Five-level Inverter Employing WRPWM Switching Scheme

by

Chia-Tsung Chaing

Submitted in partial fulfillment of the requirements for the degree
Master of Engineering (Electrical Engineering)
in the
Faculty of Engineering, the Built Environment and Information Technology
UNIVERSITY OF PRETORIA

14 February 2005

Supervisor: Prof. M. N. Gitau

SUMMARY

Five-level Inverter Employing WRPWM Switching Scheme

By Chia-Tsung Chaing

Promoter: Prof. M. N. Gitau

Master of Electrical Engineering in Department of Electrical, Electronic and Computer Engineering

Multilevel Random Pulse Width Modulation (RPWM) schemes have drawn increasing attention in the past few years. Multilevel topologies provide high voltage and high power capabilities and random PWM schemes offer reduction in discrete harmonics spectral.

This dissertation provides a generalized theory and analysis methods of the standard five-level Weighted RPWM (WRPWM). Equations have been derived to analyze the spectral performance and average switching frequency of the WRPWM output waveform using statistical approach. A modified WRPWM scheme has been proposed. The modified WRPWM scheme is then analyzed with the equations derived from the same approach. The analyzed theoretical spectrum of the standard five-level WRPWM is then compared with the three-level WRPWM scheme and the conventional carrier based PWM scheme.

A scaled laboratory prototype diode clamping five-level inverter has been built for verification of the standard and the proposed modified WRPWM schemes. It can be seen that the experimental measurements and the theoretical analyzed results are all in good agreement. Results show the two five-level WRPWM schemes offers significant improvements on the spectrum content than the conventional carrier based PWM scheme. It was found that the five-level WRPWM schemes have successfully suppress the magnitude of third harmonic below 5% of the magnitude of fundamental component and even less for the higher order harmonic components.

Research contributions made by the dissertation are:

- The proposed modified multilevel WRPWM scheme which utilizing the switching decision redundancy of multilevel inverter to manipulate the harmonic content of the output signal.
- The derived mathematical equations of the standard and modified five-level WRPWM scheme for analytical purposes.

KEY WORD

Comparison, Continuous Noise Power, Discrete Noise Power, Expected Value, Harmonic, Multilevel Inverter, Power Spectrum, Probability, Random number, Random Process, Signal power, Switching Decision, Switching frequency, WRPWM.

ABBREVIATIONS

APOD	-	Alternative Phase Opposition Disposition
DSP	-	Digital Signal Processor
EMC	-	Electromagnetic Compatibility
EMI	-	Electromagnetic Interference
MOSFET	-	Metal Oxide Field Effect Transistor
NPC	-	Neutral Point Clamped
PCB	-	Printed Circuit Board
PD	-	Phase Disposition
POD	-	Phase Opposition Disposition
PWM	-	Pulse Width Modulation
RPWM	-	Random Pulse Width Modulation
SH-PWM	-	Subharmonic Pulse Width Modulation
VCO	-	Voltage Controlled Oscillator
VSI	-	Voltage Source Inverter
WRPWM	-	Weighted Random Pulse Width Modulation

TABLE OF CONTENTS

CHAPTER 4

CHAPTER 5

CHAPTER 6

CHAPTER 7

CHAPTER 8

CHAPTER 8

CHAPTER 9

CHAPTER ONE

INTRODUCTION

Multilevel inverters are becoming popular as a viable alternative to current source inverters and conventional two-level voltage source inverters for high power applications [1,2]. With the multilevel topology, devices have to block lower voltages compared with conventional inverters for a given dc bus voltage or output voltage [1,2]. This allows utilizing currently available semiconductor switches at even higher voltages and higher power applications than previously possible. Additionally, multilevel inverters offer better quality output waveform with less harmonics and fewer electromagnetic compatibility (EMC) concerns [1,2].

Up to now many switching schemes for multilevel inverters have been proposed. This include space vector, pulse width modulation (PWM), harmonic elimination, optimal PWM and random PWM (RPWM). Each has its own advantages as well as disadvantages according to the modulation index region they operate [1]. Recently, a novel random PWM called weighted random PWM (WRPWM) has been proposed for two-level inverters. The WRPWM added some deterministic nature into the standard RPWM method to improve the harmonic content significantly [3-5]. Additionally, WRPWM scheme offers higher S/N ratio and can be consistently applied to the entire range of linear modulation index [3,5].

1.1 Background

The multilevel inverter topology leads to switch stress and losses reduction [2]. Several topologies have been given serious consideration by industry. Among them the best known are the H-bridge cascade inverter (cascade inverter with separated dc sources) [2,7], the capacitor clamping inverter [7,8] and the diode clamping inverter [6,7].

Originating from the neutral-point-clamped (NPC) inverter the diode clamp method became popular due to its similarity to conventional two-level inverter and ease of control [6,7]. The major problems besides achieving balanced voltage supplies within the dc link include indirect clamping of the inner devices and multiple blocking voltages of the clamping diodes [6,8]. As for multiple blocking voltages of the clamping diodes concerned, conventional solution is to put an appropriate number of diodes in series. It requires using large RC snubbing networks

leading to expensive and voluminous systems [6]. A new diode clamping inverter has been proposed and works without the series association of the clamping diodes [6]. The need for the large RC network to deal with the voltage-sharing problem among series diodes is therefore removed.

One of the main performance parameters that requires serious attention when designing an inverter is harmonic content of the output voltage. In general, PWM schemes provide an output waveform with a large fundamental voltage component while low-order harmonics are suppressed [9]. However, the harmonic power is usually concentrated in the high frequency range due to the high switching frequency of the inverter [9]. These high frequency harmonics can have adverse effects such as acoustic noise, harmonic heating in electric machines and radio interference. It has been shown that when randomness is introduced in a PWM waveform it can cause the harmonic power to spread over the harmonic spectrum so that no harmonic component has significant magnitude [5,9]. If the pulse position or the switching frequency is varied in a random manner, the power spectrum of the output voltage of the inverter acquires a continuous part, while the discrete (harmonic) part is significantly reduced [5].

Generally, the quality of RPWM waveforms depends largely on the sampling frequency and the quality of the random number generator. Due to the random nature, there is very little control on the quality of the RPWM harmonic content and the inverter switching decision for a given random number generator [3].

To have more control on the resulting frequency spectra of the RPWM signal a modified RPWM scheme called weighted random PWM (WRPWM) has been proposed [3]. Basically, WRPWM scheme makes several comparisons between the random number and sinusoidal reference within each sampling period. The number of comparison is an odd integer; the majority decision can then be used to determine the switching state of the RPWM output. If the weighted decision process is applied to the entire fundamental period, the probability of having a rectangular voltage block in the central region of each half cycle of fundamental is high because the weighed switching decision makes it more likely that the switching state is +1 (-1) in the positive (negative) half cycle [3,10]. The presence of this voltage block tends to increase the third harmonic component. This may be very useful in some three-phase drive applications. However, the WRPWM can be modified to eliminate the third harmonic by applying weighted switching decision process to the region, where the sinusoidal reference signal is near or equal to zero-crossing point. This weighted process can be consistently applied to the entire range of modulation index.

The combination of multi-level topologies with various RPWM has drawn interest of researchers in the last few years. The WRPWM method originally developed for two-level inverters has been extended to three-level inverter [4]. Although performance of the inverter has not been fully and properly characterized, analysis has indicated that multilevel inverter employing WRPWM has great potential to have better spectral performance (i.e., less harmonic components) than both the two-level RPWM scheme and two-level WRPWM scheme.

Chapter 2 first introduces the conventional two-level inverters and their operating principle and the advantages of multilevel topologies. Then the operating features, principle and constraints of the three most common topologies and a modified topology are discussed. This is followed by a comparison between the advantages and disadvantages of those four multilevel topologies.

In chapter 3 the operation of the two most basic PWM schemes is reviewed. This is followed by a discussion of the disadvantages of the traditional PWM and the reason of the existence of RPWM schemes. Then a literature review on the available RPWM switching schemes for conventional two-level inverters is carried out. The various RPWM schemes are categorized and concepts of their operation are briefly discussed, a conclusion based on the literature that has been reviewed is made after that. The final section of chapter 3 deals with a well known multilevel carrier-based PWM method. An analytical expression of the spectral components of the output waveforms covering all the operating conditions is presented for later comparison.

At the beginning of chapter 4 some basic mathematical background and analytical methods are provided as a tool for later analysis of random switching PWM and WRPWM waveform. This is followed by the derivation of the mathematical equations for theoretical analysis and characterization of five-level inverter with WRPWM scheme

Chapter 5 presents the theoretical results and discussion of the five-level WRPWM scheme. A comparison between the five-level WRPWM scheme and the five-level SH-PWM scheme, and a comparison between the five-level WRPWM scheme and three-level WRPWM scheme.

In chapter 6 a modified WRPWM is proposed and the mathematical equations for theoretical analysis are derived. This is followed by the theoretical results and discussion of the modified five-level WRPWM scheme and a comparison with the standard five-level WRPWM presented in chapter 4.

Chapter 7 first presents the concepts of hardware implementation and is followed by a design outline of the five-level inverter and the discussion of the WRPWM schemes implementation.

Chapter 8 presents the experimental results obtained from the implemented five-level inverter. This is followed by a comparison between the experimental results and theoretical predictions. Chapter 9 concludes this report and includes recommendation for further work in this field is given.

1.2 Objective

The objectives of this dissertation are:

1) Derive mathematical equations which characterize the performance of the five-level WRPWM schemes.
2) Design and build a scaled five-level phase leg inverter for experimental purpose.
3) Implement five-level WRPWM scheme using a DSP.
4) Analyze and characterize the five-level WRPWM schemes and verify the theoretical predictions using experimental results.

1.3 Approach

This research involves the following key aspects: research, design, analysis, characterization, implementation and laboratory analysis. First, a comprehensive literature study on various types of RPWM and investigation of the new diode clamping multi-level inverter is done. Equations which characterize the performance of the five-level WRPWM scheme are then derived. A circuit of five-level diode clamping inverter is designed based on the topology proposed on [6]. A control circuitry is designed; this includes the gate drive circuit, sensor circuitry and comparator. The designed circuits are then simulated using PSCAD. This is followed by design and implementation of the five-level WRPWM on a DSP. After the completion of the whole system a thoroughly laboratory analysis is then carried out to verify the theoretical analysis results.

CHAPTER TWO

LITERATURE STUDY ON INVERTER TOPOLOGIES

2.1 Harmonics in Electrical Systems

One of the biggest problems in power quality aspects is the harmonic contents in the electrical system. Harmonics can be generated by either the source or the load side. Harmonics generated by load are caused by nonlinear operation of devices, including power converters, arc-furnaces, gas discharge lighting devices, etc [11-13]. Load harmonics can cause the overheating of the magnetic cores of transformer and motors. On the other hand, source harmonics are mainly generated by a power supply with non sinusoidal voltage waveform. Harmonics imply power losses, Electromagnetic Interference (EMI) and pulsating torque in ac motor drives [1,2,5,14]. Any periodic waveform can be decomposed into a fundamental plus a set of harmonic components. By applying Fourier decomposition, these harmonic components can be extracted [15,16]. In switch mode inverters, the frequency of each harmonic component is a multiple of its fundamental and switching frequencies [17-19].

2.2 Inverter Topologies

2.2.1 Conventional Two-Level Voltage Source Inverter

Switch mode dc to ac inverters are used in ac power supplies and ac motor drives, where the objective is to produce a sinusoidal ac output whose magnitude and frequency can both be controlled. In practice inverters are used to generate both single-phase and three-phase voltage systems and a half-bridge is the simplest topology, which is used to produce a two-level pulse width output waveform. Fig. 2.1 shows a half bridge inverter. A center-tapped voltage source is needed in such a topology to provide two dc voltages. It may be possible to use two identical capacitors in series across the dc input to provide the center tap at point *o*. The full bridge topology consists of two half-bridge inverters, and is preferred over other arrangements in higher power rating. With the same dc input voltage, the maximum output voltage of the

full bridge inverter is twice that of the half bridge inverter. Fig. 2.2 shows the full bridge configuration of the single phase voltage source inverter.

In a single phase half bridge inverter, only two switches are needed. The two switches are switched in such a way that when one of them is in its off state, the other switch is on. Since the two switches are never off simultaneously, the output v_{ao} fluctuates between two values ($V_{dc}/2$ and $-V_{dc}/2$). When S_a is turned on and $S_{a'}$ is turned off, v_{ao} is equal to $V_{dc}/2$. When $S_{a'}$ is turned on and S_a is turned off the output voltage v_{ao} will be $-V_{dc}/2$. In a full-bridge configuration as shown in Fig. 2.2, two switching schemes can be applied, they are 1) bipolar voltage switching and 2) unipolar voltage switching [11].

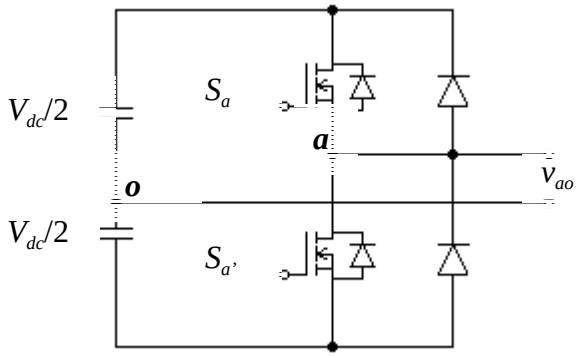

Fig. 2.1: Half-bridge configuration.

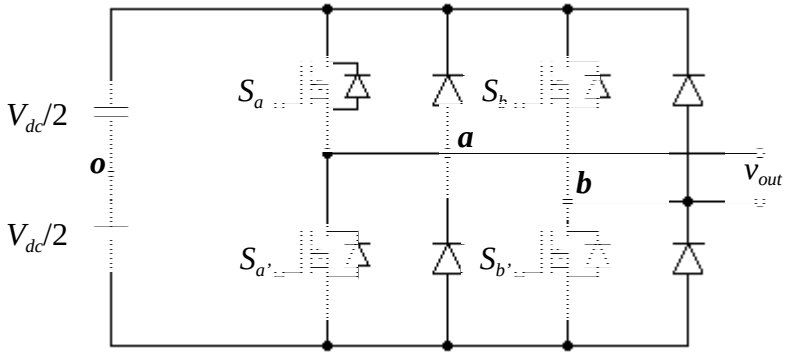

Fig. 2.2: Full-bridge configuration.

2.2.1.1 Bipolar Voltage Switching

For this control scheme, the diagonally opposite switches (S_a, $S_{b'}$) and (S_b, $S_{a'}$) are switched as switch pairs 1 and 2, respectively. With this type of switching, the output voltage waveform

between leg *a* and the point *o* (v_{ao}) is identical to the output of the half bridge inverter. The output of inverter leg *b* is 180° out of phase to the leg *a* output. When switch pair S_a and $S_{b'}$ is on, v_{ao} is equal to $V_{dc}/2$ and v_{bo} is equal to $-V_{dc}/2$. Therefore, $v_{ao} = -v_{bo}$ and $v_{out} = v_{ao} - v_{bo} = 2\ v_{ao}$. The voltage waveform for bipolar voltage switching is shown in Fig. 2.3, where v_{out1} is the fundamental output voltage.

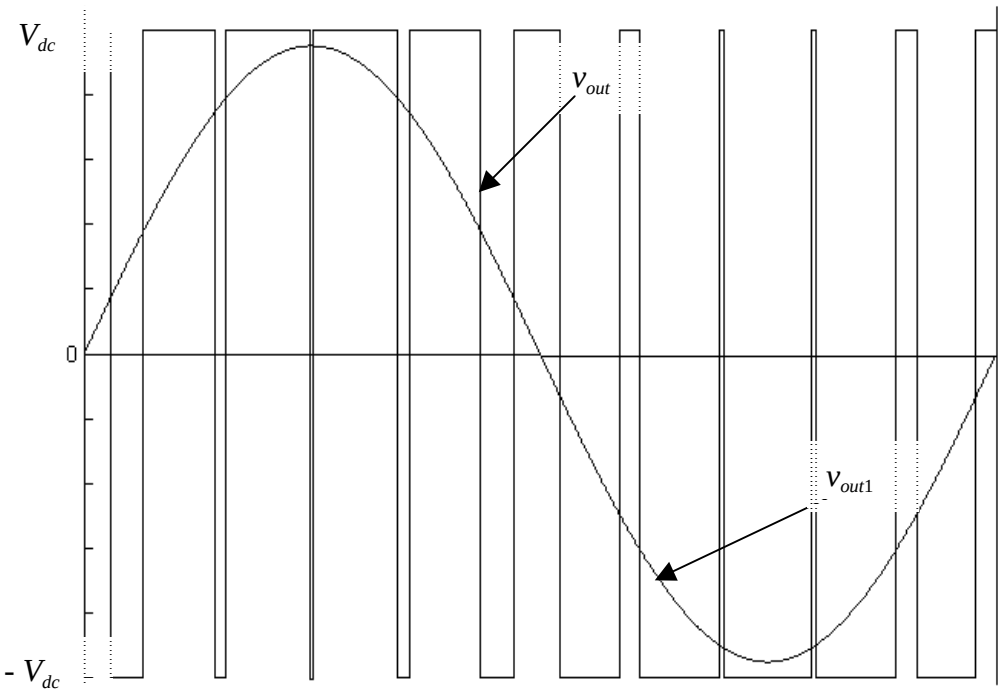

Fig. 2.3: Bipolar switching waveform.

2.2.1.2 Unipolar Voltage Switching

For this switching scheme, the full bridge inverter is used to synthesize a three level pulse width output waveform. The switches in the two legs of the inverter are not switched simultaneously, as in bipolar voltage switching scheme. There are four switching states and the corresponding voltage levels [11]:

1. S_a, $S_{b'}$ on: $v_{ao} = V_{dc}/2$, $v_{bo} = -V_{dc}/2$; $v_{out} = V_{dc}$.
2. S_b, $S_{a'}$ on: $v_{ao} = -V_{dc}/2$, $v_{bo} = V_{dc}/2$; $v_{out} = -V_{dc}$.
3. S_a, S_b on: $v_{ao} = V_{dc}/2$, $v_{bo} = V_{dc}/2$; $v_{out} = 0$.
4. $S_{a'}$, $S_{b'}$ on: $v_{ao} = -V_{dc}/2$, $v_{bo} = -V_{dc}/2$; $v_{out} = 0$.

Please note that, whenever the two top or two bottom switches are on, the output voltage is zero. In this type of switching scheme, the output voltage changes between zero and V_{dc} or

between zero and $-V_{dc}$ voltage level as shown in Fig. 2.4. Unipolar voltage switching scheme has the advantage of effectively doubling the switching frequency as far as the output waveform is concerned, compared to the bipolar voltage switching scheme. Moreover, the voltage jumps in the output voltage at each switching are reduced to V_{dc}, as compared to $2V_{dc}$ in the bipolar voltage switching scheme.

The advantage of effectively doubling the switching frequency appears in the harmonic spectrum of the output voltage waveform, where the lowest harmonic (in the ideal circuit) appear as sidebands at twice the switching frequency thus it is easier to filter out the harmonic components. As for bipolar voltage switching, the harmonic components appear at odd multiples of the switching frequency and their side-bands, and aside-bands centered around the even multiples of switching frequency. This makes it slightly more difficult to filter out the harmonic components.

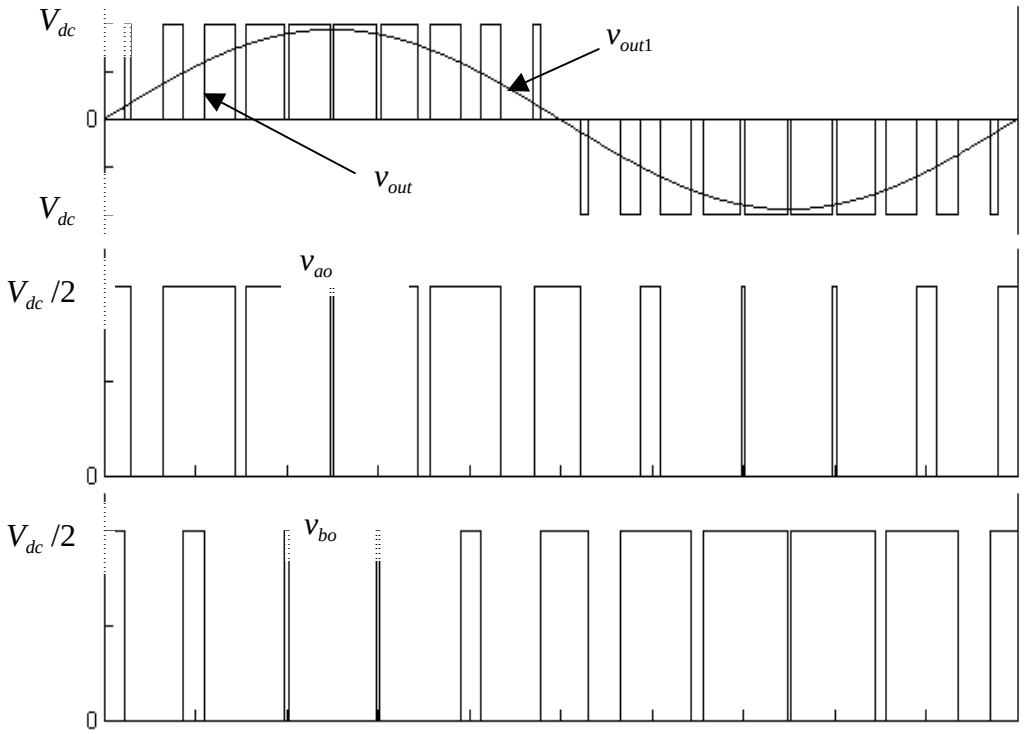

Fig. 2.4: Unipolar switching waveform.

2.2.1.3 Multilevel Voltage Source Inverter

The shift to variable voltage variable frequency inverters in ac drives and power supplies with associated emphasis on improved performance and increased power ratings is again focusing

on the problem of inverter harmonic distortion and can be thought of as a generator of harmonics. By increasing the switching frequency the harmonic content can be improved since the harmonics will shift to higher frequency regions and thus is easier to filter out. But high frequency switching requires significant de-rating of switching devices and generates large switching losses. Moreover, high frequency switching generates broadband EMI to nearby communication or other electronic equipment [1,2,5,14]. Many journal and conference articles have been issued on various switching schemes to pulse width modulate the inverter switches in order to shape the output ac voltages to be as close to a sine wave as possible [1,20-22].

Recently the multilevel inverter has drawn tremendous interest in the power industry [1,2,4,6-8,12,14,20-31]. The concept multi-level actually started from three-level neutral clamped converter [23]. The three-level neutral clamped converter makes use of two series connected capacitors to realize a voltage divider and uses the center tap as the neutral. Each phase leg of the three-level converter has two pairs of switching devices in series. The center of each device pair is clamped to neutral through clamping diodes. The output waveform of the three-level inverter is a three-level PWM wave.

It is intuitive that having more than two voltage levels to build a sinusoidal wave shape can lead to a reduction of the harmonics in the output waveform. The general premise of the multilevel inverter is to synthesize a sinusoidal voltage waveform from several levels of voltages, typically obtained from capacitor voltage sources. As the number of levels increases, the synthesized output waveform has more steps, which produces a staircase wave that approaches a sinusoidal waveform. Also, as more steps are added to the waveform, the harmonic distortion of the output wave decreases until it reaches zero with infinite number of levels. As the number of levels increases, the higher the voltage can be spanned by connecting devices in series. The structure of the multilevel inverter is such that no voltage sharing problems are encountered by series connected devices. In general the main advantages of multilevel inverters are as follows [1,7,12,14,22-32].

1) Voltage and power output increase with number of levels.
2) For multilevel inverter, increase in output voltage and power does not require an increase in rating of individual power switches.
3) Dynamic and static voltage sharing among power switches is built into the structure.
4) A multilevel inverter reduces the high dV/dt experienced in traditional inverters because switching is between several smaller voltage levels.
5) With multi-level topology, the devices ratings can be reduced due to the voltage sharing within the inverter structure.

6) A multilevel inverter offers better quality output waveform with less harmonic content and therefore reduces electromagnetic interference (EMI).

There are several multilevel topologies under serious consideration from industry. The easiest approach to generate multilevel waveforms is through phase shifting of multiple single level inverter output waveforms which are added together vertically using series connected transformer windings [25,26]. Problems of this magnetic transformer coupling method are that the resulting system is bulky, heavy and costly. Therefore, the capacitor voltage synthesis method is preferred over magnetic coupling method. Here, three capacitor voltage synthesis based multilevel inverters are briefly discussed:

1) Flying capacitor multilevel inverter [7,25,26,28].
2) Cascaded inverter with separated dc source [7,14,20,25,27,28].
3) Diode clamped multilevel inverter [2,6,7,14,23,24-26,28].

2.2.1.4 Flying Capacitor Multilevel Inverter

Fig. 2.5 illustrates the fundamental building block of a single phase leg of a flying capacitor based five-level converter. In a three phase system, each phase leg has an identical structure. The capacitor clamped inverter uses a ladder structure of dc side capacitor bank where the voltage on each capacitor bank differs from that of the next capacitor bank. Assuming all capacitors are identical, the series connection of capacitors in Fig. 2.5 is an indication of the ratio of voltage level to the dc bus voltage. Three inner loop balancing capacitors for phase leg a, C_{a1}, C_{a2} and C_{a3} are independent from those for other phase leg in the system. All phase legs share the same dc link capacitors, C_1 to C_4.

The voltage level defined in the flying capacitor inverter is similar to that of the diode clamp type inverter. However, the voltage synthesis in the flying capacitor inverter has more flexibility than a diode clamp inverter. The capacitor clamped inverter output voltage synthesis is performed by turning on switches so that adding or subtracting of the capacitor voltages takes place. For the five-level inverter in Fig. 2.5, there are four capacitor banks used in synthesizing the output voltage. The switching operations are constrained so that the capacitor banks are never shorted to each other and current continuity to the main dc bus capacitor is maintained.

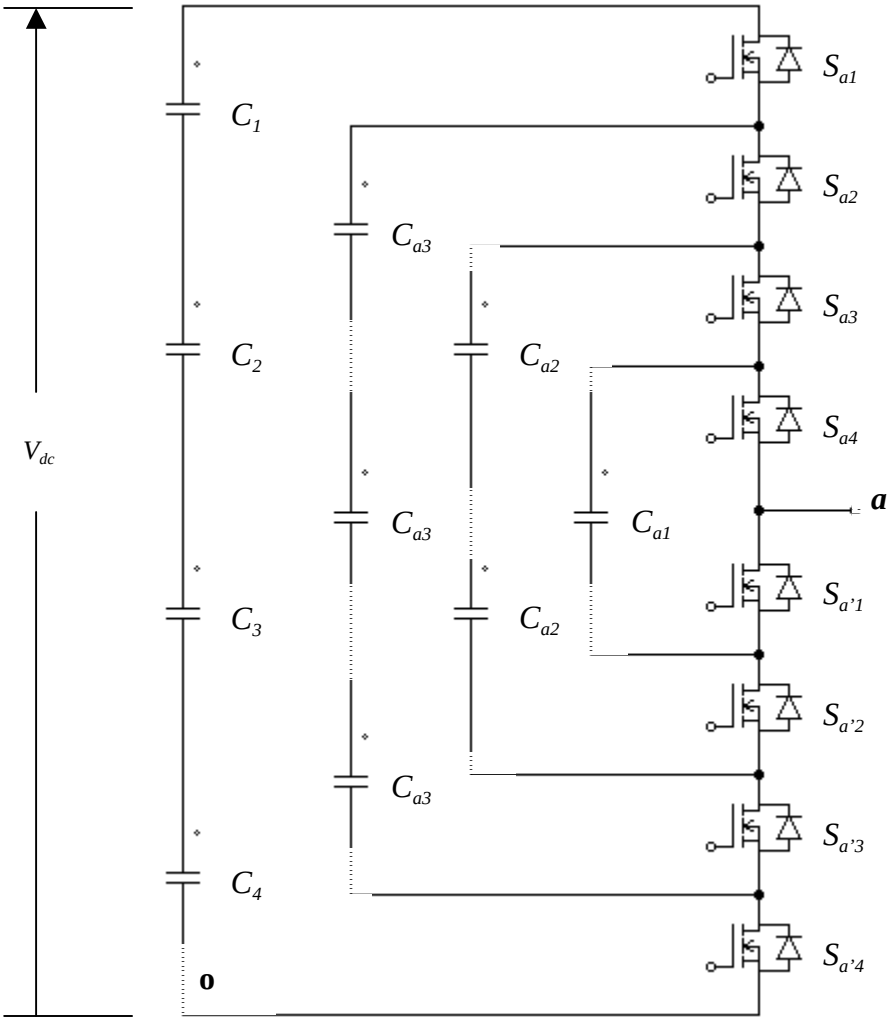

Fig. 2.5: Circuit diagram of a single phase leg of flying capacitor based five-level voltage source inverter.

As an example, the voltage of the five level phase leg a output with respect to the negative dc rail, V_{ao}, can be synthesized by the following switch combinations.

1) For voltage level $V_{ao} = V_{dc}$, turn on all upper switches S_{a1} through S_{a4}.
2) For voltage level $V_{ao} = 3V_{dc}/4$, there are four combinations:
   a) S_{a1}, S_{a2}, S_{a3} and $S_{a'1}$ ($V_{ao} = V_{dc} - V_{dc}/4$),
   b) S_{a2}, S_{a3}, S_{a4} and $S_{a'1}$ ($V_{ao} = 3V_{dc}/4$),
   c) S_{a1}, S_{a3}, S_{a4} and $S_{a'3}$ ($V_{ao} = V_{dc} - 3V_{dc}/4 + V_{dc}/2$), and
   d) S_{a1}, S_{a2}, S_{a4} and $S_{a'2}$ ($V_{ao} = V_{dc} - V_{dc}/2 + V_{dc}/4$).
3) For voltage level $V_{ao} = V_{dc}/2$, there are six combinations:
   a) S_{a1}, S_{a2}, $S_{a'1}$ and $S_{a'2}$ ($V_{ao} = V_{dc} - V_{dc}/2$),

b) S_{a3}, S_{a4}, $S_{a'3}$ and $S_{a'4}$ ($V_{ao} = V_{dc}/2$),
c) S_{a1}, S_{a3}, $S_{a'1}$ and $S_{a'3}$ ($V_{ao} = V_{dc} - 3V_{dc}/4 + V_{dc}/4$),
d) S_{a1}, S_{a4}, $S_{a'2}$ and $S_{a'3}$ ($V_{ao} = V_{dc} - 3V_{dc}/4 + V_{dc}/4$),
e) S_{a2}, S_{a4}, $S_{a'2}$ and $S_{a'4}$ ($V_{ao} = 3V_{dc}/4 - V_{dc}/2 + V_{dc}/4$) and
f) S_{a2}, S_{a3}, $S_{a'1}$ and $S_{a'4}$ ($V_{ao} = 3V_{dc}/4 - V_{dc}/4$).

4) For voltage level $V_{ao} = V_{dc}/4$, there are four combinations:
a) S_{a1}, $S_{a'1}$, $S_{a'2}$ and $S_{a'3}$ ($V_{ao} = V_{dc} - 3V_{dc}/4$),
b) S_{a4}, $S_{a'2}$, $S_{a'3}$ and $S_{a'4}$ ($V_{ao} = V_{dc}/4$),
c) S_{a3}, $S_{a'1}$, $S_{a'3}$ and $S_{a'4}$ ($V_{ao} = V_{dc}/2 - V_{dc}/4$) and
d) S_{a2}, $S_{a'1}$, $S_{a'2}$ and $S_{a4'}$ ($V_{ao} = 3V_{dc}/4 - V_{dc}/2$).

5) For voltage level $V_{ao} = 0$, turn on all lower switches $S_{a1'}$ through $S_{a4'}$.

If only one set of switch combination of the voltage levels is used, according to the turn on time requirement of their corresponding switch states the flying capacitor multi-level inverter has unequal device duty problems. Thus, the voltage across dc link capacitors is unbalanced. However, the flying capacitor has redundancy at its inner voltage level. By employing two or more proper switch combinations for middle voltage levels, it is possible to maintain the balance for capacitor charge and discharge.

Besides the difficulty of balancing voltage in real power conversion, the major problem is the requirement of a large number of storage capacitors. Provided that the voltage rating of each capacitor used is the same as switching devices, an m-level inverter will require a total of (m-1) × (m-2) / 2 auxiliary capacitors [7,26,28]. With the assumption that all capacitors have the same voltage rating, an m-level diode clamp inverter only requires (m-1) dc link capacitors [7,26,28].

2.2.1.5 Cascaded Inverter with Separate dc Sources

The general structure of this multilevel inverter is to synthesizes a sinusoidal voltage from several levels of dc voltages, which may be obtained from batteries, fuel cells, solar cells, or capacitors charged from a rectified ac voltage source. Fig. 2.6 shows a single phase leg structure of the cascaded inverter with separate dc sources. Each separate dc source is connected to a single phase full bridge inverter. Each inverter level can generate three different voltage outputs, $+V_{dc}$, 0, and $-V_{dc}$ by connecting the dc source sequentially to the ac output side using different combination switching state of the four switches, S_1, S_2, S_3 and S_4. To obtain $+V_{dc}$, turn on switches S_3 and S_4, and to obtain $-V_{dc}$ turn on switches S_2 and S_3. By

turning on S_1 and S_2 or S_3 and S_4, the output voltage is 0. The ac terminal voltages of different level inverters are connected in series such that the synthesized voltage waveform is the inverter output.

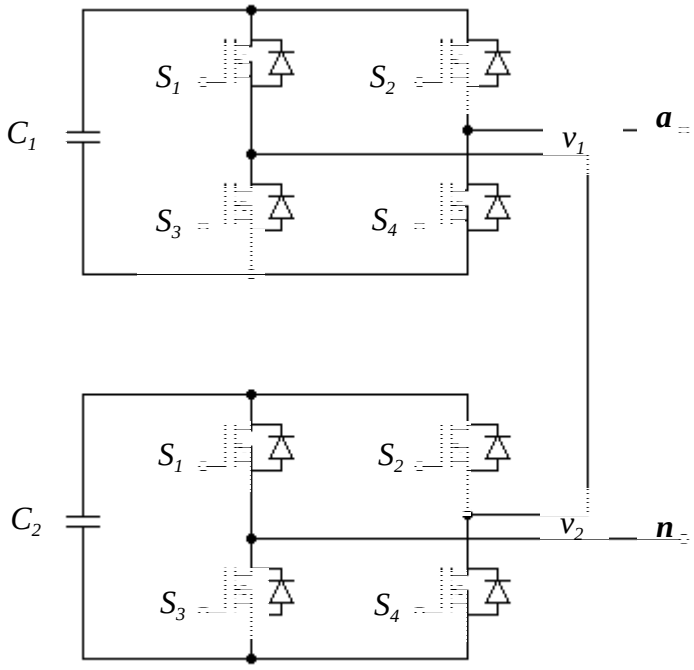

Fig. 2.6: Circuit diagram of a single phase of cascaded inverter with separated dc source.

The level in a cascaded inverter is defined by m = 2s + 1, where m is the output phase voltage level and s is the number of separate dc sources [7,14,27,28]. An example of a phase voltage waveform for a five level cascaded inverter with five separated dc sources is shown in Fig. 2.7, where the phase voltage $v_{an} = v_1 + v_2$ [7,14,27,28]. Note that the duty cycle for each of the voltage level is different. If this same pattern of duty cycle is used on a real power operation continuously, then the battery connected to C_1, is cycled on for much longer duration the battery connected to C_2. This means that the C_1 battery will be discharged much sooner than C_2 battery. However, multilevel cascaded inverter has the highest switching redundancy among the other two topologies. The batteries can be charged and discharged by rotating the duty cycles among the switches.

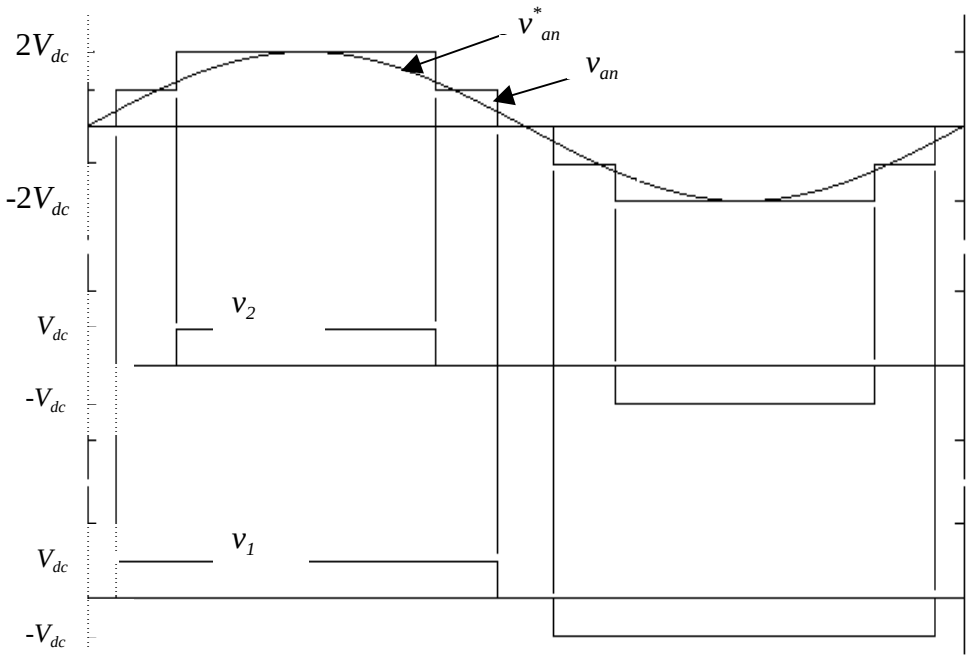

Fig. 2.7: The phase voltage waveform of the cascaded multilevel inverter with separated dc sources.

2.2.1.6 Diode Clamped Multilevel Inverter

2.2.1.6.1 Conventional Diode Clamped Multilevel Inverter

The diode clamp multilevel inverter uses a series string of capacitors to divide up the dc bus voltage into a set of voltage levels with equivalent amplitude. Each phase leg consists of a number of switching devices in series which are connected by diodes to the tap points along the dc bus capacitor. The forward voltage across each main device is clamped by the connection of diodes between the main devices and tap points along the string of dc bus capacitors. The tap points provide clamping voltage levels. To comply with the definition of the previously mentioned capacitor clamp and cascade multilevel inverters, an m level diode clamp inverter consists of m-1 capacitors on the dc bus and produces an m level phase voltage waveform [2,7,14,23,26-28]. A single-phase leg five level diode clamped inverter is shown in Fig. 2.8. The dc bus consists of four capacitors C_1, C_2, C_3 and C_4. For dc bus voltage V_{dc}, the voltage across each capacitor is V_{dc} / 4, and each device voltage stress will be limited to one capacitor voltage level (i.e. V_{dc} / 4), through clamping diodes.

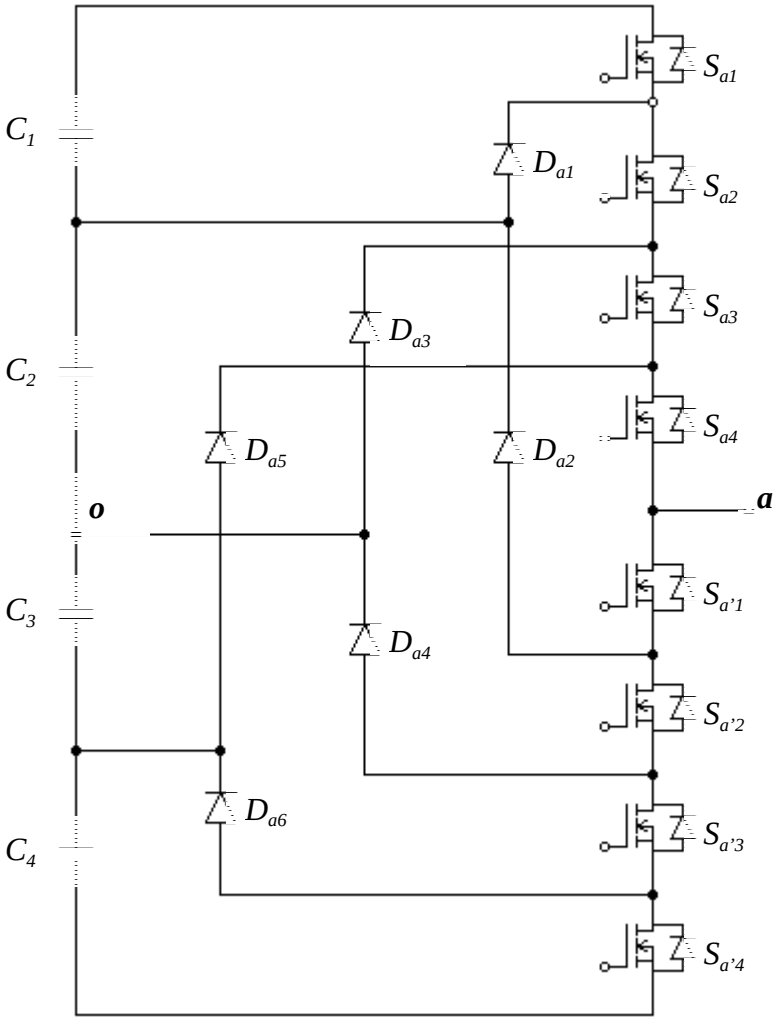

Fig.2. 8: Circuit diagram of a phase leg of conventional diode clamped inverter.

Table 1.1 lists the output voltage levels and their corresponding switching states for a five-level diode clamped inverter. State condition 1 means the switch is switched on, and 0 means the switch is switched off. Using the five-level inverter shown in Fig. 2.8 as an example, consider the center tap *o* as the output voltage reference point, there are five switching combinations to synthesize output voltage waveform across *a* and *o*.

1) For voltage level $V_{ao} = V_{dc}/2$, turn on all upper switches S_{a1} through S_{a4}.
2) For voltage level $V_{ao} = V_{dc} / 4$, turn on three upper switches S_{a2} through S_{a4} and one lower switch $S_{a'1}$.
3) For voltage level $V_{ao} = 0$, turn on two upper switches S_{a3} and S_{a4} and two lower switches $S_{a'1}$ and $S_{a'2}$.

4) For voltage level $V_{ao} = -V_{dc} / 4$, turn on one upper switch S_{a4} and three lower switches $S_{a'1}$ through $S_{a'3}$.
5) For voltage level $V_{ao} = -V_{dc}/2$, turn on all lower switches $S_{a'1}$ through $S_{a'4}$.

Note that in each phase leg there exist four complementary switch pairs. Turning on one of the switches of a switch pair requires the other switch to be turned off. The four complementary switch pairs for the phase leg shown in Fig. 2.8 are (S_{a1}, $S_{a'1}$), (S_{a2}, $S_{a'2}$), (S_{a3}, $S_{a'3}$) and (S_{a4}, $S_{a'4}$). Fig. 2.9 shows the output voltage V_{ao} of the five level inverter phase leg.

TABLE 1.1

Diode Clamped Five Level Inverter Voltage Levels and Their Switching States [7,14].

Output V_{ao}	Switch state							
	S_{a1}	S_{a2}	S_{a3}	S_{a4}	$S_{a'1}$	$S_{a'2}$	$S_{a'3}$	$S_{a'4}$
$V_5 = V_{dc}/2$	1	1	1	1	0	0	0	0
$V_4 = V_{dc}/4$	0	1	1	1	1	0	0	0
$V_3 = 0$	0	0	1	1	1	1	0	0
$V_2 = -V_{dc}/4$	0	0	0	1	1	1	1	0
$V_1 = -V_{dc}/2$	0	0	0	0	1	1	1	1

Even though each switching device is only required to block a voltage level of $V_{dc} / (m -1)$, the blocking voltage of each clamping diode in the diode clamping multilevel inverter is dependent on its position in the structure. Therefore, the clamping diodes need to have different voltage ratings for reverse voltage blocking [6,7,14]. From Fig. 2.8, if S_{a1} through S_{a4} are turned on, D_{a1} need to block one capacitor voltage, or $V_{dc} / 4$, D_{a3} need to block $V_{dc} / 2$ and D_{a5} need to block $3 V_{dc} / 4$. Table 2.2 shows the diode blocking voltages corresponding to the output voltage levels. The conventional solution is to put an appropriate number of diodes in series [6,7,26], as shown in Fig. 2.10. The possible over voltage across the series connected clamping diodes due to the diversities of diode switching characteristics as well as their stray parameters call for large RC over voltage snubbing network to be introduced leading to expensive and space consuming system.

When operating at unity power factor, the charging or discharging time for each capacitor is different, this is shown in Fig. 2.9. Such a capacitor discharging profile repeats every half cycle and result in unbalanced capacitor voltage between different levels. Unfortunately, the

diode clamped multilevel inverter does not have phase voltage switching redundancies due to the switching operation constrain imposed by its structure. Thus, it is not easy to overcome the capacitor charge balancing problem by modifying the switching scheme and often additional hardware is needed to ensure capacitor charge balancing.

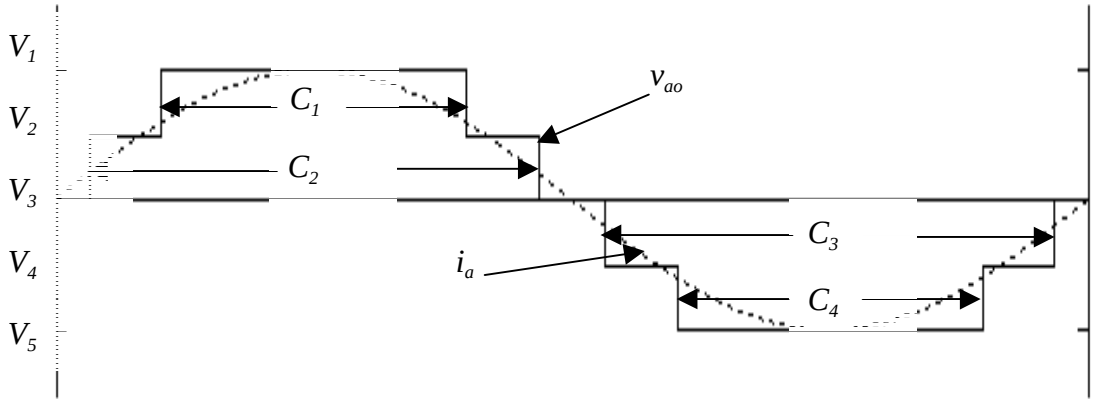

Fig. 2.9: Output waveform and capacitor discharging profile of the conventional diode clamped inverter.

TABLE 2.2

Diode Clamped Five-Level Inverter Voltage Levels and diode blocking voltages.

Output V_{ao}	Diode blocking voltage					
	D_{a1}	D_{a2}	D_{a3}	D_{a4}	D_{a5}	D_{a6}
$V_5 = V_{dc}/2$	$V_{dc}/4$	0	$V_{dc}/2$	0	$3V_{dc}/4$	0
$V_4 = V_{dc}/4$	0	0	$V_{dc}/4$	0	$V_{dc}/2$	0
$V_3 = 0$	0	$V_{dc}/4$	0	0	$V_{dc}/4$	0
$V_2 = -V_{dc}/4$	0	$V_{dc}/2$	0	$V_{dc}/4$	0	0
$V_1 = -V_{dc}/2$	0	$3V_{dc}/4$	0	$V_{dc}/2$	0	$V_{dc}/4$

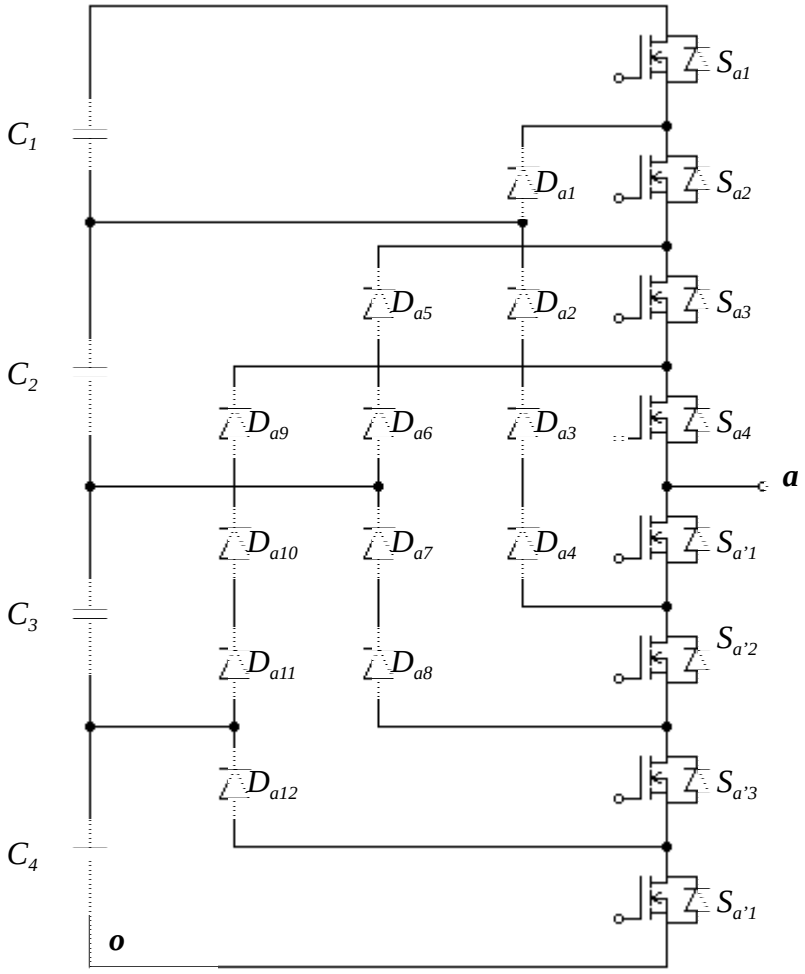

Fig. 2.10: Structure of the conventional diode clamped inverter with series clamping diodes.

2.2.1.6.2 New Diode Clamped Multilevel Inverter

A new diode clamped inverter has been introduced by Yuan and Barbi [6]. In this new structure, not only the main switches are clamped by the clamping diodes, the clamping diodes are clamped mutually by other clamping diodes. Thus, the need for the large RC network to deal with voltage sharing problem among series connected diode in the traditional topology discussed in section 2.2.1.6.1 is removed.

A five-level inverter using the new diode clamping inverter is shown in Fig. 2.11. A total of eight switches and twelve diodes of equal voltage rating are used. Thus, an equal number of diodes are used as in the case of conventional diode clamping inverter with diodes connected in series. A single, m-level inverter phase leg requires (m - 1) storage capacitors, 2 (m - 1) switches and (m-1) (m-2) clamping diodes [6].

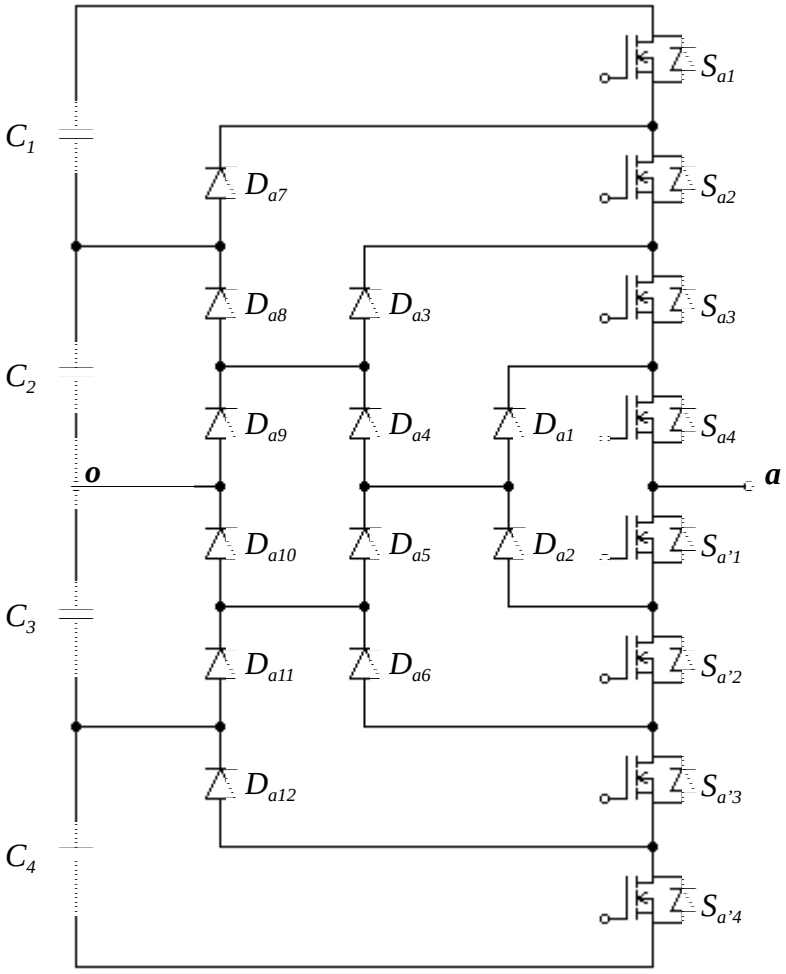

Fig. 2.11: Structure of the new diode clamped inverter.

For the five-level case, just like the conventional diode clamping inverter previously mentioned, the new diode clamping five-level inverter has five switching combinations and four complementary switch pairs (S_{a1}, $S_{a'1}$), (S_{a2}, $S_{a'2}$), (S_{a3}, $S_{a'3}$) and (S_{a4}, $S_{a'4}$) to synthesize output voltage waveform. The output voltage levels and their corresponding switching states are identical to the conventional diode clamping inverter in table 1.1. For the sake of simplicity, the new diode clamping inverter is decomposed into two level switching cells as its basic operation units [6]. In cell (a), switches S_{a2}, S_{a3} and S_{a4} are always on, while S_{a1} and $S_{a'1}$ work alternately to give the output voltage V_{ao} of V_{dc} and $3V_{dc}$ / 4 respectively. Similarly, in cell (b), switches S_{a3}, S_{a4} and $S_{a'1}$ are always on, while S_{a2} and $S_{a'2}$ work alternately to give the output voltage V_{ao} of $3V_{dc}$ / 4 and V_{dc} / 2 respectively. In cell (c), switches S_{a4}, $S_{a'1}$ and $S_{a'2}$ are always on, while S_{a3} and $S_{a'3}$ work alternately connecting the output voltage to V_{dc} / 2 and V_{dc} / 4 respectively. Finally, in cell (d), switches $S_{a'1}$, $S_{a'2}$ and $S_{a'3}$ are always on, while S_{a4} and $S_{a'4}$ work alternately to give the output voltage V_{ao} of V_{dc} / 4 and 0 respectively.

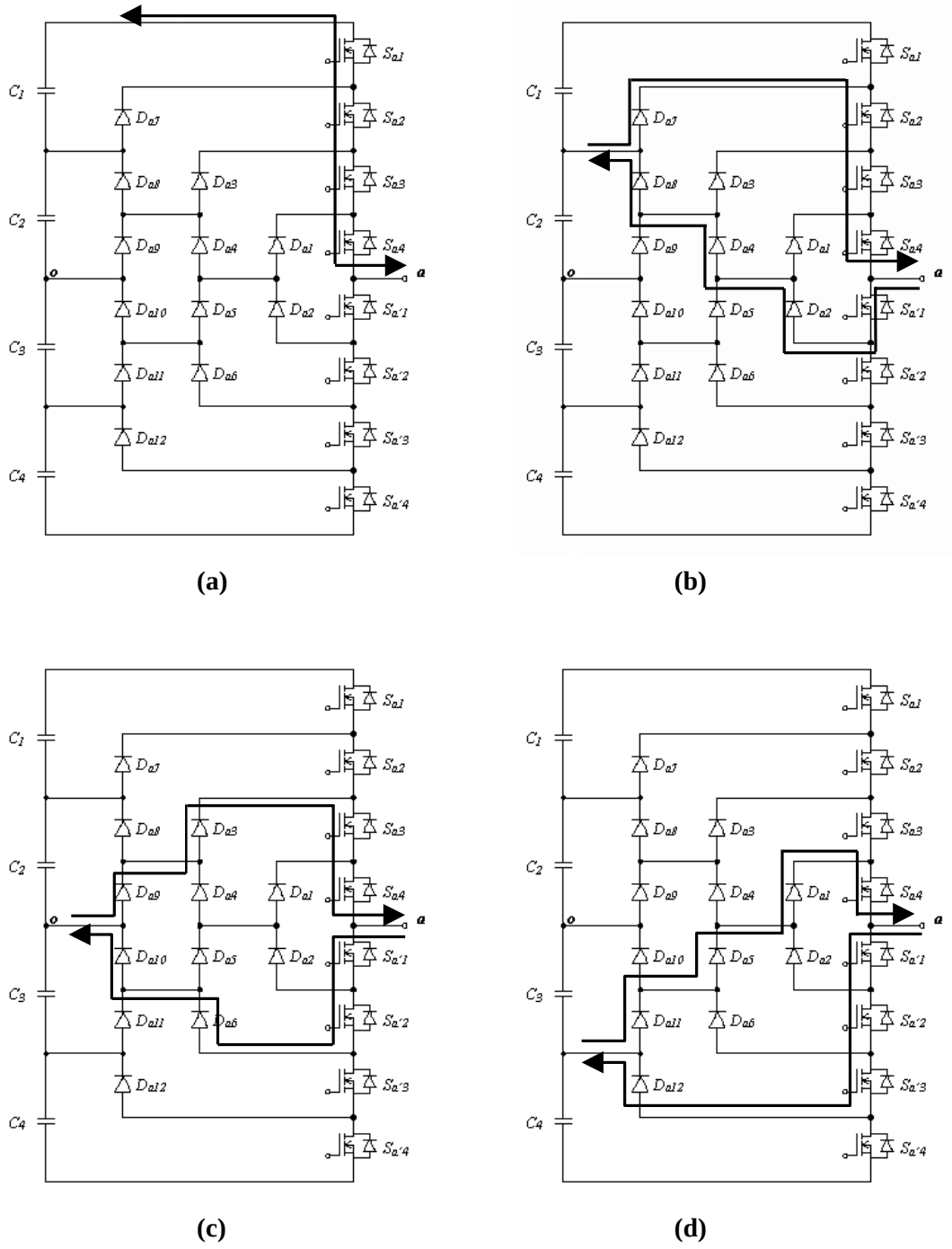

Fig. 2.12: Forward and freewheeling paths for each switching combinations [6].

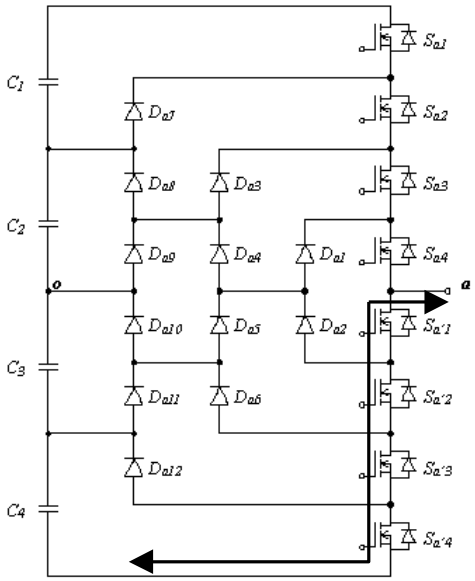

(e)

Fig. 2.12: (continued) [6].

The operation of the switching combinations is identical to the conventional diode clamping inverter, except for the forward and freewheeling path due to the clamping diode rearrangement. Figs. 2.12 (a), (b), (c), (d) and (e) show the forward and freewheeling paths corresponding to the active devices switching combination list in table 1.1.

(a) Both the forward and freewheeling path involves S_{a1}, S_{a2}, S_{a3} and S_{a4} connecting the inverter output to V_{dc} level for either positive or negative current flow.

(b) The forward path of the down arm involves D_{a3}, S_{a2}, S_{a3} and S_{a4}, whereas the freewheeling path involves S_{a4}, D_{a2}, D_{a4} and D_{a8} connecting the inverter output to $3V_{dc}$ / 4 level for either positive or negative current flow.

(c) The forward path of the down arm involves D_{a9}, D_{a3}, S_{a3} and S_{a4}, whereas the freewheeling path involves $S_{a'1}$, $S_{a'2}$, D_{a6} and D_{a10} connecting the inverter output to V_{dc} / 2 level for either positive or negative current flow.

(d) The forward path of the down arm involves D_{a11}, D_{a5}, D_{a1} and S_{a4}, whereas the freewheeling path involves $S_{a'1}$, $S_{a'2}$, $S_{a'3}$ and D_{a12} connecting the inverter output to V_{dc} / 4 level for either positive or negative current flow.

(e) Both the forward and freewheeling path involves $S_{a'1}$, $S_{a'2}$, $S_{a'3}$ and $S_{a'4}$ connecting the inverter output to 0 level for either positive or negative current flow.

As the name of the diode clamping topology implies, all the switches in the string at blocking state must be clamped to a corresponding dc link capacitors via relevant clamping diodes. By which, blocking voltage of the switches will be constrained to the nominal value. Clamping diodes change their blocking states as the switches change their states. With output of the inverter connected to certain level by relevant switches, the involved clamping diodes will block zero voltage whereas the remaining clamping diodes will block zero or the nominal voltage (V_{dc} / 4) depending on their position in the clamping network. From Figs. 2.12 (a), (b), (c), (d) and (e), the following clamping diode blocking states relating to switching states can be derived.

(a) When inverter output is connected to level V_{dc} with switches S_{a1} through S_{a4} turned on, in this case, there is no clamping diode involved. D_{a2}, D_{a4}, D_{a6}, D_{a8}, D_{a10} and D_{a12} will all block zero voltage in order to clamp switches $S_{a'1}$ through $S_{a'4}$ to nominal voltage. Then D_{a1}, D_{a3}, and D_{a7}, must block the nominal voltage as their cathode terminals are at level V_{dc} and anode terminals are at level $3V_{dc}$ / 4. D_{a5} and D_{a9} must block the nominal voltage as their cathode terminals are at level $3V_{dc}$ / 4 and anode terminals are at level V_{dc} / 2. D_{a11} must block the nominal voltage as its cathode terminal is at level V_{dc} / 2 and anode terminals are at level V_{dc} / 4.

(b) When inverter output is connected to level $3V_{dc}$ / 4 with switches S_{a2} through S_{a4} and $S_{a'1}$ turned on, the clamping diode involved include D_{a1}, D_{a2}, D_{a3}, D_{a4}, D_{a7} and D_{a8} and will all block zero voltage. D_{a6}, D_{a10} and D_{a12} will all also block zero voltage in order to clamp switches $S_{a'2}$ through $S_{a'4}$ to nominal voltage. Then D_{a5} and D_{a9} must block the nominal voltage as their cathode terminals are at level $3V_{dc}$ / 4 and anode terminals are at level V_{dc} / 2. D_{a11} must block the nominal voltage as its cathode terminal is at level V_{dc} / 2 and anode terminals are at level V_{dc} / 4.

(c) When inverter output is connected to level V_{dc} / 2 with switches S_{a3}, S_{a4} $S_{a'1}$ and $S_{a'2}$ turned on, the clamping diode involved include D_{a1}, D_{a2}, D_{a3}, D_{a4}, D_{a5}, D_{a6}, D_{a9} and D_{a10} will all block zero voltage. D_{a7} and D_{a12} will also block zero voltage in order to clamp switches S_{a1}, S_{a2}, $S_{a'3}$ and $S_{a'4}$ to nominal voltage. Then D_{a8} must block the nominal voltage as its cathode terminals are at level $3V_{dc}$ / 4 and anode terminals are at level V_{dc} / 2. D_{a12} must block the nominal voltage as its cathode terminal is at level V_{dc} / 2 and anode terminals are at level V_{dc} / 4.

(d) When inverter output is connected to level V_{dc} / 4 with switches $S_{a'1}$ through $S_{a'3}$ and S_{a4} turned on, the clamping diode involved include D_{a1}, D_{a2}, D_{a5}, D_{a6}, D_{a11} and D_{a12} will all block zero voltage. D_{a3}, D_{a7} and D_{a9} will also block zero voltage in order to clamp switches S_{a1} through S_{a3} to nominal voltage. Then D_{a4} and D_{a10} must block the nominal voltage as their cathode terminals are at level V_{dc} / 2 and anode terminals

are at level V_{dc} / 4. D_{a8} must block the nominal voltage as its cathode terminal is at level $3V_{dc}$ / 4 and anode terminals are at level V_{dc} / 2.

(e) When inverter output is connected to level 0 with switches $S_{a'1}$ through $S_{a'4}$ turned on, in this case, there are no clamping diodes involved. D_{a1}, D_{a3}, D_{a5}, D_{a7}, D_{a9} and D_{a11} will all block zero voltage in order to clamp switches S_{a1} through S_{a4} to nominal voltage. Then D_{a2}, D_{a4}, and D_{a8}, must block the nominal voltage as their cathode terminals are at level $3V_{dc}$ / 4 and anode terminals are at level V_{dc} / 2. D_{a6} and D_{a10} must block the nominal voltage as their cathode terminals are at level V_{dc} / 2 and anode terminals are at level V_{dc} / 4. D_{a12} must block the nominal voltage as its cathode terminal is at level V_{dc} / 4 and anode terminals are at level 0.

Notice that, for the new diode clamping inverter, not only are the switches clamped, so are the clamping diodes

2.2.1.7 Chapter Summary

The multilevel inverters can immediately replace the existing systems that use traditional multipulse converters without the need for transformers. All three multilevel inverter topologies can be applied to reactive power applications (e.g., static var generator) without the capacitor voltage balancing problems since they do not draw real power.

Both the flying capacitor and cascaded topologies are able to control real power flow utilizing their switching redundancy. But either an excessive number of storage capacitors or dc sources is required when number of inverter level is high, thus, they are more difficult to package and more expensive too with the required bulky components. The problem of voltage balancing for diode clamped multilevel inverters can be solved by several approaches, such as PWM regulators (back-to-back) or batteries.

The new diode clamped inverter solves the problems associated with series connected diodes of the conventional diode clamped inverter. In this new topology, not only are the power switches clamped by the clamping diodes, the clamping diodes are also clamped mutually by other clamping diodes. The need for large RC networks dealing with voltage sharing problem among series diode is removed.

Since the new diode clamped inverter topology has many advantages to offer. It is chosen to verify the theoretical predictions in this research.

CHAPTER THREE

LITERATURE STUDY ON RANDOM PULSE WIDTH MODULATION TECHNIQUES

3.1 Principle of Standard PWM

The task of power electronics is to control the power flow by shaping the input voltage waveform by means of power semiconductor devices and power reactors. One of the most important goals in controlling a voltage source inverter (VSI) with variable amplitude and frequency of the output voltage is to obtain an output waveform as close to the ideal sinusoidal waveform as possible employing simple techniques. The most common schemes are the triangular carrier PWM scheme and space vector PWM scheme.

3.1.1 Triangular Carrier PWM Scheme

In order to produce a sinusoidal output voltage waveform at a desired frequency, a reference control signal at the desired frequency is compared with carrier waveform (usually a triangular waveform), as shown in Fig. 3.1. The frequency of the triangular waveform establishes the inverter switching frequency and is generally kept constant along with its amplitude $\hat{V}_{tri}$. The triangular waveform $v_{tri}(t)$ in Fig. 3.1 is at a switching frequency f_s, which establishes the frequency with which the inverter switches are switched (f_s is also called the carrier frequency). The control signal $v_{control}$ (t) is used to modulate the switching duty ratio and has a frequency f_r, which is the desired fundamental frequency of the inverter voltage output (f_r is also called the modulating frequency). The amplitude modulation ratio m_a is defined as [11]

$$m_a = \frac{\hat{V}_{control}}{\hat{V}_{tri}}, \tag{3.1}$$

where $\hat{V}_{control}$ is the peak amplitude of the control signal. The amplitude $\hat{V}_{tri}$ of the triangular signal is generally kept constant.

In the inverter of Fig. 2.1, the switches S_a and $S_{a'}$ are controlled based on the comparison of $v_{control}(t)$ and $v_{tri}(t)$, and the following output voltage results, independent of the direction of i_o:

$$v_{control}(t) > v_{tri}(t), \qquad S_a \text{ is on}, \qquad v_{ao} = \frac{1}{2}V_{dc}$$

or

$$v_{control}(t) < v_{tri}(t), \qquad S_{a'} \text{ is on}, \qquad v_{ao} = -\frac{1}{2}V_{dc}.$$

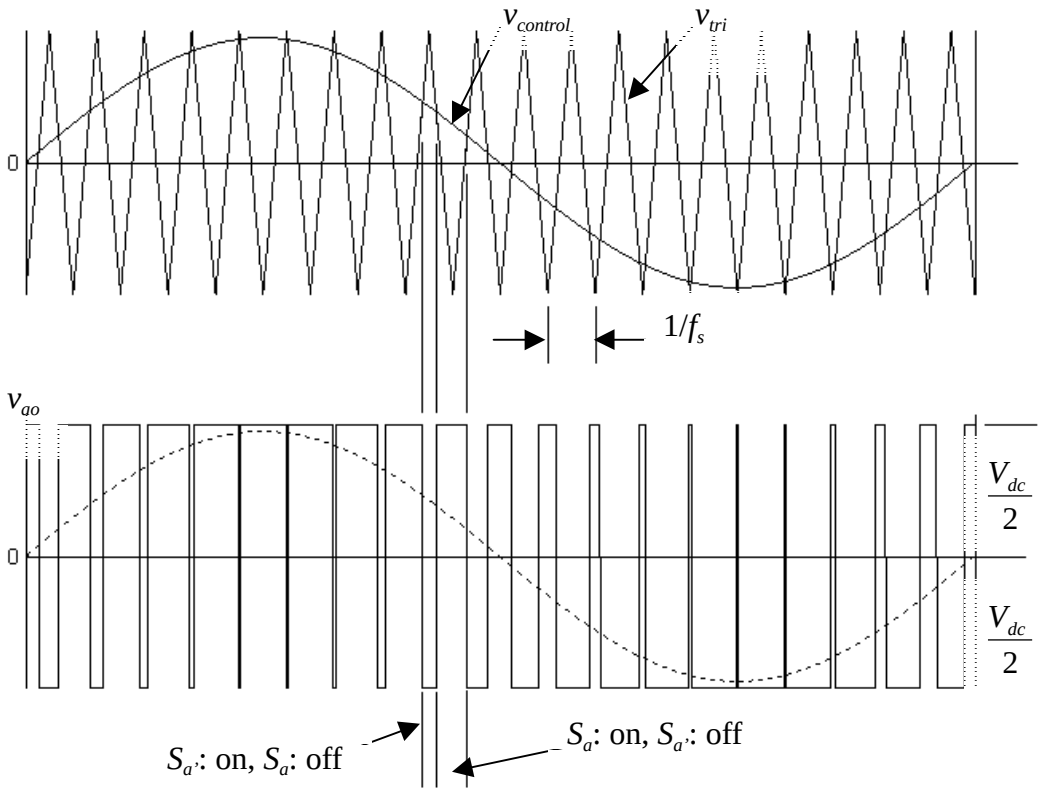

Fig. 3.1: Pulse width modulation.

3.1.2 Space Vector PWM

Fig. 3.2 (a) shows the schematic diagram of a three phase inverter. The three switching states (P, O, N) are summarized in table 3.1 for the three phases A, B and C. The space vector method operates in a complex plane divided into six 60° wide sectors separated by the switching state vectors [12,32]. The six 60° wide sectors correspond to 60° long subcycles of the cycle of the output voltage of the inverter. Each sector can be divided into a constant integer number of N_s intervals by a constant T_s switching period. The switching state vectors are defined by a combination of conducting/non conducting switches in the power circuit of the inverter [Fig. 3.2 (a)]. In order to generate desired output waveform, the rotating complex reference vector $\boldsymbol{V}_r$ with angular frequency ω_r is used to locate two adjacent switching state vectors (e.g., $\boldsymbol{V}_1$ and $\boldsymbol{V}_2$ in the first sector, see Fig. 3.3 (a)) and to compute the time (T_1 and T_2, respectively) for which each one is active, where $\omega_r = 2\pi f_r$ and α is the central angle of the switching interval in the $\omega_r t$ domain. For the remaining sampling time $T_0 + T_7 = T_s - T_1 - T_2$, zero state vectors $\boldsymbol{V}_0$ or $\boldsymbol{V}_7$ (connecting the entire three phase output terminal to positive or negative rail of the dc bus) are active. Fig. 3.3 (b) illustrates the sequence and timing of application of zero vectors ($\boldsymbol{V}_0$ and $\boldsymbol{V}_7$) and active vectors ($\boldsymbol{V}_1$ and $\boldsymbol{V}_2$) in the first sector and the time interval expressions associated with each state are given by [12]

$$T_X = \frac{3}{2}|V_r|T_s\left(\cos(\alpha) - \frac{1}{\sqrt{3}}\sin(\alpha)\right), \tag{3.2}$$

$$T_Y = \sqrt{3}|V_r|T_s\sin(\alpha) \tag{3.3}$$

and

$$T_0 + T_7 = T_s - (T_X + T_Y). \tag{3.4}$$

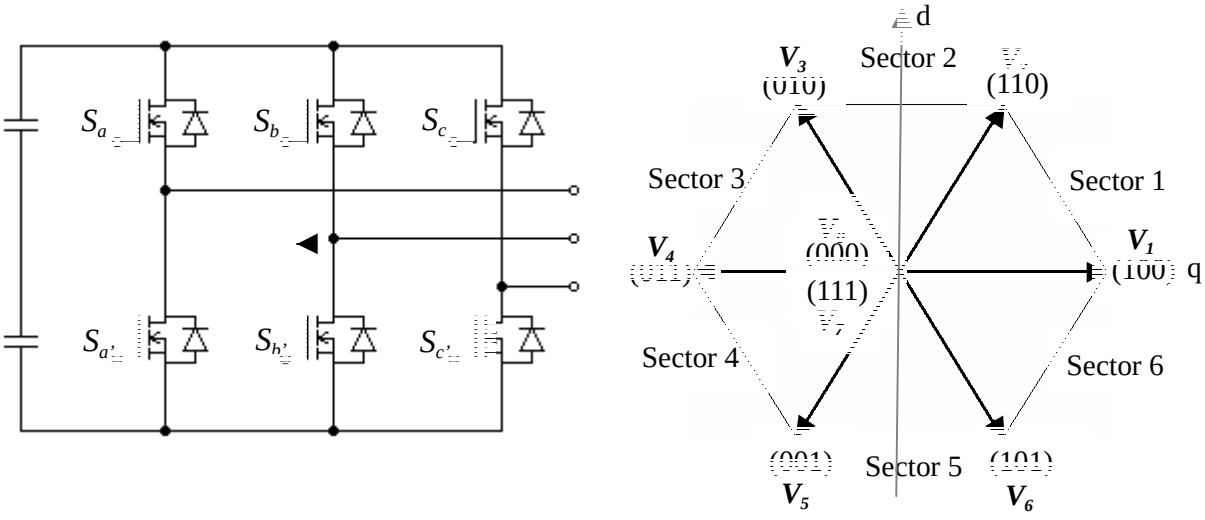

(a) **(b)**

Fig. 3.2: (a) Three phase inverter with switches S_a, $S_{a'}$, S_b, $S_{b'}$, S_c and $S_{c'}$. (b) The definition of switching state vectors in the complex *dq* plane [12, 32].

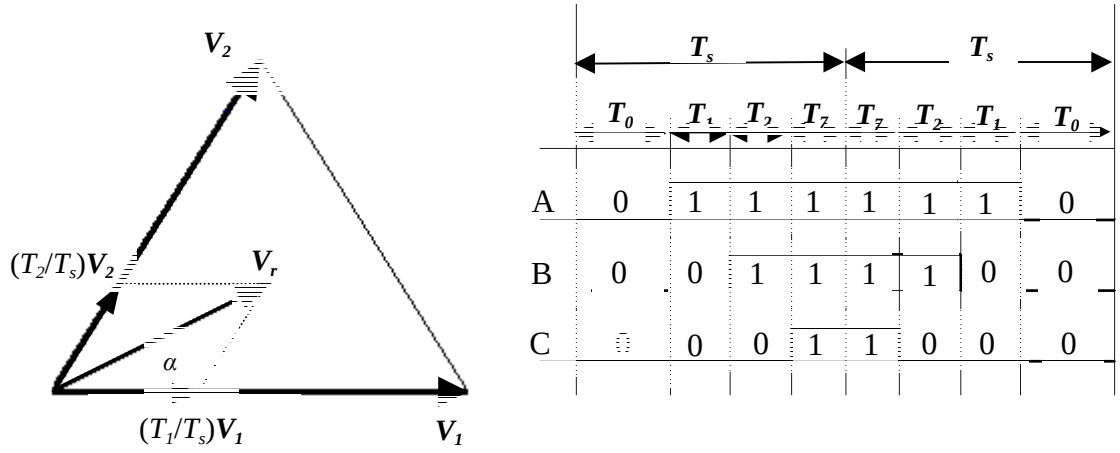

(a) **(b)**

Fig. 3.3: (a) Illustration of the voltage space vector PWM techniques in sector 1 [12]. (b) Illustration of timing and sequence of the voltage space vector PWM techniques in sector 1 [32].

TABLE 3.1

Summary of the Switching States of Three Phase Two level Inverter.

Three phase switches combination (A B C)	Switch state					
	S_a	$S_{a'}$	S_b	$S_{b'}$	S_c	$S_{c'}$
000	OFF	ON	OFF	ON	OFF	ON
100	ON	OFF	OFF	ON	OFF	ON
110	ON	OFF	ON	OFF	OFF	ON
010	OFF	ON	OFF	ON	OFF	ON
011	OFF	ON	ON	OFF	ON	OFF
001	OFF	ON	OFF	ON	ON	OFF
101	ON	OFF	OFF	ON	ON	OFF
111	ON	OFF	ON	OFF	ON	OFF

3.2 RPWM

Many PWM schemes have been developed and implemented successfully for different applications. However, the harmonic power is usually concentrated in the high-frequency range due to the high-frequency switching of the power inverter. These high-frequency harmonics can have adverse effects, such as acoustic noise, harmonic heating in electric machines, and radio interference [33-37].

Voltage control in pulse width modulated static power converters is performed by means of enforcing appropriate duty ratio of the converter switches. The duty ratio, which is the ratio of the on-time of the switch to the length of the switching (sampling) interval, does not depend on the location of the on interval within the switching interval, for example, the pulse position, or on the length of the switching interval (i.e., the switching frequency). In general, if either the pulse position or the switching frequency is varied in a random manner, the power spectrum of the output voltage of the converter acquires a continuous part, while the discrete (harmonics) part is significantly reduced. This is the basic principle of the random pulse modulation (RPWM), which has recently attracted the increasing interest of researchers [38].

The fundamental difference between classic PWM and RPWM methods is that the power carried by the PWM signal is no longer restricted to a few dominating frequencies that are normally determine by the switching frequency and the modulated signal. The total power is conserved, but the spread of power results in two major advantages due to the RPWM operation. The discrete harmonics are significantly reduced and the harmonic power is spread over the spectrum as continuous spectrum. Due to the reduction of discrete harmonics, the dc/ac randomized switching methods have been shown to have obvious advantage of acoustic reduction and mechanical vibration reduction in electronic drive systems. And conducted electromagnetic interference requirements may be met with reduced size of the filter components compared to standard PWM [33-37].

An ideal RPWM technique would result in power spectra of the inverter voltage containing a fixed harmonic (the fundamental) and a continuous noise spectral density, totally free of higher harmonics, over the entire frequency range. In practice such an ideal spectrum is not possible because of the technical limitations imposed on the feasible switching patterns [34,39].

According to the literature survey that was carried out, the RPWM techniques can be, generally, divided into two classes, which are 1) techniques with random variation of PWM parameters (PWM parameter varying modulation) and 2) techniques with direct modulation of random variables (direct random modulation) [38].

3.2.1PWM Parameter Varying Modulation

Common for this class is to randomize parameter of deterministic PWM technique in order to utilize the advantages of such a technique in its modified, random version. The known means of randomization usually involves the classic triangular carrier modulation) [40-41] and space vector modulation methods [33,34,39,42-47]. The following basic concepts are utilized in the existing RPWM strategies.

3.2.1.1 Randomization of Triangular Carrier Modulation

A simple concept diagram of an analogue randomly modulated carrier PWM is illustrated in Fig. 3.4.

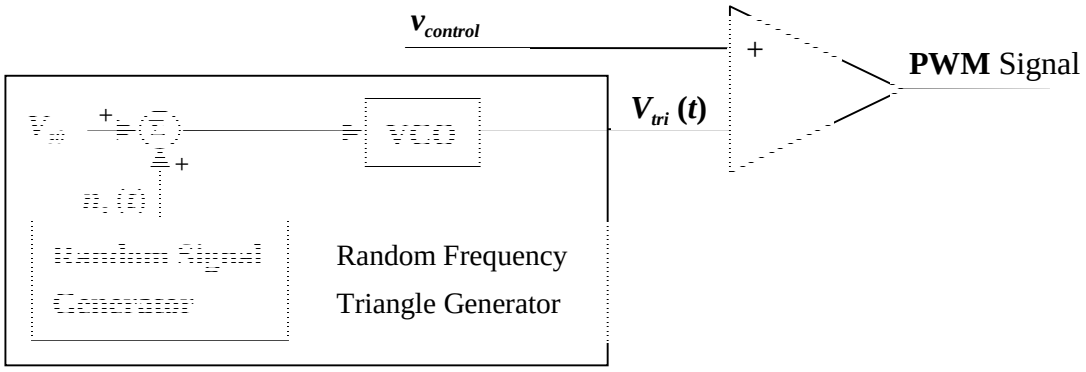

Fig. 3.4: Block diagram illustrating the concept of analogue random modulated carrier PWM [41].

In the random frequency triangular generator as shown in Fig. 3.4, an average control voltage V_{s0} is augmented with a zero mean random signal n_s (t). The resultant total control voltage v_s (t) is then used as the input of the voltage controlled oscillator (VCO) to yield the triangular wave

v_{tri} (t) with randomly varied frequency over a specific range as shown in Fig. 3.5. The reference sinusoidal signal $v_{control}$ is then compared to v_{tri} (t) to generate the PWM switching signals.

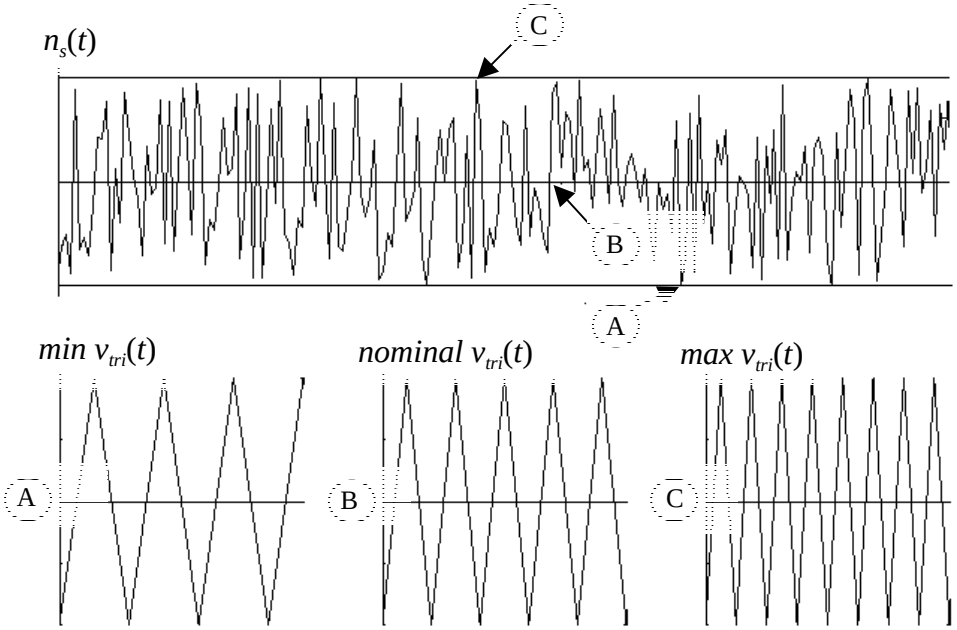

Fig. 3.5: Frequency of triangle wave $v_{tri}(t)$ randomly modulated by random signal $n_s(t)$.

3.2.1.2 Randomization of Space Vector Modulation Parameter

Here, various space vector based RPWM schemes are further classified into random switching frequency RPWM [42,43,47] and fixed switching frequency RPWM [44-46].

3.2.1.2.1 Random Switching Frequency PWM

This modified space vector PWM has been, thus far, the most common means of RPWM. It can be performed in either the regular or natural sampling mode. The regular sampling mode is characterized by an integer number N of the switching intervals per cycle of the output frequency. As an alternative, an integer number N_s of switching intervals is used for each 60° subcycle, an approach typical for space vector PWM techniques. Either N or N_s can be randomly changed from cycle to cycle or from subcycle to subcycle, respectively. The calculation of the switching time of a success pulse is unchanged but T_s is now either taken from a look-up table stored in memory or generated separately using a pseudorandom number

generator [42-44,47].

In the case of the natural sampling mode, it randomizes the consecutive increments of the angular position of the reference voltage vector [37].

3.2.1.2.2 Fixed Switching Frequency RPWM

Three methods of fixed switching frequency RPWM are discussed here. Those are random lead-lag modulation, random displacement of the pulse center and random distribution of the zero voltage vector. Those methods either utilize the position of PWM pulses or the second degree freedom of zero state vector time T_0 and T_7. It is known, that, in three phase system the duration of the zero voltage vector does not alter the phase voltages. This fact when utilized in the random distribution of the zero voltage vector, result in randomizing the switching frequency [42-44,47]. All of them have the common property that the switching frequency is constant. Fig. 3.6 shows the three phase switching functions F_a, F_b and F_c of the three methods, and T_s is the switching period.

3.2.1.2.2.1 Random Lead-Lag Modulation

The random lead-lag modulation is also called random pulse position modulation [33,46]. It constitutes a simple but effective RPWM strategy. The cycle of the reference frequency f_r of the inverter is divided into N equal switching intervals of width T_s. As illustrated in Fig. 3.6 (a), pulse of the switching intervals, F_a, F_b and F_c either start at the beginning of the switching interval (lead mode) or cease at the end of the interval (lag mode). The mathematical expressions for the lead/lag mode switching patterns at *k*th switching interval are given below [46]:

$$F(k)=\begin{cases}1 & \text{for } \left(t_k-\dfrac{T_s}{2}\le t\le t_k-\dfrac{T_s}{2}+\delta(k)\right)\\ 0 & \text{otherwise}\end{cases} \qquad \text{lead mode} \qquad (3.5)$$

or

$$F(k)=\begin{cases}1 & \text{for } \left(t_k+\dfrac{T_s}{2}\le t\le t_k+\dfrac{T_s}{2}-\delta(k)\right)\\ 0 & \text{otherwise}\end{cases} \qquad \text{lag mode.} \qquad (3.6)$$

The pulse position is controlled by a random number *R*. If the random *R* is 0, the pulse

position is changed to lead mode, whereas the random *R* is 1, the pulse position is changed to lag mode.

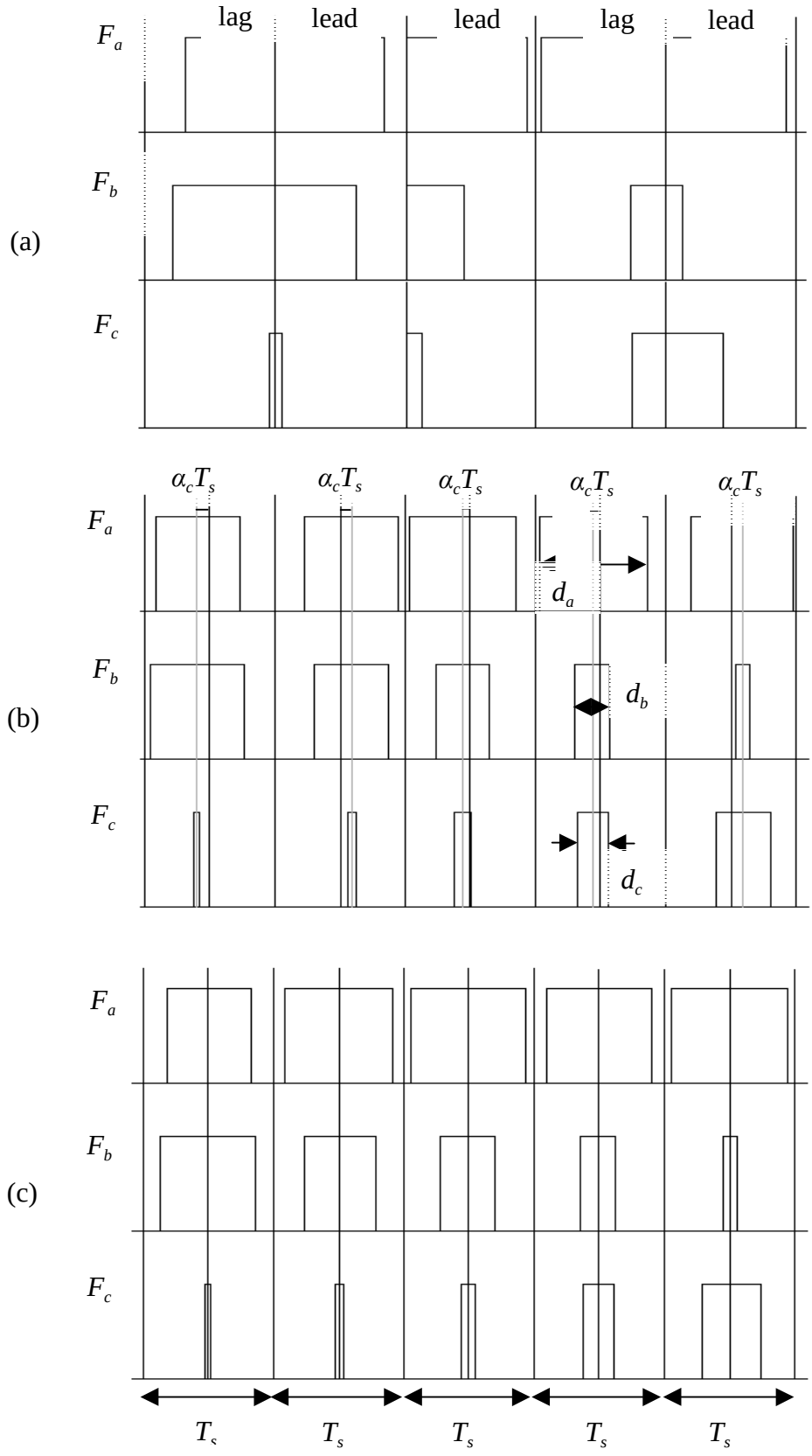

Fig. 3.6: Different fixed switching frequency modulation schemes. (a) Random pulse position

modulation. (b) Random center displacement. (c) Random zero vector distribution [45].

3.2.1.2.2.2 Random Displacement of the Pulse Center

Fig. 3.6 (b) shows the method where the pulses for each phase are mutually center-aligned as in standard space vector modulation, but the common pulse center is displaced by amount $\alpha_c T_s$ from the middle of the period. The parameter α_c is varied randomly within a band limited by the maximum duty cycle.

Fig. 3.7 shows how the modulation strategy can be implemented. The reference for the modulator is the reference voltage vector defined by its magnitude U and its position θ. This is used in a standard voltage space vector modulator. The output is three duty ratios d_a, d_b and d_c for each phase. The one with largest duty ratio is then used to calculate the maximum possible displacement α_{max} [45].

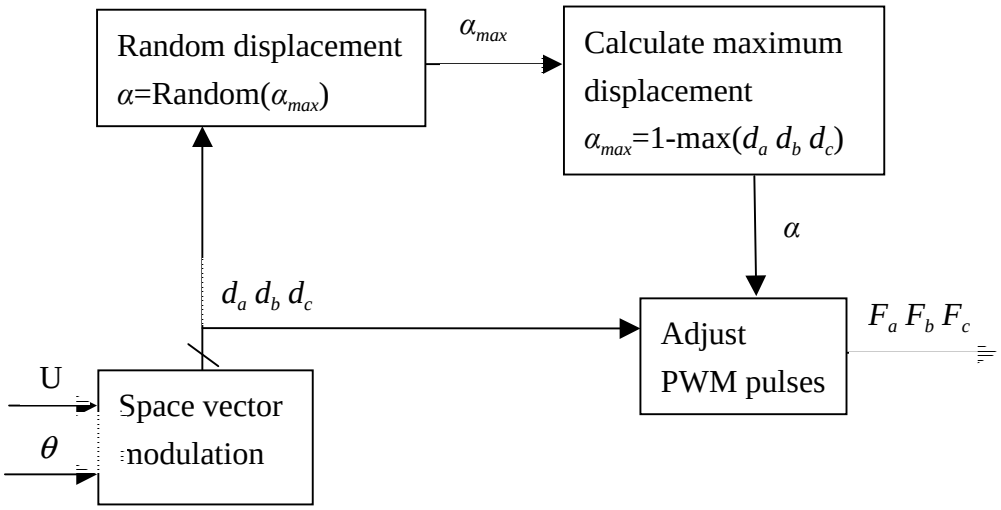

Fig. 3.7: Block diagram of implementation of random modulation with center displacement [45].

3.2.1.2.2.3 Random Distribution of the Zero Voltage Vector

This method, similar to the random switching frequency technique in natural sampling mode utilizes the second degree of freedom of zero state vector time T_0 and T_7. In order to keep the switching frequency constant, instead of randomly varying the total duration time of the two zero state vector ($T_0 + T_7$), this method keeps the total duration time constant, where the

proportion between the time duration for the two zero state vector is randomized in a switching interval (see Fig. 3.6 (c)) [44].

Fig. 3.8 illustrates the sequence and timing of application of zero state vectors ($\boldsymbol{V_0}$ and $\boldsymbol{V_7}$) and active vectors ($\bar{V}_1$ and $\bar{V}_2$) in the first sector. Note that vectors $\bar{V}_0$ and $\bar{V}_7$ are applied for time k_0T_0 and (1- k_0) T_0, respectively, where k_0 randomly varies within the range between 0 and 1. In the standard space vector PWM scheme, zero vectors $\bar{V}_0$ and $\bar{V}_7$ are applied for the same time interval T_0 / 2 (i.e., k_0 = 0.5). Duration T_a , T_b and T_c of switching pulse for switches S_a, S_b and S_c in Fig. 3.2 (a) are [44]

$$T_a = k_0(T_0 + T_7) + T_2 + T_1, \tag{3.7}$$

$$T_b = k_0(T_0 + T_7) + T_2 \tag{3.8}$$

and

$$T_c = k_0(T_0 + T_7). \tag{3.9}$$

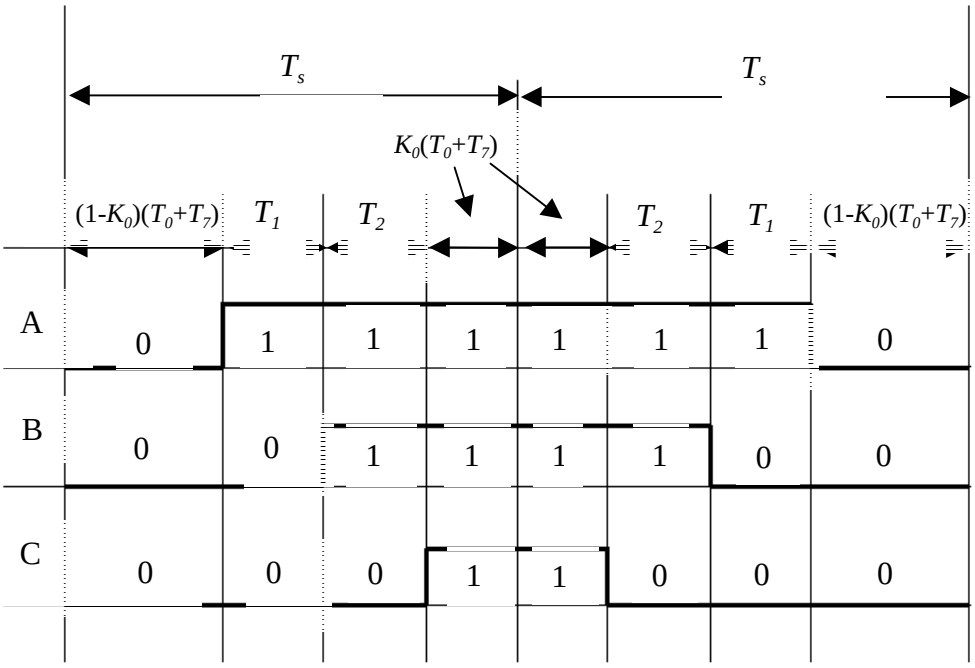

Fig. 3.8: Timing of space vector sequence in first sector [44].

3.2.2 Direct Random Modulation

The following two basic concepts are utilized in the existing direct random modulation strategies [3-5,10,48-50].

3.2.2.1 Random Switching

The random switching PWM technique is very simple; no precise timing of the switching signal is required. The basic principle of random switching is illustrated in Fig. 3.9. Randomly generated numbers, R_i, having uniform probability distribution, are compared with the desired duty ratio $v_{control}$ (reference signal) of the switching signal of the inverter [48-50].

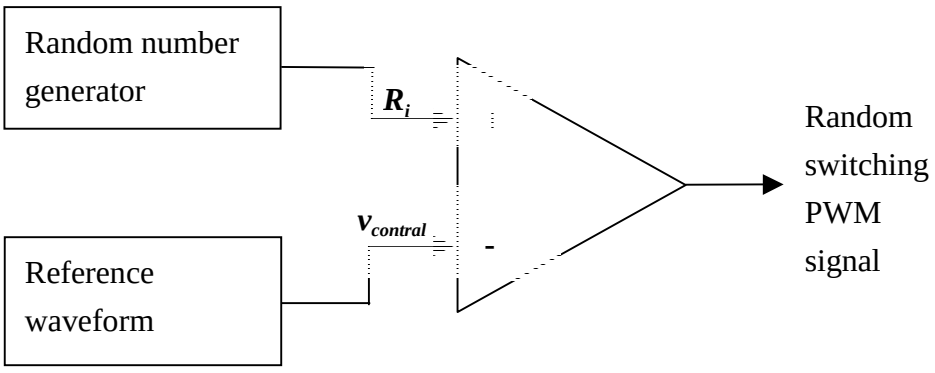

Fig. 3.9: Concept block diagram of random switching PWM [3].

The switching decisions are made according to the comparison as illustrated in Fig. 3.10. If, for instance, $R_i < v_{control}$ or $R_i > v_{control}$, then the switching signal a are set to 1 or 0, respectively. Inverter switching decision is made at sampling frequency f_{sp}, which affects the average switching frequency of the power inverter. The quality of the random switching PWM depends on the quality of the random number generator and f_{sp} [3].

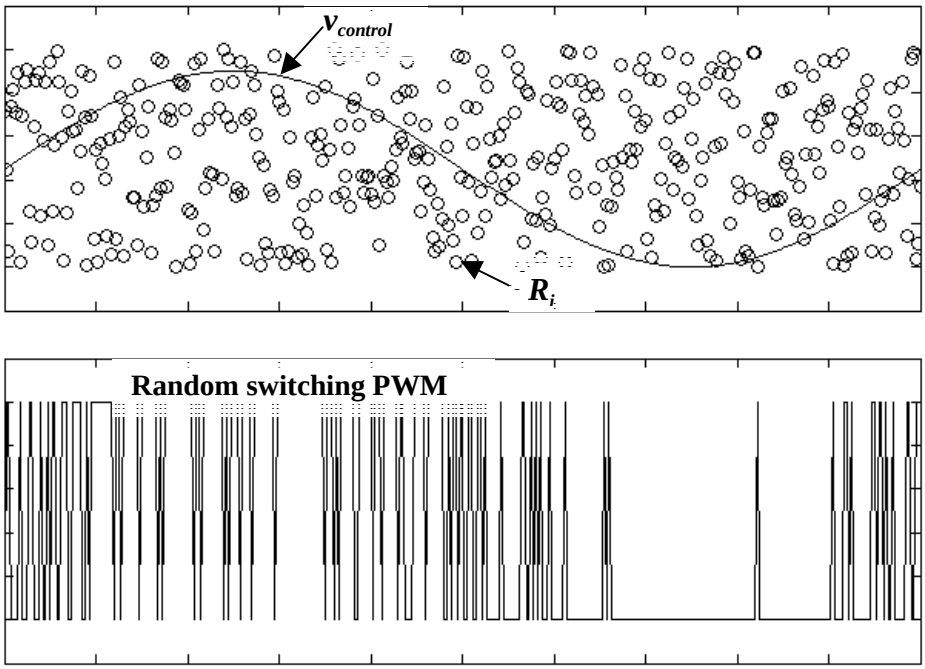

Fig. 3.10: Illustration of the random switching technique.

3.2.2.2 Random Switching with Weighted Switching Decision (WRPWM)

In standard random switching PWM, the output of the PWM depends on a single comparison of a random number and the instantaneous reference value in each sampling interval. In WRPWM scheme, it is suggested that *N* (where *N* is an odd integer) random numbers are generated and compared with the instantaneous reference signal in each sampling interval. The PWM output is determined from the majority or weighted switching decision of the *N* comparisons. Such majority or weighted decision process essentially introduces some deterministic nature into the PWM switching pattern because it increases the probability for the scheme to provide a more accurate switching decision in each sampling interval. When operating at low modulation index the probabilities of random number on both sides of the reference waveform become closer (approach 0.5), making it difficult for standard random switching PWM scheme to accurately provide a PWM waveform of good spectrum content. Therefore, standard random switching PWM is not effective when the magnitude of the reference waveform is close of or equal to the mid point of the number range. The weighted switching decision therefore provides better quality output waveform at low modulation index [3-5].

If the weighted decision process is applied to the entire fundamental period, the probability of having a rectangular voltage block in the central region of each half cycle (during the vicinity of time when the reference waveform has largest magnitude) is high because the weighted switching decision makes it more likely that the switching state is +1 or -1 in the positive or negative half cycle as shown in Fig. 3.11.

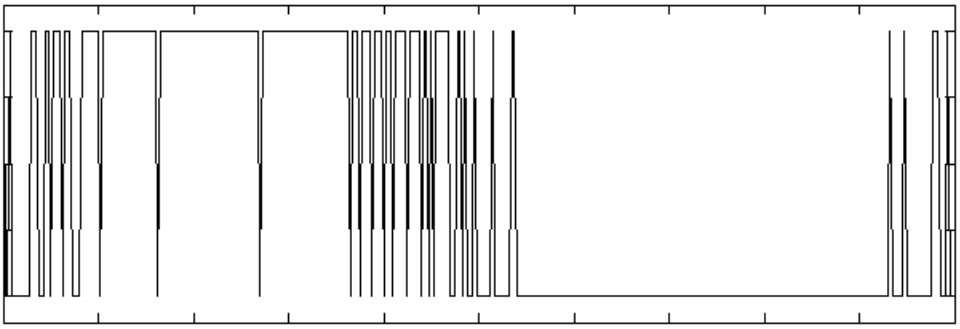

Fig. 3.11: WRPWM output waveform using five comparisons (N = 5) illustrate the third harmonic boosting effect.

The existence of the third harmonic may not be desirable in some applications, especially for the single phase applications. The WRPWM scheme can, however, be modified to eliminate the third harmonic. This can be achieved if the weighted switching decision process is applied in the region, where the reference waveform is in the vicinity of zero crossing point, which is within the band of ± 15% of the number range around the zero crossing level of the reference signal. That is, if the full ranges of reference signal for the random switching PWM implementation is from zero to one, the zero crossing level is then 0.5 and the weighted switching is applied within $0.5 \pm 0.15m_a$. Fig. 3.12 illustrates how the weighted switching process applied to enable the third harmonic boosting effect and the output waveform.

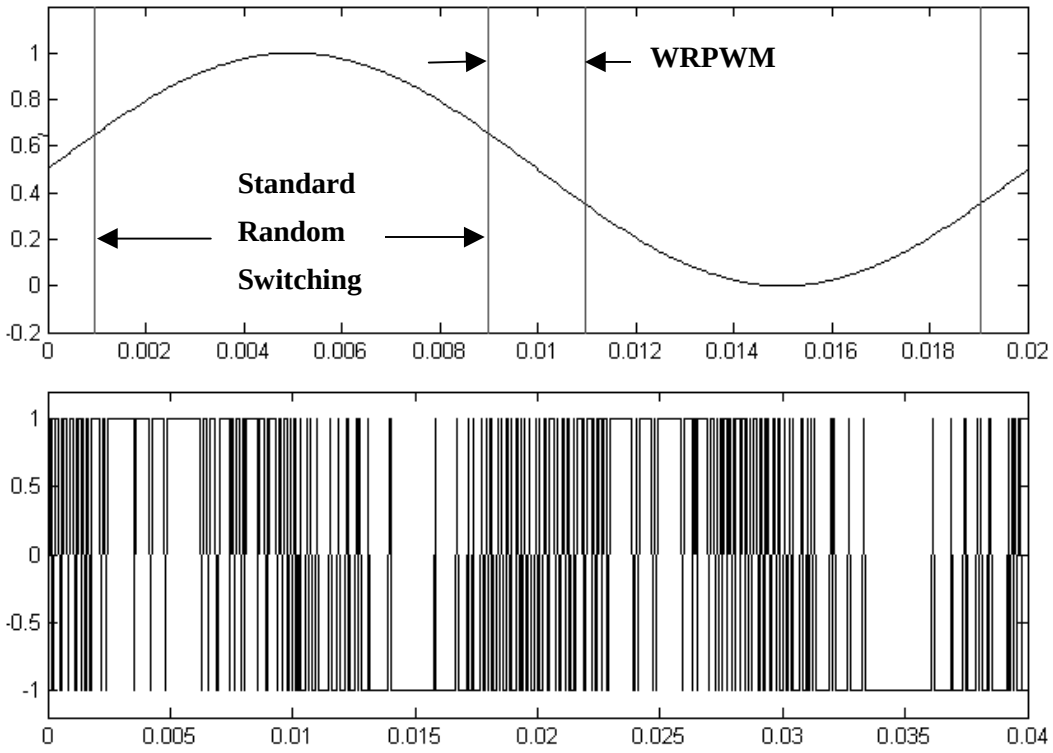

Fig. 3.12: WRPWM output waveform using five comparisons (N = 5) illustrate the elimination of third harmonic boosting effect.

3.2.3 Chapter Summary

In most of the researches, the classic space vector PWM strategy is used with randomly varied position of the switching pulses within consecutive switching intervals, or with a randomly varied number of switching intervals per cycle or subcycle of the output voltage. In both cases, certain harmonics still appear in the power spectrum, since the fixed or limited number of switching intervals per cycle introduces a deterministic factor to the spectrum. By using random switching PWM the closest approximation of the ideal spectrum can be obtained. However, the quality of the random switching PWM depends on the quality of the random number generator and f_{sp}. Moreover, when operating at low modulation index the probabilities of random number on both sides of the reference waveform become closer (approach 0.5), making it difficult for standard random switching PWM scheme to accurately provide a PWM waveform of good spectrum content. Therefore, standard random switching PWM is not effective when the magnitude of the reference waveform is close to or equal to the mid point of the number range. The weighted switching decision provides better quality output waveform at low modulation index and it is less dependent on the quality of the random number generator and f_{sp}.

3.3 Standard Carrier Based Multilevel PWM Method

In chapter 2, the operation principle of the three well known topologies of multilevel inverter were discussed. On the other hand, section 3.1 presented the basic operation principle of the standard PWM methods. To illustrate the performance of the standard multilevel PWM method so the reason of emerging RPWM can be understand, a brief discussion on the harmonic spectrum of a well known carrier based PWM method called multilevel subharmonic PWM (SH-PWM) [29] is presented. In this section an analytical expression of the spectral components of the output waveforms is presented.

3.3.1 Multilevel PWM Technique

As previously discussed, for conventional two-level inverter, the carrier based PWM is generated by comparing a reference waveform with a triangular carrier waveform to determine when the switching devices are to be turned on and off. If an N-level inverter is employed, N – 1 carriers will be needed. The carriers have the same frequency f_s and the same peak-to-peak amplitude V_{tri} and are disposed so that the bands they occupy are contiguous. The zero of the reference is placed in the middle of the carrier set [29]. The reference signal is a sinusoidal wave of frequency f_r and amplitude $V_{control}$. The amplitude modulation ratio m_a is defined as [51]

$$m_a = \frac{V_{control}}{\left(N' V_{tri}\right)}, \tag{3.10}$$

where $N' = (N - 1)/2$. At every instant each carrier is compared with the reference waveform. Each comparison gives +1/-1 if the reference signal is greater/lower than the triangular carrier in the positive/negative half of the fundamental period, 0 otherwise. The results are added to give a voltage level, which is required at the output terminal of the multilevel inverter.

Notice that, the phase displacement between two contiguous triangular carriers offers a degree of freedom. As shown in Figs. 3.13 (a), (b) and (c), using five-level inverters as an example, the three most commonly employed dispositions are [29]:

1) Alternative phase opposition disposition (APOD, see Fig. 3.13 (a)), where each

carrier is phase shifted by 180° from its adjacent carrier.

2) Phase opposition disposition (POD, see Fig. 3.13 (b)), where the carriers above the sinusoidal reference zero point are 180° out of phase with those below the zero point.

3) Phase disposition (PD, see Fig. 3.13 (c)), where all carriers are in phase.

Note that, for three-level inverter, the APOD and POD are identical.

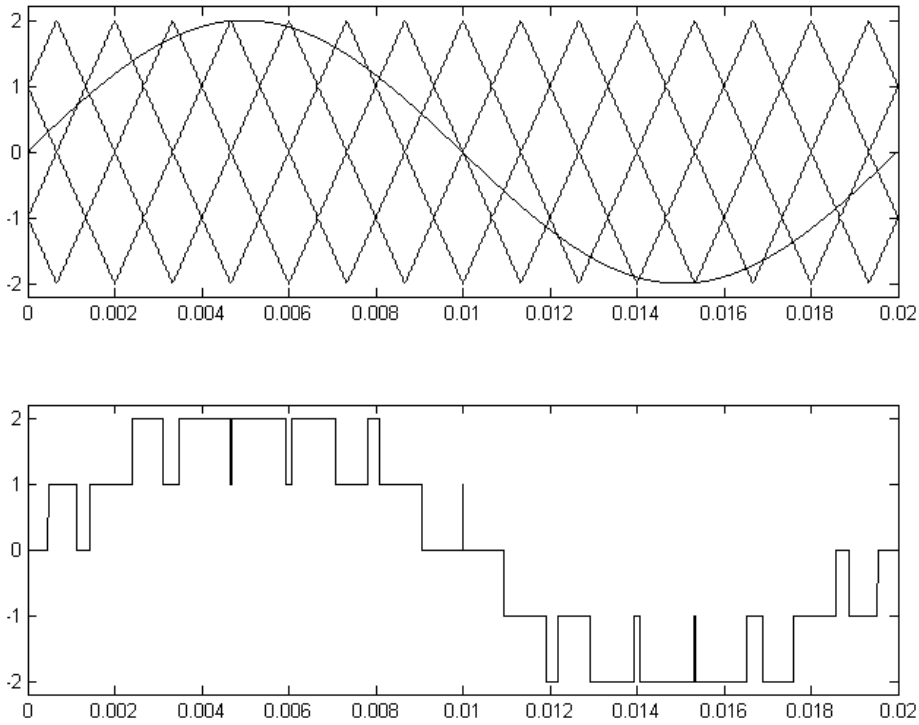

(a)

Fig. 3.13: Illustration of the three disposition techniques. (a) APOD.

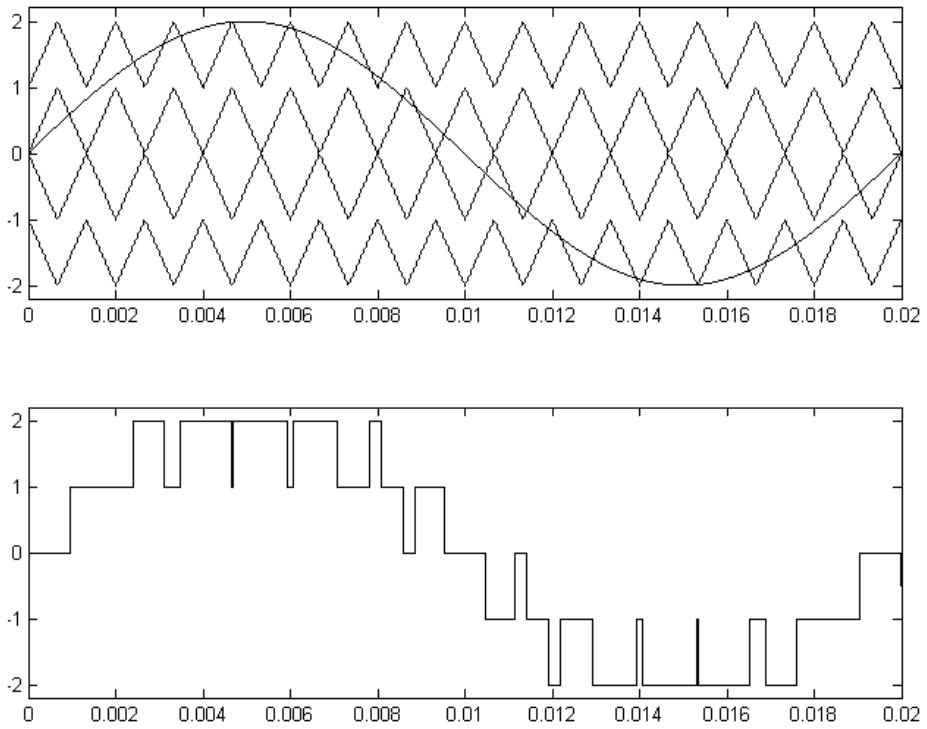

(b)

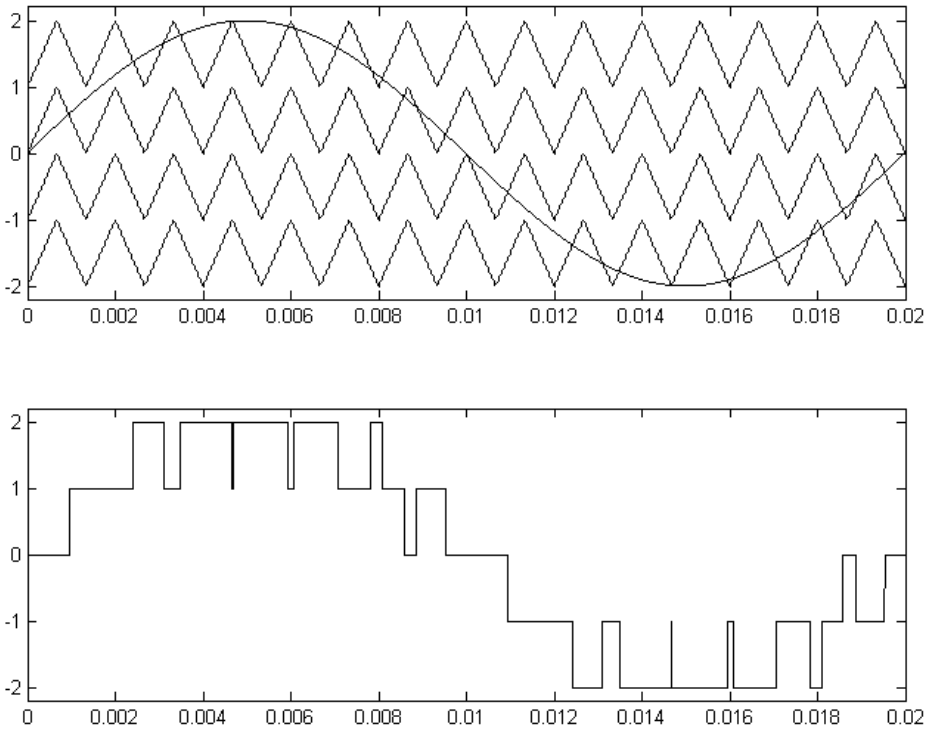

(c)

Fig. 3.13: Illustration of the three disposition techniques. (b) POD. (c) PD [29].

While these three techniques create quite different spectra, it is known from multilevel modulation theory that PD disposition strategy is superior for diode clamped inverters [51]. From [51], the general phase leg solution for multilevel PD PWM under linear modulation conditions

$$\begin{aligned} v_a(t) = {} & N' V_{dc} m_a \cos(\omega_r t) + \frac{8V_{dc}}{\pi^2} \sum_{m=1}^{\infty} \frac{1}{2m-1} \sum_{k=1}^{\infty} C_{m0} \cos([2m-1]\omega_s t) \\ & + \frac{2V_{dc}}{\pi^2} \sum_{m=1}^{\infty} \frac{1}{2m} \sum_{n=-\infty}^{\infty} C_{m_{even} n_{odd}} \cos(2m\omega_s t + [2n+1]\omega_r t) \\ & + \frac{4V_{dc}}{\pi^2} \sum_{m=1}^{\infty} \frac{1}{2m-1} \sum_{\substack{n=-\infty \\ (n\neq 0)}}^{\infty} \sum_{k=1}^{\infty} C_{m_{odd} n_{even}} \cos([2m-1]\omega_s t + 2n\omega_r t), \end{aligned} \tag{3.11}$$

where k, m and n are integers, ω_r is the angular frequency ($2\pi f_r$) of the reference signal and ω_c is the angular frequency ($2\pi f_s$) of the carrier wave. $N' V_{dc} m_a$ is the amplitude of the fundamental component. C_{m0} is the coefficient for the harmonics components for multiple of carrier frequency. $C_{mevennodd}$ is the coefficient of the harmonic components for sidebands about the even multiple carrier frequency and odd multiple fundamental frequency (i.e., reference frequency) and $C_{moddneven}$ is the coefficient of the harmonic components for sidebands about the odd multiple carrier frequency and even multiple fundamental frequency. To illustrate the performance of multilevel PD PWM technique the harmonic spectrum of five level PD PWM is plotted in Fig. 3.14, with m_a =1, f_r = 50 Hz and f_s = 2000 Hz. It can be seen that the spectrum consists of components at the fundamental frequency f_r, odd multiples of carrier frequency $(2m\text{-}1)f_s$, sidebands about the even multiple carrier frequency $2m\ f_s$, odd multiple fundamental frequency $(2m\text{-}1)f_r$, odd multiple carrier frequency $(2m\text{-}1)f_s$ and even multiple fundamental frequency $2m\ f_r$ [29].

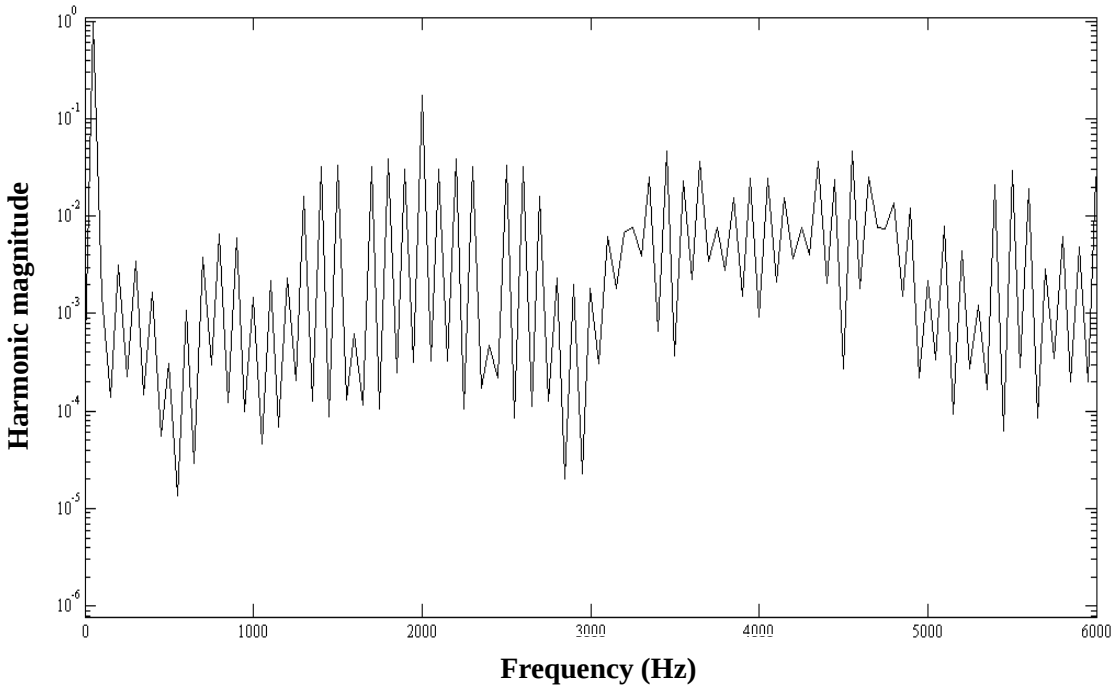

Fig.3.14: Five-level PD PWM phase leg voltage spectrum.

CHAPTER FOUR

THEORETICAL ANALYSIS OF FIVE-LEVEL INVERTER ADOPTING RANDOM SWITCHING PWM TECHNIQUE

This chapter deals with the derivation of equations which characterize the five-level WRPWM scheme. A statistical approach is used to derive equations which are used to analyze and characterize the performance of the five-level WRPWM scheme. Hence at the beginning of this chapter some basic mathematical background and theories are provided for the derivation of equations for WRPWM characterization. This is then followed by the actual derivation of characterization equations of the five-level WRPWM scheme.

4.1 Introduction of Random Process Analysis Method

A random signal may be thought of as a signal selected from an ensemble (family) of possible signals by a random experiment governed by some specification of probabilities. The ensemble and the specification of probabilities together comprise what is called the random process (or stochastic process) generating the random signal. The signal is therefore the realization of the process [16]. At the beginning of this chapter, some mathematical background and theories are provided for later analysis of random switching PWM and WRPWM waveform, which can be thought of as the realization of the random process.

4.1.1 The Binomial Probability Law

A Bernoulli trial involves performing an experiment once and noting whether a particular event occurs. The outcome of the Bernoulli trial is said to be a “success” if the event occurs and a “failure’ otherwise. The aim here is to find the probability of m successes in N independent repetitions of a Bernoulli trial. The outcome of a single Bernoulli trial can be viewed as the outcome of comparing a random number R in the range [0, 1] with uniform

probability distribution and a given number x in the range [0, 1]. The event (success) of this Bernoulli trial occurs if the random number R is smaller than or equal to the given number x. The probability of the event for R smaller than or equal to the given number x is $P_r[\{R \le x\}] = x$ [53].

Suppose that three uniformly distributed random numbers R_1, R_2 and R_3 are generated and compared with a given number chosen from the range [0, 1]. The probability for the sequences of success and failure is obtained as follows

$$
\begin{aligned}
&P_r[\{R_1 \le x, R_2 \le x, R_3 \le x\}] = P_r[\{R_1 \le x\}]\, P_r[\{R_2 \le x\}]\, P_r[\{R_3 \le x\}] = x^3,\\
&P_r[\{R_1 \le x, R_2 \le x, R_3 \ge x\}] = P_r[\{R_1 \le x\}]\, P_r[\{R_2 \le x\}]\, P_r[\{R_3 \ge x\}] = x^2(1-x),\\
&P_r[\{R_1 \le x, R_2 \ge x, R_3 \le x\}] = P_r[\{R_1 \le x\}]\, P_r[\{R_2 \ge x\}]\, P_r[\{R_3 \le x\}] = x^2(1-x),\\
&P_r[\{R_1 \ge x, R_2 \le x, R_3 \le x\}] = P_r[\{R_1 \ge x\}]\, P_r[\{R_2 \le x\}]\, P_r[\{R_3 \le x\}] = x^2(1-x),\\
&P_r[\{R_1 \ge x, R_2 \ge x, R_3 \le x\}] = P_r[\{R_1 \ge x\}]\, P_r[\{R_2 \ge x\}]\, P_r[\{R_3 \le x\}] = x^1(1-x)^2,\\
&P_r[\{R_1 \ge x, R_2 \le x, R_3 \ge x\}] = P_r[\{R_1 \ge x\}]\, P_r[\{R_2 \le x\}]\, P_r[\{R_3 \ge x\}] = x^1(1-x)^2,\\
&P_r[\{R_1 \le x, R_2 \ge x, R_3 \ge x\}] = P_r[\{R_1 \le x\}]\, P_r[\{R_2 \ge x\}]\, P_r[\{R_3 \ge x\}] = x^1(1-x)^2,\\
&P_r[\{R_1 \ge x, R_2 \ge x, R_3 \ge x\}] = P_r[\{R_1 \ge x\}]\, P_r[\{R_2 \ge x\}]\, P_r[\{R_3 \ge x\}] = (1-x)^3.
\end{aligned}
\tag{4.1}
$$

Let m be the number of successes in three trials, then from (4.1)

$$
\begin{aligned}
P_r[m = 0] &= P_r[\{R_1 \ge x, R_2 \ge x, R_3 \ge x\}] = (1-x)^3,\\
P_r[m = 1] &= P_r[\{R_1 \ge x, R_2 \ge x, R_3 \le x\}] + P_r[\{R_1 \ge x, R_2 \le x, R_3 \ge x\}]\\
&\quad + P_r[\{R_1 \le x, R_2 \ge x, R_3 \ge x\}]\\
&\quad = 3\, x^1(1-x)^2,\\
P_r[m = 2] &= P_r[\{R_1 \le x, R_2 \le x, R_3 \ge x\}] + P_r[\{R_1 \le x, R_2 \ge x, R_3 \le x\}]\\
&\quad + P_r[\{R_1 \ge x, R_2 \le x, R_3 \le x\}]\\
&\quad = 3\, x^2(1-x)
\end{aligned}
$$

and

$$P_r[m = 3] = P_r[\{R_1 \le x, R_2 \le x, R_3 \le x\}] = x^3.$$

The result is the $N = 3$ case of the binomial probability law. Therefore, let m be the number of successes in N independent Bernoulli trials, then the probabilities of m are given by the binomial probability law [52] as:

$$P_r(m) = \binom{N}{m} x^m (1-x)^{N-m} \qquad \text{for} \quad m = 0, \ldots, N, \tag{4.2}$$

where $P_r(m)$ is the probability of m successes in N trials, and

$$\binom{N}{m} = \frac{N!}{m!(N-m)!} \tag{4.3}$$

is the binomial coefficient. It means the number of different combinations of size m from a set of size N, where $m \leq N$. The term $N!$ in (4.3) is called N factorial and is defined by $N! = N(N-1)\ldots(2)(1)$. By definition 0! is equal to 1.

4.1.2 Random Process Analysis Method

For conventional deterministic PWM schemes, one usually analyzes the spectral properties of a signal by applying the Fourier transform to the signal. Power distribution density is then given by the square of the amplitude of the Fourier transform. However, for random schemes, such as the random switching PWM, the PWM signal is the result of a random process. The Fourier transform of a random signal is itself a random function (i.e., it is a random variable at each frequency) and does not yield any useful information about the signal power distribution. Autocorrelation function is an appropriate measure for the average rate of change of a random process. The Fourier transform of an autocorrelation function of a random signal gives the expected power spectral density of that random signal. The expected power spectral density gives the average power distribution of a random signal at different frequencies. Consequently, for random schemes it is more meaningful to study the expected power spectral density [36].

4.1.2.1 Autocorrelation and Power Spectrum

The (time-averaged) autocorrelation of a random process $k(t)$ is defined [4,16,36] as

$$R_k(\tau) = \lim_{W\to\infty} \frac{1}{2W} \int_{-W}^{W} E\{k(t)k(t+\tau)\}dt\,, \tag{4.4}$$

where the expectation operation $E\{\cdot\}$ is taken over the whole ensemble. This definition is slightly different from the one found in standard textbooks [36], where only the strictly stationary random processes are dealt with. For the strictly stationary random processes $E\{k(t)k(t+\tau)\}$ is independent of t and depends only on τ, thus, the time averaging in (4.4) is unnecessary. Therefore, this definition is a generalisation of the more usual definition where time averaging is performed. Also this definition reduces to the usual definition for

deterministic signals where the ensemble consists of just one number, and as a result $E\{\cdot\}$ is unnecessary. The RPWM signals which are dealt with in this report are considered as cyclostationary random signals. Consequently, the definition in (4.4) leads to meaningful results for them. It should be noted that $R_k\{\tau\}$ is symmetrical about the origin i.e. $R_k\{\tau\} = R_k\{-\tau\}$. The power spectral density $S_k\{f\}$ of *k(t)* is the Fourier Transform of $R_k\{\tau\}$ [15,16,36], i.e.,

$$S_k(f) = \int_{-\infty}^{\infty} e^{-j2\pi f\tau} R_k(\tau) d\tau \,. \tag{4.5}$$

$S_k(f)$ can have both continuous and an impulsive part [4,5]. The impulsive part of $S_k(f)$ is referred to as the discrete spectrum, and is characterized entirely by the locations $f_1, f_2, \ldots$ of the impulses and by positive numbers $c_1, c_2, \ldots$ representing the strengths of the impulses, which equal to the signal power at the harmonic frequencies. When integrated over a frequency range, the continuous part of $S_k(f)$ yields the signal power in that frequency range.

4.1.3 Classification of Randomized Switching Strategy

The main elements characterizing randomized modulation schemes are the underlying (deterministic) nominal switching patterns and the probability laws governing the random dithering of the nominal patterns. The other issue is the time variation of the probability densities used to pick the dithering from cycle to cycle. If the random switching function has a mean and autocorrelation that are independent of time origin (so the time averaging in (4.4) becomes unnecessary), it is then called wide-sense stationary [16]. The random switching function is called cyclostationary if both the mean and the autocorrelation function are periodic in t with some period T_0 [16]. In general, the direct random modulation RPWM techniques in section 3.2.2 are considered as cyclostationary processes.

4.2 Characterization of Five-Level Inverter Adopting Weighted Random Switching

PWM Technique

In this section the equations which characterize the five-level WRPWM scheme will be derived based on analysis similar to that carried out in [4] for three-level inverters.

4.2.1 Distribution Functions of Five-Level Random Switching PWM

During any one time interval [nT, (n+1)T] where n is an integer and T is the sampling period, the output of the five-level random switching inverter can be switched among 2A, A, 0, -A and –2A, where 2A and –2A is the rail dc-bus voltage (+V_d/2 and -V_d/2) referenced to the center tap point o of the dc voltage source. The presence of a 2A, A, 0, -A and –2A at output terminals of the five-level inverter, at any one time interval [nT, (n+1) T] is determined by the following process.

- Generate random numbers $R_1,\ldots, R_N$ (where N is an integer) with a uniform distribution in the range [0, 1].
- Compare the random number with a sampled reference signal $r(t)$, which is a sinusoidal waveform. Let c be the number of times that these random numbers are smaller than or equal to $r(t)$. The sinusoidal reference $r(t)=0.5[1+m_a \sin(2\pi f_r t)]$, where m_a is the modulation index, f_r is the frequency of the sinusoidal waveform, and t is the time variable.
- For five-level inverter topology, the number of comparisons in one sampling period has to be at least five (i.e., $N \geq 5$). That is in order for the system to have enough comparisons to make a decision which level of dc-bus should the switches connect to. The WRPWM signal $k(t)$ is defined as

$$k(t)=\begin{cases} 2A, & \text{if } \left\lceil \frac{N}{2} \right\rceil + q \leq c \leq N, \\ A, & \text{if } \left\lceil \frac{N}{2} \right\rceil + 1 \leq c \leq \left\lceil \frac{N}{2} \right\rceil + q - 1, \\ 0, & \text{otherwise} \left(i.e. \left\lfloor \frac{N}{2} \right\rfloor \leq c \leq \left\lceil \frac{N}{2} \right\rceil \right), \\ -A, & \text{if } \left\lfloor \frac{N}{2} \right\rfloor - q + 1 \leq c \leq \left\lfloor \frac{N}{2} \right\rfloor - 1, \\ -2A, & \text{if } \quad 0 \leq c \leq \left\lfloor \frac{N}{2} \right\rfloor - q, \end{cases} \tag{4.6}$$

where q is an integer and $2 \leq q \leq \lfloor N/2 \rfloor$. The symbol $\lfloor \cdot \rfloor$ refers to round towards -∞ and $\lceil \cdot \rceil$

refers to round towards +∞. From (4.6) it can be seen that q is one of the parameters needed by the inverter to make a decision which level of dc-bus should the switches connect to. The effects of q will be discussed in a short while. Note that for $q \geq \lfloor N/2 \rfloor + 1$, $k(t) = 0$, that is PWM output is zero.

Five probability distribution functions are of interest for a five-level inverter. They are

$$\begin{aligned} F_{N,q}^{(1)}(x) &= P_r\{k(t) = 2A \mid r(nT) = x\}, \\ F_{N,q}^{(2)}(x) &= P_r\{k(t) = A \mid r(nT) = x\}, \\ F_{N,q}^{(3)}(x) &= P_r\{k(t) = 0 \mid r(nT) = x\}, \\ F_{N,q}^{(4)}(x) &= P_r\{k(t) = -A \mid r(nT) = x\}, \\ F_{N,q}^{(5)}(x) &= P_r\{k(t) = -2A \mid r(nT) = x\}, \end{aligned} \tag{4.7}$$

where the bracketed superscripts correspond to the $k(t)$ of $2A$, A, 0, $-A$ and $-2A$, respectively, and $r(nT)$ is the sampled value of the reference signal. The probabilities $P_r\{k(t) \mid r(nT)\}$ are obtained from (4.2) and (4.6) as

$$\begin{aligned} &P_r\{k(t) = 2A \mid r(nT) = x\} = P_r[m = \lceil N/2 \rceil + q] + P_r[m = \lceil N/2 \rceil + q + 1] + \ldots + P_r[m = N], \\ &P_r\{k(t) = A \mid r(nT) = x\} = P_r[m = \lceil N/2 \rceil + 1] + P_r[m = \lceil N/2 \rceil + 2] + \ldots + P_r[m = \lceil N/2 \rceil + q - 1], \\ &P_r\{k(t) = 0 \mid r(nT) = x\} = P_r[m = \lfloor N/2 \rfloor] + P_r[m = \lfloor N/2 \rfloor + 1] + P_r[m = \lfloor N/2 \rfloor + 2] + \ldots + P_r[m = \lceil N/2 \rceil], \\ &P_r\{k(t) = -A \mid r(nT) = x\} = P_r[m = \lfloor N/2 \rfloor - q + 1] + P_r[m = \lfloor N/2 \rfloor - q] + \ldots + P_r[m = \lfloor N/2 \rfloor - 1] \end{aligned}$$

and

$$P_r\{k(t) = -2A \mid r(nT) = x\} = P_r[m = 0] + P_r[m = 1] + \ldots + P_r[m = \lfloor N/2 \rfloor - q]. \tag{4.8}$$

It can be seen from (4.8) that it is necessary to include a summation term in (4.2). Therefore, each of the five probability distribution functions for the five-level scheme is a cumulative distribution functions [16, 52] of the probabilities of m successes in N independent Bernoulli trials of the five-level scheme and are formulated as

$$F_{N,q}^{(1)}(x) = \begin{cases} 1 & \text{for } x > 1 \\ \displaystyle\sum_{m=\left\lceil \frac{N}{2} \right\rceil + q}^{N} \binom{N}{m} x^m (1-x)^{N-m} & \text{for } 0 \leq x \leq 1 \\ 0 & \text{for } x < 0 \end{cases} \tag{4.9}$$

$$F_{N,q}^{(2)}(x)=\begin{cases}0 & \text{for } x>1\\ \displaystyle\sum_{m=\left\lceil\frac{N}{2}\right\rceil+1}^{\left\lceil\frac{N}{2}\right\rceil+q-1}\binom{N}{m}x^m(1-x)^{N-m} & \text{for } 0\le x\le 1\\ 0 & \text{for } x<0\end{cases} \tag{4.10}$$

$$F_{N,q}^{(3)}(x)=\begin{cases}0 & \text{for } x>1\\ \displaystyle\sum_{m=\left\lfloor\frac{N}{2}\right\rfloor}^{\left\lceil\frac{N}{2}\right\rceil}\binom{N}{m}x^m(1-x)^{N-m} & \text{for } 0\le x\le 1\\ 0 & \text{for } x<0\end{cases} \tag{4.11}$$

$$F_{N,q}^{(4)}(x)=\begin{cases}0 & \text{for } x>1\\ \displaystyle\sum_{m=\left\lfloor\frac{N}{2}\right\rfloor-q+1}^{\left\lfloor\frac{N}{2}\right\rfloor-1}\binom{N}{m}x^m(1-x)^{N-m} & \text{for } 0\le x\le 1\\ 0 & \text{for } x<0\end{cases} \tag{4.12}$$

$$F_{N,q}^{(5)}(x)=\begin{cases}0 & \text{for } x>1\\ \displaystyle\sum_{m=0}^{\left\lfloor\frac{N}{2}\right\rfloor-q}\binom{N}{m}x^m(1-x)^{N-m} & \text{for } 0\le x\le 1\\ 1 & \text{for } x<0\end{cases} \tag{4.13}$$

Obviously

$$F_{N,q}^{(1)}(x)+F_{N,q}^{(2)}(x)+F_{N,q}^{(3)}(x)+F_{N,q}^{(4)}(x)+F_{N,q}^{(5)}(x)=1.$$

A typical plot of the five distribution functions (expected value of five-level WRPWM signal) for N = 5, q = 2 and m_a = 1 is shown in Fig. 4.1.

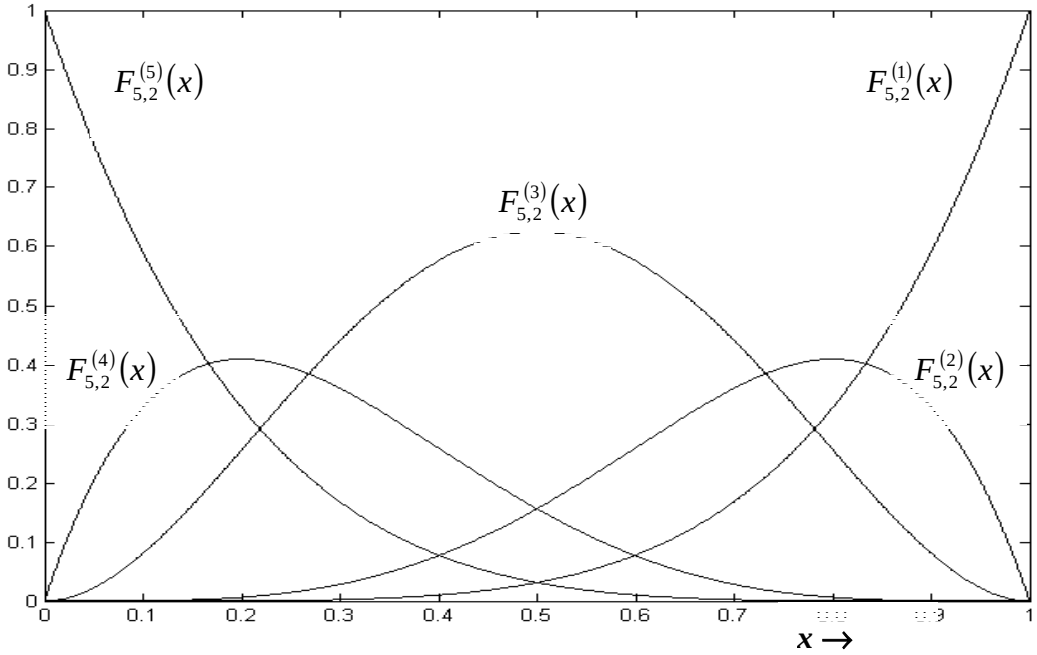

Fig. 4.1: Probability distribution functions for $N = 5$, $q = 2$ and $m_a = 1$.

For the five-level scheme, the probability $F_{N,q}^{(3)}(x)$ of having the switches connect the output terminals to the center tap point of the dc-bus is highest when the reference signal x is equal to 0.5. Probabilities $F_{N,q}^{(2)}(x)$, $F_{N,q}^{(3)}(x)$ and $F_{N,q}^{(4)}(x)$ approach zero as x approaches zero or one. When x approaches to one, the possibility of having the switches connect the output terminals to the fifth level of the dc-bus voltage (i.e., $2A$ V) approaches to one. Likewise, as x approaches to one, the possibility of having the switches connect the output terminals to the first level of the dc-bus voltage (i.e., $-2A$ V) approaches to zero. The probability distribution functions are in agreement with the manner in which the switching should be decided for a five-level inverter.

4.2.2 Expected Value of Five-Level WRPWM Signal

To predict the WRPWM signal $k(t)$, it is necessary to determine the expected value of $k(t)$. The expected value $E\{k(t)\}$ provides an expected value of $k(t)$ for an equivalent averaged WRPWM waveform pattern despite the fact that the actual WRPWM pattern is chaotic in practice. This expected value avoids the uncertainty performance due to the nondeterministic behavior of the WRPWM switching pattern in the theoretical prediction of the WRPWM

scheme and provides the mean $m_k(t)$ of the random signal $k(t)$ at each time interval. Since the Fourier transformation of a random process is itself a random process. The expected value of a random signal is defined [16] as

$$E\{k(t)\} = m_k(t) = \int k f_{k(t)}(k)\, dk\,, \tag{4.14}$$

where k is the outcome of the random signal (i.e., $2A$, A, $-A$ or $-2A$) and $f_{k(t)}$ is the probability of the outcome of the random signal and is defined [16] as

$$f_{k(t)}(x) = \frac{d}{dx} F_{N,q}^{(\cdot)}(x). \tag{4.15}$$

Thus, from (4.14) and (4.15) the expected value of the random WRPWM output function $E\{k(t)\}$ is obtained as

$$\begin{aligned} E\{k(t)\} &= P_r\{k(t)=2A\}(2A) + P_r\{k(t)=A\}(A) + P_r\{k(t)=0\}(0) \\ &\quad + P_r\{k(t)=-A\}(-A) + P_r\{k(t)=-2A\}(-2A) \\ &= 2AF_{N,q}^{(1)}(x) + AF_{N,q}^{(2)}(x) - AF_{N,q}^{(4)}(x) - 2AF_{N,q}^{(5)}(x). \end{aligned} \tag{4.16}$$

Define $\alpha = (f_{sp}/f_r)$, where f_{sp} is the sampling frequency (i.e. $f_{sp} = (1/T)$). Figs. 4.2 (a) and (b) present the expected random switching signal when $N = 5$, $q = 2$, $A = 1$ and $m_a = 1$ with sampling frequencies of 20 kHz and 667 Hz, respectively. It can be seen that that $E\{k(t)\}$ is periodic with the fundamental frequency f_r if α is an integer [3,4], i.e. sampling frequency f_{sp} is an integer multiple of the frequency f_r, of the reference signal $r(t)$. However, if α is not an integer, but a fairly large number [i.e. $f_{sp} >> f_r$], $E\{k(t)\}$ will be almost periodic with f_r [3,4]. For example, if a sampling frequency of 20 kHz is employed for a fundamental frequency of 50 Hz, $\alpha = 400$ which is a fairly large integer. Any slight change of either f_{sp} or f_r that leads to an noninteger value of α can be still considered to be almost periodic with f_r. As for small and noninterger value of α, it can be seen from Fig. 4.2 (b) that $E\{k(t)\}$ can not be considered to be periodic with f_r.

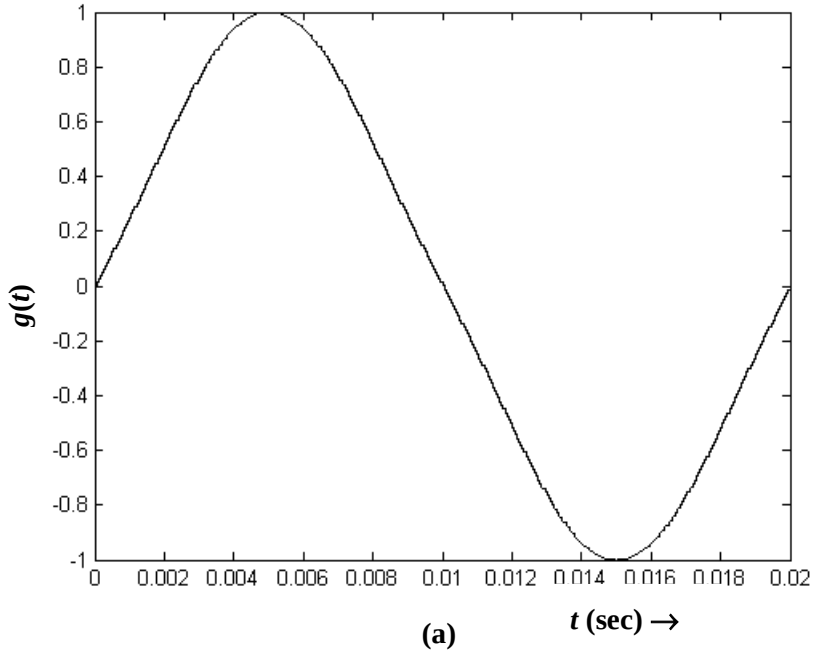

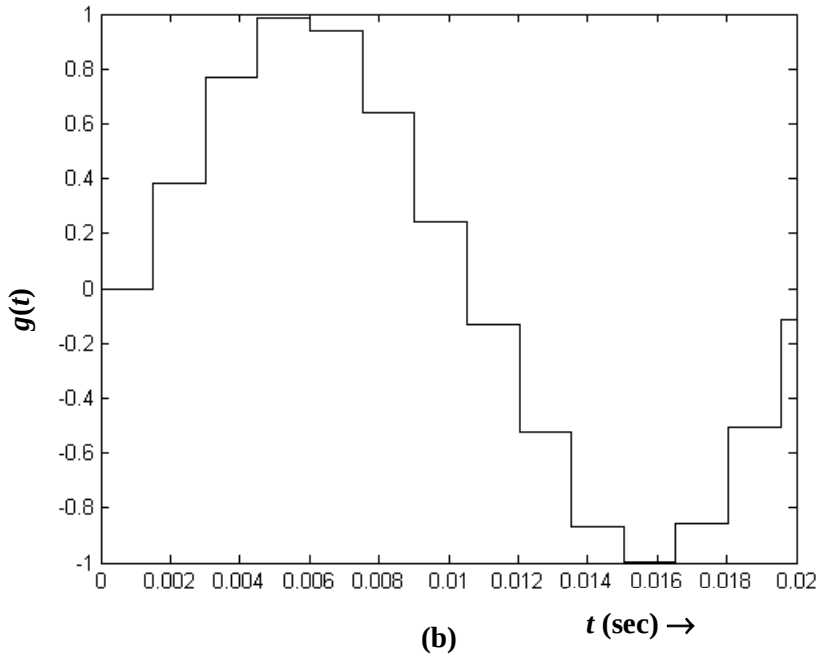

Fig. 4.2: Expected random switching signal $E\{k(t)\}$ for $N = 5$, $q = 2$, $A = 1$ and $m_a = 1$ (a) $\alpha = 400$ (b) $\alpha = 13.3$.

4.2.3 Expected Power Spectral Density

The Fourier series components of $E\{k(t)\}$ represent the discrete parts of the spectrum. The expected power spectral density is

$$S(f) = \Im[R_k(\tau)], \tag{4.17}$$

where the general expression of autocorrelation is given by

$$R_k(\tau) = \lim_{W\to\infty} \frac{1}{2W} \int_{-W}^{W} E\{k(t)k(t+\tau)\}dt\,. \tag{4.18}$$

To evaluate $R_k(\tau)$, it is necessary to determine $E\{k(t_1)\ k(t_2)\}$. If the continuous variable x is replaced by the discrete sampled value of the modulating function $r(\lfloor t/T \rfloor T)$, two cases need to be considered [4].

1. The first one is when $\left\lfloor \frac{t_1}{T} \right\rfloor = \left\lfloor \frac{t_2}{T} \right\rfloor$, i.e., t_1 and t_2 are in the same sampling period. Then making use of analysis techniques similar to those adopted in [4,10,16], an expression for $E\{k(t_1)\ k(t_2)\}$ for a five-level inverter is obtained as follows

$$\begin{aligned}
E\{k(t_1)k(t_2)\} = {} & P_r\{k(t_1)=2A, k(t_2)=2A\}(4A^2) + P_r\{k(t_1)=A, k(t_2)=A\}(A^2) + \\
& P_r\{k(t_1)=-2A, k(t_2)=-2A\}(4A^2) + P_r\{k(t_1)=-A, k(t_2)=-A\}(A^2) + \\
& P_r\{k(t_1)=2A, k(t_2)=A\}(2A) + P_r\{k(t_1)=2A, k(t_2)=-A\}(-2A^2) + \\
& P_r\{k(t_1)=2A, k(t_2)=-2A\} + P_r\{k(t_1)=A, k(t_2)=2A\}(2A^2) + \\
& P_r\{k(t_1)=A, k(t_2)=-A\}(-A^2) + P_r\{k(t_1)=A, k(t_2)=-2A\}(-2A^2) + \\
& P_r\{k(t_1)=-A, k(t_2)=2A\}(-2A^2) + P_r\{k(t_1)=-A, k(t_2)=A\}(-A^2) + \\
& P_r\{k(t_1)=-A, k(t_2)=-2A\}(2A^2) + P_r\{k(t_1)=-2A, k(t_2)=2A\}(-4A^2) + \\
& P_r\{k(t_1)=-2A, k(t_2)=A\}(-2A^2) + P_r\{k(t_1)=-2A, k(t_2)=-A\}(2A^2)
\end{aligned}$$

$$\begin{aligned}
E\{k(t_1)k(t_2)\} = {} & 4A^2 F_{N,q}^{(1)}\left(r\left(\left\lfloor \frac{t_1}{T} \right\rfloor T\right)\right) + A^2 F_{N,q}^{(2)}\left(r\left(\left\lfloor \frac{t_1}{T} \right\rfloor T\right)\right) \\
& + A^2 F_{N,q}^{(4)}\left(r\left(\left\lfloor \frac{t_1}{T} \right\rfloor T\right)\right) + 4A^2 F_{N,q}^{(5)}\left(r\left(\left\lfloor \frac{t_1}{T} \right\rfloor T\right)\right) \\
= {} & U_1
\end{aligned} \tag{4.19}$$

According to [16] the average power content of a signal can be obtain as follows

$$P = \lim_{T\to\infty} \int_{-T/2}^{T/2} E\{k^2(t)\}dt. \tag{4.20}$$

Thus, from (4.20) it can be seen that U_1 represents the instantaneous expected power of signal $k(t)$. Since $\left\lfloor \frac{t_1}{T} \right\rfloor = \left\lfloor \frac{t_2}{T} \right\rfloor$, the probability of signal $k(t)$ having different value at t_1 and t_2 is zero. Therefore when $\left\lfloor \frac{t_1}{T} \right\rfloor = \left\lfloor \frac{t_2}{T} \right\rfloor$

$$\begin{aligned}
P_r\{k(t_1)=2A, k(t_2)=A\} &= P_r\{k(t_1)=2A, k(t_2)=-A\} \\
&= P_r\{k(t_1)=A, k(t_2)=2A\} \\
&= P_r\{k(t_1)=A, k(t_2)=-A\} \\
&= P_r\{k(t_1)=A, k(t_2)=-2A\} \\
&= P_r\{k(t_1)=-A, k(t_2)=2A\} \\
&= P_r\{k(t_1)=-A, k(t_2)=A\} \\
&= P_r\{k(t_1)=-A, k(t_2)=-2A\} \\
&= P_r\{k(t_1)=-2A, k(t_2)=2A\} \\
&= P_r\{k(t_1)=-2A, k(t_2)=A\} \\
&= P_r\{k(t_1)=-2A, k(t_2)=-A\} \\
&= P_r\{k(t_1)=2A, k(t_2)=-2A\} \\
&= 0.
\end{aligned} \tag{4.21}$$

2. The second case that needs to be considered is when $\left\lfloor \frac{t_1}{T} \right\rfloor \neq \left\lfloor \frac{t_2}{T} \right\rfloor$, i.e., t_1 and t_2 are in different sampling periods. Again, by making use of analysis techniques similar to those adopted in [4,10,16] an expression for $E\{k(t_1)\,k(t_2)\}$ is obtained as

$$\begin{aligned}
E\{k(t_1)k(t_2)\} = {} & P_r\{k(t_1)=2A, k(t_2)=2A\}(4A^2) + P_r\{k(t_1)=A, k(t_2)=A\}(A^2) + \\
& P_r\{k(t_1)=-2A, k(t_2)=-2A\}(4A^2) + P_r\{k(t_1)=-A, k(t_2)=-A\}(A^2) + \\
& P_r\{k(t_1)=2A, k(t_2)=A\}(2A^2) + P_r\{k(t_1)=2A, k(t_2)=-A\}(-2A^2) + \\
& P_r\{k(t_1)=2A, k(t_2)=A\}(2A^2) + P_r\{k(t_1)=A, k(t_2)=2A\}(2A^2) + \\
& P_r\{k(t_1)=A, k(t_2)=-A\}(-A^2) + P_r\{k(t_1)=A, k(t_2)=-2A\}(-2A^2) + \\
& P_r\{k(t_1)=-A, k(t_2)=2A\}(-2A^2) + P_r\{k(t_1)=-A, k(t_2)=A\}(-A^2) + \\
& P_r\{k(t_1)=-A, k(t_2)=-2A\}(2A^2) + P_r\{k(t_1)=-2A, k(t_2)=2A\}(-4A^2) + \\
& P_r\{k(t_1)=-2A, k(t_2)=A\}(-2A^2) + P_r\{k(t_1)=-2A, k(t_2)=-A\}(2A^2)
\end{aligned} \tag{4.22}$$

Substitution of (4.9)-(4.13) into (4.22) yields

$$
\begin{aligned}
E\{k(t_1)k(t_2)\} = {} & 4A^2F_{N,q}^{(1)}\left(r\left(\left\lfloor\frac{t_1}{T}\right\rfloor T\right)\right)F_{N,q}^{(1)}\left(r\left(\left\lfloor\frac{t_2}{T}\right\rfloor T\right)\right)+A^2F_{N,q}^{(2)}\left(r\left(\left\lfloor\frac{t_1}{T}\right\rfloor T\right)\right)F_{N,q}^{(2)}\left(r\left(\left\lfloor\frac{t_2}{T}\right\rfloor T\right)\right) \\
& +4A^2F_{N,q}^{(5)}\left(r\left(\left\lfloor\frac{t_1}{T}\right\rfloor T\right)\right)F_{N,q}^{(5)}\left(r\left(\left\lfloor\frac{t_2}{T}\right\rfloor T\right)\right)+A^2F_{N,q}^{(4)}\left(r\left(\left\lfloor\frac{t_1}{T}\right\rfloor T\right)\right)F_{N,q}^{(4)}\left(r\left(\left\lfloor\frac{t_2}{T}\right\rfloor T\right)\right) \\
& +2A^2F_{N,q}^{(1)}\left(r\left(\left\lfloor\frac{t_1}{T}\right\rfloor T\right)\right)F_{N,q}^{(2)}\left(r\left(\left\lfloor\frac{t_2}{T}\right\rfloor T\right)\right)-2A^2F_{N,q}^{(1)}\left(r\left(\left\lfloor\frac{t_1}{T}\right\rfloor T\right)\right)F_{N,q}^{(4)}\left(r\left(\left\lfloor\frac{t_2}{T}\right\rfloor T\right)\right) \\
& +2A^2F_{N,q}^{(2)}\left(r\left(\left\lfloor\frac{t_1}{T}\right\rfloor T\right)\right)F_{N,q}^{(1)}\left(r\left(\left\lfloor\frac{t_2}{T}\right\rfloor T\right)\right)-A^2F_{N,q}^{(2)}\left(r\left(\left\lfloor\frac{t_1}{T}\right\rfloor T\right)\right)F_{N,q}^{(4)}\left(r\left(\left\lfloor\frac{t_2}{T}\right\rfloor T\right)\right) \\
& -2A^2F_{N,q}^{(2)}\left(r\left(\left\lfloor\frac{t_1}{T}\right\rfloor T\right)\right)F_{N,q}^{(5)}\left(r\left(\left\lfloor\frac{t_2}{T}\right\rfloor T\right)\right)-2A^2F_{N,q}^{(4)}\left(r\left(\left\lfloor\frac{t_1}{T}\right\rfloor T\right)\right)F_{N,q}^{(1)}\left(r\left(\left\lfloor\frac{t_2}{T}\right\rfloor T\right)\right) \\
& -A^2F_{N,q}^{(4)}\left(r\left(\left\lfloor\frac{t_1}{T}\right\rfloor T\right)\right)F_{N,q}^{(2)}\left(r\left(\left\lfloor\frac{t_2}{T}\right\rfloor T\right)\right)+2A^2F_{N,q}^{(4)}\left(r\left(\left\lfloor\frac{t_1}{T}\right\rfloor T\right)\right)F_{N,q}^{(5)}\left(r\left(\left\lfloor\frac{t_2}{T}\right\rfloor T\right)\right) \\
& -4A^2F_{N,q}^{(5)}\left(r\left(\left\lfloor\frac{t_1}{T}\right\rfloor T\right)\right)F_{N,q}^{(1)}\left(r\left(\left\lfloor\frac{t_2}{T}\right\rfloor T\right)\right)-2A^2F_{N,q}^{(5)}\left(r\left(\left\lfloor\frac{t_1}{T}\right\rfloor T\right)\right)F_{N,q}^{(2)}\left(r\left(\left\lfloor\frac{t_2}{T}\right\rfloor T\right)\right) \\
& +2A^2F_{N,q}^{(5)}\left(r\left(\left\lfloor\frac{t_1}{T}\right\rfloor T\right)\right)F_{N,q}^{(4)}\left(r\left(\left\lfloor\frac{t_2}{T}\right\rfloor T\right)\right)-4A^2F_{N,q}^{(1)}\left(r\left(\left\lfloor\frac{t_1}{T}\right\rfloor T\right)\right)F_{N,q}^{(5)}\left(r\left(\left\lfloor\frac{t_2}{T}\right\rfloor T\right)\right) \\
= {} & U_2.
\end{aligned}
\tag{4.23}
$$

With the use of Kronecker δ function defined as [52]

$$
\delta_{i,j} = \begin{cases} 1 & \text{if } i = j \\ 0, & \text{if } i \neq j \end{cases} \tag{4.24}
$$

the preceding two cases can be treated in a unified fashion. Therefore, the expression for $E\{k(t_1)\, k(t_2)\}$ can be re-written as follows:

$$
\begin{aligned}
E\{k(t_1)k(t_2)\} &= U_1\delta_{\left\lfloor\frac{t_1}{T}\right\rfloor,\left\lfloor\frac{t_2}{T}\right\rfloor}+U_2\left[1-\delta_{\left\lfloor\frac{t_1}{T}\right\rfloor,\left\lfloor\frac{t_2}{T}\right\rfloor}\right] \\
&= U_2+(U_1-U_2)\delta_{\left\lfloor\frac{t_1}{T}\right\rfloor,\left\lfloor\frac{t_2}{T}\right\rfloor}
\end{aligned}
\tag{4.25}
$$

By defining a few new signals, $E\{k(t_1)\, k(t_2)\}$can be re-arranged as follows

$$E\{k(t_1)k(t_2)\} = g(t_1)g(t_2) + d(t_1)\delta_{\lfloor t_1/T \rfloor, \lfloor t_2/T \rfloor}, \tag{4.26}$$

where

$$\begin{aligned} g(t) &= E\{k(t)\} = m_k(t) \\ &= A\left(2F_{N,q}^{(1)}\left(r\left(\left\lfloor \frac{t}{T} \right\rfloor T\right)\right) + F_{N,q}^{(2)}\left(r\left(\left\lfloor \frac{t}{T} \right\rfloor T\right)\right) - F_{N,q}^{(4)}\left(r\left(\left\lfloor \frac{t}{T} \right\rfloor T\right)\right) - 2F_{N,q}^{(5)}\left(r\left(\left\lfloor \frac{t}{T} \right\rfloor T\right)\right)\right) \end{aligned} \tag{4.27}$$

and

$$\begin{aligned} d(t) &= 4A^2F_{N,q}^{(1)}\left(r\left(\left\lfloor \frac{t}{T} \right\rfloor T\right)\right) + A^2F_{N,q}^{(2)}\left(r\left(\left\lfloor \frac{t}{T} \right\rfloor T\right)\right) \\ &\quad + A^2F_{N,q}^{(4)}\left(r\left(\left\lfloor \frac{t}{T} \right\rfloor T\right)\right) + 4A^2F_{N,q}^{(5)}\left(r\left(\left\lfloor \frac{t}{T} \right\rfloor T\right)\right) \\ &\quad - A^2\left(2F_{N,q}^{(1)}\left(r\left(\left\lfloor \frac{t}{T} \right\rfloor T\right)\right) + F_{N,q}^{(2)}\left(r\left(\left\lfloor \frac{t}{T} \right\rfloor T\right)\right) - F_{N,q}^{(4)}\left(r\left(\left\lfloor \frac{t}{T} \right\rfloor T\right)\right) - 2F_{N,q}^{(5)}\left(r\left(\left\lfloor \frac{t}{T} \right\rfloor T\right)\right)\right)^2. \end{aligned} \tag{4.28}$$

It is observed that the first term on the right hand side of (4.26) is a product of two one dimensional functions, while the second term is a two dimensional function (i.e., the second term $d(t)\delta_{\lfloor t1/T \rfloor, \lfloor t2/T \rfloor}$ equals to $d(t)$ if $\left\lfloor \frac{t_1}{T} \right\rfloor = \left\lfloor \frac{t_2}{T} \right\rfloor$ and equals to zero if $\left\lfloor \frac{t_1}{T} \right\rfloor \neq \left\lfloor \frac{t_2}{T} \right\rfloor$) and $g(t)$ of (4.27) is identical to the $E\{k(t)\}$ of (4.16). The plot of the waveform $g(t)$ was presented in Fig. 4.2.

From (4.28) it can be seen that $d(t)$ is equal to $U_1 - (g(t))^2$ which is the variance of the random signal [52] (i.e., $E\{k(t_1)\ k(t_2)\}$- $m_k(t_1)m_k(t_2)$ where $t_1 = t_2$). It is known that by varying the switching patterns the discrete spectral components can be transformed into continuous components. Thus, $d(t)$ represents the instantaneous continuous noise of the five-level WRPWM signal. Fig. 4.3 shows the waveform of $d(t)$, which is an even periodic function at twice the reference frequency f_r. It can be seen from Figs. 4.2 (a) and 4.3 that $d(t)$ reaches its minimum value when $g(t)$ reaches its maximum value since $d(t) = U_1 - (g(t))^2$.

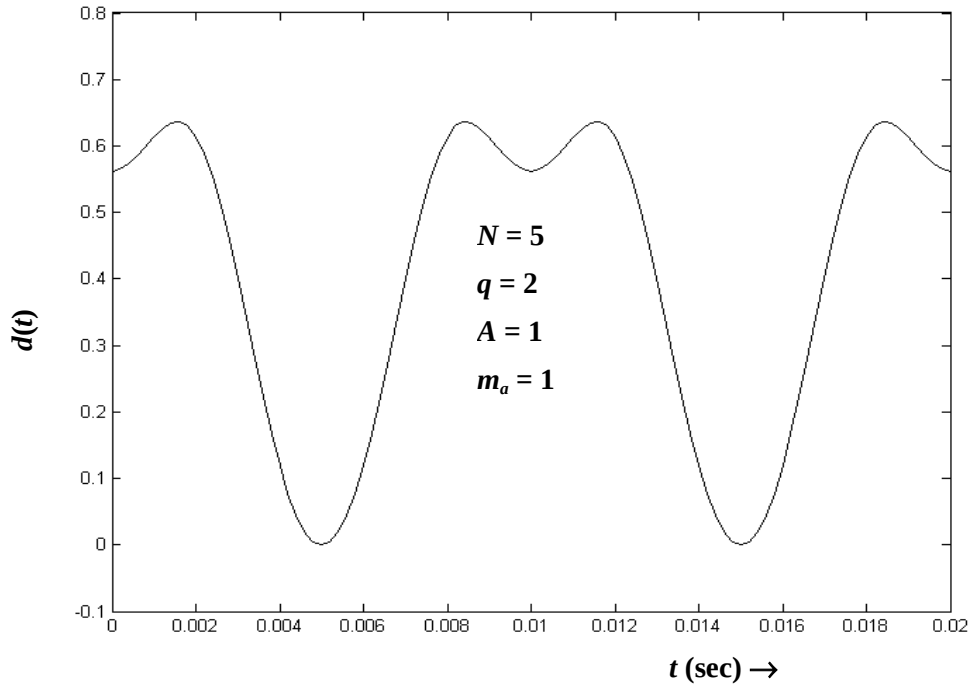

Fig. 4.3: Waveform of $d(t)$ for $N = 5$, $q = 2$, $A = 1$ and $m_a = 1$.

From Fig. 4.2 and (4.26), it is seen that the expectation $E\{k(t)\}$ with mean $m_k(t+nT_r) = m_k(t)$ and $E\{k(t_1)k(t_2)\}$ are periodic with period $T_r = 1/f_r$ (since $g(t)$ has the dominant amplitude and is periodic with period T_r). Therefore, it is a cyclostationary process. From Wiener-Khinchin theorem [16], in a cyclostationary process, if

$$\left| \int_0^{T_r} R_k(t+\tau, t)dt \right| < \infty, \tag{4.29}$$

then the power spectral density is obtained [16] as

$$S_k(f) = \Im(R_k(\tau)), \tag{4.30}$$

where the autocorrelation function $R_k(\tau)$ is obtained by defining $W = T_r / 2$ in (4.18) and thus, (4.18) can be re-written as

$$R_k(\tau) = \frac{1}{T_r} \int_{-T_r/2}^{T_r/2} E\{k(t_1)k(t_2)\}dt. \tag{4.31}$$

Since the expression $E\{k(t_1)\, k(t_2)\}$ is the sum of two terms, so is $R_k(\tau)$. Thus the autocorrelation

function can be expressed as

$$R_k(\tau) = R_1(\tau) + R_2(\tau), \tag{4.32}$$

where the first term on the right hand side of (4.32) can be expressed as

$$R_1(\tau) = \lim_{W\to\infty} \frac{1}{2W} \int_{-W}^{W} g(t)g(t+\tau)dt = R_1(-\tau) \tag{4.33}$$

and the second term on the right hand side of (4.32) can be expressed as

$$R_2(\tau) = \lim_{W\to\infty} \frac{1}{2W} \int_{-W}^{W} d(t)\delta_{\lfloor t/T \rfloor, \lfloor t+\tau/T \rfloor} dt = R_2(-\tau). \tag{4.34}$$

These definitions follow directly from (4.4). This decomposition leads to two distinctly behaving terms in the power spectral density which will be explained later. For the first term $R_1(\tau)$, note that $g(t)$ is periodic, with period $(1/f_r)$ if α is an integer. Then a Fourier series expansion for $g(t)$ exists, i.e.,

$$g(t) = \sum_{-\infty}^{\infty} c_n \, \mathrm{e}^{j2\pi m f_r t}, \tag{4.35}$$

where

$$c_n = f_r \int_0^{1/f_r} g(t)\mathrm{e}^{-j2\pi m f_r t} dt \tag{4.36}$$

and as $g(t)$ is real, $c_{-n} = c^*_n$ and (4.33) can be re-written as

$$\begin{aligned} R_1(\tau) &= \lim_{W\to\infty}\left(\frac{1}{2W}\right)\int_{-W}^{W} \sum_{n=-\infty}^{\infty}\sum_{m=-\infty}^{\infty} c_n c_m^* e^{j2\pi m f_r \tau} e^{j2\pi(m-n)f_r t} dt \\ &= \frac{1}{T_r}\int_{-T_r/2}^{T_r/2} \sum_{n=-\infty}^{\infty}\sum_{m=-\infty}^{\infty} c_n c_m^* e^{j2\pi m f_r \tau} e^{j2\pi(m-n)f_r t} dt. \end{aligned} \tag{4.37}$$

Now using the fact that

$$\frac{1}{T_r}\int_{-\frac{T_r}{2}}^{\frac{T_r}{2}} e^{j2\pi(m-n)f_r}dt = \delta_{m,n}, \tag{4.38}$$

then (4.37) may be expressed as

$$R_1(\tau) = \sum_{n=-\infty}^{\infty} |c_n|^2 e^{j2\pi n f_r \tau}, \tag{4.39}$$

where c_n are the Fourier series coefficients of the periodic signal $g(t)$. Since $g(t)$ is periodic with the frequency f_r , the time average autocorrelation of $g(t)$ it periodic with the same frequency. Equation (4.39) defines the discrete part of the spectrum.

For the second term $R_2(\tau)$, $d(t)$ is periodic with period $1/(2f_r)$ if α is an integer and has the average value [4,5]

$$d_{av} = 2f_r\int_0^{1/2f_r} d(t)dt = \frac{\sum_{n=0}^{\alpha/2-1} d(nT)}{\alpha/2}. \tag{4.40}$$

Thus, $R_2(\tau)$ can be evaluated in the following manner

1) For $|\tau| \geq T$, $\lfloor t/T \rfloor \neq \lfloor t+\tau/T \rfloor$ (i.e., $\lfloor t_1/T \rfloor \neq \lfloor t_2/T \rfloor$) and thus $\delta_{\lfloor t1/T \rfloor, \lfloor t2/T \rfloor} = 0$ then the second term of (4.26) is eliminated, thus, $R_2(\tau)=0$.
2) For $0 \leq \tau \leq T$, let $W = MT$ (where M is an integer) then $\lfloor t/T \rfloor = \lfloor t+\tau/T \rfloor = n$ (i.e., $\lfloor t_1/T \rfloor = \lfloor t_2/T \rfloor$) for $\forall t \in [nT, nT + T - \tau)$ and thus $\delta_{\lfloor t1/T \rfloor, \lfloor t2/T \rfloor} = 1$ then the second term of (4.26) exist, thus, $R_2(\tau)\neq 0$.

Therefore, the following holds true.

$$\delta_{\lfloor t/T \rfloor, \lfloor t+\tau/T \rfloor} = \begin{cases} 1 & \forall t \in [nT, nT+T-\tau) \\ 0 & \forall t \in [nT+T-\tau, nT+T) \end{cases} \tag{4.41}$$

and (4.34) can be re-written as

$$R_2(\tau) = \lim_{M\to\infty} \frac{1}{2MT} \cdot \sum_{n=-M}^{M-1} \int_{nT}^{nT+T} d(t)\delta_{\lfloor t/T \rfloor, \lfloor t+\tau/T \rfloor}\, dt. \tag{4.42}$$

Since the product of $d(t)$ and $\delta_{\lfloor t1/T \rfloor, \lfloor t2/T \rfloor}$ is nonzero value at the time interval $\forall t \in [nT, nT + T - \tau)$ and from (4.40) the expression in (4.42) can be simplified as

$$R_2(\tau) = d_{av} \cdot \frac{1}{T} \int_{nT}^{nT+T-\tau} dt. \tag{4.43}$$

This allows (4.43) to be rewritten as.

$$R_2(\tau) = d_{av} \cdot \left(1 - \frac{\tau}{T}\right). \tag{4.44}$$

3) For $0 \geq \tau > -T, R_2(\tau) = d_{av}(1 + \tau/T)$, thus

$$R_2(\tau) = \begin{cases} 0, & \text{for } |\tau| \geq T \\ d_{av}\left(1 - \dfrac{|\tau|}{T}\right) & \text{for } |\tau| < T \end{cases} \tag{4.45}$$

From (4.32), the autocorrelation function $R_k(\tau)$ consists of a periodic part $R_1(\tau)$ and finite duration part $R_2(\tau)$.Thus, the power density $S_k(f)$ is just the sum of the Fourier transforms of $R_1(\tau)$ and $R_2(\tau)$,

$$\begin{aligned} S_k(f) &= \Im(R_1(\tau)) + \Im(R_2(\tau)) \\ &= S_1(f) + S_2(f). \end{aligned} \tag{4.46}$$

Since $R_1(\tau)$ is periodic, its Fourier transform simply consists of the harmonics at integer multiples of f_r,

$$\begin{aligned} S_1(f) &= \Im\left(\sum_{n=-\infty}^{\infty} |c_n|^2 e^{-j2\pi n f_r} \right) \\ &= \sum |c_n|^2 \delta(f + nf_r), \end{aligned} \tag{4.47}$$

where δ(·) denotes the Dirac-delta function. Thus, (4.47) represents the impulse part of the power spectral density in (4.30), i.e., the discrete spectrum. The discrete spectrum was characterized by impulses whose magnitudes are square of the Fourier series coefficients of the periodic signal $g(t)$ at location of integer multiples of f_r.

Given that $R_2(\tau)$ is a finite duration signal, its Fourier transform is spread over a wide range of frequencies. Thus the component of power spectral density $S_2(f)$ is obtained as

$$S_2(f) = Td_{av} \sin c^2(fT). \tag{4.48}$$

From (4.47) and (4.48) an expression for the power spectral density is obtained as

$$S_k(f) = \sum_{n=-\infty}^{\infty} |c_n|^2 \delta(f + nf_r) + Td_{av} \sin c^2(fT). \tag{4.49}$$

A statistical approach for analysis of WRPWM scheme is presented and important equations derived. The derivations are used to predict the spectral performance of the five-level WRPWM scheme. The performance of the five-level WRPWM scheme and the effect of various parameters on the five-level WRPWM scheme such as the sampling frequency, the modulation index and value of N, sampling frequency, will be discussed and characterized in the next chapter.

CHAPTER FIVE

ANALYTICAL RESULTS AND DISCUSSIONS

The mathematical equations that characterize the five-level WRPWM scheme was derived in chapter 4 and its power spectral density was found to have two components:

1) An impulsive part $S_1(f)$ referred to as the discrete spectrum.
2) A continuous part $S_2(f)$ referred to as continuous spectrum.

Provided that the ratio $\alpha = (f_{sp}/f_r)$ is an integer, the discrete spectrum was characterized by impulses at locations …, -2 f_r, - f_r, 0, f_r, -2 f_r,… (i.e., integer multiples of f_r) having strength equal to the distribution of power at these frequencies. The continuous spectrum on the other hand is distributed over all frequencies and has to be integrated over a frequency range in order to obtain the signal power distribution in that frequency range. For deterministic periodic signal $y(t)$ having frequency f_r, the power spectral density only consists of the discrete spectrum which has impulses at locations nf_r having a strength equal to the square of the absolute values of the Fourier series coefficients of the signal. Thus, for the random switching schemes, $|c_1|^2$ gives the power at desired ac signal frequency f_r and $|c_n|^2$ corresponds to the power in the usual discrete harmonics in the deterministic schemes.

5.1 Relationship between Harmonics Content and *N*

Typical plots of the functions $F_{N,q}(x)$ are shown in Figs. 5.1 (a), (b), (c), (d) and (e), and the plots of normalized expected random PWM signal $g(t)$ (with base value of V_d / 2) are shown in Fig. 5.2 for various values of comparison, N, with modulation index m_a = 1. From these plots, it is clear that there is a harmonic boosting effect on $g(t)$ for N > 5. The expected value $g(t)$ provides an expected value of $k(t)$ for an equivalent averaged WRPWM waveform pattern. Theoretically, as the inverter is more likely to have the output terminal connected to the first and fifth level voltage (i.e., 2A V and -2A V, respectively), $g(t)$ approaches a square wave like function. So, as N increases, the fundamental component $|c_1|$ increases for a given reference.

From Figs. 5.1 (a) and (c) it is evident that as N increases (i.e. for both odd and or even increments of N), the probability of inverter output terminals being connected to the first and fifth level of dc-bus voltage (i.e., $2A$ V and $-2A$ V, respectively) increases and the probability of output terminals connected to the second, third, and fourth level of dc-bus voltage (i.e., A V, 0 V and $-A$ V, respectively) decreases. From Figs. 5.1 (b) and (d), it can be seen that the first and fifth level of dc-bus voltage are more likely to be connected to the output terminal of the inverter when the WRPWM scheme operates with even number of comparisons, N, than the WRPWM scheme operating with N odd. On the other hand, the third level of dc-bus voltage is more likely to be connected to the output terminal of the inverter when the WRPWM scheme operates with odd number of N than the WRPWM scheme operating with N even number of N. Thus, from above discussions and Fig.5.2, it can be expected that with N even the WRPWM scheme will have higher fundamental component ($|c_1|$) than with N odd. Moreover, as N increases with odd or even increment, $|c_1|$ increases. For example, in Fig. 5.1 it can be seen that the value of $F^{(1)}_{101,2}(x)$ and $F^{(5)}_{101,2}(x)$ is higher than the value of $F^{(1)}_{8,2}(x)$ and $F^{(5)}_{8,2}(x)$, whereas the value of $F^{(2)}_{101,2}(x)$, $F^{(3)}_{101,2}(x)$ and $F^{(4)}_{101,2}(x)$ is lower than the value of $F^{(2)}_{8,2}(x)$, $F^{(3)}_{8,2}(x)$ and $F^{(4)}_{8,2}(x)$, thus the expected value $g(t)$ is a more square wave like function with N = 102 than with N = 8, hence $|c_1|$ is higher with N = 101 than with N = 8. When the WRPWM scheme operates with $N = \infty$ (which corresponds to a square wave signal and thus totally deterministic signal), it gives the highest fundamental component. However, it is important to note that this increase in fundamental component is accompanied by an increase in other harmonic components.

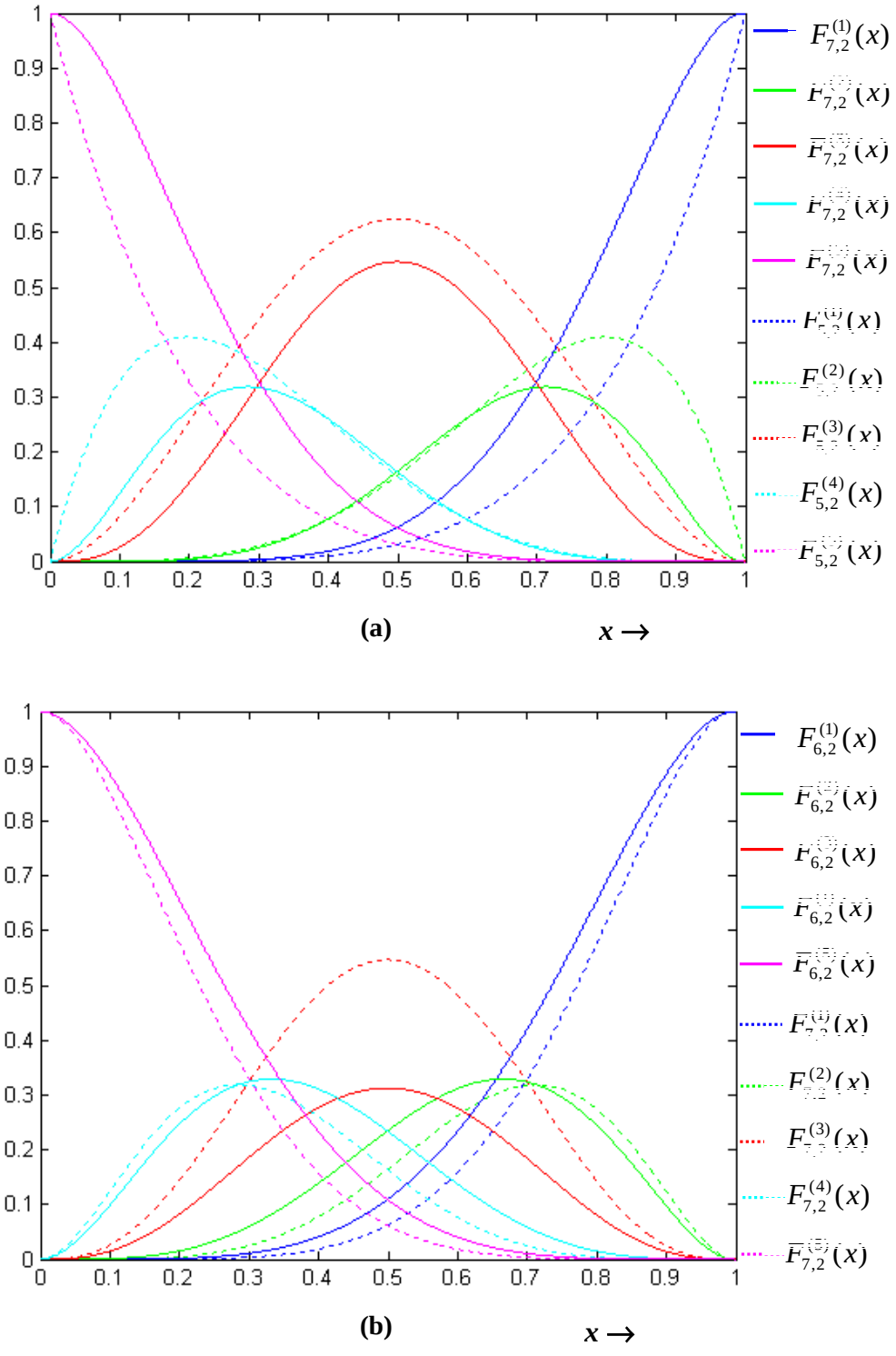

Fig. 5.1: Probability distribution functions with (a) N = 5 and 7 (b) N = 6 and 7.

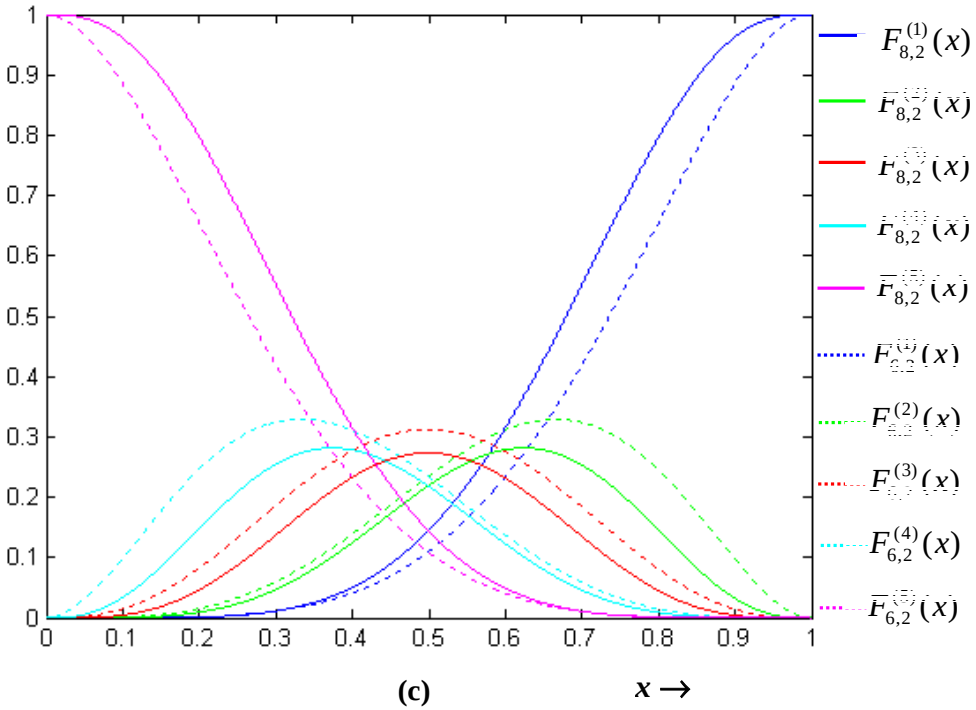

(c) $x \rightarrow$

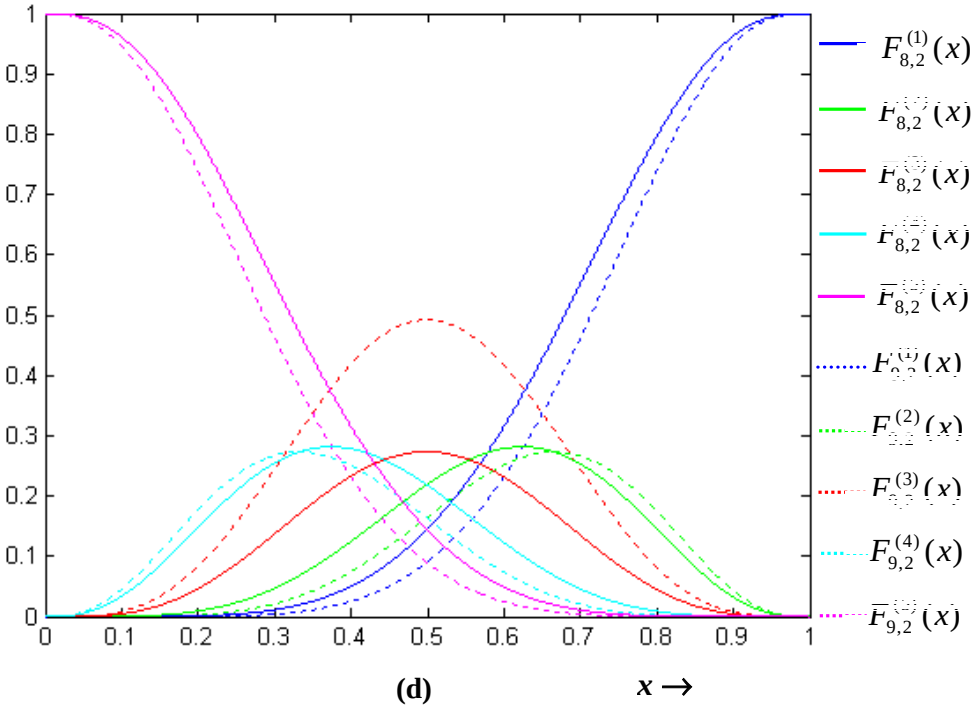

(d) $x \rightarrow$

Fig. 5.1: (continued) (c) N = 6 and 8. (d) N = 8 and 9.

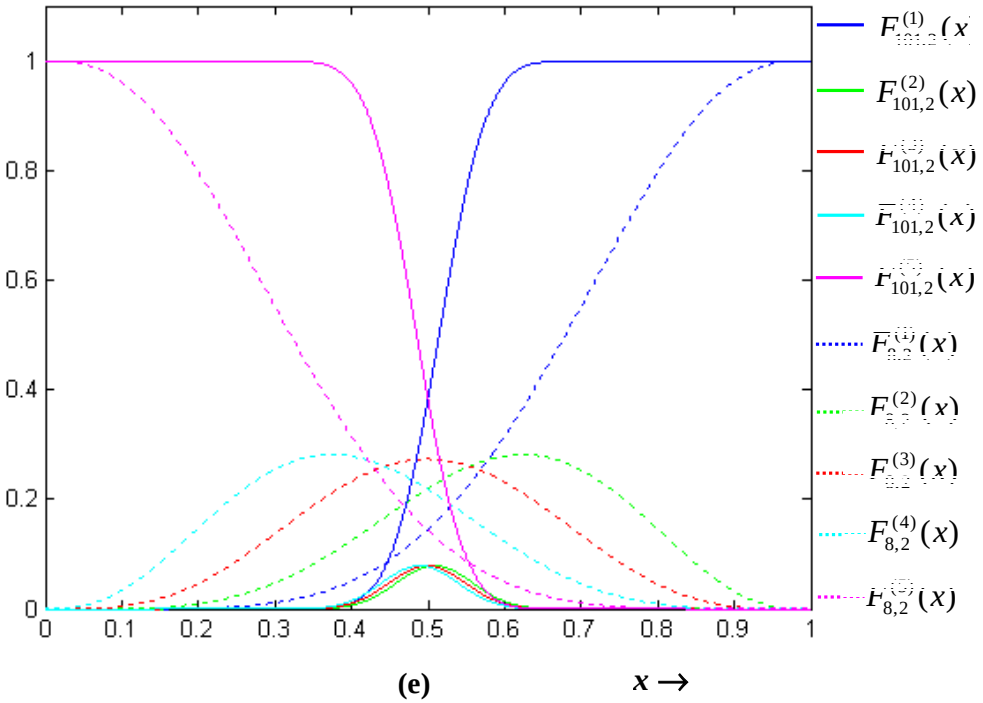

Fig. 5.1: (continued) (e) N = 8 and 102.

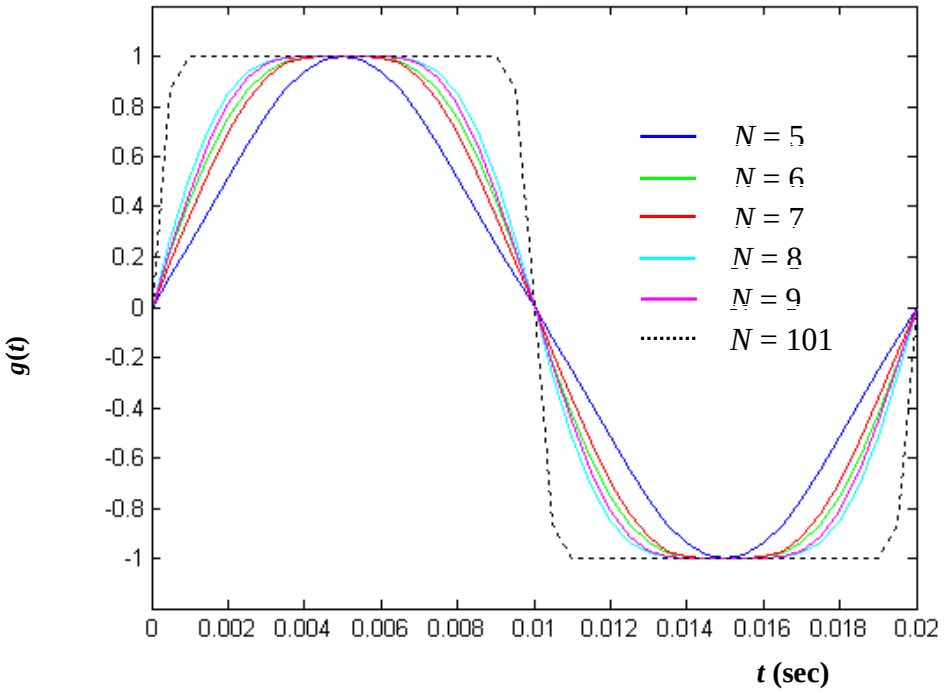

Fig.5.2: Expected random PWM signal $g(t)$.

5.2 Theoretical Predictions with $q = 2$ for Various Values of N

Typical plots of the normalized fundamental component $2|c_1|$ for a base value of $V_{dc}/2$ ($|c_1|$ represents the half of the fundamental component in the positive or negative of frequency domain) versus modulation index for various numbers of comparisons N (N = 5, 6, 7, 8, 9) is shown in Fig. 5.3.

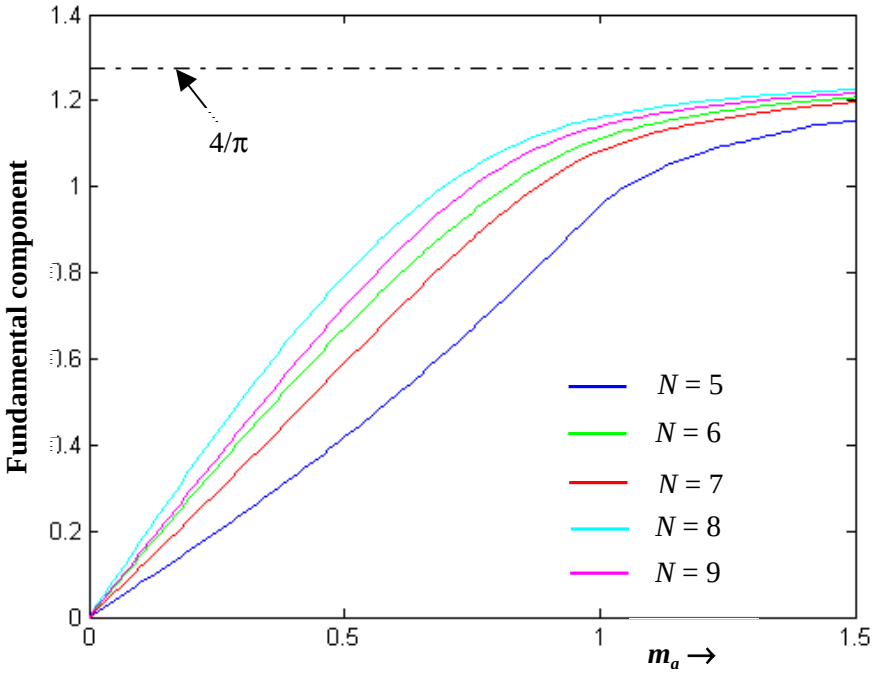

Fig. 5.3: Theoretical fundamental component versus modulation index.

From Fig. 5.3 it can be seen that as the number of comparison, N increases (in odd or even increments) the fundamental component increases. Moreover, the fundamental for WRPWM schemes operating with even numbers of N is higher than that with odd numbers of N. This is in agreement with the findings of section 5.1. For all values of N, the WRPWM scheme has fairly linear fundamental-modulation index characteristic within the range $m_a < 1$. However, these characteristics saturate when the modulation index increases beyond one which is similar to the conventional sinusoidal PWM techniques. For sinusoidal PWM techniques in the linear modulation region, the width of the PWM output pulses has a linear relationship with the ratio m_a of the amplitude of the reference sinusoidal signal to the triangle carrier wave in (3.1) [11]. In overmodulation operation ($m_a > 1$) as m_a increases the width of the notches of the sinusoidal PWM pulses start to decrease. Thus, the pulses at positive (negative) half of the fundamental cycle start to join together leaving little or no space for the width of the pulses to expand any

further. Consequently, the fundamental component start to saturate since the fundamental component is proportional to the total volt-time area of the PWM pulses. Similarly for WRPWM in overmodulation operation, as m_a increases the notches of the pulses start to disappear, thus, the pulses at positive (negative) half of the fundamental cycle start to merge together. Therefore, the fundamental component starts to saturate. For a sufficiently large value of m_a, the inverter voltage degenerates from a PWM waveform into a square wave, hence, it can be concluded that in the overmodulation region with $m_a > 1$

$$\frac{V_d}{2} < 2|c_1| < \frac{4}{\pi}\frac{V_d}{2}. \tag{5.1}$$

Thus, for a dc-bus voltage of 2 V the first harmonic component can not exceed 4/π as shown in Fig. 5.3.

Typical plots of the third harmonic component $2|c_3|$ versus modulation index for various numbers of comparisons N (N = 5, 6, 7, 8, 9) are shown in Fig. 5.4.

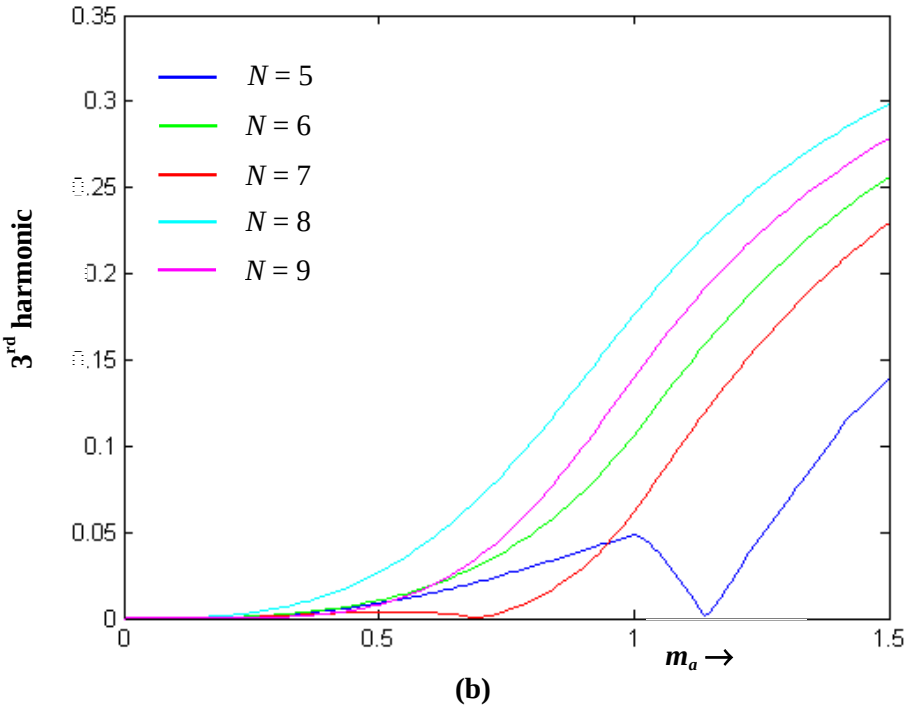

Fig. 5.4: Theoretical third harmonic component versus modulation index.

From Fig. 5.4, it can be seen that the five-level WRPWM scheme with various numbers of comparisons gives rise to third harmonic boosting effect and the WRPWM scheme with $N = 8$ has the highest $|c_3|$ in the entire range of modulation index. For the range of $m_a < 0.5$, the WRPWM schemes with numbers of comparisons $N = 5$, 6, 7 and 9 have negligible third harmonic component (i.e., $(|c_3| / |c_1|) \times 100\% \leq 1\%$, since in signal processing, a signal to noise ratio of -40 dB is considered insignificant). In the linear modulation region, both the magnitude and the $|c_3| / |c_1|$ ratio of the WRPWM scheme with $N = 7$ are the lowest compared to the WRPWM schemes operating with the other four values of N. While third harmonic boosting is beneficial for electric drives, the third harmonic component increases the harmonic loss and, therefore, reduces the efficiency of the drive system. Thus, $N = 7$ scheme has the least third harmonic heating effect in the linear modulation region. In the overmodulation region the WRPWM scheme with $N = 5$ has the lowest value of $|c_3|$ and is approximately zero at $m_a = 1.14$. In general, the third harmonic increases with the modulation index and the number of comparisons (i.e., N increases in odd or even increment), and with N even the third harmonic is higher than with odd numbers of N (i.e., $N = 6$ yields a higher third harmonic than $N = 7$ and $N = 8$ yields a higher third harmonic than $N = 9$).

In the linear region the WRPWM scheme operating with $N = 7$ offers the best performance as it has the lowest $|c_3|$ compared with the WRPWM schemes operating with other values of N. For overmodulation region, the WRPWM scheme operating with $N = 5$ offers the best performance as it has the lowest $|c_3|$ compared with the WRPWM schemes operating with other values of N.

The presence of other low order harmonics is also a concern because they could cause torque pulsation and increase harmonic heating.

The theoretical fifth harmonic $2|c_5|$ versus m_a characteristics for various values of N are plotted in Fig. 5.5.

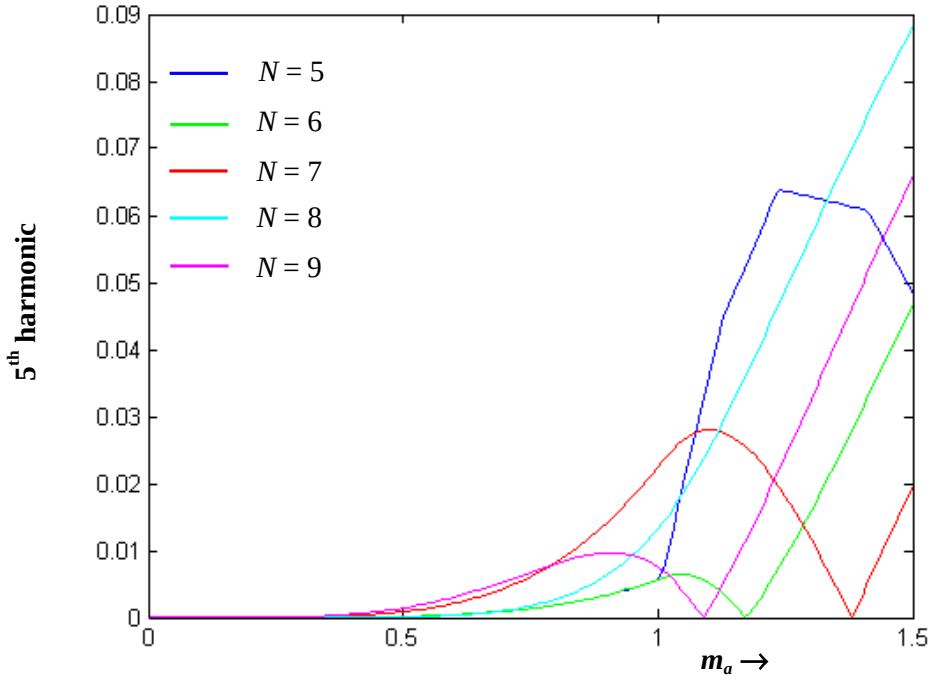

Fig. 5.5: Theoretical fifth harmonic component versus modulation index.

From Fig. 5.5 it is seen that the WRPWM scheme for five-level inverter generates a fifth harmonic for all the different values of N considered (i.e., N = 5, 6, 7, 8 and 9) in the entire modulation index region. In the linear modulation region, the fifth harmonic of the WRPWM scheme operating with the values of N under consideration are insignificant and can be considered negligible at m_a < 0.75 ($|c_5|/|c_1| << 1$ %). Note that, the WRPWM scheme operating with N = 5 and N = 6 yields approximately the same $|c_5|$ versus m_a characteristic in the linear modulation region. In the overmodulation region, the fifth harmonic of the WRPWM scheme operating with N = 6, 7 or 9 are insignificant ($|c_5|/|c_1| < 5$ %). In the overmodulation region, the fifth harmonic of the WRPWM scheme operating with N = 5 and 8 exceed 5 % of the fundamental component, for N = 5 the fifth harmonic reaches its maximum value (5.834 % of the fundamental component) at m_a = 1.24 and for N = 8 the fifth harmonic reaches its maximum value (7.2 % of the fundamental component) at m_a = 1.5. In the overmodulation region, the fifth harmonic reaches approximately zero at m_a = 1.17 with N = 6, at m_a = 1.38 the fifth harmonic reaches approximately zero with N = 7 and the fifth harmonic reaches approximately zero with N = 8 at m_a = 1.09.

In the linear region the WRPWM scheme operates with N = 6 and N = 5 offers the best performance as they have the lowest $|c_5|$ compared with the WRPWM schemes operating with other values of N. For the slightly overmodulated region $1 < m_a < 1.2$ (which could be part of the operation region in some applications), the WRPWM schemes operating with N = 6 and N = 9 offers the best performance as it has the lowest $|c_5|$ compared with the WRPWM schemes operating with other values of N. The WRPWM scheme with N = 6 offers the best overall fifth harmonic performance, since in general it has the lowest value of $|c_5|$ at $0 < m_a < 1.2$.

The theoretical seventh harmonic $2|c_7|$ versus m_a characteristics for various values of N are plotted in Fig. 5.6.

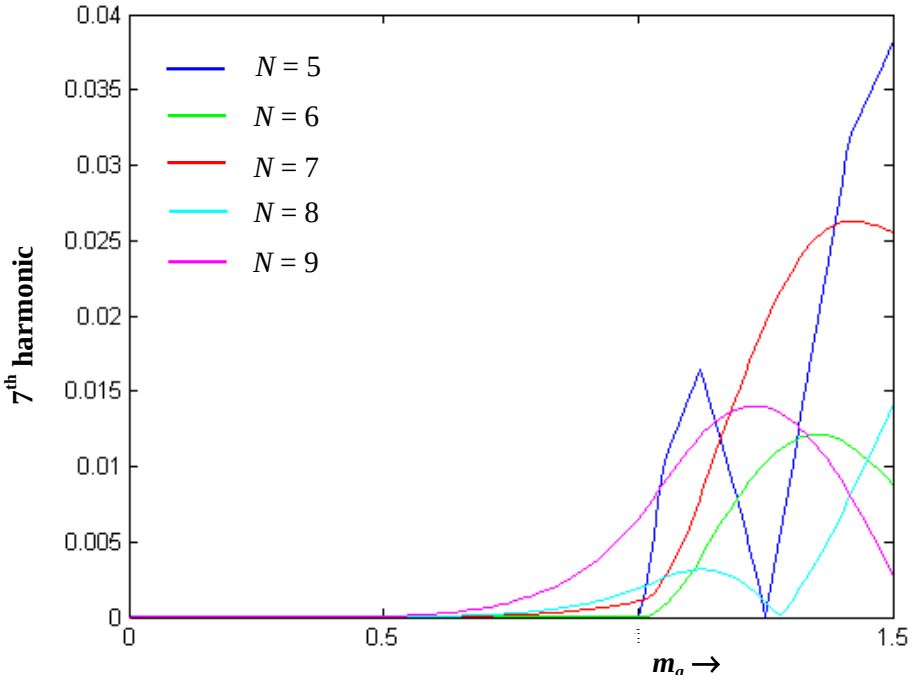

Fig. 5.6: Theoretical seventh harmonic component versus modulation index.

From Fig. 5.6 it can be seen that in the entire modulation region, the seventh harmonic of the WRPWM scheme operating with the values of N under consideration (i.e. N = 5, 6, 7, 8 and 9) are insignificant, and can be considered negligible at $m_a < 1$. In the overmodulation region, the seventh harmonic reaches approximately zero at m_a = 1.25 with N = 5 and at m_a = 1.28 the seventh harmonic reaches approximately zero with N = 8.

In the linear region, and for all values of comparisons, N, the WRPWM scheme offers a good

performance as it gives rise to insignificant $|c_7|$. For the slightly overmodulated region $1 < m_a < 1.2$, the WRPWM scheme operating with $N = 6$ and $N = 8$ offers the best performance as they have the lowest $|c_7|$ compared with the WRPWM schemes operating with other value of N.

Figs. 5.7 and 5.8 show the characteristic plots of the ninth harmonic $|c_9|$ and eleventh harmonic $|c_{11}|$ versus modulation index m_a, respectively.

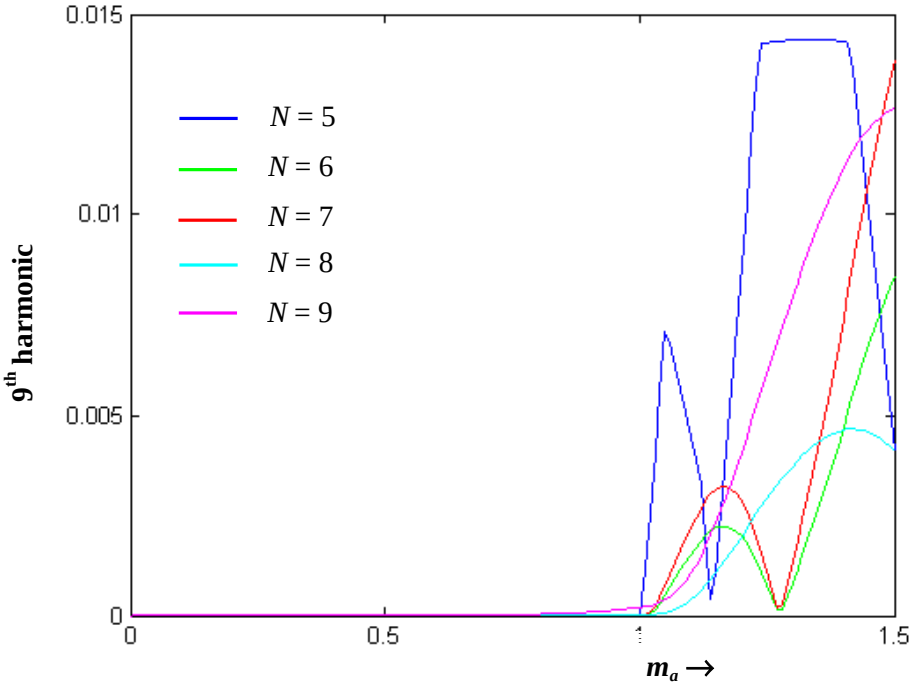

Fig. 5.7: Theoretical ninth harmonic component versus modulation index.

From Fig. 5.7 it can be seen that in the entire modulation region, the ninth harmonic of the WRPWM scheme operating with the value of N under consideration (i.e., $N = 5$, 6, 7, 8 and 9) are insignificant and can be considered negligible at $m_a < 1.05$. The ninth harmonic of the WRPWM scheme operating with $N = 5$ reaches its minimum value (0.0415 % of the fundamental component) in the overmodulation region at $m_a = 1.14$. In the overmodulation region, the ninth harmonic reaches approximately zero at $m_a = 1.27$ with $N = 6$ and 7.

In the linear region, and for all values of comparisons, N, the WRPWM scheme offers a good performance as they generate negligible $|c_9|$. For the slightly overmodulated region $1 < m_a < 1.2$, the WRPWM scheme operating with $N = 8$ offers the best performance as it has the lowest value of $|c_9|$ compared with the WRPWM schemes operating with other values of N.

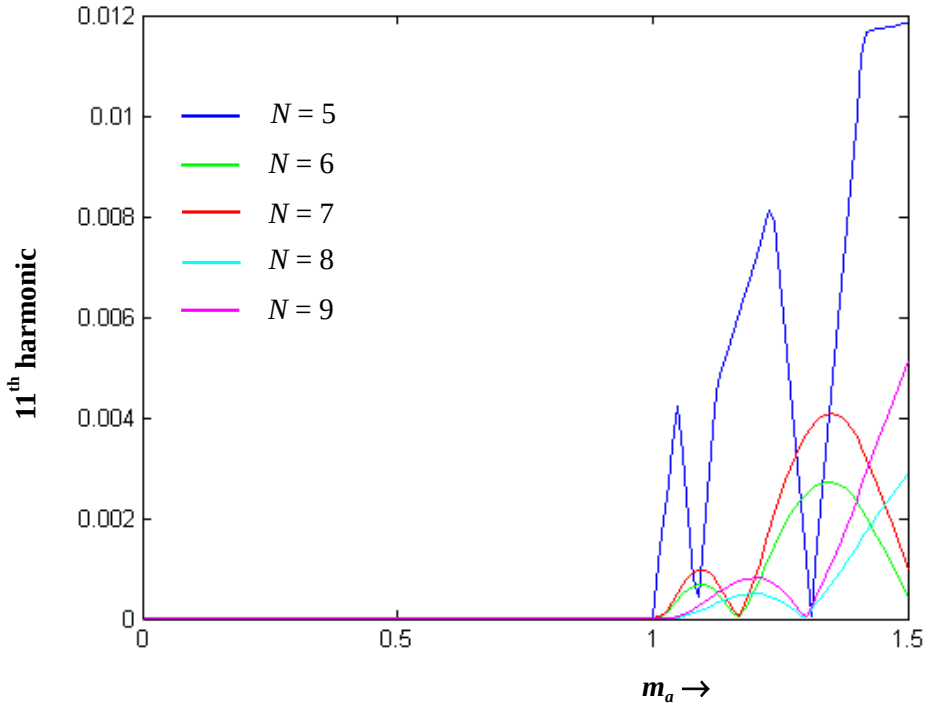

Fig. 5.8: Theoretical eleventh harmonic component versus modulation index.

From Fig. 5.8 it can be seen that in the entire modulation region, the eleventh harmonic of the WRPWM scheme operating with the values of N under consideration (i.e., N = 5, 6, 7, 8 and 9) is insignificant and can be considered negligible at m_a < 1.17. In the overmodulation region, the eleventh harmonic reaches approximately zero at m_a = 1.31 with N = 5, the eleventh harmonic reaches approximately zero at m_a = 1.17 with both N = 6 or 7 operations, and the eleventh harmonic reaches approximately zero at m_a = 1.29 with both N = 8 and 9 operations.

In the linear region, and for all values of comparisons, N, the WRPWM schemes offer a good performance as they have negligible $|c_{11}|$. For the overmodulation region, the WRPWM scheme operating with N = 5 offers the worst performance compared to the other values of N, as it has overall the highest value of $|c_{11}|$ compared with the WRPWM schemes operating with other values of N.

5.2.1 Comparison of the Five-Level and Three-Level WRPWM Schemes

In this section, a comparison is made between the performance of five-level WRPWM and that of three-level WRPWM with N = 3 and N = 4. However, it should be noted that the five-level WRPWM would most likely be used in a system with higher dc-bus voltages than that for the

three-level WRPWM making any improvements in harmonic performance that much more significant. The plot of fundamental component versus modulation index is shown in Fig. 5.9. The plots of third, fifth, seventh, ninth and eleventh harmonic components versus modulation index are shown in Figs. 5.10, 5.11, 5.12, 5.13 and 5.14, respectively.

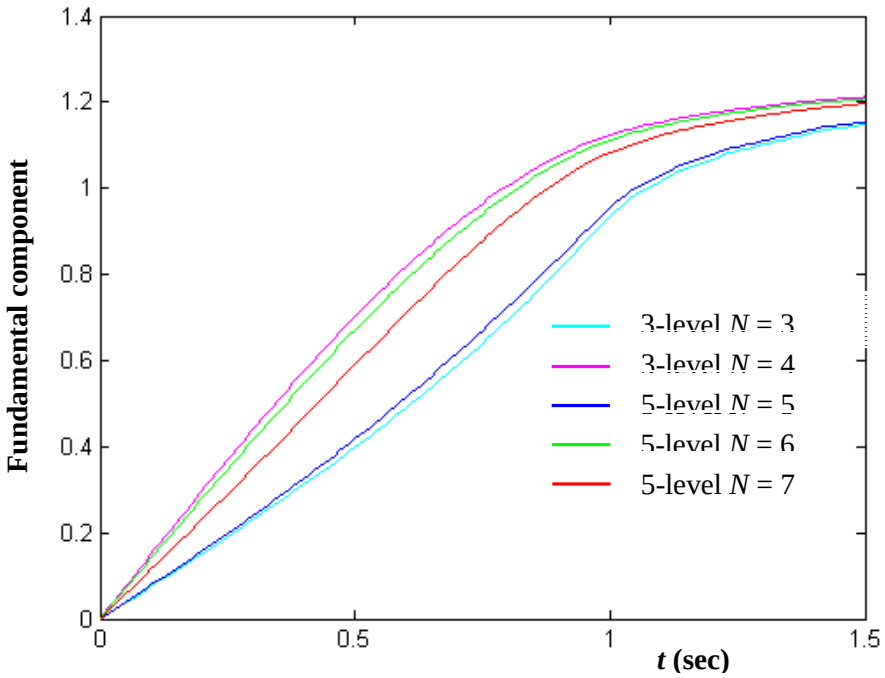

Fig. 5.9: Theoretical fundamental component versus modulation index.

From Fig. 5.9, it can be seen that the three-level WRPWM operating with $N = 3$ has the lowest fundamental component and the three-level WRPWM operating with $N = 4$ has the highest fundamental component. The five-level WRPWM schemes operating with $N = 6$ has a slightly lower fundamental component than the three-level WRPWM scheme operating with $N = 4$. However, the five-level WRPWM scheme with $N = 5$ has a slightly higher fundamental component than the three-level WRPWM scheme operating with $N = 3$. The plot of the fundamental component of the five-level WRPWM scheme operating with $N = 7$ lies between the plots of the fundamental component of the five-level WRPWM schemes operating with $N = 5$ and 6.

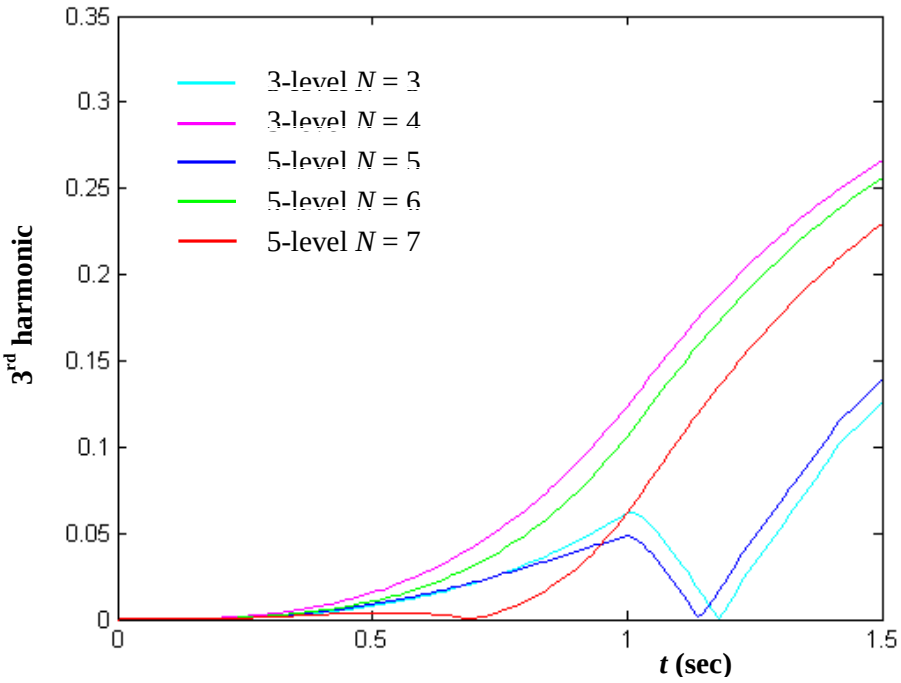

Fig. 5.10: Theoretical third harmonic component versus modulation index.

From Fig. 5.10 it can be seen that the five-level WRPWM scheme with $N = 7$ offers the best third harmonic performance since it has the lowest third harmonic to fundamental component ratio at $0 < m_a < 1.0$. Note that the plots for the three-level WRPWM scheme operating with $N = 3$ and the five-level WRPWM scheme operating with $N = 5$ are similar. Further, the plots for the three-level WRPWM scheme operating with $N = 4$ and the five-level WRPWM scheme operating with $N = 6$ are similar. The third harmonic of the three-level WRPWM scheme operating with $N = 4$ is higher than that of the five-level WRPWM scheme operating with $N = 6$ in the entire modulation region. The third harmonic of the three-level WRPWM scheme operating with $N = 3$ is higher than the fifth harmonic of the five-level WRPWM scheme operating with $N = 5$ at $0.6 < m_a < 1.2$.

From Fig. 5.11 it can be seen that the three-level WRPWM scheme with $N = 4$ and 3 offers the best fifth harmonic performance since it has the lowest fifth harmonic to fundamental component ratio at $0 < m_a < 1$. In the overmodulation region, both the three-level WRPWM scheme with $N = 3$ and the five-level WRPWM scheme operating with $N = 5$ have large fifth harmonic component with the three-level WRPWM scheme with $N = 3$ having the highest.

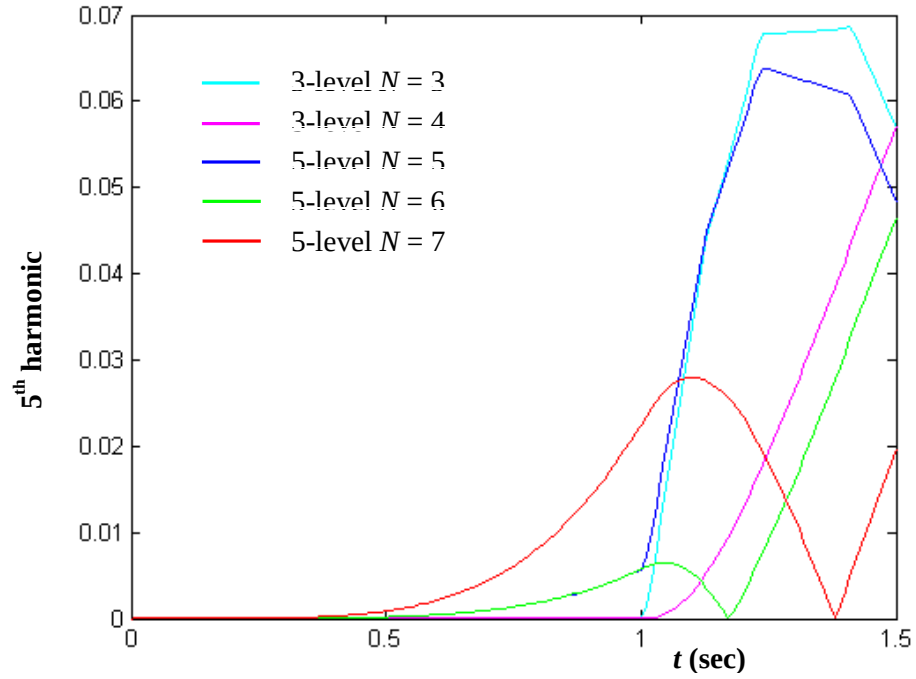

Fig. 5.11: Theoretical fifth harmonic component versus modulation index.

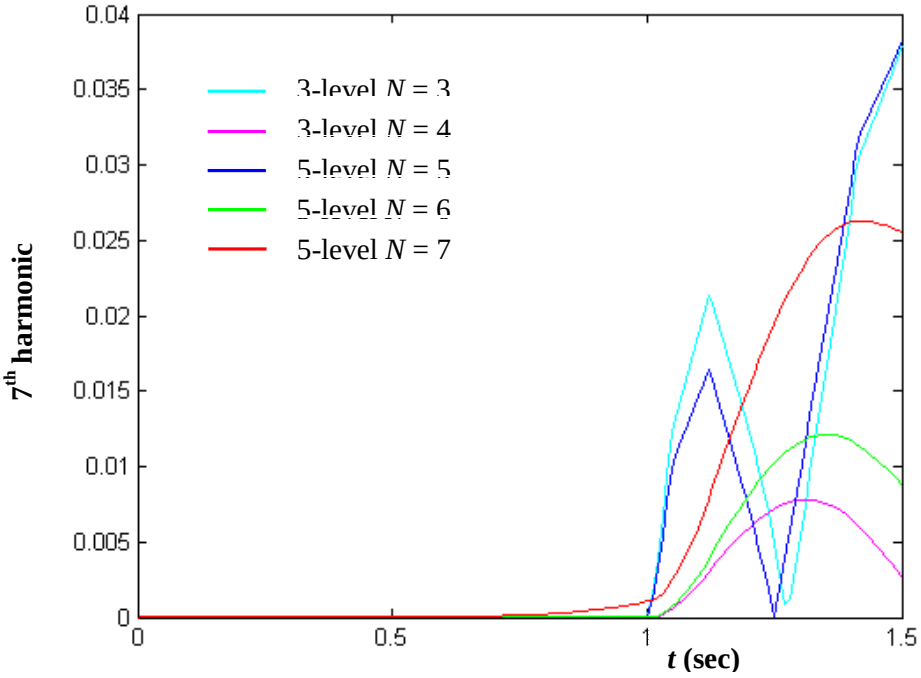

Fig. 5.12: Theoretical seventh harmonic component versus modulation index.

From Fig. 5.12 it can be seen that both WRPWM schemes operating with the value of *N* under consideration have negligible seventh harmonic content in the linear modulation region. In the

overmodulation region, both the three-level WRPWM scheme with $N = 4$ and the five-level WRPWM scheme operating with $N = 6$ give rise to fairly low seventh harmonic components.

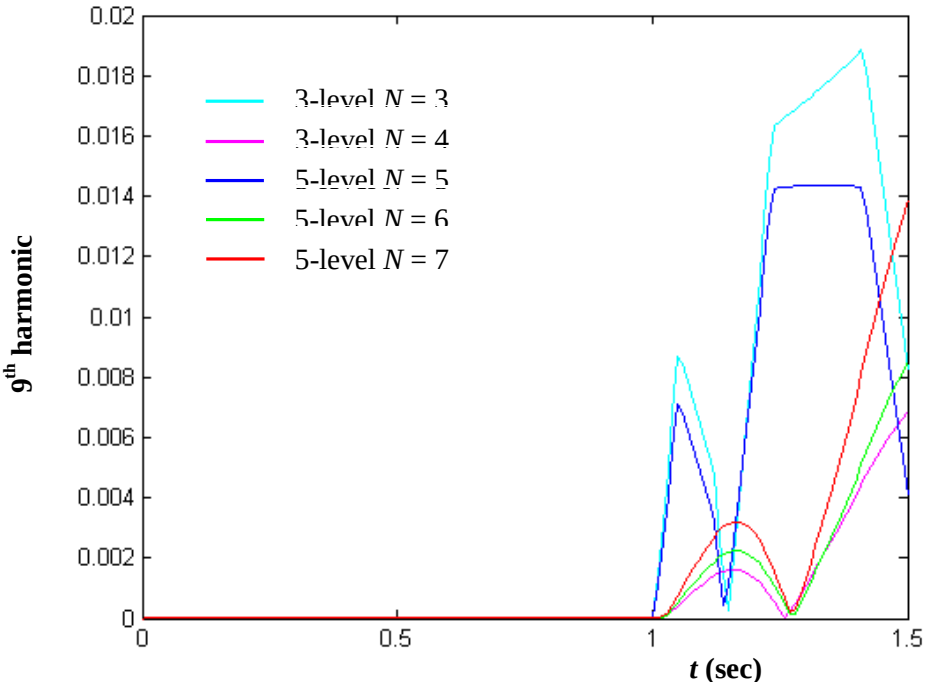

Fig. 5.13: Theoretical ninth harmonic component versus modulation index.

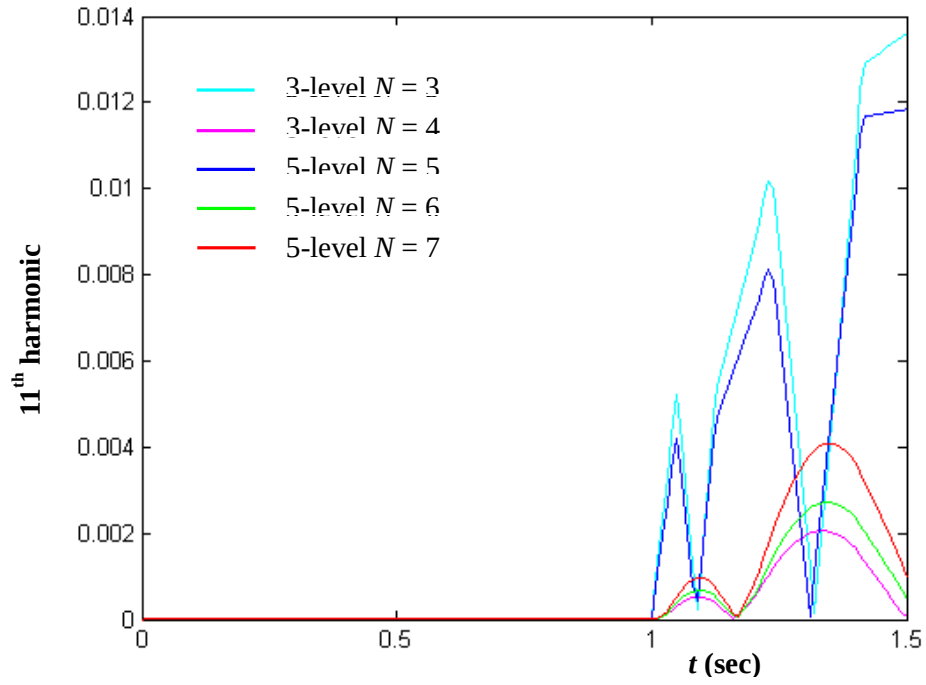

Fig. 5.14: Theoretical eleventh harmonic component versus modulation index.

In Figs. 5.13 and 5.14, both WRPWM schemes operating with the values of N under consideration have negligible ninth and eleventh harmonic content in the linear modulation region. In the overmodulation region, both the three-level WRPWM scheme operating with N = 4 and the five-level WRPWM scheme operating with N = 6 generate lower and similar ninth and eleventh harmonic components. Note that, as the level of inverter increases the number of comparisons necessary for the inverter to make switching decisions increases making the scheme more deterministic and hence the harmonics will increase.

From Figs. 5.9-5.14 and also from the above discussions the following conclusions can be drawn. In general, both the three-level WRPWM scheme operating with N = 4 and the five-level WRPWM scheme operating with N = 6 have the best fundamental and least harmonics components in the entire modulation region. The five-level WRPWM scheme operating with N = 6 has slightly higher seventh, ninth and eleventh harmonics than the three-level WRPWM scheme operating with N = 4 but can be considered as insignificant. The third harmonic content of the five-level WRPWM scheme operating with N = 6 is better than that of three-level WRPWM scheme operating with N = 4. However, the fifth harmonic content of the three-level WRPWM scheme operating with N = 4 is better than that of the five-level WRPWM scheme operating with N = 6. Thus, for lower power three-phase drive applications, the three-level WRPWM scheme operating with N = 4 is the better choice whereas the five-level WRPWM scheme operating with N = 6 is the better choice for high power single and three-phase applications.

5.3 Absence of Even Harmonics in Five-Level WRPWM Scheme

Fig. 5.15 shows the theoretical discrete harmonic spectra of the five-level WRPWM scheme (q = 2, N = 5 and m_a = 1) obtained by solving (4.36) and (4.47). It is interesting to see, that, similar to the three-level WRPWM scheme [4] all the even discrete harmonic components are absent from the spectrum. It can be proved mathematically that the even discrete harmonics are absent from the spectrum if α is an even number. Note that, for a sufficiently large α, the quantitative picture remains the same, i.e., even harmonic are very small.

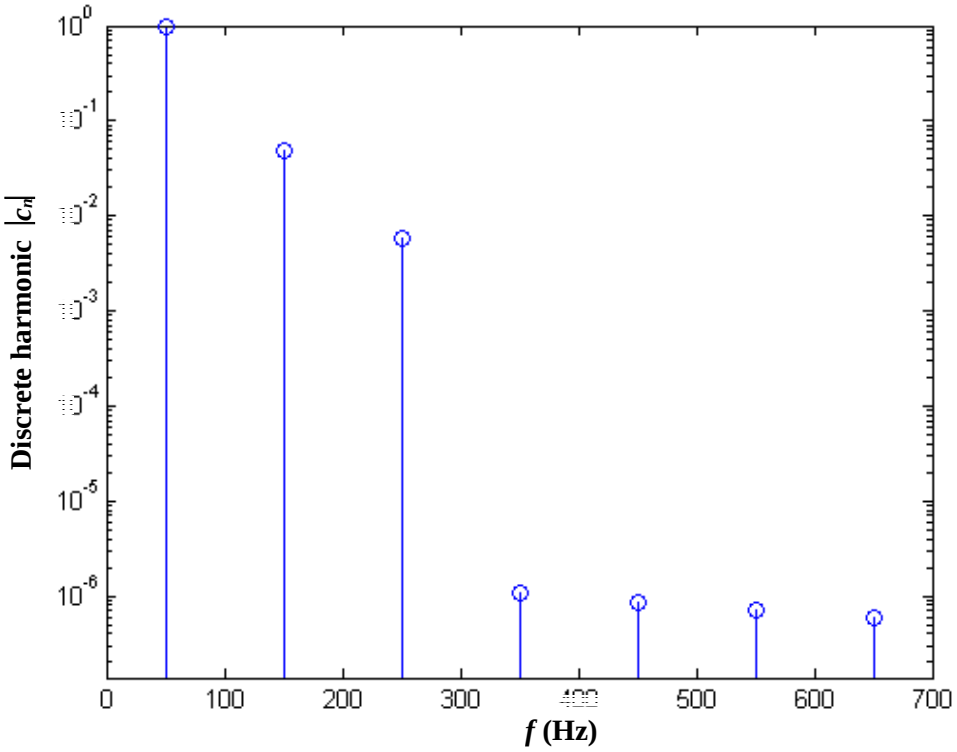

Fig. 5.15: The theoretical discrete spectra of five-level WRPWM (q = 2, N = 5 and m_a = 1).

A was previously mentioned $g(t)$ is a periodic signal with a period $1/f_r$ provided α is an integer. For a periodic signal $g(t)$, all even harmonics are absent if it is antisymmetric over its midway point in period, i.e., $g(t) + g(1 + 1/(2f_r)) = 0$. This is the case when α is an even number. To prove this a number of lemmas are needed [4]. These are derived following the same approach that was adopted in [4] for a three-level inverter.

Lemma 1:

$$F_{N,q}^{(1)}(x)+F_{N,q}^{(1)}(1-x)=F_{N,q}^{(5)}(x)+F_{N,q}^{(5)}(1-x)$$

Proof: For value of $x>1$ or $x<0$, the lemma can be seen to be true trivially as both sides of the equation equal one.

For $0 \le x \le 1$ and with reference to (4.9) the following expression is obtained

$$F_{N,q}^{(1)}(x)+F_{N,q}^{(1)}(1-x)=\sum_{m=\left\lfloor \frac{N}{2} \right\rfloor+q}^{N}\binom{N}{m}x^{m}(1-x)^{N-m}+\sum_{m=\left\lfloor \frac{N}{2} \right\rfloor+q}^{N}\binom{N}{m}(1-x)^{m}x^{N-m}. \quad (5.2)$$

By defining $\hat{m}=N-m$ and substituting into (5.2) and rearranging yields

$$F_{N,q}^{(1)}(x)+F_{N,q}^{(1)}(1-x)=\sum_{\hat{m}=\left\lfloor \frac{N}{2} \right\rfloor-q}^{0}\binom{N}{N-\hat{m}}x^{N-\hat{m}}(1-x)^{\hat{m}}+\sum_{\hat{m}=\left\lfloor \frac{N}{2} \right\rfloor-q}^{0}\binom{N}{N-\hat{m}}(1-x)^{N-\hat{m}}x^{\hat{m}}, \quad (5.3)$$

since $\binom{N}{N-\hat{m}}=\binom{N}{\hat{m}}$ and also with reference to (4.13), then (5.3) can be modified to yield

$$\begin{aligned}F_{N,q}^{(1)}(x)+F_{N,q}^{(1)}(1-x)&=\sum_{\hat{m}=0}^{\left\lfloor \frac{N}{2} \right\rfloor-q}\binom{N}{\hat{m}}x^{N-\hat{m}}(1-x)^{\hat{m}}+\sum_{\hat{m}=0}^{\left\lfloor \frac{N}{2} \right\rfloor-q}\binom{N}{\hat{m}}(1-x)^{N-\hat{m}}x^{\hat{m}}\\&=F_{N,q}^{(5)}(x)+F_{N,q}^{(5)}(1-x).\end{aligned}$$

Lemma 2:

$$F_{N,q}^{(2)}(x)+F_{N,q}^{(2)}(1-x)=F_{N,q}^{(4)}(x)+F_{N,q}^{(4)}(1-x)$$

proof: With reference to (4.10) the following expression is obtained

$$F_{N,q}^{(2)}(x)+F_{N,q}^{(2)}(1-x)=\sum_{m=\left\lfloor\frac{N}{2}\right\rfloor+1}^{\left\lceil\frac{N}{2}\right\rceil+q-1}\binom{N}{m}x^{m}(1-x)^{N-m}+\sum_{m=\left\lfloor\frac{N}{2}\right\rfloor+1}^{\left\lceil\frac{N}{2}\right\rceil+q-1}\binom{N}{m}(1-x)^{m}x^{N-m}$$
$$=\sum_{\hat{m}=\left\lfloor\frac{N}{2}\right\rfloor-1}^{\left\lfloor\frac{N}{2}\right\rfloor-q+1}\binom{N}{N-\hat{m}}x^{N-\hat{m}}(1-x)^{\hat{m}}+\sum_{\hat{m}=\left\lfloor\frac{N}{2}\right\rfloor-1}^{\left\lfloor\frac{N}{2}\right\rfloor-q+1}\binom{N}{N-\hat{m}}(1-x)^{N-\hat{m}}x^{\hat{m}}, \quad (5.4)$$

again since $\binom{N}{N-\hat{m}}=\binom{N}{\hat{m}}$ and also with reference to (4.12), then (5.4) can be modified to yield

$$F_{N,q}^{(2)}(x)+F_{N,q}^{(2)}(1-x)=\sum_{\hat{m}=\left\lfloor\frac{N}{2}\right\rfloor-q+1}^{\left\lfloor\frac{N}{2}\right\rfloor-1}\binom{N}{\hat{m}}x^{N-\hat{m}}(1-x)^{\hat{m}}+\sum_{\hat{m}=\left\lceil\frac{N}{2}\right\rceil-q+1}^{\left\lceil\frac{N}{2}\right\rceil-1}\binom{N}{\hat{m}}(1-x)^{N-\hat{m}}x^{\hat{m}}$$
$$=F_{N,q}^{(4)}(x)+F_{N,q}^{(4)}(1-x).$$

Lemma 3:

$$r\left(t+\frac{1}{2f_r}\right)=1-r(t)$$

proof: Modifying the sinusoidal reference signal defined previously (see section 4.2.1) to yield

$$r\left(t+\frac{1}{2f_r}\right)=0.5\left[1+m\sin\left(2\pi f_r\left(t+\frac{1}{2f_r}\right)\right)\right]$$
$$=0.5[1+m\sin(2\pi f_r t+\pi)]$$
$$=0.5[1-m\sin(2\pi f_r t)]$$

and

$$1-r(t)=1-0.5[1+m\sin(2\pi f_r t)]$$
$$=1-0.5-0.5m\sin(2\pi f_r t)$$
$$=0.5-0.5m\sin(2\pi f_r t)$$
$$=0.5[1-m\sin(2\pi f_r t)].$$

Therefore

$$r\left(t+\frac{1}{2f_r}\right)=1-r(t).$$

Making use of the above three lemmas and also with reference to (4.2.7), it is possible to prove that $g(t)+g\left(t+\frac{1}{2f_r}\right)=0$

Proof:

$$\begin{aligned}
&g(t)+g\left(t+\frac{1}{2f_r}\right)\\
&=A\left[2F_{N,q}^{(1)}\left(r\left(\left\lfloor\frac{t}{T}\right\rfloor T\right)\right)+F_{N,q}^{(2)}\left(r\left(\left\lfloor\frac{t}{T}\right\rfloor T\right)\right)-F_{N,q}^{(4)}\left(r\left(\left\lfloor\frac{t}{T}\right\rfloor T\right)\right)-2F_{N,q}^{(5)}\left(r\left(\left\lfloor\frac{t}{T}\right\rfloor T\right)\right)\right]\\
&+A\left[2F_{N,q}^{(1)}\left(r\left(\left\lfloor\frac{t+\frac{1}{2f_r}}{T}\right\rfloor T\right)\right)+F_{N,q}^{(2)}\left(r\left(\left\lfloor\frac{t+\frac{1}{2f_r}}{T}\right\rfloor T\right)\right)-F_{N,q}^{(4)}\left(r\left(\left\lfloor\frac{t+\frac{1}{2f_r}}{T}\right\rfloor T\right)\right)\right.\\
&\left.-2F_{N,q}^{(5)}\left(r\left(\left\lfloor\frac{t+\frac{1}{2f_r}}{T}\right\rfloor T\right)\right)\right],
\end{aligned}\tag{5.5}$$

since α is an even integer, so is $\frac{1/(2f_r)}{T}$. Therefore (5.5) becomes

$$
\begin{aligned}
&g(t)+g\left(t+\frac{1}{2f_r}\right)\\
&=A\left[2F_{N,q}^{(1)}\left(r\left(\left\lfloor\frac{t}{T}\right\rfloor T\right)\right)+F_{N,q}^{(2)}\left(r\left(\left\lfloor\frac{t}{T}\right\rfloor T\right)\right)-F_{N,q}^{(4)}\left(r\left(\left\lfloor\frac{t}{T}\right\rfloor T\right)\right)-2F_{N,q}^{(5)}\left(r\left(\left\lfloor\frac{t}{T}\right\rfloor T\right)\right)\right]\\
&+A\left[2F_{N,q}^{(1)}\left(r\left(\frac{1}{2f_r}+\left\lfloor\frac{t}{T}\right\rfloor T\right)\right)+F_{N,q}^{(2)}\left(r\left(\frac{1}{2f_r}+\left\lfloor\frac{t}{T}\right\rfloor T\right)\right)-F_{N,q}^{(4)}\left(r\left(\frac{1}{2f_r}+\left\lfloor\frac{t}{T}\right\rfloor T\right)\right)\right.\\
&\left.-2F_{N,q}^{(5)}\left(r\left(\frac{1}{2f_r}+\left\lfloor\frac{t}{T}\right\rfloor T\right)\right)\right]\\
&=A\left[2F_{N,q}^{(1)}\left(r\left(\left\lfloor\frac{t}{T}\right\rfloor T\right)\right)+F_{N,q}^{(2)}\left(r\left(\left\lfloor\frac{t}{T}\right\rfloor T\right)\right)-F_{N,q}^{(4)}\left(r\left(\left\lfloor\frac{t}{T}\right\rfloor T\right)\right)-2F_{N,q}^{(5)}\left(r\left(\left\lfloor\frac{t}{T}\right\rfloor T\right)\right)\right]\\
&+A\left[2F_{N,q}^{(1)}\left(1-r\left(\left\lfloor\frac{t}{T}\right\rfloor T\right)\right)+F_{N,q}^{(2)}\left(1-r\left(\left\lfloor\frac{t}{T}\right\rfloor T\right)\right)-F_{N,q}^{(4)}\left(1-r\left(\left\lfloor\frac{t}{T}\right\rfloor T\right)\right)-2F_{N,q}^{(5)}\left(1-r\left(\left\lfloor\frac{t}{T}\right\rfloor T\right)\right)\right]\\
&=A\left[2F_{N,q}^{(1)}\left(r\left(\left\lfloor\frac{t}{T}\right\rfloor T\right)\right)+2F_{N,q}^{(1)}\left(1-r\left(\left\lfloor\frac{t}{T}\right\rfloor T\right)\right)-2F_{N,q}^{(5)}\left(r\left(\left\lfloor\frac{t}{T}\right\rfloor T\right)\right)-2F_{N,q}^{(5)}\left(1-r\left(\left\lfloor\frac{t}{T}\right\rfloor T\right)\right)\right]\\
&+A\left[F_{N,q}^{(2)}\left(r\left(\left\lfloor\frac{t}{T}\right\rfloor T\right)\right)+F_{N,q}^{(2)}\left(1-r\left(\left\lfloor\frac{t}{T}\right\rfloor T\right)\right)-F_{N,q}^{(4)}\left(r\left(\left\lfloor\frac{t}{T}\right\rfloor T\right)\right)-F_{N,q}^{(4)}\left(1-r\left(\left\lfloor\frac{t}{T}\right\rfloor T\right)\right)\right]\\
&=A[0]+A[0]\\
&=0,
\end{aligned}
$$

which shows that $g(t)$ is antisymmetric over its midway point period. This explains the reason for the absence of any even discrete harmonics.

5.4 Comparison of the Five-Level WRPWM and Five-Level SH-PWM Schemes

To illustrate how the five-level WRPWM improves the harmonic content, the five-level SH-PWM scheme with PD disposition strategy [51,52] is used for comparison. Fig. 5.16 shows the voltage spectrum of the five-level WRPWM with N = 5. For comparison purposes the voltage spectrum of the five-level SH-PWM scheme with PD disposition strategy shown in Fig. 3.14 is again plotted in Fig. 5.17.

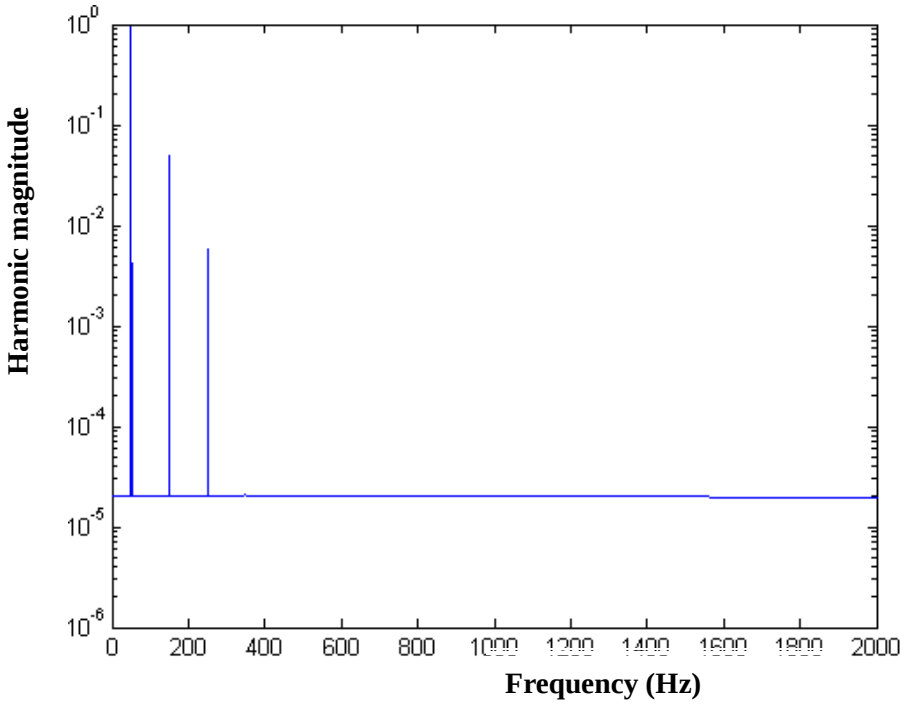

Fig.5.16: Voltage spectrum of five-level WRPWM scheme with *N* = 5.

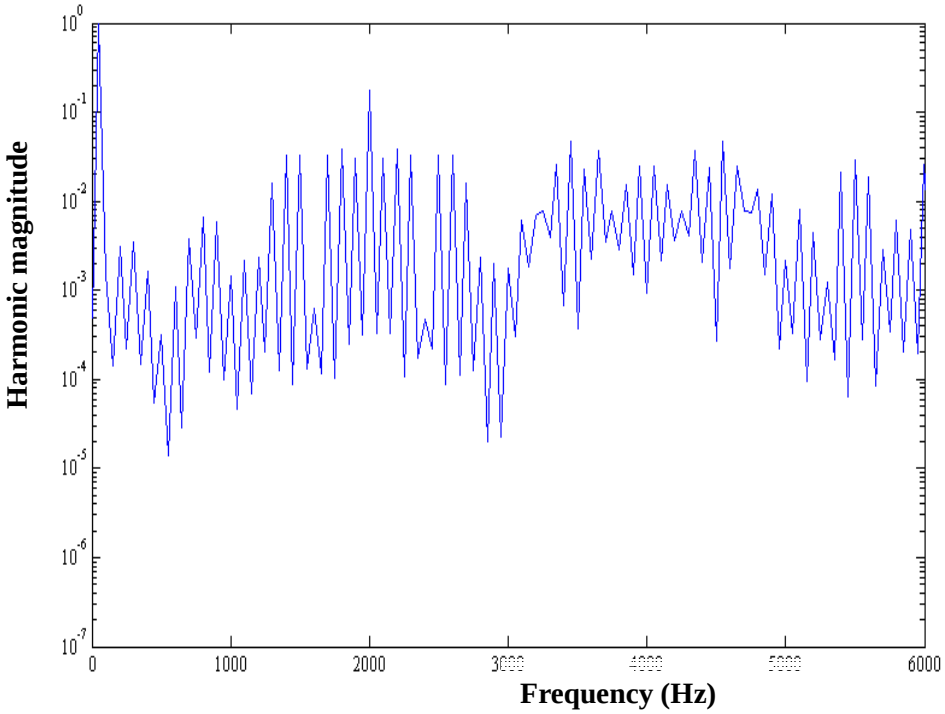

Fig.5.17: Five-level PD PWM phase leg voltage spectrum.

From Fig. 5.16 it can be seen that due to the random nature of the switching, the harmonic components of the five-level WRPWM scheme are spread over the spectrum to form a continuous spectrum and the discrete harmonic components are reduced. In the case of the five-level SH-PWM scheme in Fig. 5.17, it can be seen that the spectrum consists of components at the fundamental frequency, odd multiples of carrier frequency and sidebands about the even multiple carrier frequency, odd multiple fundamental frequency, odd multiple carrier frequency and even multiple fundamental frequency.

From Figs. 5.16 and 5.17 it can be seen that the magnitudes of the fundamental components of the five-level WRPWM scheme and the five-level PD PWM scheme are approximately the same. However, the largest harmonic of the WRPWM scheme is smaller than that of the PD PWM scheme. Moreover, for the five-level WRPWM scheme, except for the third and fifth harmonics, the rest of the harmonics are significantly smaller than most of the harmonics of the five-level PD PWM scheme.

Thus, from the above discussions it can be said that the five-level WRPWM scheme has better harmonic content than the five-level SH-PWM scheme. Since the five-level WRPWM scheme not only significantly improves the harmonic content it also provides approximately the same fundamental component as the five-level PD PWM.

5.5 Noise Analysis of WRPWM Scheme

The study of noise power is the major focus of this section. Effects of various parameters on the noise power (P_{noise}) are investigated. In chapter 4, the power spectrum density (4.49) was derived. The first term of (4.49) represents the discrete component spectra and the second term represents the general noise level. A typical plot of the general noise ($S_2(f)$ / ($T \times d_{av}$)) from (4.48) is shown in Fig. 5.18.

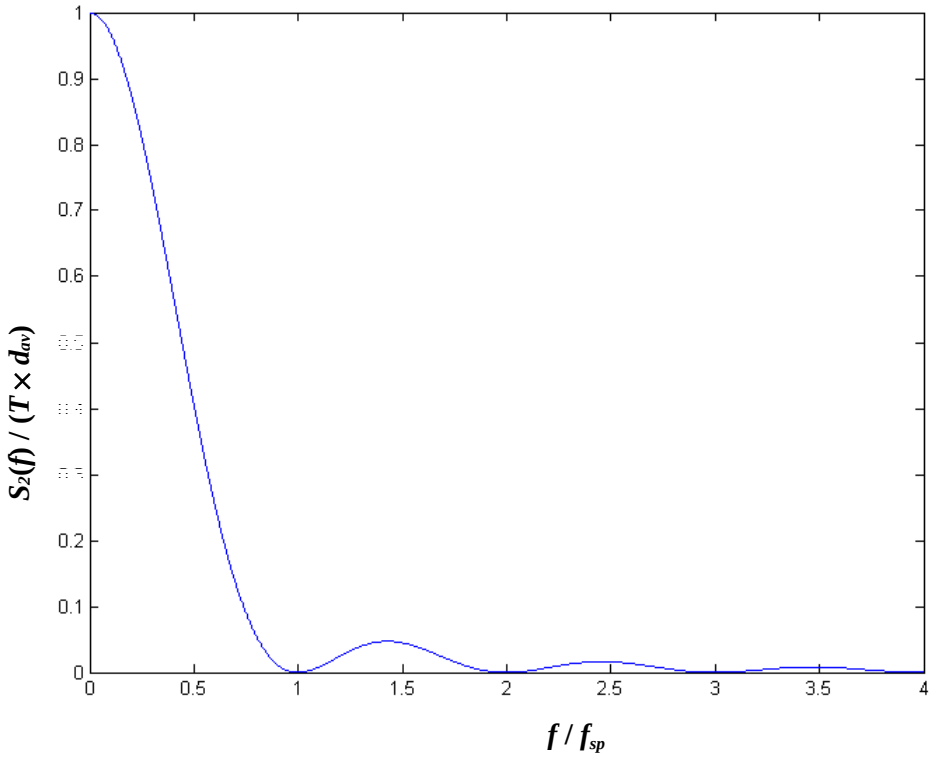

Fig. 5.18: Plot of general noise level.

The total expected power of the WRPWM signal $P_{k(t)}$ is obtained as

$$\begin{aligned} P_{k(t)} &= \int_{-\infty}^{\infty} S_k(f)df \\ &= \sum_{n=-\infty}^{\infty} |c_n|^2 + d_{av}. \end{aligned} \tag{5.6}$$

From Parseval's theorem [16], an expression for the first term on the right hand side of (5.6) is obtained as

$$\sum_{n=-\infty}^{\infty} |c_n|^2 = f_r \int_0^{1/f_r} |g(t)|^2 dt \tag{5.7}$$

and from (4.19), (4.27) and (4.28), it is clear that $d(t) = U_1 - |g(t)|^2$. Therefore (5.7) can be re-written as

$$\begin{aligned} f_r \int_0^{1/f_r} |g(t)|^2 dt &= f_r \int_0^{1/f_r} (U_1 - d(t)) dt \\ &= f_r \int_0^{1/f_r} U_1 dt - d_{av} \\ &= P_{k(t)} - d_{av}, \end{aligned} \tag{5.8}$$

and from(5.8) an expression for d_{av} is

$$d_{av} = f_r \int_0^{1/f_r} \left(U_1 - |g(t)|^2\right) dt, \tag{5.9}$$

where $P_{k(t)}$ is the average total expected power of $k(t)$ (as it should be since $R(0) = E\{k(t)\ k(t)\} = U_1$).

For the sake of simplicity, it is necessary to make a certain assumption. In most of the applications, the WRPWM signal will be low pass filtered (e.g., by the machine dynamics). The effect of power spectrum on the system can therefore be approximated by passing $S_k(f)$ through an ideal low pass filter (e.g., by the machine dynamics). The approximation does not change the qualitative dependence of the noise on various parameters. For the sake of theoretical investigation, f_r is chosen as 50Hz, A = 1 V (which will result in normalized output voltage e.g., the maximum amplitude of the output voltage is $2A$ = 2 V), and an ideal low pass filter with a cut off frequency 2 kHz (i.e., up to 40th harmonic for a 50 Hz system, this is to reduce the PC calculation time and still keep good approximation of the actual result, since the harmonics after that should be negligible). This implies that the noise power (P_{noise}) in the filtered signal obtained by integrating $S_k(f)$ over the filter pass band consists of two parts corresponding to the discrete spectrum ($P_{1,noise}$) and continuous spectrum ($P_{2,noise}$), respectively. In particular

$$P_{noise} = P_{1,noise} + P_{2,noise}, \tag{5.10}$$

where the first term on the right hand side of (5.10) is given by

$$P_{1,noise} = 2\sum_{n=2}^{40} |c_n|^2 + |c_0|^2 \tag{5.11}$$

and the second term on the right hand side of (5.10) is obtained as

$$P_{2,noise} = 2\int_0^{2000} S_2(f)df = 2d_{av}\int_0^{2000/f_{sp}} \sin c^2(y)dy. \quad (5.12)$$

The factor of 2 in (5.12) accounts for negative frequencies, namely, $S_k(-f) = S_k(f)$. As mentioned previously $g(t)$ is a periodic signal of period $1/f_r$ and has a staircase appearance with a number of stairs in a period equal to α. As discrete spectrum consists of Fourier series coefficients of $g(t)$, it is virtually independent of f_{sp} as long as α is large enough (typically ≥ 100) [5]. So the discrete noise component $P_{1,noise}$ is virtually independent of f_{sp} (which will be confirmed later experimentally). By the same argument the signal power (i.e., the fundamental component) is virtually independent of f_{sp} as well. Fig. 5.19 shows the plots of normalized signal power (i.e., $2|c_1|^2 / (V_d / 2)^2$) versus f_{sp}. Figs. 20 and 21 show the plots of ratio of discrete noise and continuous noise power as a percentage of signal power. The effects of various parameters on the noise power are discussed in the sections that follow.

5.5.1 The Effect of the Sampling Frequency

As already mentioned, the signal power and the discrete noise power are virtually independent of f_{sp} for $\alpha \geq 100$. This is evident from Figs. 5.19 and 5.20. Note that U_1 is virtually independent of f_{sp} as well since it consists of four probability distribution functions that are independent of f_{sp}. Since both $g(t)$ and U_1 are virtually independent of f_{sp}, and d_{av} is the average value of the signal $U_1 - |g(t)|^2$, d_{av} is also virtually independent of f_{sp}. Consequently, from (5.6), $P_{2,noise}$ is directly proportional to the area under the $sinc^2(y)$ curve in the range of $[0, (2000/f_{sp})]$. As f_{sp} increases, this area decreases due to reducing range, thus, $P_{2,noise}$ decreases as f_{sp} increases. Furthermore, if f_{sp} is large enough ($f_{sp} >>$ 2kHz), then $sinc^2(y) \approx 1$ in the range of integration and thus $P_{2,noise} \propto 1/f_{sp}$. Typical plots of $P_{2,noise}$ versus f_{sp} are shown in Fig. 5.21, which proves the inverse relationship of $P_{2,noise}$ and f_{sp}. Notice that for a reference frequency of f_r = 50 Hz, the reduction in $P_{2,noise}$ is insignificant for f_{sp} exceeding 30 kHz. So even if the digital signal processor (DSP) and the hardware are capable of operating at f_{sp} over 30 kHz, the comparative gain in $P_{2,noise}$ is insignificant. On the other hand, the increase in switching losses due to an increase in switching frequency may wipe out any marginal gains in the reduction of $P_{2,noise}$. Additionally, note that $P_{1,noise}$ is significantly lower than $P_{2,noise}$ especially at low values of f_{sp}. Thus, it is desirable not to operate at sampling frequencies exceeding 30 kHz for a fundamental output frequency of 50 Hz.

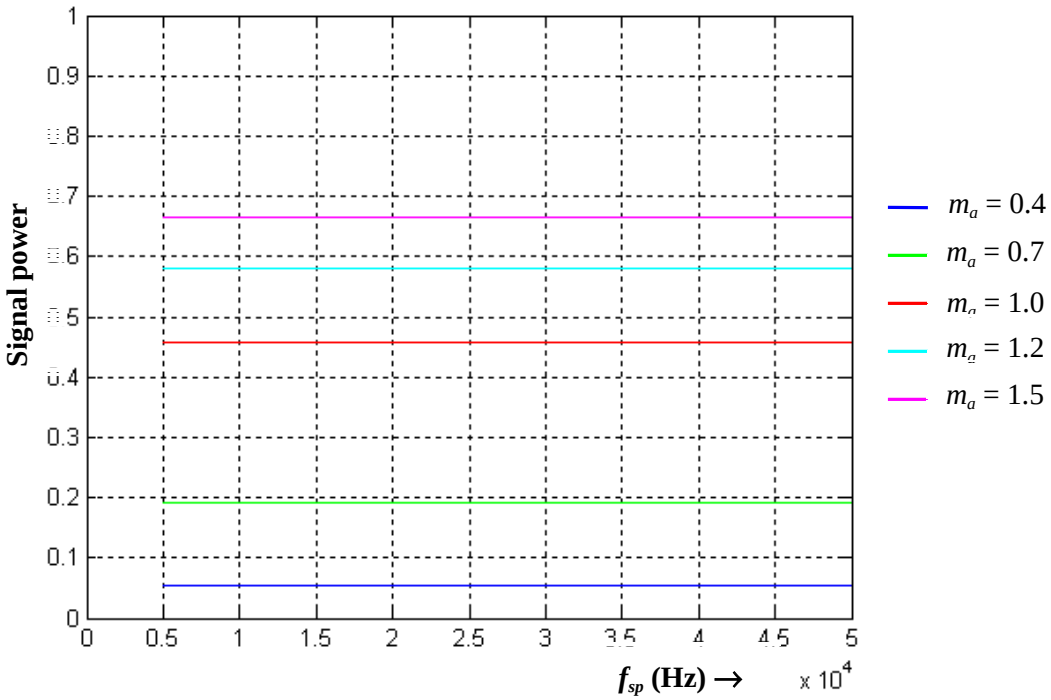

(a)

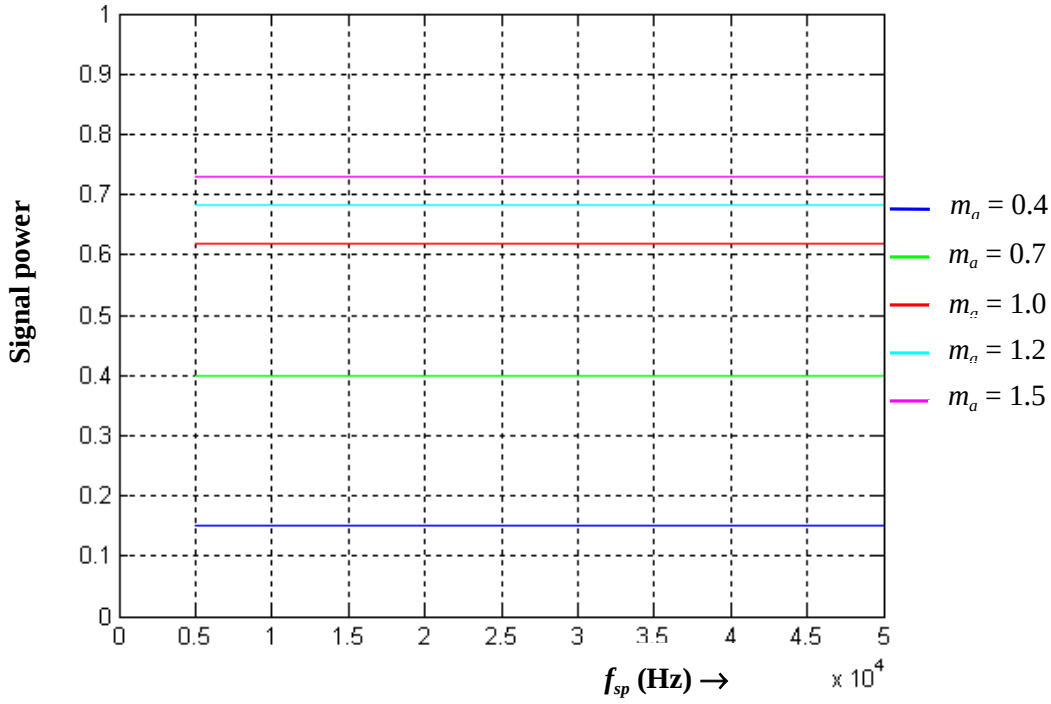

(b)

Fig. 5.19: Theoretical signal power ($2|c_1|^2$) versus f_{sp} (a) WRPWM with N = 5. (b) WRPWM with N = 6.

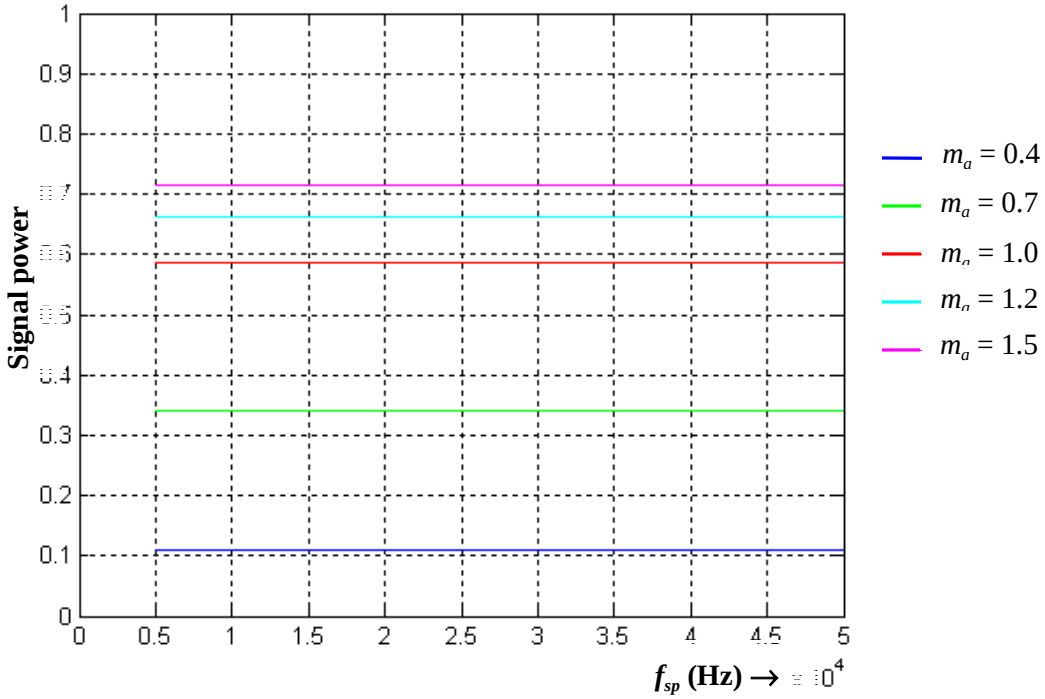

(c)

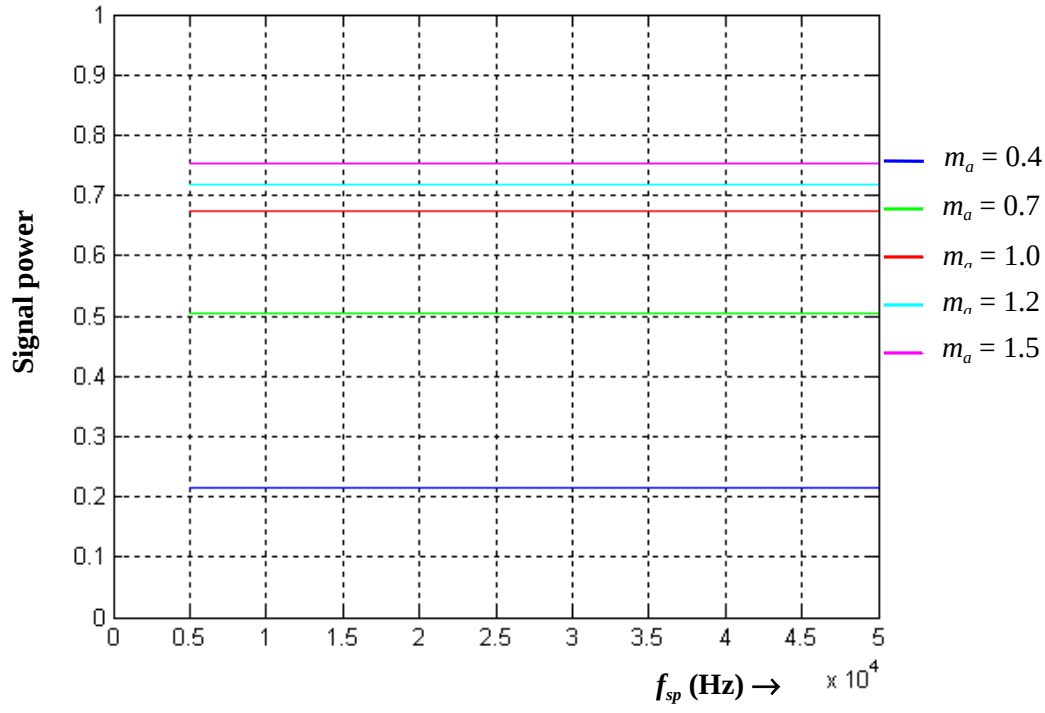

(d)

Fig. 5.19: (Continued) (c) WRPWM with *N* = 7. (d) WRPWM with *N* = 8.

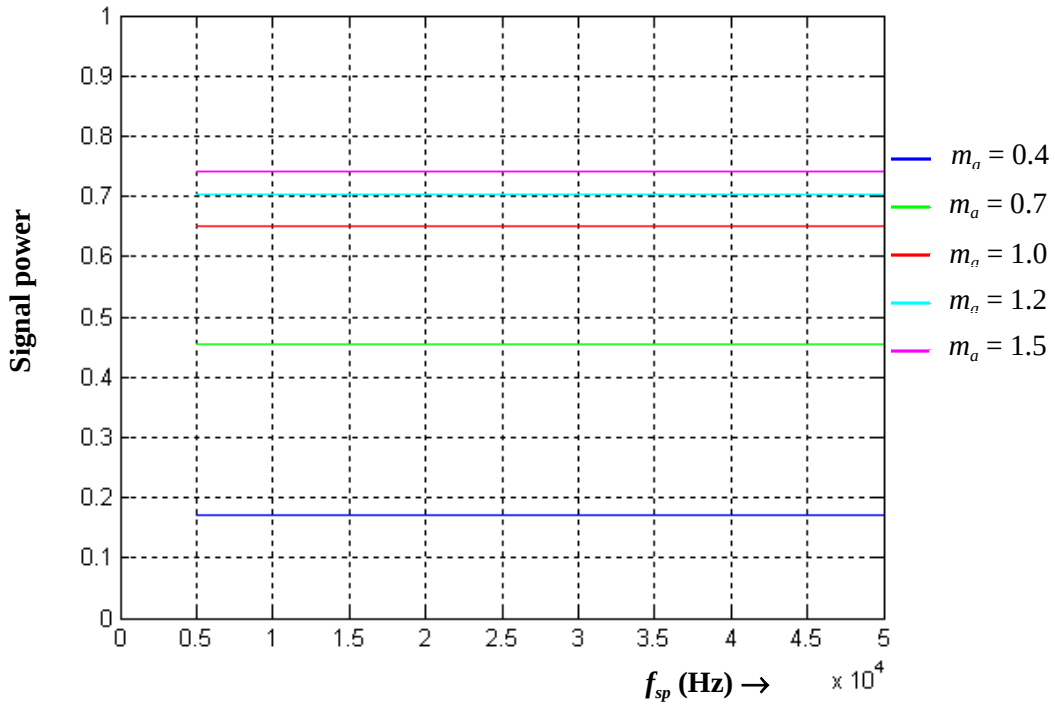

(e)

Fig. 5.19: (continued) (e) WRPWM with N = 9.

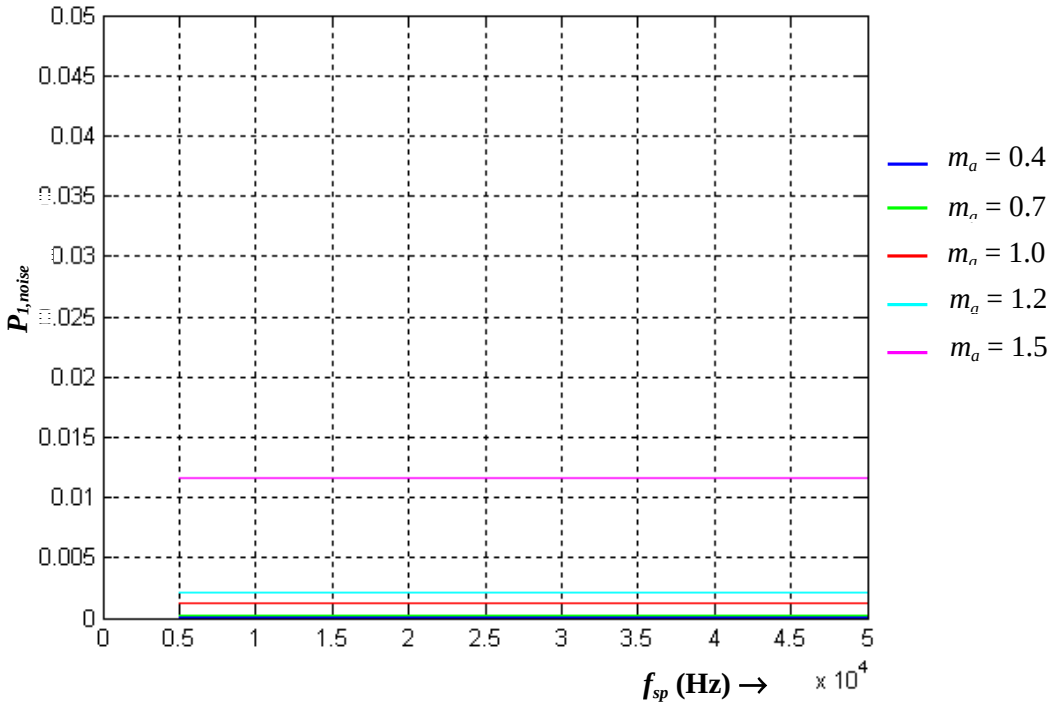

(a)

Fig. 5.20: Theoretical discrete noise ($P_{1,noise}$) power versus f_{sp} (a) WRPWM with N = 5.

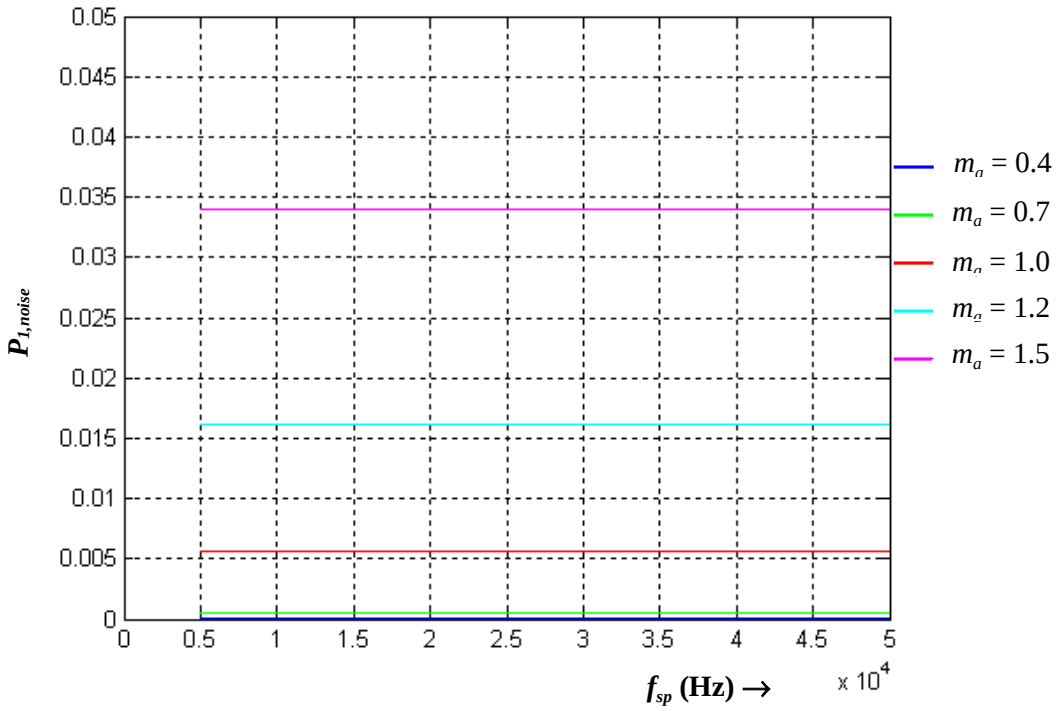

(b)

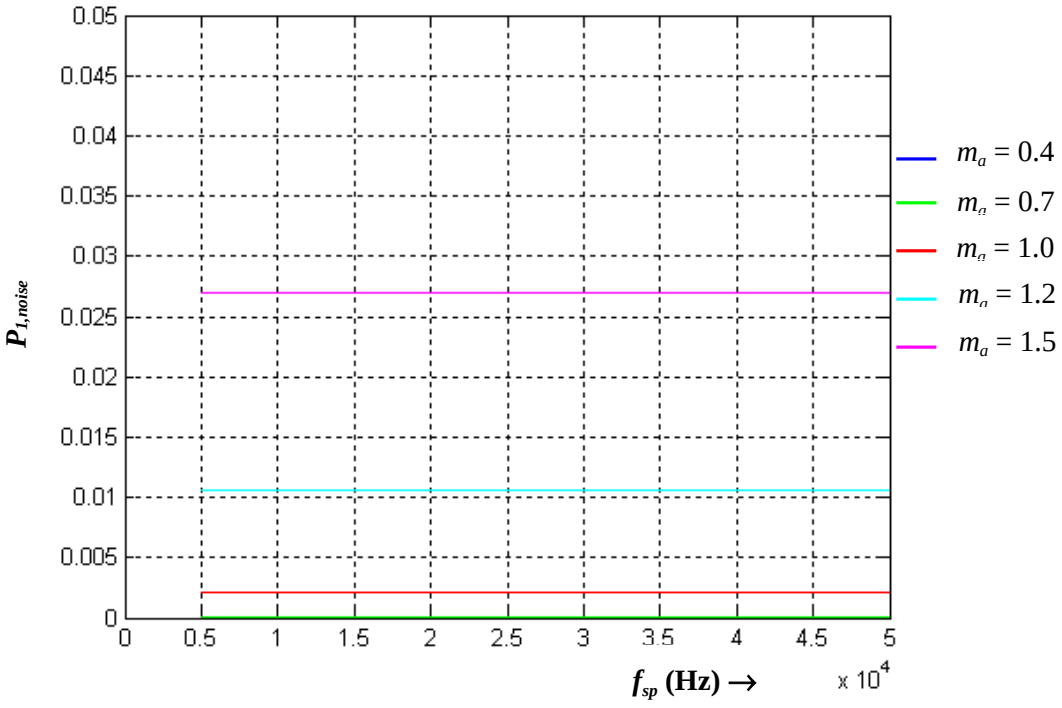

(c)

Fig. 5.20: Theoretical discrete noise ($P_{1,noise}$) power versus f_{sp} (b) WRPWM with N = 6. (c) WRPWM with N = 7.

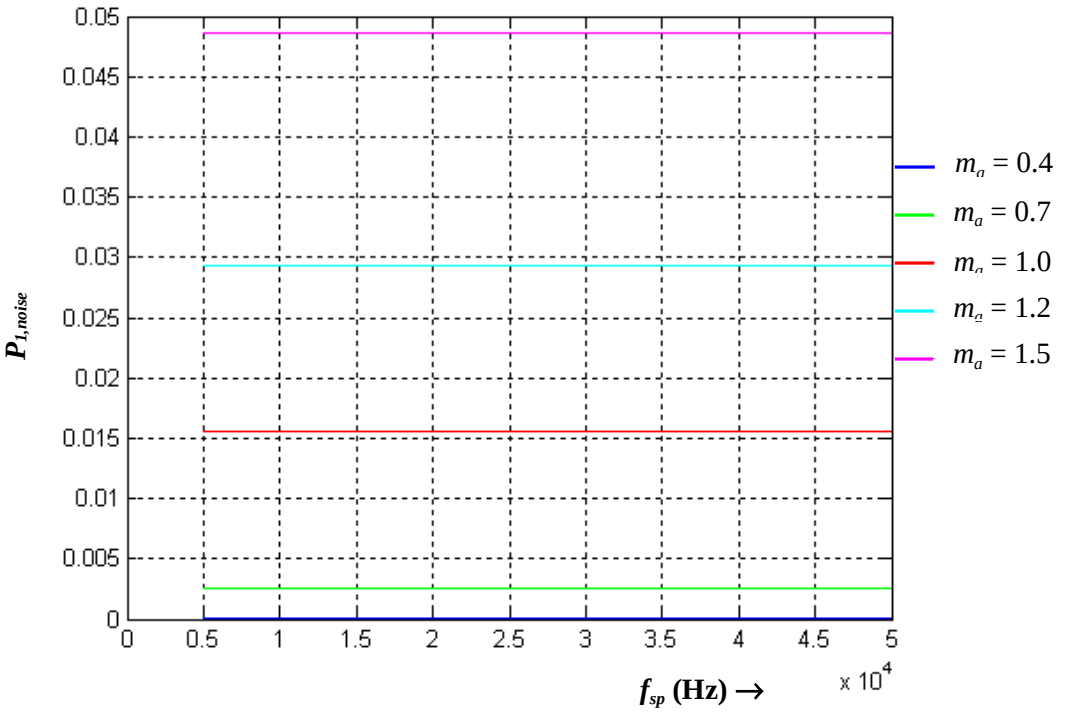

(d)

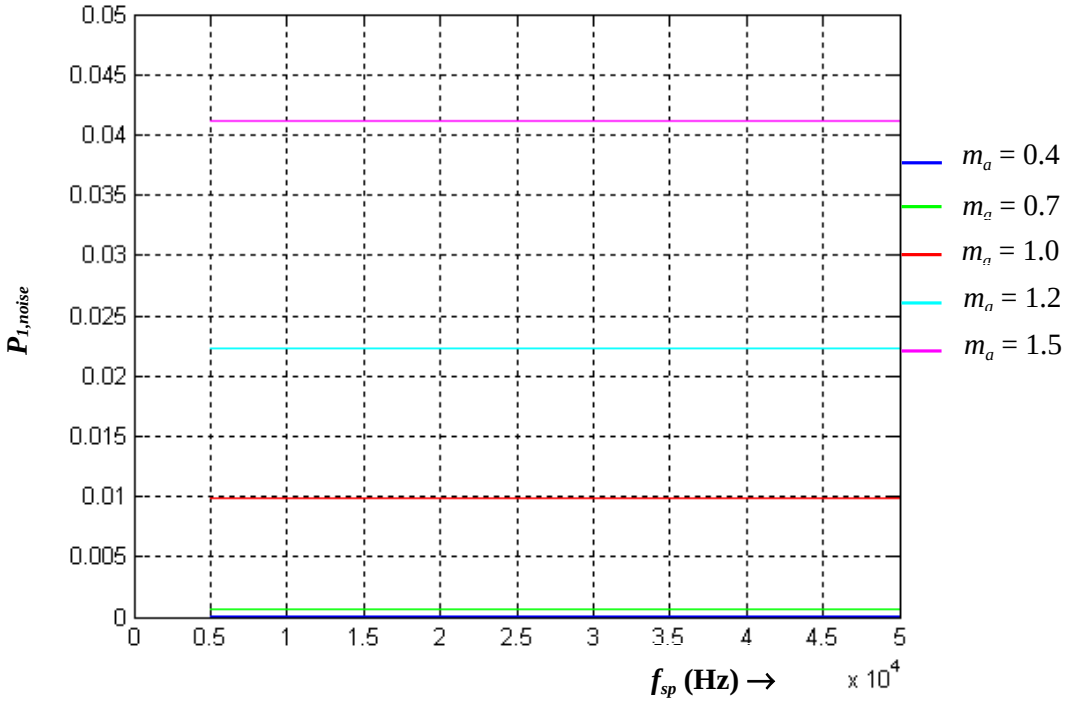

(e)

Fig. 5.20: (continued) (d) WRPWM with N = 8. (e) WRPWM with N = 9.

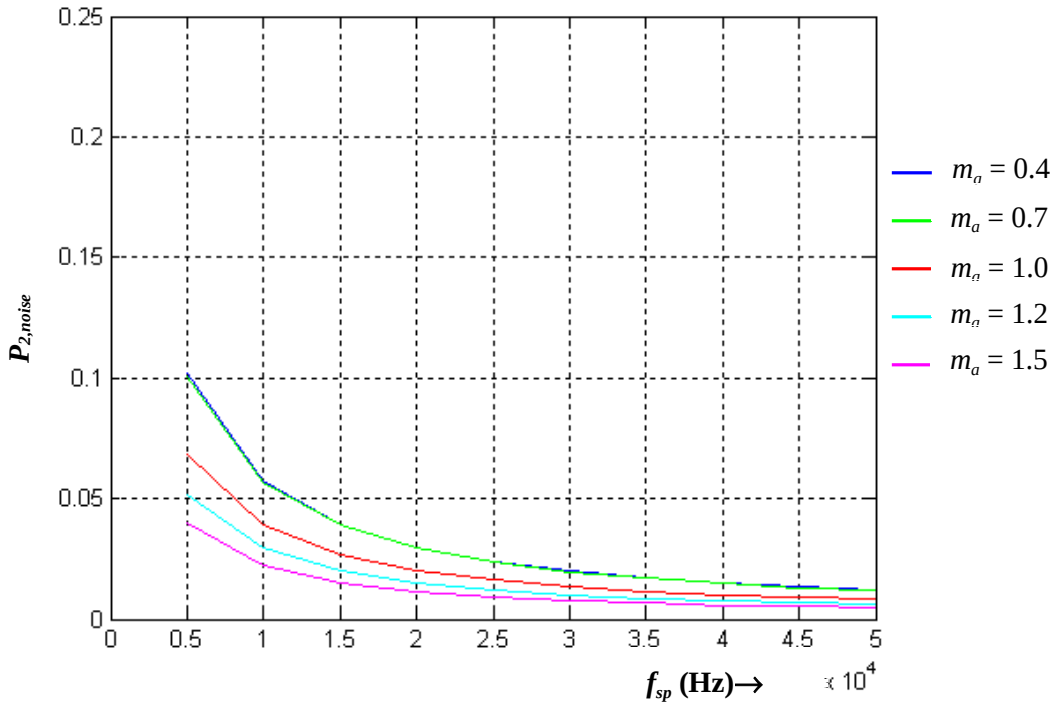

(a)

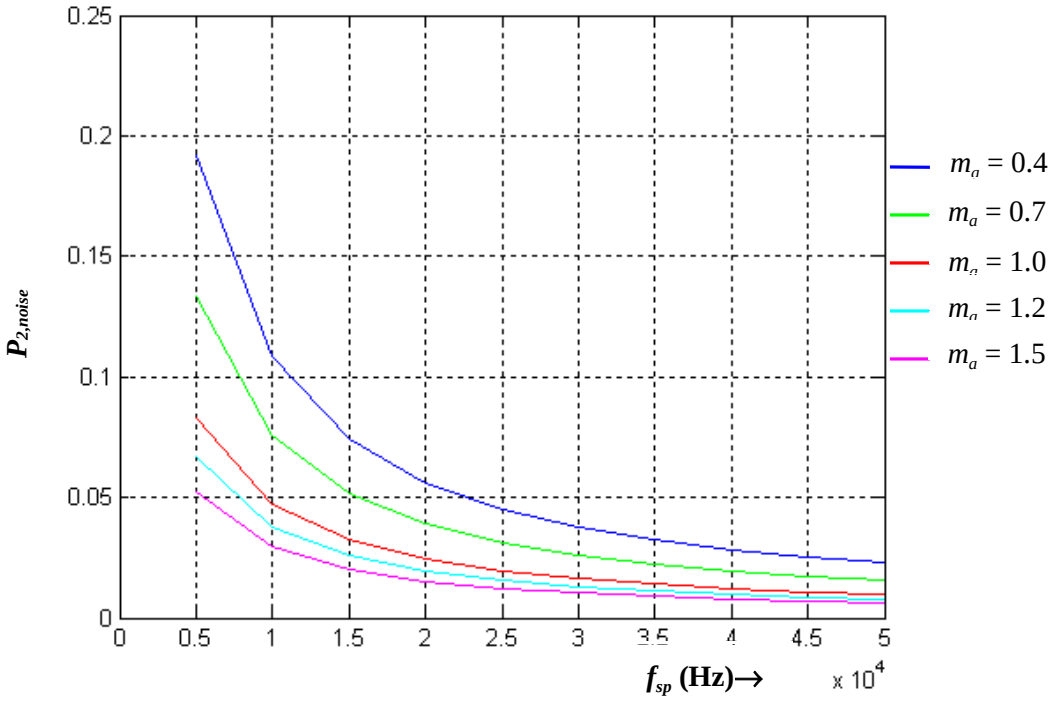

(b)

Fig. 5.21: Theoretical continuous noise ($P_{2,noise}$) power versus f_{sp} (a) WRPWM with N = 5. (b) WRPWM with N = 6.

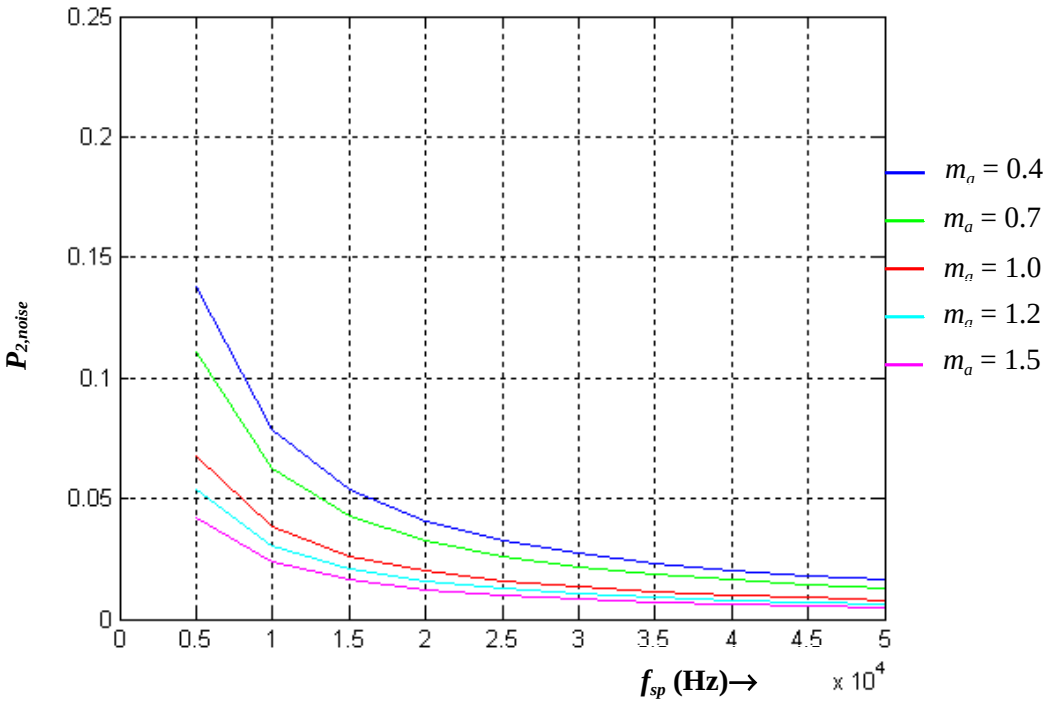

(c)

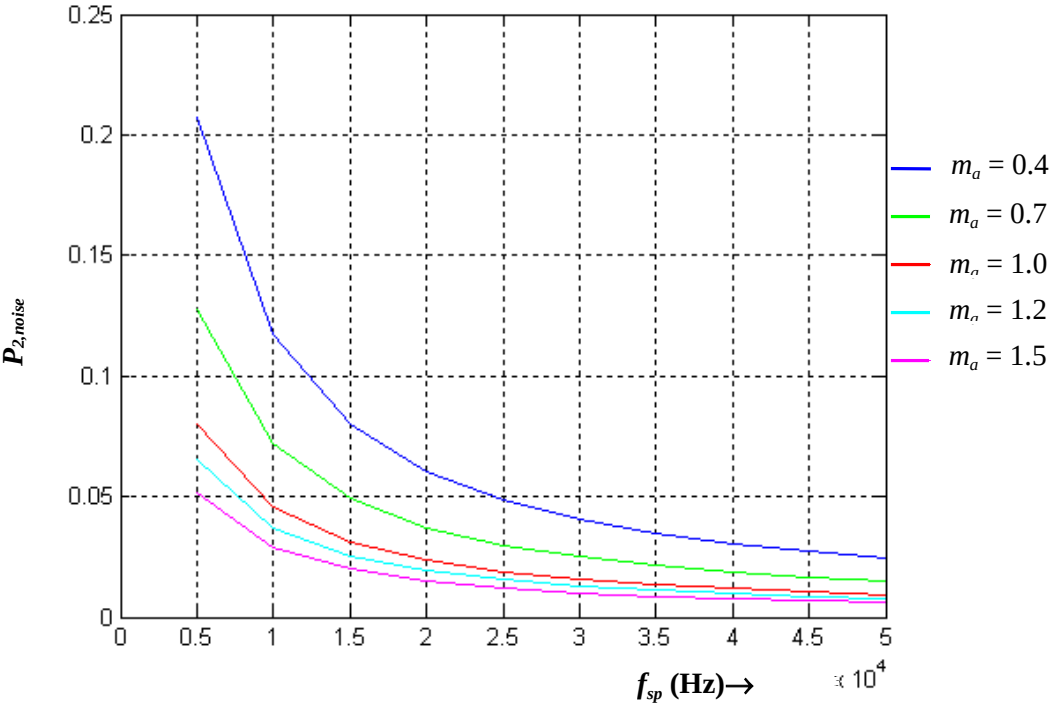

(d)

Fig. 5.21: (continued) (c) WRPWM with N = 7. (d) WRPWM with N = 8.

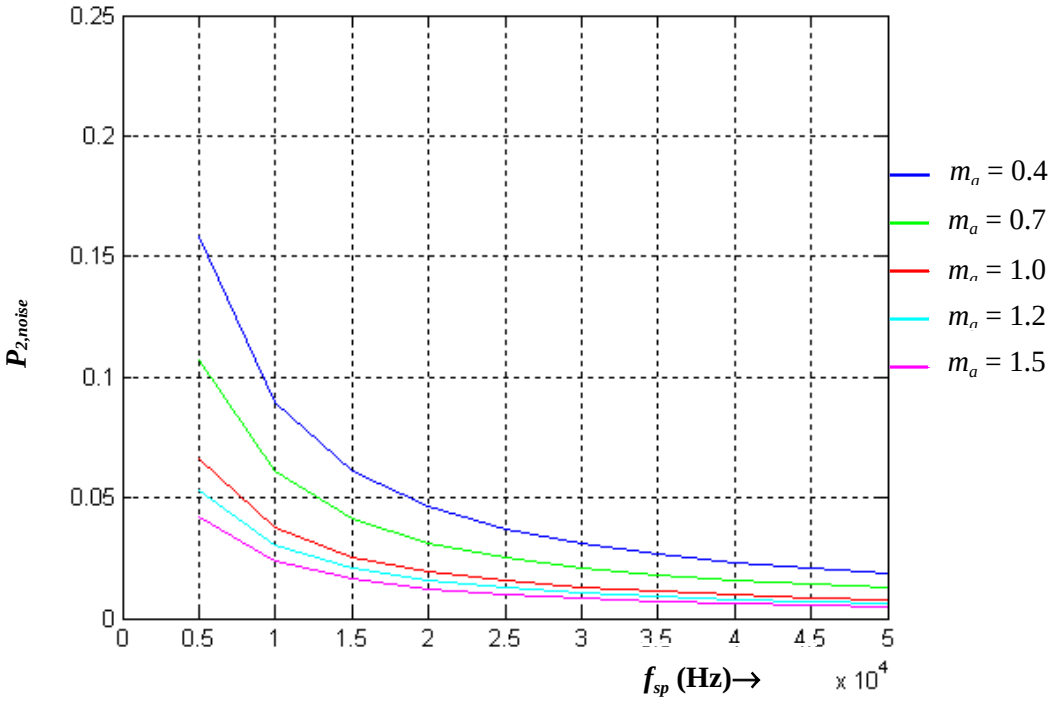

(e)

Fig. 5.21: (continued) (e) WRPWM with N = 9.

5.5.2 The Effect of Modulation Index

From (4.9) to (4.13), (4.27), and Figs. 5.2 and 5.22, it can be observed that as modulation index m_a increases $g(t)$ becomes more and more square wave like function (especially for N > 5 or m_a >1). Moreover, from Fig. 5.23, it can be seen that as modulation index m_a increases the average of U_1 over one fundamental period increases as well. This results in an increasing value of the fundamental component $|c_1|$ as m_a increases. From Fig.5.20 it can be seen that as the modulation index increases, the discrete noise power increases too. Note that for large values of m_a, $g(t)$ approaches a square wave and by using the mean square error (MSE) the approximated value of $P_{1,noise}$ can be found. The mean square error is obtained as [15]

$$MSE = \frac{1}{2\pi}\left(\int_0^{2\pi} g^2(t)dt - c_1^2 k_1 - c_2^2 k_1 - \cdots \right), \tag{5.13}$$

where $k_1 = k_2 = \ldots = \pi$ in this case. Thus the mean square error is

$$MSE = \frac{1}{2\pi}\left[2\pi - \pi\left(c_1^2 + c_2^2 + \cdots\right)\right]$$
$$= 1 - \frac{1}{2}\left(c_1^2 + c_2^2 + \cdots\right),$$

where c_n's equal $2A \times 4/\pi n$ for odd n and 0 for even n [15]. Thus, if $n = 1$ (the fundamental component), the mean square error is

$$MSE = 1 - \frac{1}{2}\left(\frac{2A \times 4}{\pi}\right)^2 \approx 0.19(2A)^2. \tag{5.14}$$

Hence, for large values of m_a, $P_{1,noise}$ will approach $0.19(2A)^2$. As for the continuous noise power $P_{2,noise}$, note that the rate of increase with m_a for the average of $|g(t)|^2$ over one fundamental period is higher than the average U_1 over one fundamental period. Thus, when m_a starts increasing, $g(t)$ becomes more square wave like and the area under the curve U_1- $|g(t)|^2$ decreases, resulting in a reduction of d_{av}. Since $S_2(f)$ is directly proportional to d_{av} for a fixed f_{sp}, $P_{2,noise}$ decreases as m_a increases for a given sampling frequency. This relationship can be obtained from Fig. 5.21.

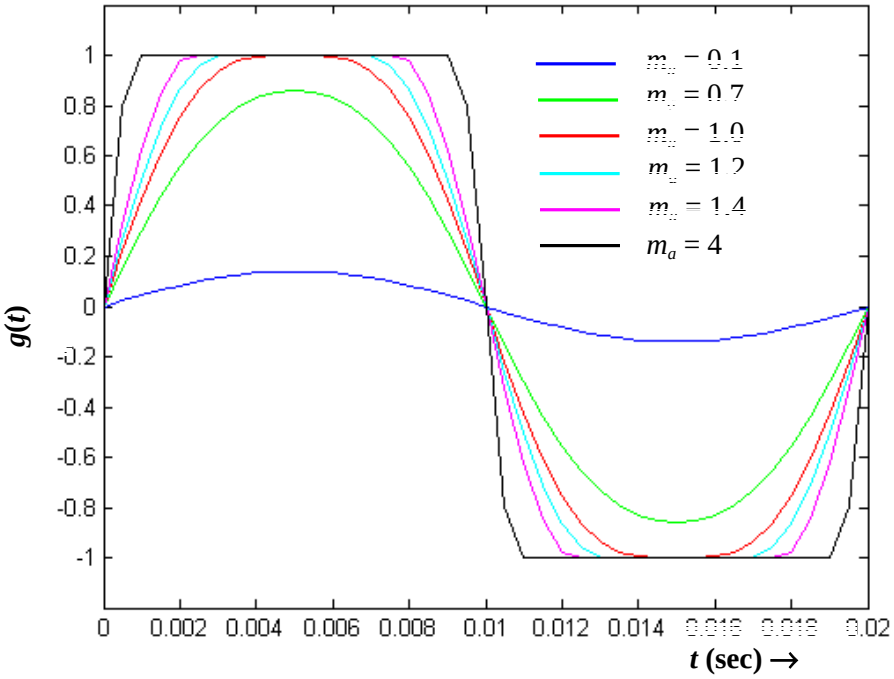

Fig. 5.22: Expected random PWM signal $g(t)$ (N = 6) with various modulation index.

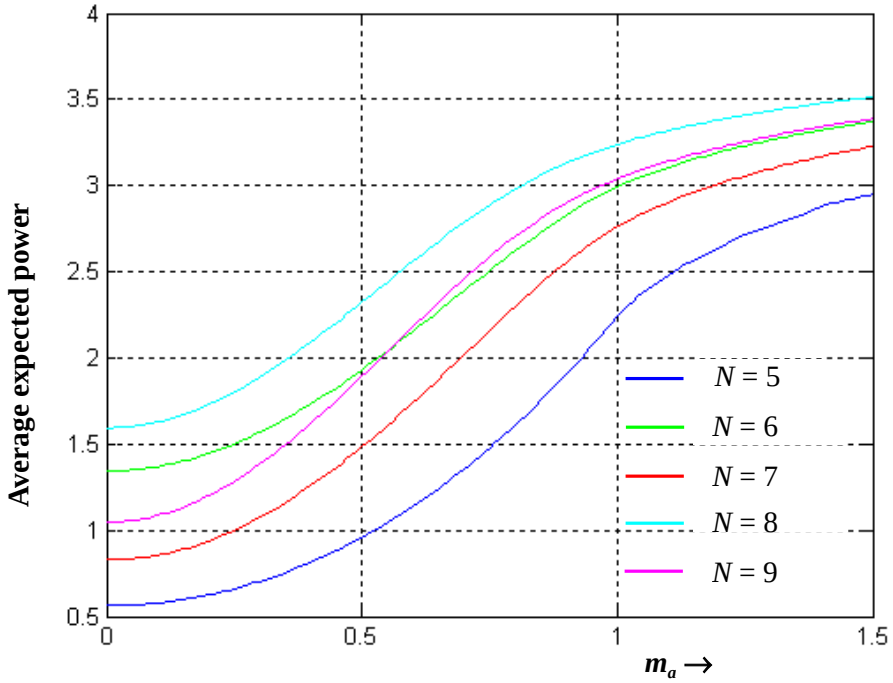

Fig. 5.23: Average expected power U_1 for N = 5, 6, 7, 8 and 9 versus m_a.

5.5.3 The Effect of N

The effect of N is similar to that of modulation index m_a on the discrete noise power $P_{1,noise}$ and the continuous noise power $P_{2,noise}$. Qualitatively, $g(t)$ tends to a square wave as N increases resulting in a larger fundamental component (see Figs. 5.1 and 5.2). However, the effect on other harmonics is mixed and thus qualitative dependence of $P_{1,noise}$ on N is hard to predict. But for large values of N, it will approach a square wave like value of $(1-(8/\pi^2))\times(2A)^2 \approx 0.19(2A)^2$ (see equation 5.8). In general, for N = 5, 6, 7, 8 and 9, it was found that $P_{1,noise}$ increased with odd/even increment of N (see Fig. 5.20), and the discrete noise power for even numbers of N is higher than the discrete noise power for the odd number of N. This is because for the value of q that was chosen (i.e., q = 2) the probabilities of the inverter output connecting to the fifth and first dc-bus voltage levels are higher (the inverter is more likely to make the decision to switch to the first and fifth voltage level of the dc bus) than the other voltage levels compared to the WRPWM scheme with odd number of comparisons N. Hence as the value of N increases, the expected value $g(t)$ for even numbers of N becomes more square wave like function than $g(t)$ for odd numbers of N. Moreover, from Fig. 5.23 the total expected power $P_{k(t)}$ for even numbers of N is larger than the $P_{k(t)}$ for odd numbers of N (e.g., $P_{k(t)}$ for N = 6 is larger than N = 5 and 7). Thus, the WRPWM scheme with even numbers of N has stronger boosting effect on the fundamental and other harmonics components. Furthermore, as N

increases (in odd increment or in even increment), $g(t)$ becomes more square wave like and the area under the curve $U_1 - |g(t)|^2$ decreases, resulting in a reduction of d_{av}, therefore, $P_{2,noise}$ decreases as N increases. Note that, from Fig. 5.23, for N even, the value of the average of expected power U_1 is larger than with an odd number of comparisons N. This is due to the probability of the inverter output connecting to third dc-bus voltage level (0 V) when operating with N odd being higher than when operating with an even number of comparisons, N. This suggests that for an even number of comparisons, N, the inverter is more likely to connect its output terminals to first, second, fourth and fifth voltage level than it does when N is an odd number. From Fig. 5.21 it can be observed that $P_{2,noise}$ decreases with even/odd increment of N. Furthermore, $P_{2,noise}$ for N even is larger than $P_{2,noise}$ for N odd even though the harmonic components for operation with N even are larger than for N odd. This is due to the total expected power of $k(t)$ for operation with N even being higher than that for N odd (see Fig. 5.23).

5.5.4 Comparison of the Five-Level and Three-Level WRPWM Schemes

In section 5.2.2, comparisons have been made between the five-level WRWPM scheme and the three-level WRPWM scheme regarding to the harmonic content and it was found that the optimal values of comparisons, N, for the five-level and three-level WRPWM schemes are N = 6 and 4, respectively. In this section the three-level WRPWM with N = 4 is compared with the five-level scheme operating with the various values of N considered in the previous section (i.e. N = 5, 6, 7, 8 and 9). The comparison is made with reference to the discrete noise power $P_{1,noise}$ and the continuous noise power $P_{2,noise}$. The plots of normalized $P_{1,noise}$ and $P_{2,noise}$ versus modulation index are shown in Figs. 5.24 and 5.25, respectively.

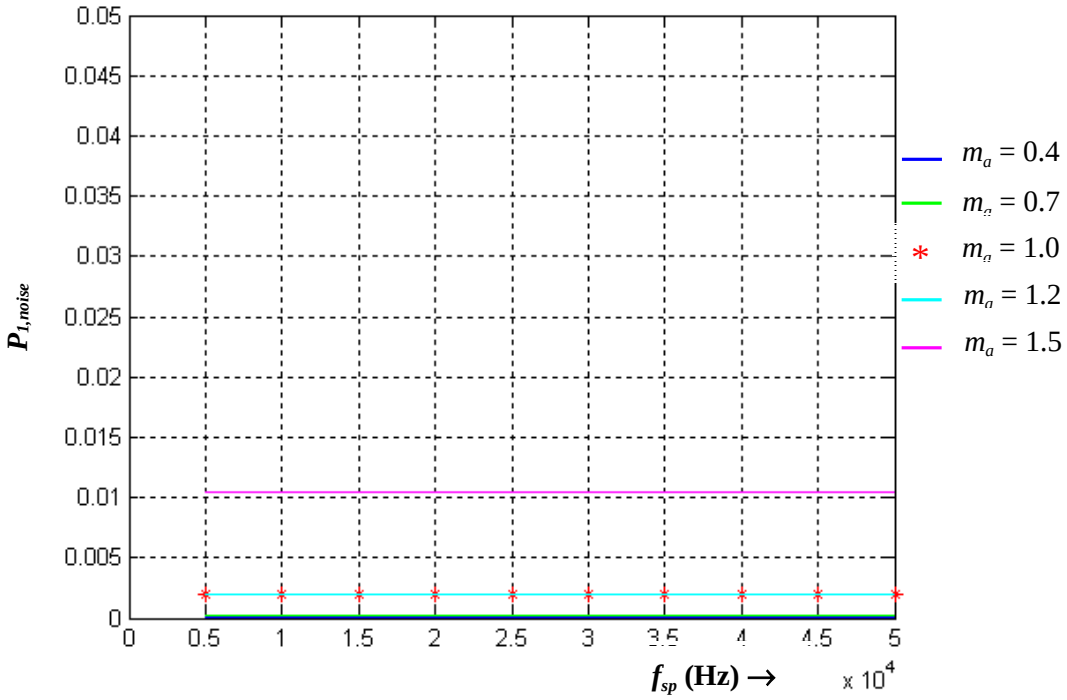

Fig. 5.24: Theoretical discrete noise ($P_{1,noise}$) power versus f_{sp} for three-level WRPWM scheme with N = 4.

From Figs. 5.20 and 5.24, it can be seen that the five-level WRPWM operating with various values of N has higher discrete noise power $P_{1,noise}$ than the three-level WRPWM scheme operating with N = 4. This is true for all the values of modulation index under consideration (i.e., m_a = 0.4, 0.7, 1.0, 1.2 and 1.5) except at m_a = 1.0 and 1.2 where $P_{1,noise}$ for the five-level WRPWM operating with N = 5 is lower.

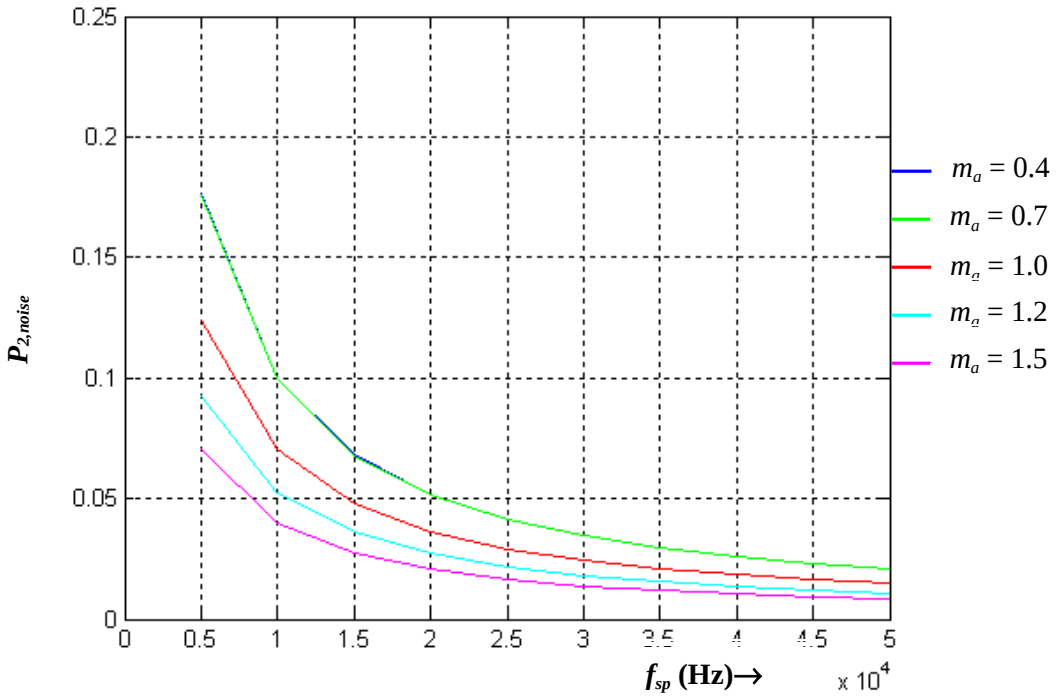

Fig. 5.25: Theoretical discrete noise ($P_{2,noise}$) power versus f_{sp} for three-level WRPWM scheme with N = 4.

From Figs. 5.21 and 5.25, it can be seen that the five-level WRPWM scheme operating with various values of N has lower continuous noise power $P_{2,noise}$ than the three-level WRPWM scheme operating with N = 4. Again, this is true for all the values of modulation index under consideration except for m_a = 0.4 where $P_{2,noise}$ for the five-level WRPWM scheme operating with N = 6 and 8 are higher. Note that the three-level WRPWM scheme operating with N = 4, $P_{2,noise}$ for m_a = 0.4 is slightly higher than that for m_a = 0.7 at 5000 Hz < f_{sp} < 20 kHz.

It is known [37] that high continuous noise (wide-band excitation) is likely to excite system resonances. This can be improved by increasing switching frequency, but the increase in switching loss caused by increasing the switching frequency may wipe out any marginal gains in the reduction of $P_{2,noise}$. Thus, for the various aspects under consideration (i.e., the harmonics, discrete noise, continuous noise and switching loss), the five-level WRPWM scheme with N = 6 seems to be the optimal choice.

5.6 Average Switching Frequency of WRPWM Scheme

In the WRPWM scheme, the probability that the output signal takes a value +2*A*, *A*, 0, -*A* or -2*A* depends on the reference signal and the number of comparisons (see (4.9)-(4.13)). So the probability of successive pulses merging together to form a wider pulse is nonzero and depends on the relative position within the reference waveform period. This leads to an average switching frequency that is smaller than f_{sp}. In this section, the precise theoretical value of the average switching frequency, f_{sw}, for a WRPWM scheme is calculated.

The easiest way to derive the average switching frequency is to first consider the following simpler problem. Consider a random signal $k(t)$ taking values +2*A*, *A*, 0, -*A* or -2*A* in every sampling interval of duration T_{sp} as follows: $x(t)$ takes a value +2*A* with probability of P_1, +*A* with probability of P_2, 0 with probability of P_3, -*A* with probability of P_4 and -2*A* with probability of P_5 in each interval independently of other intervals. The expected number of switching in *M* sampling periods of $k(t)$, i.e., the averaged switching frequency, can be estimated as follows [5].

First, start with $M = 2$ (i.e., 2 sampling periods), table 5.1 list all the corresponding possible switching sequences, the probabilities and number of switching that occurred. From table 5.1 the expected value of number of switching is

$$E\{\text{no. of switching}\} = 2(P_1 P_2 + P_1 P_3 + P_1 P_4 + P_1 P_5 + P_2 P_3 + P_2 P_4 + P_2 P_5 + P_3 P_4 + P_3 P_5 + P_4 P_5). \qquad (5.15)$$

The probability that the last pulse is 2*A* is

$$\begin{aligned} P_r\{\text{last pulse is } 2A\} &= P_r\{\text{sequence } (2A, 2A)\} + P_r\{\text{sequence } (A, 2A)\} + P_r\{\text{sequence } (0, 2A)\} \\ &\quad + P_r\{\text{sequence } (-A, 2A)\} + P_r\{\text{sequence } (-2A, 2A)\} \\ &= P_1 P_1 + P_2 P_1 + P_3 P_1 + P_4 P_1 + P_5 P_1 \\ &= P_1(P_1 + P_2 + P_3 + P_4 + P_5) \\ &= P_1. \end{aligned}$$

TABLE 5.1

Number of switching and the probabilities of possible switching sequence at M = 2 sampling period.

Possible sequence	Probabilities	No. of switching
-2A -2A	P_5 P_5	0
-2A -A	P_5 P_4	1
-2A 0	P_5 P_3	1
-2A A	P_5 P_2	1
-2A 2A	P_5 P_1	1
-A -A	P_4 P_4	0
-A -2A	P_4 P_5	1
-A 0	P_4 P_3	1
-A A	P_4 P_2	1
-A 2A	P_4 P_1	1
0 0	P_3 P_3	0
0 -2A	P_3 P_5	1
0 -A	P_3 P_4	1
0 A	P_3 P_2	1
0 2A	P_3 P_1	1
A A	P_2 P_2	0
A 2A	P_2 P_1	1
A 0	P_2 P_3	1
A -A	P_2 P_4	1
A -2A	P_2 P_5	1
2A 2A	P_1 P_1	0
2A A	P_1 P_2	1
2A 0	P_1 P_3	1
2A -A	P_1 P_4	1
2A -2A	P_1 P_5	1

The probability that the last pulse is A is

P_r\{last pulse is A\}

$=P_r$\{sequence (A, A)\} + P_r\{sequence (2A, A)\} + P_r\{sequence (0, A)\} + P_r\{sequence (-A, A)\} + P_r\{sequence (-2A, A)\}

$= P_2 P_2 + P_1 P_2 + P_3 P_2 + P_4 P_2 + P_5 P_2$

$= P_2(P_2 + P_1 + P_3 + P_4 + P_5)$

$= P_2$.

The probability of last pulse being 0 is

P_r{last pulse is 0}

$=P_r$\{sequence (0, 0)\} + P_r\{sequence (2*A*, 0)\} + P_r\{sequence (*A*, 0)\} + P_r\{sequence (-*A*, 0)\} + P_r\{sequence (-2*A*, 0)\}

$= P_3 P_3 + P_1 P_3 + P_2 P_3 + P_4 P_3 + P_5 P_3$

$= P_3(P_3 + P_1 + P_2 + P_4 + P_5)$

$= P_3$.

The probability of last pulse being -*A* is

P_r\{last pulse is -*A*\}

$=P_r$\{sequence (-*A*, -*A*)\} + P_r\{sequence (2*A*, -*A*)\} + P_r\{sequence (0, -*A*)\} + P_r\{sequence (*A*, -*A*)\} + P_r\{sequence (-2*A*, -*A*)\}

$= P_4 P_4 + P_1 P_4 + P_3 P_4 + P_2 P_4 + P_5 P_4$

$= P_4(P_4 + P_1 + P_3 + P_2 + P_5)$

$= P_4$

and because

$P_1 + P_2 + P_3 + P_4 + P_5 = 1$.

Hence

P_r\{last pulse is 2*A*\} + P_r\{last pulse is *A*\} + P_r\{last pulse is 0\} + P_r\{last pulse is -*A*\} + P_r\{last pulse is -2*A*\}
= 1,

thus

P_r\{last pulse is -2*A*\}
= 1-($P_1 + P_2 + P_3 + P_4$).

Mathematical induction hypothesis is now used to determine the expected value of the number

of switching for M sampling periods as follows:

$$E\{\text{no. of switching}\} = 2(M\text{-}1)\,(P_1P_2 + P_1P_3 + P_1P_4 + P_1P_5 + P_2P_3 + P_2P_4 + P_2P_5 + P_3P_4 + P_3P_5 + P_4P_5)$$
$$= 2(M\text{-}1)(X), \qquad (5.16)$$

where

$$X = (P_1P_2 + P_1P_3 + P_1P_4 + P_1P_5 + P_2P_3 + P_2P_4 + P_2P_5 + P_3P_4 + P_3P_5 + P_4P_5).$$

Probabilities for various sequences are obtained using a similar approach as that which was adopted for $M = 2$ as shown below

(No. of switching = S_1) and (last pulse is -1) → the probability is p_1
↓
(No. of switching = S_r) and (last pulse is -1) → the probability is p_r
(No. of switching = S_{r+1}) and (last pulse is -1) → the probability is p_{r+1}
↓
(No. of switching = S_{r+q}) and (last pulse is -1) → the probability is p_{r+q}
(No. of switching = S_{r+q+1}) and (last pulse is -1) → the probability is p_{r+q+1}
↓
(No. of switching = S_{r+q+p}) and (last pulse is -1) → the probability is p_{r+q+p}
(No. of switching = $S_{r+q+p+1}$) and (last pulse is -1) → the probability is $p_{r+q+p+1}$
↓
(No. of switching = $S_{r+q+p+o}$) and (last pulse is -1) → the probability is $p_{r+q+p+o}$
(No. of switching = $S_{r+q+p+o+1}$) and (last pulse is -1)→ the probability is $p_{r+q+p+o+1}$
↓
(No. of switching = $S_{r+q+p+o+n}$) and (last pulse is -1)→ the probability is $p_{r+q+p+o+n}$

It has already been shown that induction hypothesis holds for $M = 2$. Now let $M = n$ and assume the following probabilities for various sequences, as given above. Then by induction hypothesis

$$\sum_{i=1}^{r} p_i = P_1 \qquad \sum_{i=r+1}^{r+q} p_i = P_2 \qquad \sum_{i=r+q+1}^{r+q+p} p_i = P_3 \qquad \sum_{i=r+q+p+1}^{r+q+p+o} p_i = P_4 \qquad \sum_{i=r+q+p+o+1}^{r+q+p+o+n} p_i = P_5$$

then

$$\sum_{i=1}^{r+q+p+o+n} S_i p_i = 2(n-1)(P_1P_2 + P_1P_3 + P_1P_4 + P_1P_5 + P_2P_3 + P_2P_4 + P_2P_5 + P_3P_4 + P_3P_5 + P_4P_5).$$

(5.17)

Now for $M = n+1$, each of above sequences leads to different scenarios on whether the signal has a value $+2A$, A, 0, $-A$ or $-2A$ in the $(n+1)th$ switching interval. Therefore

$$\begin{aligned} P_r\{\text{last pulse is } 2A\} &= \sum_{i=1}^{r} p_i(P_1) + \sum_{i=r+1}^{r+q} p_i(P_1) + \sum_{i=r+q+1}^{r+q+p} p_i(P_1) + \sum_{i=r+q+p+1}^{r+q+p+o} p_i(P_1) + \sum_{i=r+q+p+o+1}^{r+q+p+o+n} p_i(P_1) \\ &= P_1P_1 + P_2P_1 + P_3P_1 + P_4P_1 + P_5P_1 \\ &= P_1, \end{aligned}$$

$$\begin{aligned} P_r\{\text{last pulse is } A\} &= \sum_{i=1}^{r} p_i(P_2) + \sum_{i=r+1}^{r+q} p_i(P_2) + \sum_{i=r+q+1}^{r+q+p} p_i(P_2) + \sum_{i=r+q+p+1}^{r+q+p+o} p_i(P_2) + \sum_{i=r+q+p+o+1}^{r+q+p+o+n} p_i(P_2) \\ &= P_1P_2 + P_2P_2 + P_3P_2 + P_4P_2 + P_5P_2 \\ &= P_2, \end{aligned}$$

$$\begin{aligned} P_r\{\text{last pulse is } 0\} &= \sum_{i=1}^{r} p_i(P_3) + \sum_{i=r+1}^{r+q} p_i(P_3) + \sum_{i=r+q+1}^{r+q+p} p_i(P_3) + \sum_{i=r+q+p+1}^{r+q+p+o} p_i(P_3) + \sum_{i=r+q+p+o+1}^{r+q+p+o+n} p_i(P_3) \\ &= P_1P_3 + P_2P_3 + P_3P_3 + P_4P_3 + P_5P_3 \\ &= P_3, \end{aligned}$$

$$\begin{aligned} P_r\{\text{last pulse is } -A\} &= \sum_{i=1}^{r} p_i(P_4) + \sum_{i=r+1}^{r+q} p_i(P_4) + \sum_{i=r+q+1}^{r+q+p} p_i(P_4) + \sum_{i=r+q+p+1}^{r+q+p+o} p_i(P_4) + \sum_{i=r+q+p+o+1}^{r+q+p+o+n} p_i(P_4) \\ &= P_1P_4 + P_2P_4 + P_3P_4 + P_4P_4 + P_5P_4 \\ &= P_4, \end{aligned}$$

$$\begin{aligned} P_r\{\text{last pulse is } -2A\} &= \sum_{i=1}^{r} p_i(P_5) + \sum_{i=r+1}^{r+q} p_i(P_5) + \sum_{i=r+q+1}^{r+q+p} p_i(P_5) + \sum_{i=r+q+p+1}^{r+q+p+o} p_i(P_5) + \sum_{i=r+q+p+o+1}^{r+q+p+o+n} p_i(P_5) \\ &= P_1P_5 + P_2P_5 + P_3P_5 + P_4P_5 + P_5P_5 \\ &= P_5. \end{aligned}$$

Thus the value of number of expected switchings in $n + 1$ sampling periods can be expressed as

$$
\begin{aligned}
&E\{\text{no. of switching}\}\\
&=\sum_{i=1}^{r} S_i p_i(P_1)+\sum_{i=r+1}^{r+q}(S_i+1)p_i(P_1)+\sum_{i=r+q+1}^{r+q+p}(S_i+1)p_i(P_1)+\sum_{i=r+q+p+1}^{r+q+p+o}(S_i+1)p_i(P_1)\\
&+\sum_{i=r+q+p+o+1}^{r+q+p+o+n}(S_i+1)p_i(P_1)\ +\sum_{i=1}^{r}(S_i+1)p_i(P_2)+\sum_{i=r+1}^{r+q} S_i p_i(P_2)+\sum_{i=r+q+1}^{r+q+p}(S_i+1)p_i(P_2)\\
&+\sum_{i=r+q+p+1}^{r+q+p+o}(S_i+1)p_i(P_2)+\sum_{i=r+q+p+o+1}^{r+q+p+o+n}(S_i+1)p_i(P_2)\ +\sum_{i=1}^{r}(S_i+1)p_i(P_3)+\sum_{i=r+1}^{r+q}(S_i+1)p_i(P_3)\\
&+\sum_{i=r+q+1}^{r+q+p} S_i p_i(P_3)+\sum_{i=r+q+p+1}^{r+q+p+o}(S_i+1)p_i(P_3)+\sum_{i=r+q+p+o+1}^{r+q+p+o+n}(S_i+1)p_i(P_3)\ +\sum_{i=1}^{r}(S_i+1)p_i(P_4)\\
&+\sum_{i=r+1}^{r+q}(S_i+1)p_i(P_4)+\sum_{i=r+q+1}^{r+q+p}(S_i+1)p_i(P_4)+\sum_{i=r+q+p+1}^{r+q+p+o} S_i p_i(P_4)+\sum_{i=r+q+p+o+1}^{r+q+p+o+n}(S_i+1)p_i(P_4)\\
&+\sum_{i=1}^{r}(S_i+1)p_i(P_5)+\sum_{i=r+1}^{r+q}(S_i+1)p_i(P_5)+\sum_{i=r+q+1}^{r+q+p}(S_i+1)p_i(P_5)+\sum_{i=r+q+p+1}^{r+q+p+o}(S_i+1)p_i(P_5)\\
&+\sum_{i=r+q+p+o+1}^{r+q+p+o+n} S_i p_i(P_5)\\
&=\sum_{i=1}^{r+q+p+o+n} S_i p_i(P_1)+\sum_{i=r+1}^{r+q} p_i(P_1)+\sum_{i=r+q+1}^{r+q+p} p_i(P_1)+\sum_{i=r+q+p+1}^{r+q+p+o} p_i(P_1)+\sum_{i=r+q+p+o+1}^{r+q+p+o+n} p_i(P_1)\\
&\quad+\sum_{i=1}^{r} p_i(P_2)+\sum_{i=r+1}^{r+q+p+o+n} S_i p_i(P_2)+\sum_{i=r+q+1}^{r+q+p} p_i(P_2)+\sum_{i=r+q+p+1}^{r+q+p+o} p_i(P_2)+\sum_{i=r+q+p+o+1}^{r+q+p+o+n} p_i(P_2)\\
&\quad+\sum_{i=1}^{r} p_i(P_3)+\sum_{i=r+1}^{r+q} p_i(P_3)+\sum_{i=r+q+1}^{r+q+p+o+n} S_i p_i(P_3)+\sum_{i=r+q+p+1}^{r+q+p+o} p_i(P_3)+\sum_{i=r+q+p+o+1}^{r+q+p+o+n} p_i(P_3)\\
&\quad+\sum_{i=1}^{r} p_i(P_4)+\sum_{i=r+1}^{r+q} p_i(P_4)+\sum_{i=r+q+1}^{r+q+p} p_i(P_4)+\sum_{i=r+q+p+1}^{r+q+p+o+n} S_i p_i(P_4)+\sum_{i=r+q+p+o+1}^{r+q+p+o+n} p_i(P_4)\\
&\quad+\sum_{i=1}^{r} p_i(P_5)+\sum_{i=r+1}^{r+q} p_i(P_5)+\sum_{i=r+q+1}^{r+q+p} p_i(P_5)+\sum_{i=r+q+p+1}^{r+q+p+o} p_i(P_5)+\sum_{i=1}^{r+q+p+o+n} S_i p_i(P_5)\\
&=2(n-1)(X)P_1+P_1P_2+P_1P_3+P_1P_4+P_1P_5+2(n-1)(X)P_2+P_1P_2+P_2P_3+P_2P_4+P_2P_5\\
&\quad+2(n-1)(X)P_3+P_1P_3+P_2P_3+P_3P_4+P_3P_5+2(n-1)(X)P_4+P_1P_4+P_2P_4+P_3P_4+P_4P_5\\
&\quad+2(n-1)(X)P_5+P_1P_5+P_2P_5+P_3P_5+P_4P_5\\
&=2(n-1)(X)P_1+2(n-1)(X)P_2+2(n-1)(X)P_3+2(n-1)(X)P_4+2(n-1)(X)P_5\\
&\quad+2(P_1P_2+P_1P_3+P_1P_4+P_1P_5+P_2P_3+P_2P_4+P_2P_5+P_3P_4+P_3P_5+P_4P_5)\\
&=2(X)\big((n-1)(P_1+P_2+P_3+P_4+P_5)+1\big)\\
&=2(X)(n).
\end{aligned}
\tag{5.18}
$$

Equations (5.15) and (5.18) show that the statement in (5.16) holds true for $M = 2$ and $n + 1$, hence (5.17) for $M = n$ is true. If the number of sampling periods approaches infinity (i.e., $M \rightarrow \infty$) and with the sampling period T_{sp} the average switching frequency for the five-level

WRPWM scheme can be obtained by dividing the number of expected switching with a time interval $2MT_{sp}$. Therefore, the average switching frequency can be expressed as

$$f_{sw} = \lim_{M\to\infty}\left[\frac{2(M-1)(P_1P_2+P_1P_3+P_1P_4+P_1P_5+P_2P_3+P_2P_4+P_2P_5+P_3P_4+P_3P_5+P_4P_5)}{2MT_{sp}}\right]$$
$$= (P_1P_2+P_1P_3+P_1P_4+P_1P_5+P_2P_3+P_2P_4+P_2P_5+P_3P_4+P_3P_5+P_4P_5)\,f_{sp}. \quad (5.19)$$

Now the WRPWM scheme can be viewed as the simpler scheme considered above with the added proviso that the probabilities P_1, P_2, P_3, P_4 and P_5 are periodic functions $F_{N,q}^{(1)}(x), F_{N,q}^{(2)}(x), F_{N,q}^{(3)}(x)$, $F_{N,q}^{(4)}(x)$ and $F_{N,q}^{(5)}(x)$ respectively as given by (4.9)-(4.13).

This makes f_{sw} of (5.19) periodic as well. Thus, average switching frequency for the WRPWM scheme is given by

$$\frac{f_{sw}}{f_{sp}} = f_r\int_0^{1/f_r}\left\{F_{N,q}^{(1)}\left(r\left(\left\lfloor\frac{t}{T}\right\rfloor T\right)\right)F_{N,q}^{(2)}\left(r\left(\left\lfloor\frac{t}{T}\right\rfloor T\right)\right)+F_{N,q}^{(1)}\left(r\left(\left\lfloor\frac{t}{T}\right\rfloor T\right)\right)F_{N,q}^{(3)}\left(r\left(\left\lfloor\frac{t}{T}\right\rfloor T\right)\right)\right.$$
$$+F_{N,q}^{(1)}\left(r\left(\left\lfloor\frac{t}{T}\right\rfloor T\right)\right)F_{N,q}^{(4)}\left(r\left(\left\lfloor\frac{t}{T}\right\rfloor T\right)\right)+F_{N,q}^{(1)}\left(r\left(\left\lfloor\frac{t}{T}\right\rfloor T\right)\right)F_{N,q}^{(5)}\left(r\left(\left\lfloor\frac{t}{T}\right\rfloor T\right)\right)$$
$$+F_{N,q}^{(2)}\left(r\left(\left\lfloor\frac{t}{T}\right\rfloor T\right)\right)F_{N,q}^{(3)}\left(r\left(\left\lfloor\frac{t}{T}\right\rfloor T\right)\right)+F_{N,q}^{(2)}\left(r\left(\left\lfloor\frac{t}{T}\right\rfloor T\right)\right)F_{N,q}^{(4)}\left(r\left(\left\lfloor\frac{t}{T}\right\rfloor T\right)\right) \quad (5.20)$$
$$+F_{N,q}^{(2)}\left(r\left(\left\lfloor\frac{t}{T}\right\rfloor T\right)\right)F_{N,q}^{(5)}\left(r\left(\left\lfloor\frac{t}{T}\right\rfloor T\right)\right)+F_{N,q}^{(3)}\left(r\left(\left\lfloor\frac{t}{T}\right\rfloor T\right)\right)F_{N,q}^{(5)}\left(r\left(\left\lfloor\frac{t}{T}\right\rfloor T\right)\right)$$
$$\left.+F_{N,q}^{(4)}\left(r\left(\left\lfloor\frac{t}{T}\right\rfloor T\right)\right)F_{N,q}^{(5)}\left(r\left(\left\lfloor\frac{t}{T}\right\rfloor T\right)\right)\right\}dt.$$

Fig. 5.26 shows the plot of ratio of average switching frequency to sampling frequency (f_{sw}/f_{sp}) versus modulation index (m_a). From (5.19) and (5.20), it is known that f_{sw}/f_{sp} is directly proportional to the sum of products of each possible combination of the five distribution functions. Therefore, the characteristic of f_{sw}/f_{sp} versus m_a behave in a mixed manner and are therefore hard to explain. But at $0 < m_a < 0.2$ and $m_a > 1$, probabilities P_3 and P_1 (or P_5) are at their highest value, respectively (i.e., it is more likely for the inverter to connect its output terminal to the third level of the dc-bus voltage at $m_a = 0$ and first/fifth level of the dc-bus voltage at $m_a > 1$). The plots of the average P_1, P_2, P_3, P_4 and P_5 over one fundamental period versus modulation index are shown in Figs. 5.27 (a), (b), (c), (d) and (e). Thus, it is rational to say that for a given value of N, the five-level WRPWM has a higher value of f_{sw}/f_{sp}, if the

average value of $(P_1+P_2+P_4+P_5)/P_3$ over one fundamental period, at $0 < m_a < 0.2$, say $ratio_1$, is higher. Similarly, at $m_a > 1$ the value of f_{sw}/f_{sp} is higher if the average value of $(P_2+P_3+P_4)/(P_1+P_5)$ over one fundamental period, at $m_a > 1$, say $ratio_2$, is higher. Figs. 5.28 (a) and (b) show the plots of $ratio_1$ versus $0 < m_a < 0.2$ and $ratio_2$ versus $1 < m_a < 1.5$ of the five-level WRPWM scheme operating with N = 5, 6, 7, 8 and 9 over one fundamental period.

From Figs. 5.28 (a) and (b) it can be seen that for N even have a higher $ratio_1$ at $0 < m_a < 0.2$ (e.g., the value of $ratio_1$ for N = 8 is higher than the value for N = 9). On the other hand, operations with N odd have a higher $ratio_2$ at $m_a > 1$ (e.g., the value of $ratio_2$ for N = 5 is higher than the value for N = 6). Thus, for a fixed value of sampling frequency, operation with N even has a higher number of switching than when N is odd in the range $0 < m_a < 0.2$. However, operation with N odd has a higher number of switching than the even number of N at $m_a > 1$.

The ratio of the average switching frequency to the sampling frequency for various values of N at $0 < m_a < 0.2$ can be sorted in descending order as N = 8, N = 6, N = 9, N = 7 and N = 5. The ratio of the average switching frequency to the sampling frequency for various values of N at $m_a > 1$ can be sorted in descending order as N = 5, N = 7, N = 6, N = 9 and N = 8.

From Fig. 5.26 the following can be observed. For the WRPWM scheme with N = 5, at zero modulation index (m_a = 0), the ratio of f_{sw}/f_{sp} is the lowest amongst those considered and reaches a maximum value (0.3150) at m_a = 0.6. This means that when the sampling frequency is at 30 kHz the average switching frequency will not exceed 9.45 kHz. When the WRPWM scheme operates with N = 6, the ratio of f_{sw}/f_{sp} is at its maximum value (0.3843) when m_a = 0. This means that when the sampling frequency is at 30 kHz the average switching frequency will not exceed 11.5 kHz. When the WRPWM scheme operates with N = 7, the ratio of f_{sw}/f_{sp} attains its maximum value (0.3358) at m_a = 0.4. This means that when the sampling frequency is at 30 kHz the average switching frequency will not exceed 10 kHz. When the WRPWM scheme operates with N = 8, the ratio of f_{sw}/f_{sp} is at its maximum value (0.3939) when m_a = 0 and is the highest amongst all those considered. This means that when the sampling frequency is at 30 kHz the average switching frequency will not exceed 11.8 kHz. As for the WRPWM scheme with N = 9, the ratio of f_{sw}/f_{sp} is at its maximum value (0.3488) when m_a = 0.3. This means, when the sampling frequency is at 30 kHz the average switching frequency will not exceed 10.5 kHz.

Note that for conventional carrier-based PWM scheme, the switching frequency is identical to the sampling frequency (i.e., symmetrical regular sampling) and is constant over the entire linear modulation region. The switching frequency starts to decrease as m_a increases in the

overmodulation region ($m_a > 1$) since the pulses start to merge together, whereas the switching frequency of the WRPWM scheme is a fraction of the sampling frequency. Thus, for the same sampling frequency, the switching frequency of the WRPWM scheme is less than that of the conventional carrier-based PWM scheme. Hence with the same sampling frequency f_{sp}, the WRPWM scheme has lower switching losses compared with the conventional carrier-based PWM scheme.

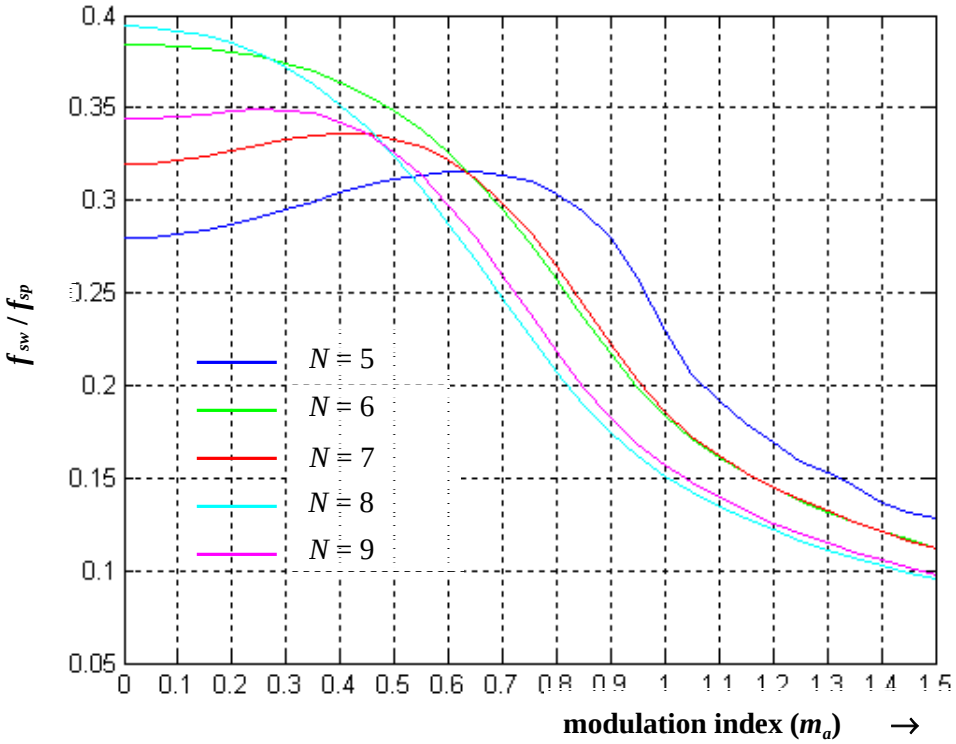

Fig. 5.26: Ratio of average switching frequency to sampling frequency versus modulation index.

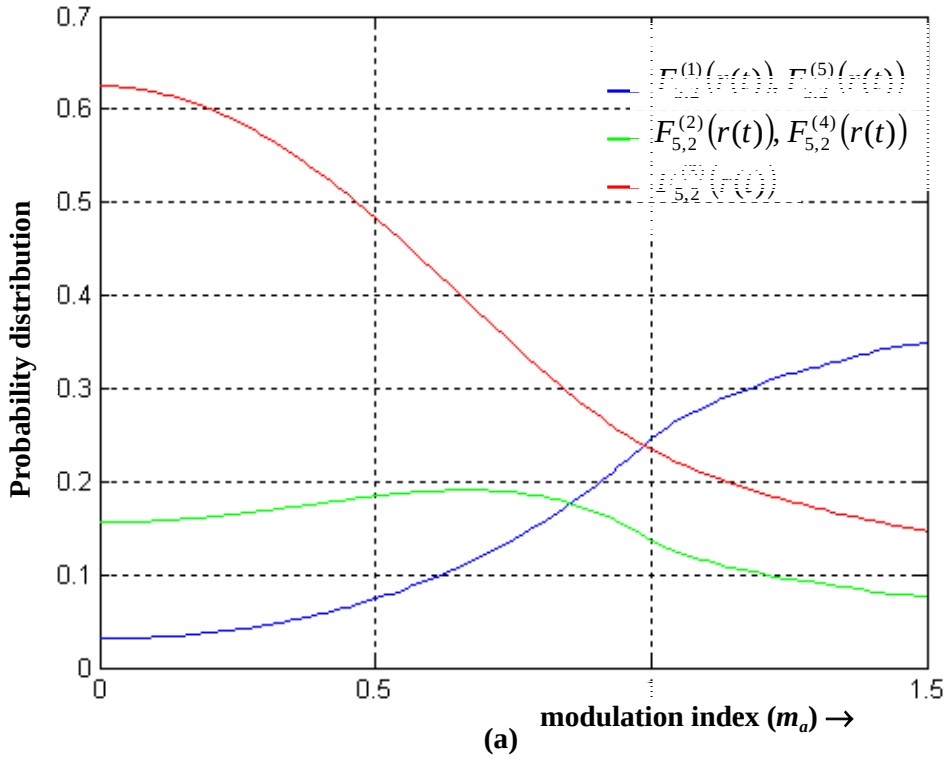

(a)

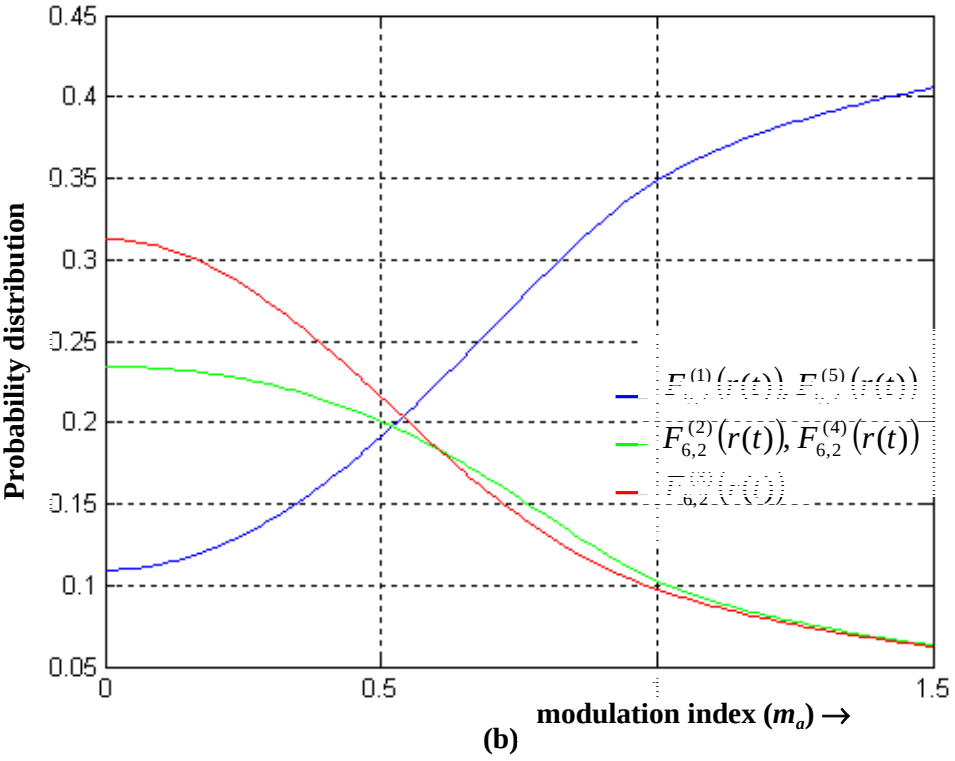

(b)

Fig. 5.27: Probability distribution functions versus modulation index for (a) N = 5 (b) N = 6.

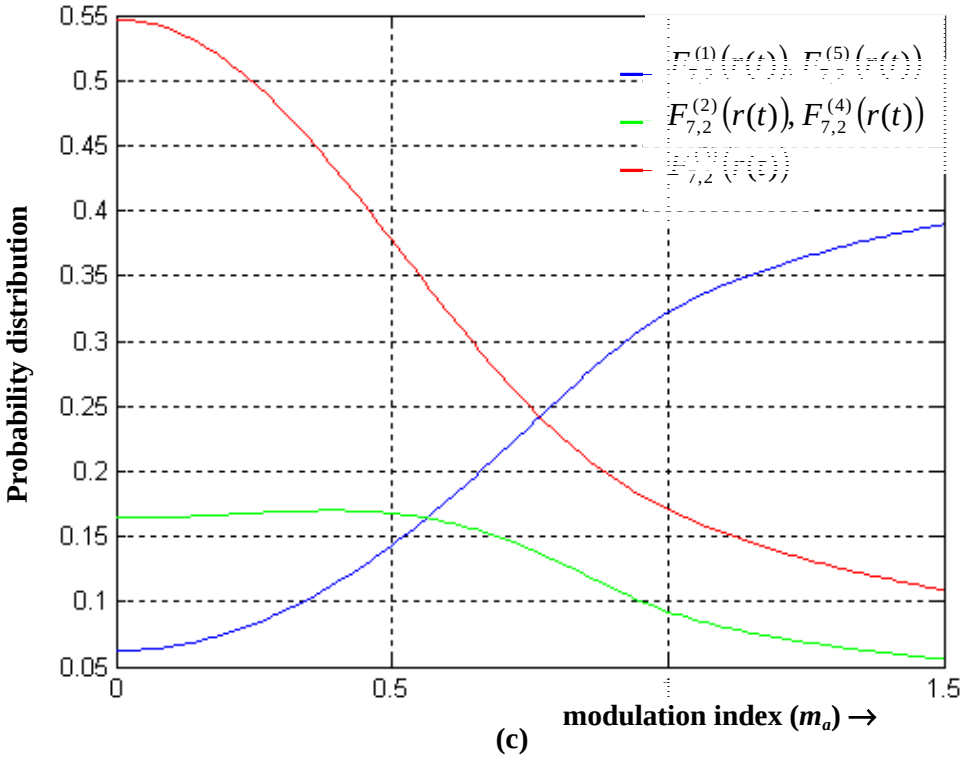

(c)

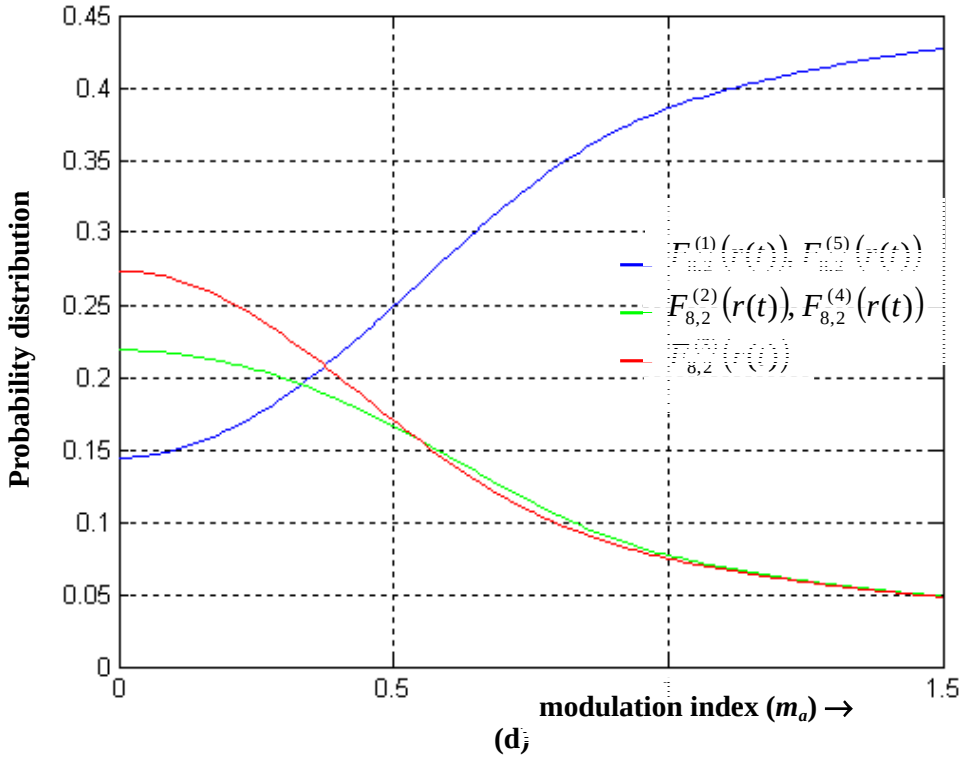

(d)

Fig. 5.27: (continued) (c) N = 7 (d) N = 8.

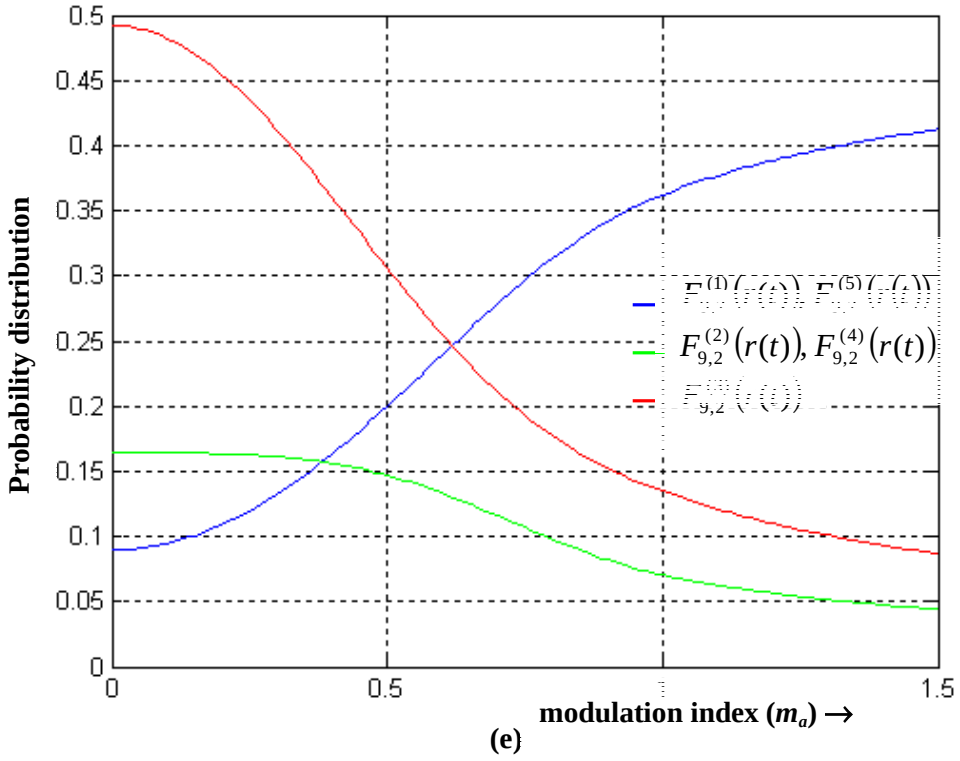

Fig. 5.27: (continued) (e) N = 9.

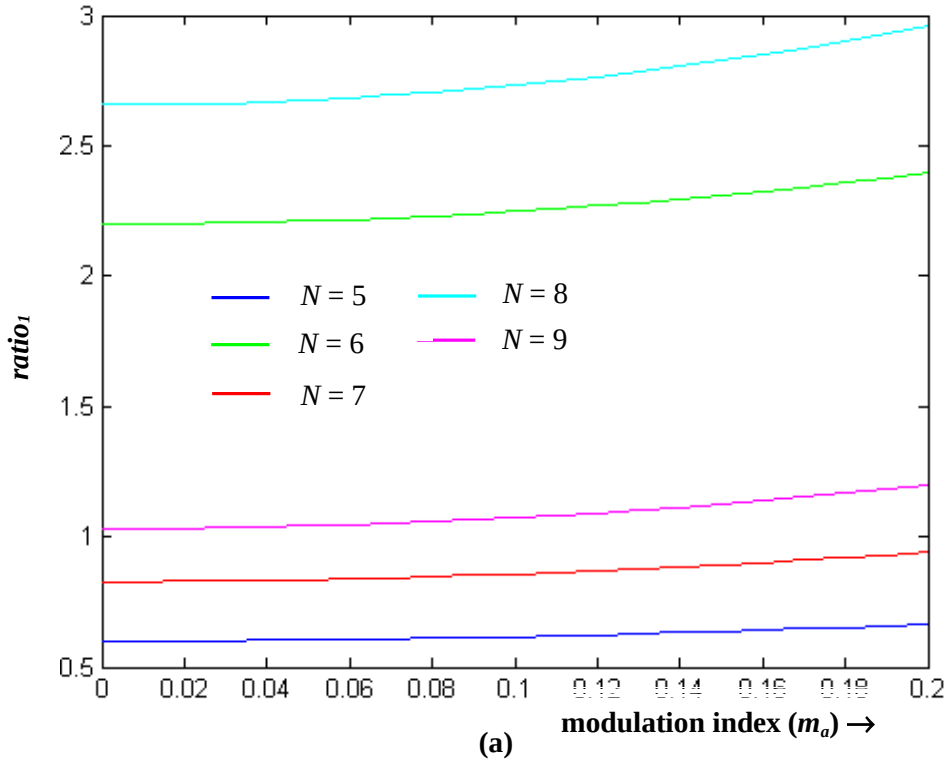

Fig. 5.28: Plot of $(P_1+P_2+P_4+P_5)/P_3$ at (a) $0 < m_a < 0.2$.

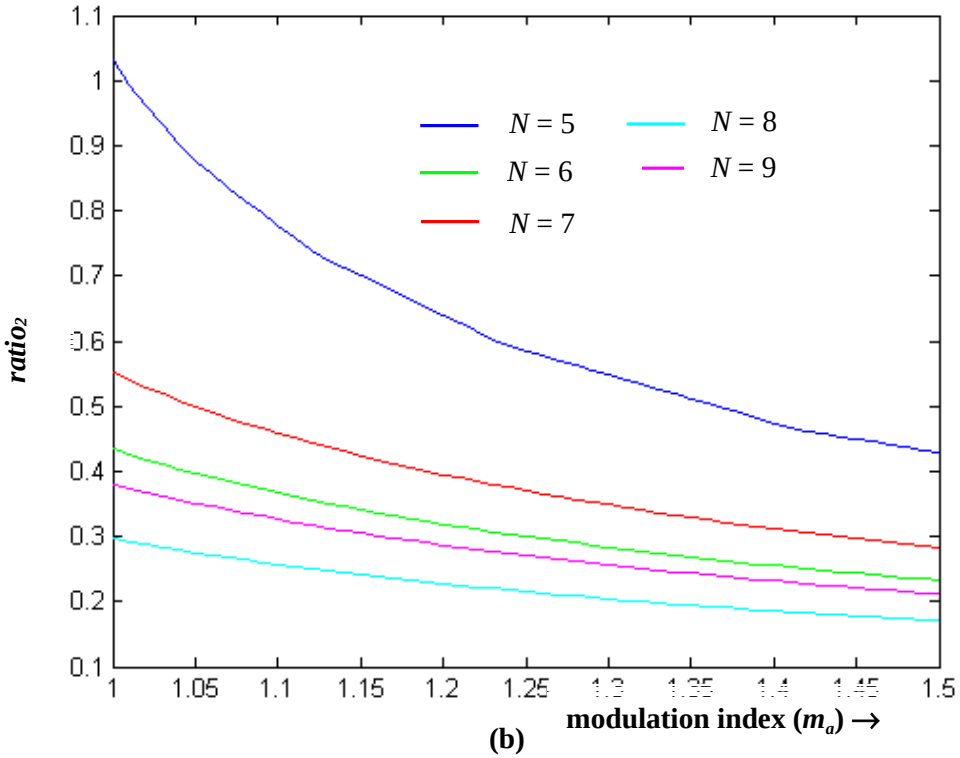

(b)

Fig. 5.28: (continued) (b) $m_a > 1$.

CHAPTER SIX

THE MODIFIED MULTILEVEL WRPWM

The performance of a five-level WRPWM scheme was discussed in detail in chapter 5. In this chapter, a modified five-level WRPWM scheme is proposed and the equations needed to characterize the proposed WRPWM scheme are derived. A detailed analysis of the performance of the new scheme and comparisons between the two five-level WRPWM schemes are carried out.

6.1 Introduction of Modified Five-Level WRPWM Scheme

For the multilevel WRPWM schemes, the multilevel inverter decides which level of dc-bus voltage is connected to the output based on the number of times that the random numbers is smaller than or equal to the instantaneous sampling value of the reference signal $r(t)$. From (4.6) it can be seen that the range of c (number of times that the random numbers are smaller than or equal to $r(t)$) for each level of voltage is dependent on the value of N and/or q. As the number of comparisons, N, increases, the value of parameter q increases (since $2 \leq q \leq \lfloor N/2 \rfloor$). Consequently, the range of c increases and this in turn provides redundancy for the multilevel inverter switching decision.

It is known that the harmonic content of the multilevel inverter has a close relationship with the probability of voltage levels the multilevel inverter output terminals connect to. Hence for each value of N, it is possible to manipulate harmonic content of the multilevel inverter by varying the value of parameter q. To increase the flexibility of c for the second, third and fourth level of dc-bus voltage, an additional parameter is therefore introduced. Consequently, the range of c is able to vary from its minimum value (e.g., $3 \leq c \leq 3$ for the third level of dc-bus voltage with $N = 6$) to its maximum value (e.g., $4 \leq c \leq 2$ for the third level of dc-bus voltage with $N = 6$). The modified WRPWM signal $k(t)$ is defined as

$$k(t)=\begin{cases} 2A, & \text{if} \quad \left\lceil \frac{N}{2} \right\rceil + q \le c \le N \\ A, & \text{if} \left\lceil \frac{N}{2} \right\rceil + a + 1 \le c \le \left\lceil \frac{N}{2} \right\rceil + q - 1 \\ 0, & \text{otherwise (i.e.} \left\lceil \frac{N}{2} \right\rceil + a \le c \le \left\lfloor \frac{N}{2} \right\rfloor - a) \\ -A, & \text{if} \left\lfloor \frac{N}{2} \right\rfloor - q + 1 \le c \le \left\lfloor \frac{N}{2} \right\rfloor - a - 1 \\ -2A, & \text{if} \quad 0 \le c \le \left\lfloor \frac{N}{2} \right\rfloor - q, \end{cases} \tag{6.1}$$

which is identical to (4.6) with the exception that an extra parameter "*a*" was introduced.

6.2 Characterization of Modified Five-Level WRPWM Scheme

The probability distribution functions of the modified multilevel WRPWM required to determine the fraction of the dc-bus voltage that will appear across the output terminals in a five-level inverter are as shown below

$$F_{N,q}^{(1)}(x)=\begin{cases} 1 & \text{for x} > 1 \\ \sum_{m=\left\lceil \frac{N}{2} \right\rceil + q}^{N} \binom{N}{m} x^m (1-x)^{N-m} & \text{for } 0 \le x \le 1 \\ 0 & \text{for x} < 0 \end{cases} \tag{6.2}$$

$$F_{N,q}^{(2)}(x)=\begin{cases} 0 & \text{for x} > 1 \\ \sum_{m=\left\lceil \frac{N}{2} \right\rceil + a + 1}^{\left\lceil \frac{N}{2} \right\rceil + q - 1} \binom{N}{m} x^m (1-x)^{N-m} & \text{for } 0 \le x \le 1 \\ 0 & \text{for x} < 0 \end{cases} \tag{6.3}$$

$$F_{N,q}^{(3)}(x)=\begin{cases} 0 & \text{for x} > 1 \\ \sum_{m=\left\lfloor \frac{N}{2} \right\rfloor - a}^{\left\lceil \frac{N}{2} \right\rceil + a} \binom{N}{m} x^m (1-x)^{N-m} & \text{for } 0 \le \text{x} \le 1 \\ 0 & \text{for x} < 0 \end{cases} \tag{6.4}$$

$$F_{N,q}^{(4)}(x)=\begin{cases}0 & \text{for } x>1\\ \sum_{m=\left\lfloor\frac{N}{2}\right\rfloor-q+1}^{\left\lfloor\frac{N}{2}\right\rfloor-a-1}\binom{N}{m}x^m(1-x)^{N-m} & \text{for } 0\le x\le 1\\ 0 & \text{for } x<0\end{cases} \tag{6.5}$$

$$F_{N,q}^{(5)}(x)=\begin{cases}0 & \text{for } x>1\\ \sum_{m=0}^{\left\lfloor\frac{N}{2}\right\rfloor-q}\binom{N}{m}x^m(1-x)^{N-m} & \text{for } 0\le x\le 1\\ 1 & \text{for } x<0\end{cases} \tag{6.6}$$

where

$$\sum_{m=Y}^{Z}\binom{N}{m}x^m(1-x)^{N-m} \tag{6 .7}$$

in (6.2)-(6.6) is the sum of probabilities of Bernoulli trials for choosing *m* objects out of a set *N* with the probability of success *x*. For the case under consideration, this is the probability of *m* random numbers out of *N* random numbers being smaller than or equal to the instantaneous sampling value of reference *r*(*t*). The inverter decides which level of voltage it will connect to based on not just a single value of *m* but a set of values of *m* (i.e., within the range of *c*). Use *N* = 6 and *q* = 2 as an example, from (4.5) and (4.7) in order for the multilevel inverter to connect the output terminals to a first level of the dc-bus voltage (i.e. $V_{dc}/2$) the random numbers that are smaller than or equal to the instantaneous sampling value of *r*(*t*) should be within the range of 5 to 6 (i.e., $5 \le c \le 6$). From (6.7) the range of *c* is defined as *Y* to *Z*. By altering *Y* and/or *Z*, the value of the probability distribution functions will change. Thus, the expected value *g*(*t*) of the switching signal *k*(*t*) will change. In order to achieve better flexibility of *c* for the second, third and fourth level of dc-bus voltage a new parameter has been introduced into the probability distribution functions. With the additional parameter that has been introduced the range of *c* for each level of voltage is able to vary from its minimum value to maximum allowable value. In equations (6.1)-(6.6), parameter *a* is introduced into the limit of summation. It can be seen that *Y* and *Z* are now functions of *N* and/or *q* and/or *a*. If *N* has been chosen, by altering *q* and/or *a* it is possible to "manipulate" the discrete harmonic spectrum, since *g*(*t*) is a function of *q* and a. Note that both *q* and *a* are integers in the range of $[2, \lfloor N/2 \rfloor]$ and $[0, \lfloor N/2 \rfloor - 2]$, respectively. Thus, an increase in *N* will increase range of *q*

and a, which means that the degree of freedom for both q and a will increase. To illustrate the function of parameter a, $N = 6$ is used as an example. From (6.1) for $q = 3$ $a = 0$, in order for the multilevel inverter to connect its output terminals to the second level of dc-bus voltage, 5 or 4 random numbers have to be smaller than or equal to the instantaneous sampling value of $r(t)$. For third level of voltage, 3 random numbers have to be smaller than or equal to the instantaneous sampling value of $r(t)$. For $q = 3$ $a = 1$ it requires 5 random numbers to be smaller than or equal to the instantaneous sampling value of $r(t)$ for the second level of voltage to be connected to the output terminals. Similarly, 4, 3 or 2 random numbers (i.e., $2 \le c \le 4$) have to be smaller than or equal to the instantaneous sampling value of $r(t)$ for the second level of voltage to be selected. Tables 6.1-6.4 show the various combinations of q and a with the summation limits corresponding to various numbers of comparisons in one sampling interval.

TABLE 6.1

Upper and Lower Summation Limit of Five level WRPWM scheme with N = 6 Probability Distribution Functions Correspond to Various Combination of *q* and *a*.

$N = 6$	Limits of Summation of Probability Distribution Functions									
	$F^{(1)}_{N,q,a}(x)$		$F^{(2)}_{N,q,a}(x)$		$F^{(3)}_{N,q,a}(x)$		$F^{(4)}_{N,q,a}(x)$		$F^{(5)}_{N,q,a}(x)$	
	upper	lower	upper	lower	upper	lower	upper	lower	upper	lower
1. $q = 2$, $a = 0$	6	5	4	4	3	3	2	2	1	0
2. $q = 3$, $a = 0$	6	6	5	4	3	3	2	1	0	0
3. $q = 3$, $a = 1$	6	6	5	5	4	2	1	1	0	0

TABLE 6.2

Upper and Lower Summation Limit of Five level WRPWM scheme with N = 7 Probability Distribution Functions Correspond to Various Combination of *q* and *a*.

$N = 7$	Limits of Summation of Probability Distribution Functions									
	$F^{(1)}_{N,q,a}(x)$		$F^{(2)}_{N,q,a}(x)$		$F^{(3)}_{N,q,a}(x)$		$F^{(4)}_{N,q,a}(x)$		$F^{(5)}_{N,q,a}(x)$	
	upper	lower	upper	lower	upper	lower	upper	lower	upper	lower
1. $q = 2$, $a = 0$	7	6	5	5	4	3	2	2	1	0
2. $q = 3$, $a = 0$	7	7	6	5	4	3	2	1	0	0
3. $q = 3$, $a = 1$	7	7	6	6	5	2	1	1	0	0

TABLE 6.3

Upper and Lower Summation Limit of Five level WRPWM scheme with N = 8 Probability Distribution Functions Correspond to Various Combination of *q* and *a*.

$N = 8$	Limits of Summation of Probability Distribution Functions

	$F^{(1)}_{N,q,a}(x)$		$F^{(2)}_{N,q,a}(x)$		$F^{(3)}_{N,q,a}(x)$		$F^{(4)}_{N,q,a}(x)$		$F^{(5)}_{N,q,a}(x)$	
	upper	lower	upper	lower	upper	lower	upper	lower	upper	lower
1. q = 2, a = 0	8	6	5	5	4	4	3	3	2	0
2. q = 3, a = 0	8	7	6	5	4	4	3	2	1	0
3. q = 4, a = 0	8	8	7	5	4	4	3	1	0	0
4. q = 4, a = 1	8	8	7	6	5	3	2	1	0	0
5. q = 4, a = 2	8	8	7	7	6	2	1	1	0	0

TABLE 6.4

Upper and Lower Summation Limit of Five level WRPWM scheme with N = 9

Probability Distribution Functions Correspond to Various Combination of *q* and *a*.

N = 9	Limits of Summation of Probability Distribution Functions									
	$F^{(1)}_{N,q,a}(x)$		$F^{(2)}_{N,q,a}(x)$		$F^{(3)}_{N,q,a}(x)$		$F^{(4)}_{N,q,a}(x)$		$F^{(5)}_{N,q,a}(x)$	
	upper	lower	upper	lower	upper	lower	upper	lower	upper	lower
1. q = 2, a = 0	9	7	6	6	5	4	3	3	2	0
2. q = 3, a = 0	9	8	7	6	5	4	3	2	1	0
3. q = 4, a = 0	9	9	8	6	5	4	3	1	0	0
4. q = 4, a = 1	9	9	8	7	6	3	2	1	0	0
5. q = 4, a = 2	9	9	8	8	7	2	1	1	0	0

For the five-level WRPWM scheme operating with N = 6 or 7, three combinations of q and a are possible. They are combination 1 (i.e., q = 2, a = 0), combination 2 (i.e., q = 3, a = 0) and combination 3 (i.e., q = 3, a = 1). For the five-level WRPWM scheme operating with N = 8 or 9, five combinations of q and a are possible. These are combination 1 (i.e., q = 2, a = 0), combination 2 (i.e., q = 3, a = 0), combination 3 (i.e., q = 4, a = 0), combination 4 (i.e., q = 4, a = 1) and combination 5 (i.e., q = 4, a = 2). From tables 6.1-6.4, it can be seen that as q increases, the range of summation limit (lower to upper limit) of distribution functions 1 and 5 decreases. Each time q increased by one, the lower (upper) limit of distribution function 1 (5) shift by one to the upper (lower) summation limit of distribution function 2 and 4 until q reached its maximum value ($\lfloor N/2 \rfloor$). Moreover, each time parameter a increased by one, the lower (upper) limit summation of distribution function 2 (3) will shift by a value of one to the upper and lower limit summation of distribution function 3. Note that for N = 5, there is no redundancy since the value of $\lfloor N/2 \rfloor$ is equal to 2, thus, parameters q and a are fixed with 2 and 0, respectively.

6.3 Fundamental and Harmonics Components

Figs. 6.1 (a) and (b) show the expected value $g(t)$ for values of N equal to 6 and 7 and with various combinations of q and a. The average probabilities of each level of the dc-bus over one fundamental cycle versus modulation index for the modified WRPWM scheme operating with N = 6 and 7 and with combinations 2 and 3 are shown in Figs. 6.2 and 6.3. Similar plots for combination 1 are shown in Fig. 5.27 (b) and (c) for N = 6 and 7 respectively. Note that the modified WRPWM scheme operating with the combination 1 (i.e., q = 2, a = 0) is identical to that of the standard multilevel WRPWM scheme discussed in chapter 5.

From Fig. 6.1 (a) and (b), tables 6.1 and 6.2, when operating with combination 2 (i.e., q = 3, a = 0), $g(t)$ for the WRPWM schemes operating with N = 6 and 7 is more sinusoidal than those for other combinations. This is due to the fact that the probability of connecting the output of inverter to the first and fifth dc-bus voltage levels has been reduced (see Fig. 6.2 (a)). For instance, if combination 3 (i.e., q = 3, a =1) is applied, it is clear that the five-level inverter is more likely to connect its output terminal to the third voltage level (see Fig. 6.2 (b)). Consequently, the probability for the inverter to connect its output terminals to the first and fifth dc-bus voltage is reduced, thus the expected value $g(t)$ become more pulse like.

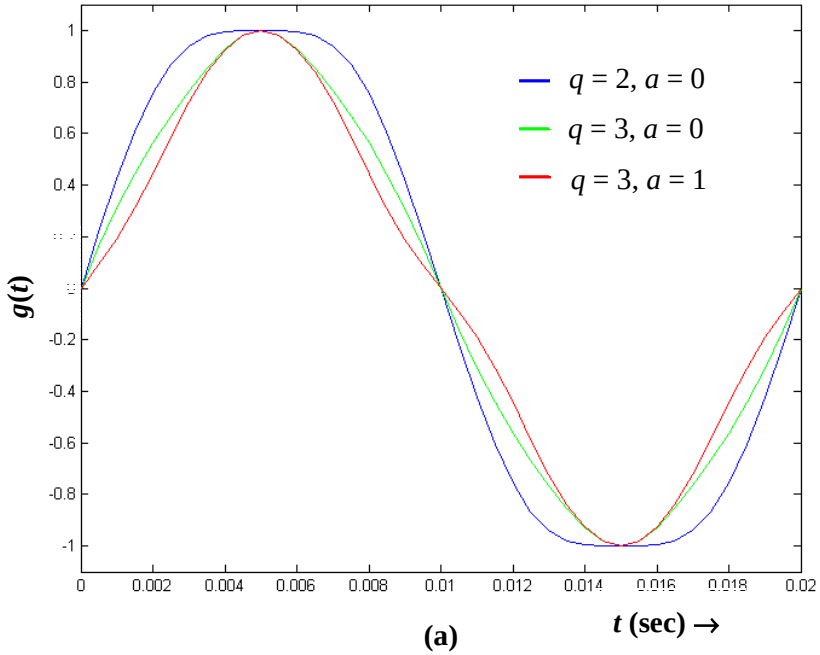

(a)

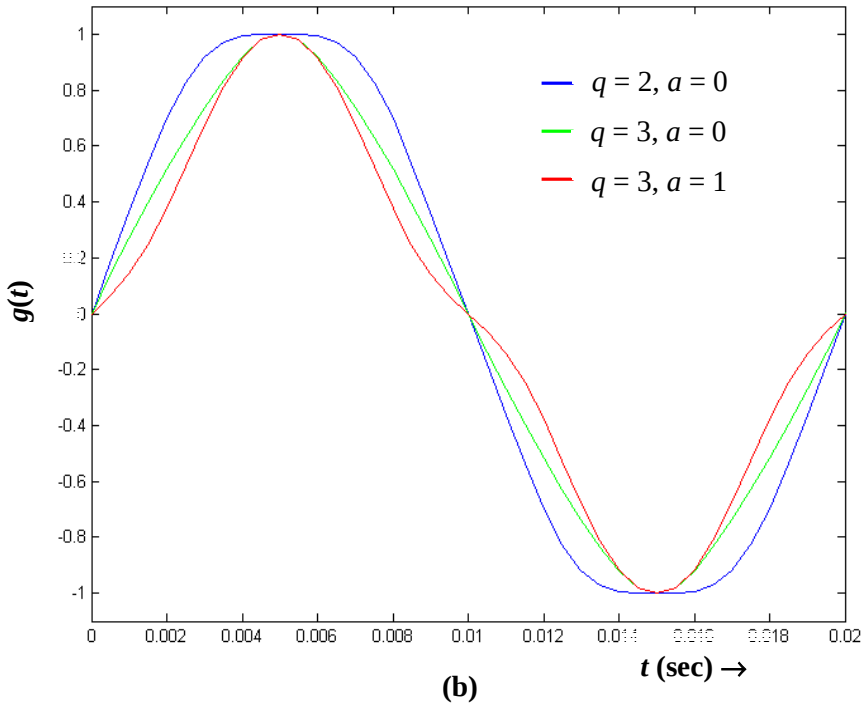

Fig. 6.1: Expected signal $g(t)$ with (a) $N = 6$ and modulation index $m_a = 1$ (b) $N = 7$ and modulation index $m_a = 1$.

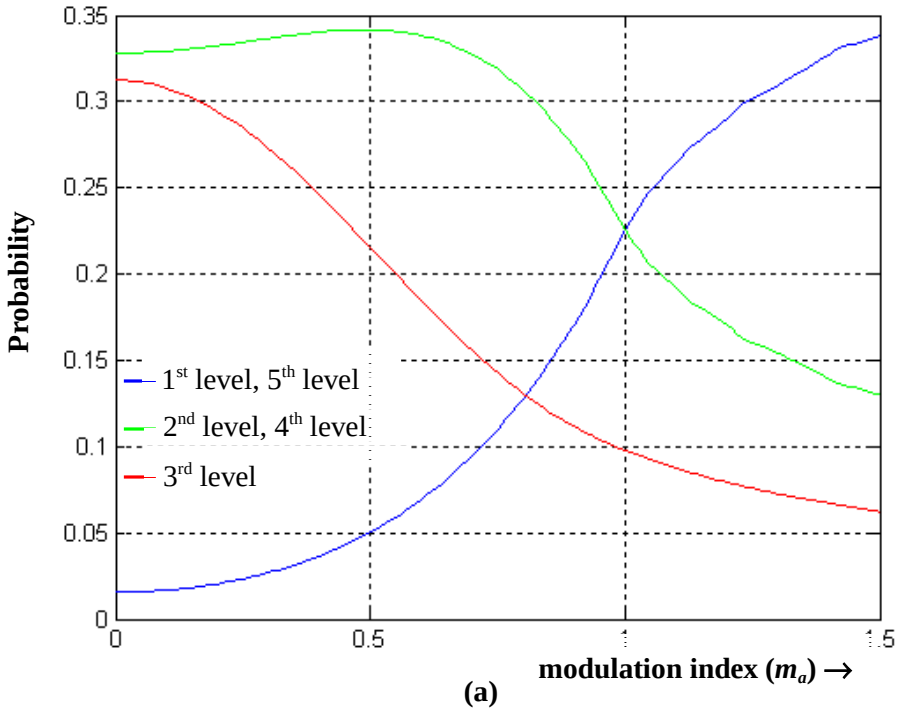

Fig. 6.2: Probability versus modulation index for $N = 6$ (a) combination 2 ($q = 3$, $a = 0$).

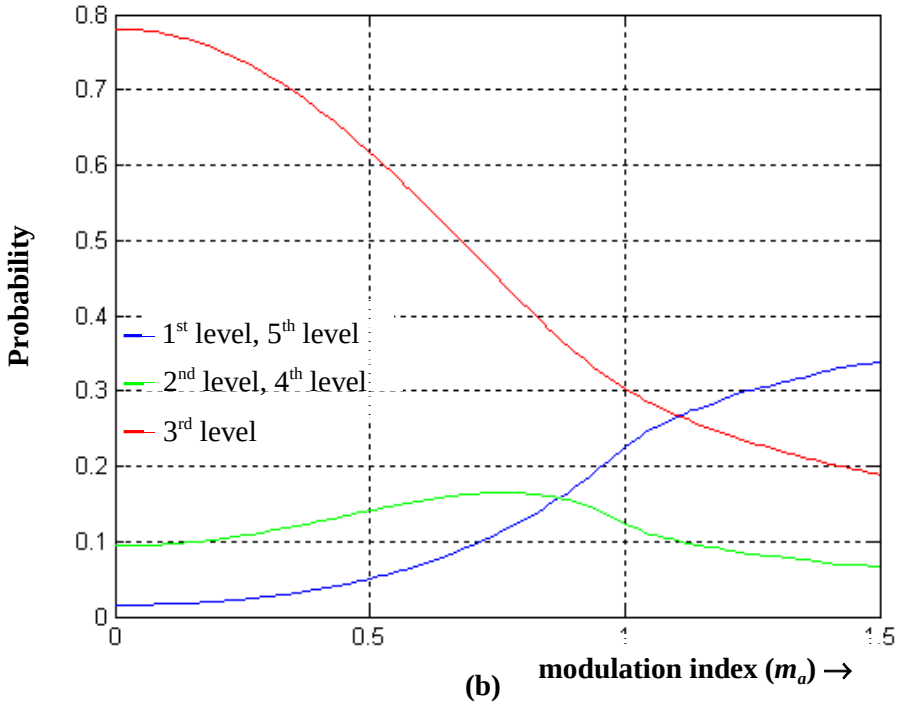

(b)

Fig. 6.2: Probability versus modulation index for N = 6 (a) combination 2 (q = 3, a = 0) (b) combination 3 (q = 3, a = 1).

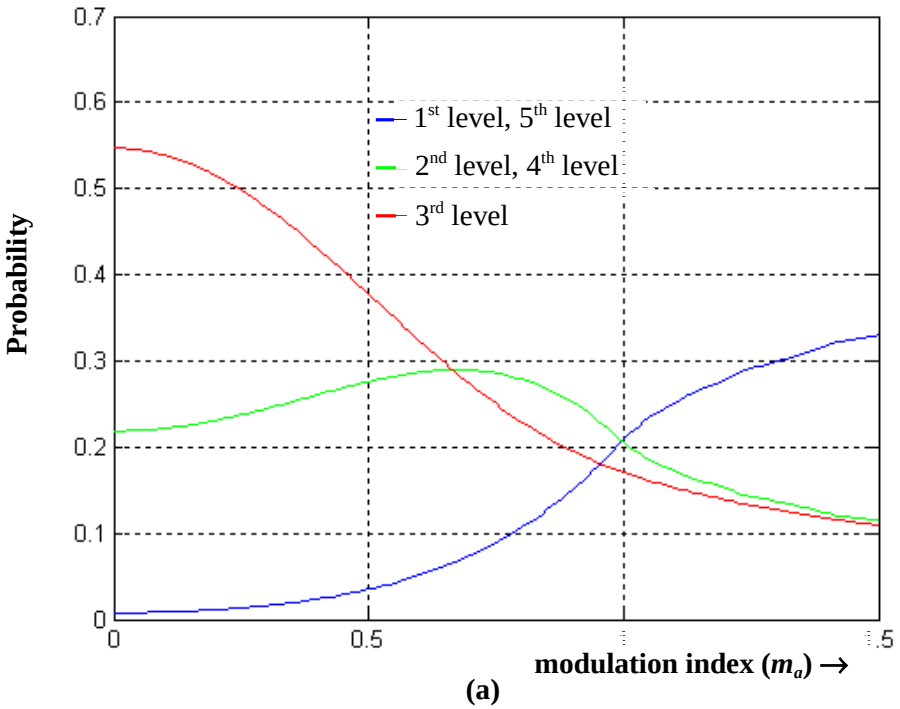

(a)

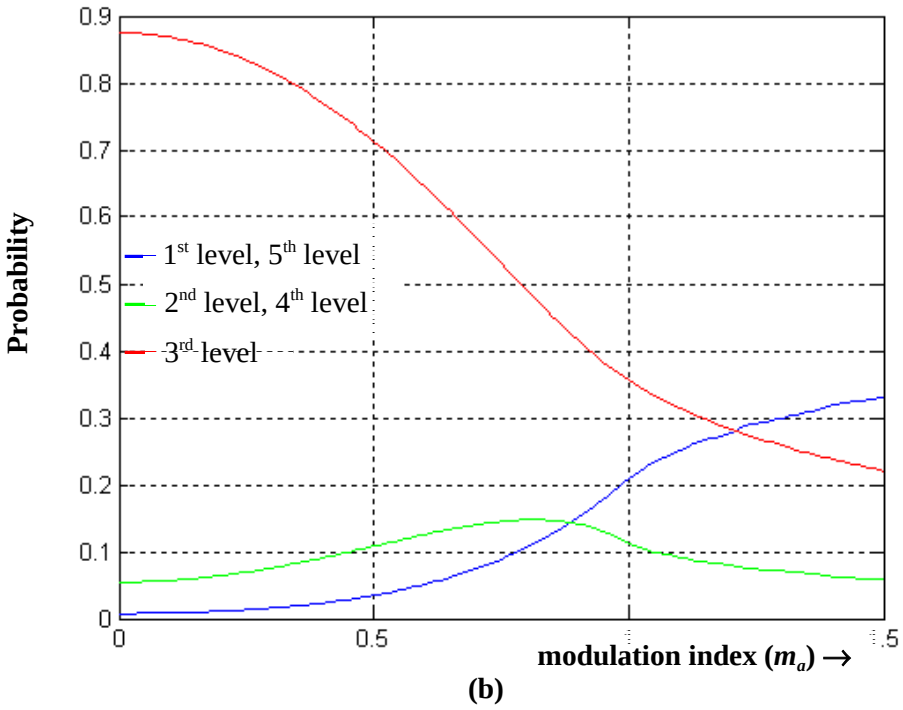

(b)

Fig. 6.3: Probability versus modulation index for N = 7 (a) combination 2 (q = 3, a = 0). (b) combination 3 (q = 3, a = 1).

Figs. 6.4 (a) and (b) show the expected value $g(t)$ for values of N equal to 8 and 9 and with various combinations of q and a. The average probabilities of each level of the dc-bus over one fundamental cycle versus modulation index for the modified WRPWM scheme operating with N = 8 and 9 and with combinations 2, 3, 4 and 5 are shown in Figs. 6.5 and 6.6. Similar plots for combination 1 are shown in Fig. 5.27 (d) and (e) for N = 8 and 9 respectively. Note that the characteristics for the modified WRPWM scheme operating with the combination 1 (i.e., q = 2, a = 0) are identical to those of the standard multilevel WRPWM scheme discussed in chapter 5.

From Fig. 6.4 (a) and (b), tables 6.3 and 6.4, when operating with combination 2 (i.e., q = 3, a = 0), combination 3 (i.e., q = 4, a = 0) and combination 4 (i.e., q = 4, a = 1), $g(t)$ is more sinusoidal for the WRPWM scheme operating with N = 8 and 9 than the standard WRPWM scheme. This is due to the fact that the probability of connecting the output terminals of the inverter to the first and fifth dc-bus voltage levels has been reduced (see Figs. 6.5 (a), (b) and (c) and Figs. 6.6 (a), (b) and (c)). Thus it is expected that one of the combinations 2, 3 or 4 will have an optimal harmonic content for a fixed value of N. Now, if combination 5 (i.e., q = 4, a =2) is applied, it is clear that the five-level inverter is more likely to connect its output

terminal to the third voltage level (see Fig. 6.2 (b)). Consequently, the probability that the inverter will connect its output terminals to the first and fifth dc-bus voltage is reduced and the expected value $g(t)$ becomes more pulse like.

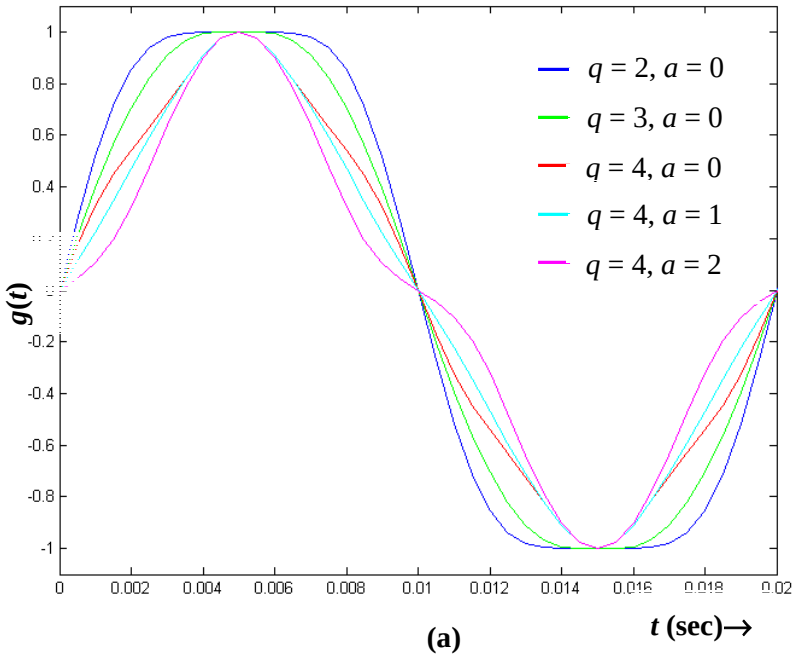

Fig. 6.4: Expected signal $g(t)$ with (a) N = 8 and modulation index m_a = 1.

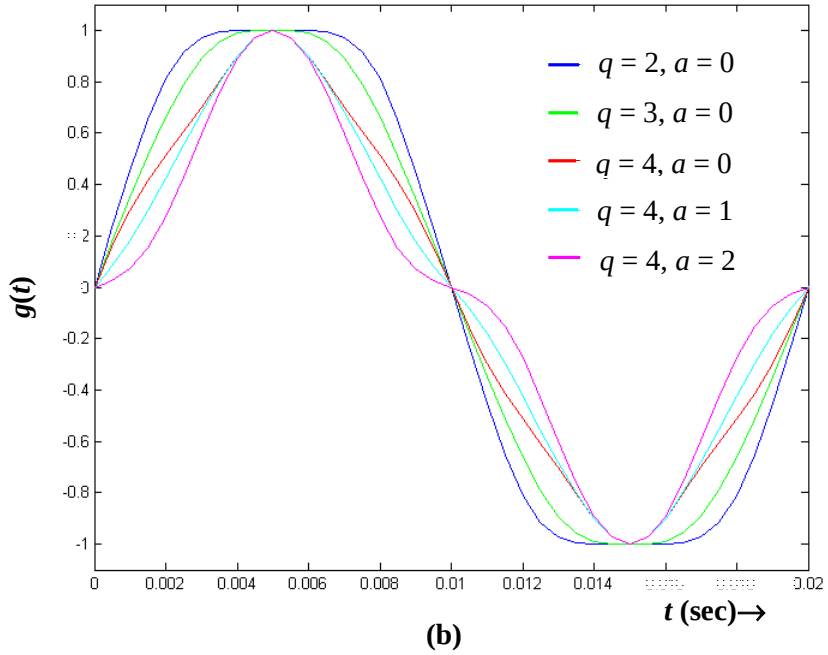

Fig. 6.4: (continued) (b) N = 9 and modulation index m_a = 1.

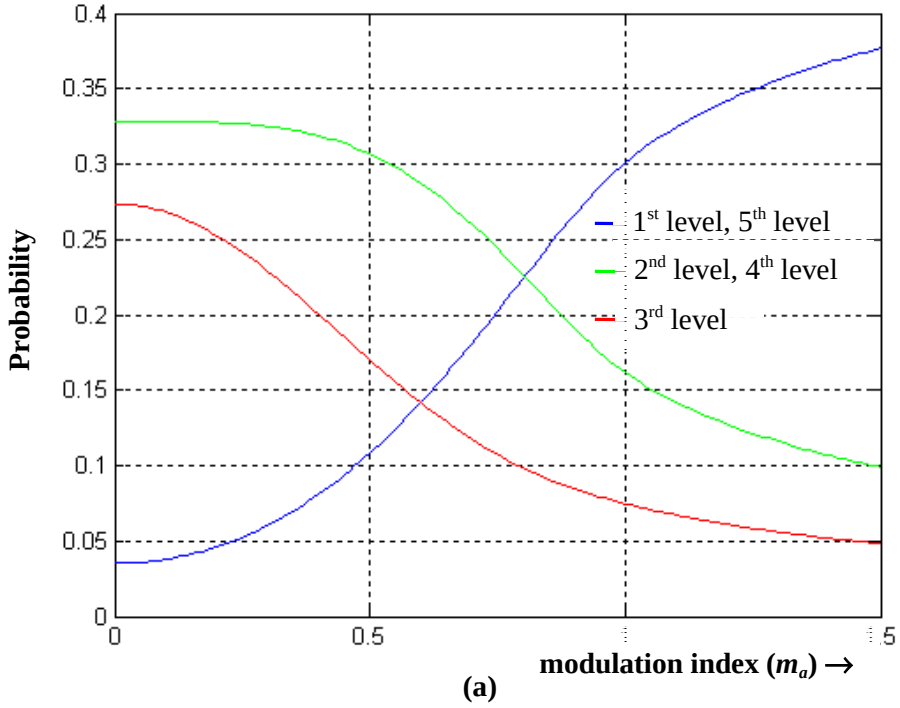

(a)

Fig. 6.5: Probability versus modulation index for N = 8 (a) combination 2 (q = 3, a = 0).

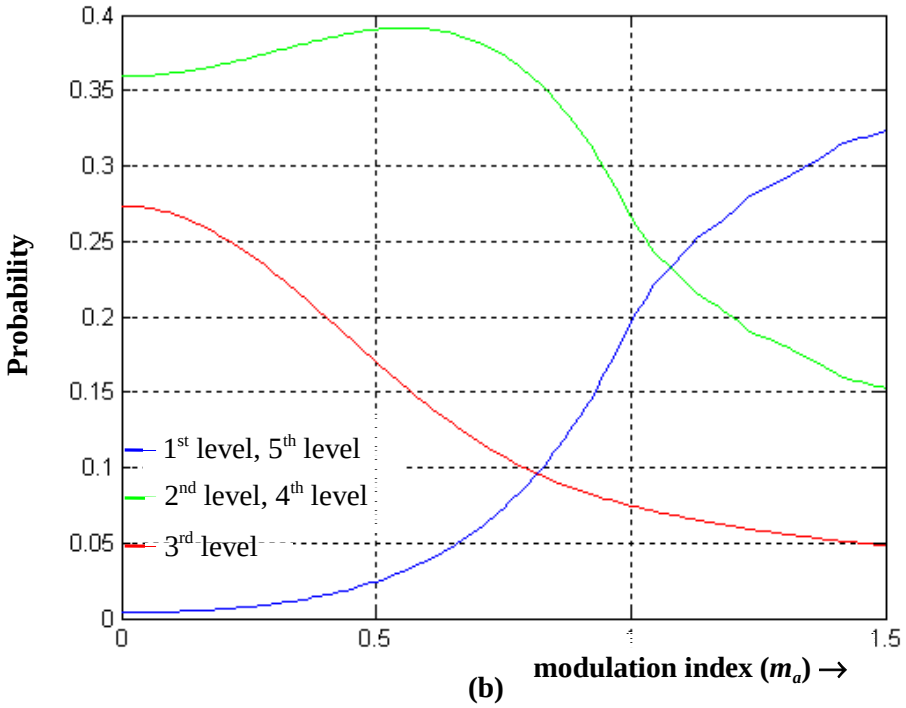

(b)

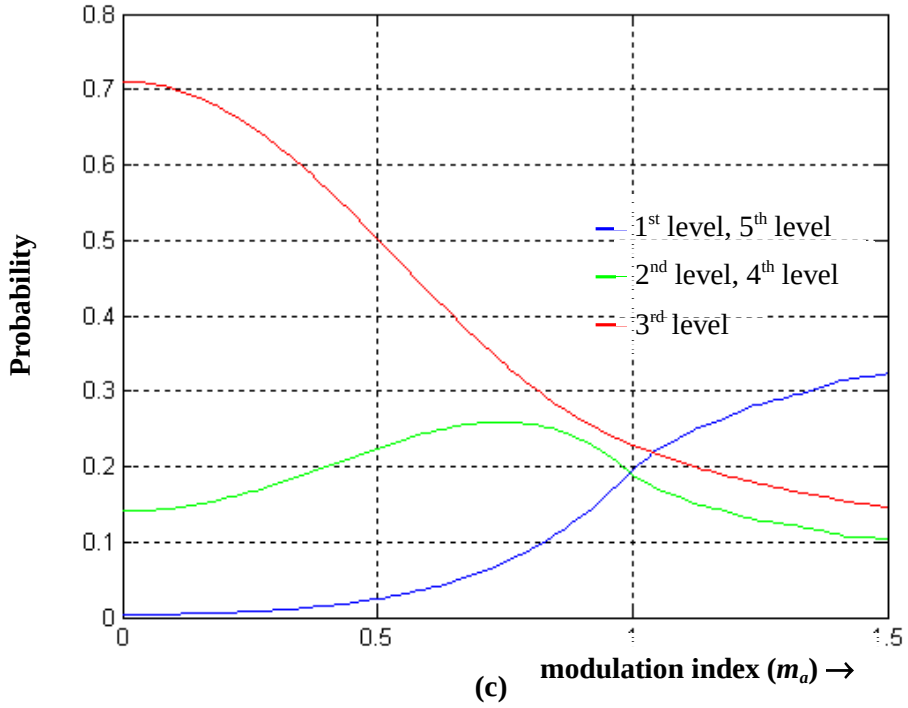

(c)

Fig. 6.5: (continued) (b) combination 3 (q = 4, a = 0) (c) combination 4 (q = 4, a = 1).

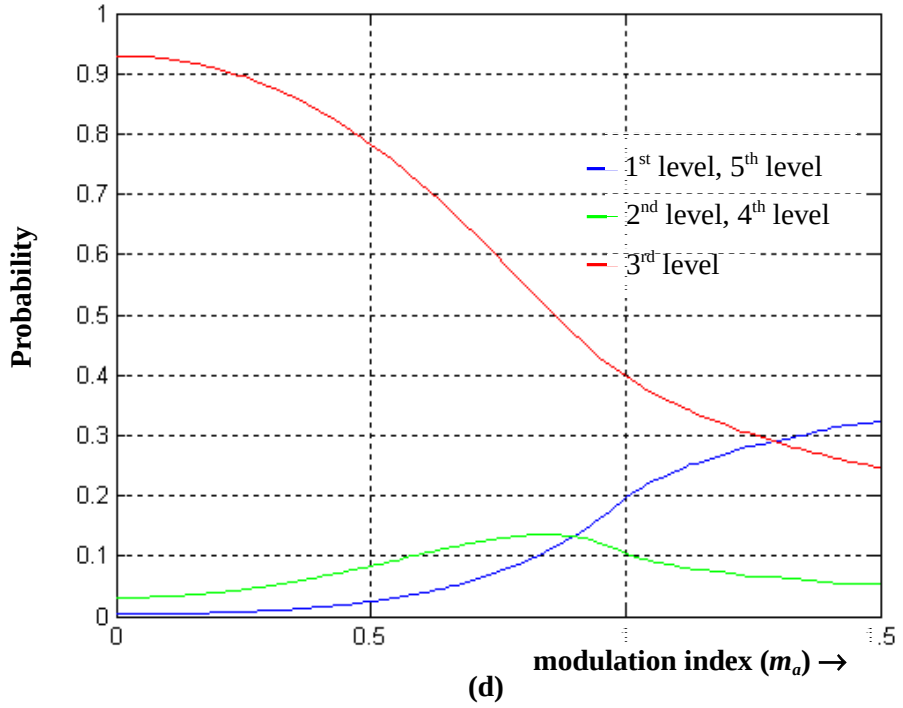

(d)

Fig. 6.5: (continued) (d) combination 5 (q = 4, a = 2).

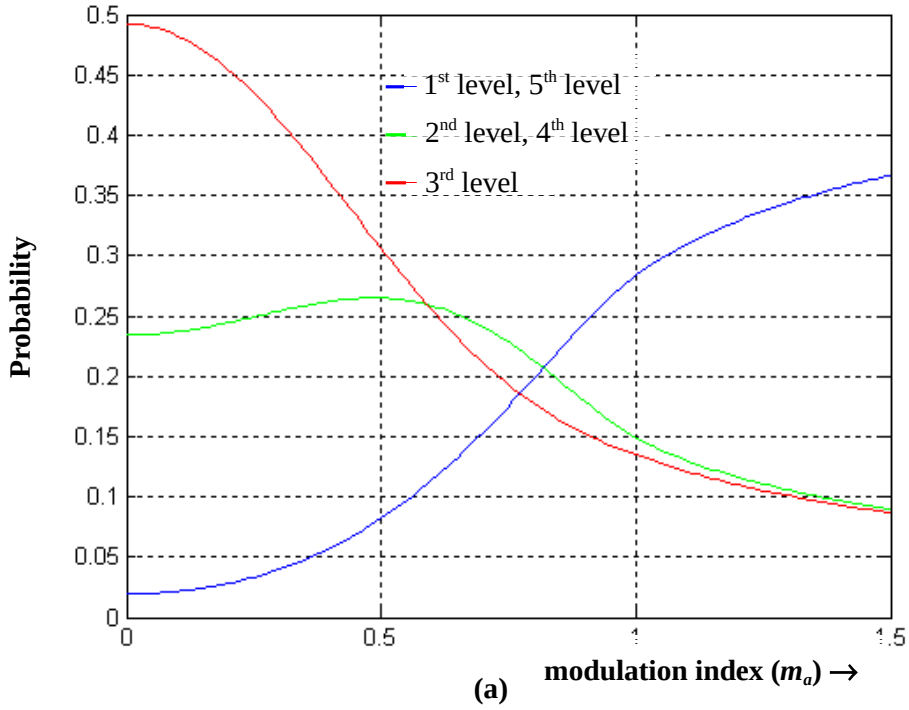

(a)

Fig. 6.6: Probability versus modulation index for N = 9 (a) combination 2 (q = 3, a = 0).

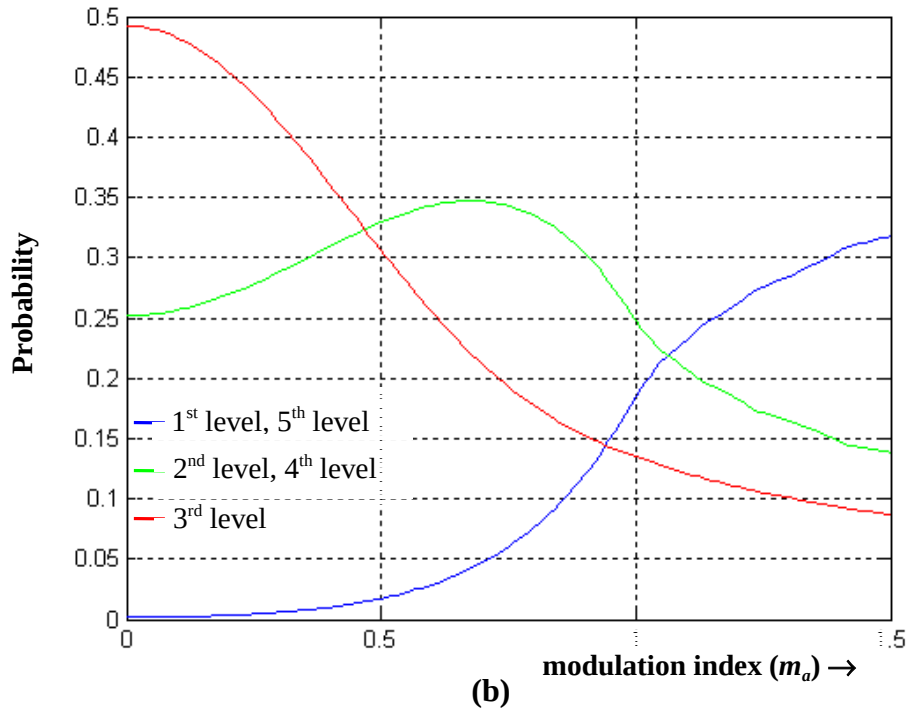

(b)

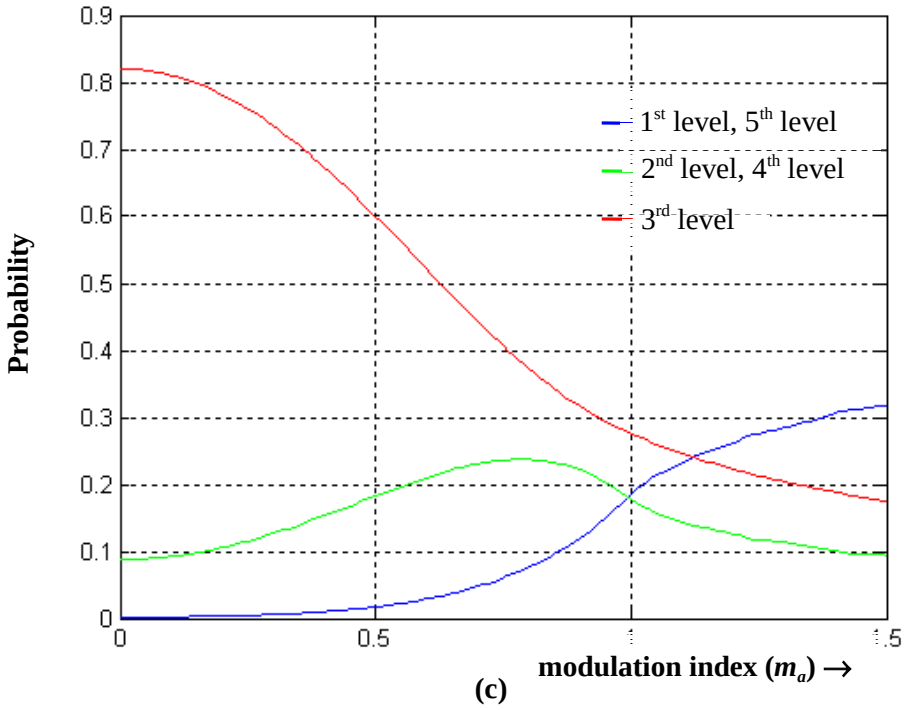

(c)

Fig. 6.6: (continued) (b) combination 3 (q = 4, a = 0) (c) combination 4 (q = 4, a = 1).

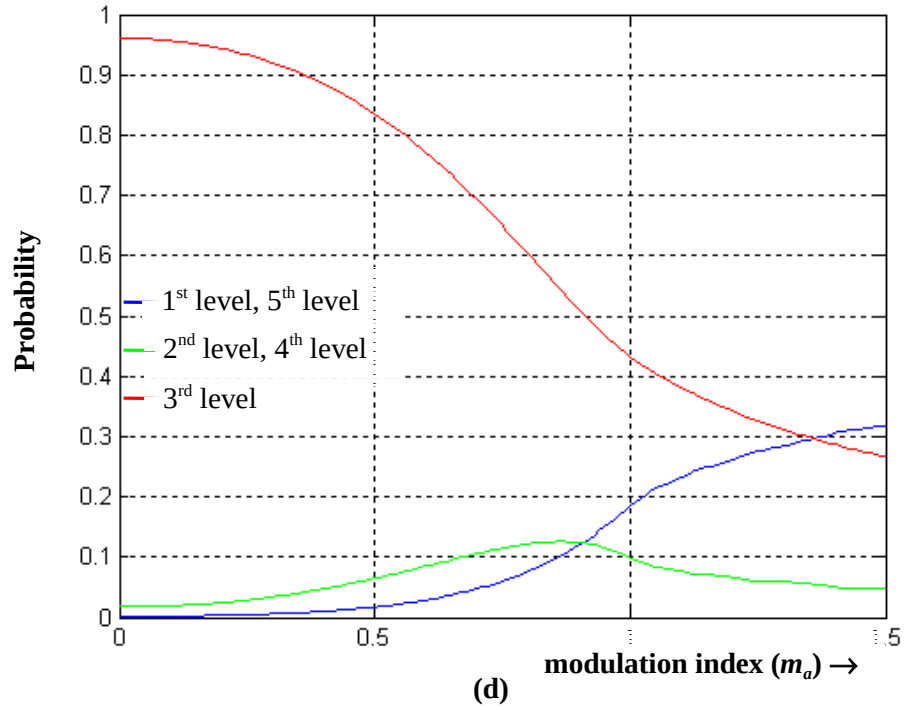

(d)

Fig. 6.6: (continued) (d) combination 5 (q = 4, a = 2).

6.3.1 Modified WRPWM Scheme Operating with N = 6

Fig. 6.7 shows typical plots of fundamental component $2|c_1|$ for the WRPWM scheme operating with N = 6 versus modulation index m_a and for various combinations of q and a.

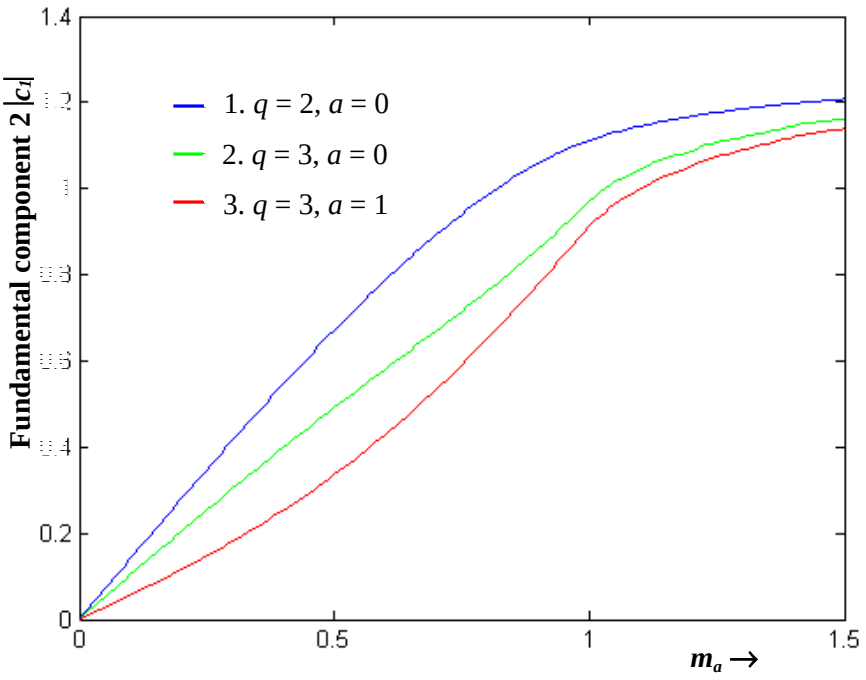

Fig. 6.7: Theoretical fundamental components versus modulation index with N = 6.

From Fig. 6.7, it is seen that unlike the standard WRPWM scheme with fixed q = 2, the modified WRPWM scheme operating with N = 6 does not give rise to linear fundamental-modulation index characteristics within the range $m_a < 1$ for all the combinations of q and a. In particular combinations 2 and 3 lead to slightly non-linear characteristics. For all the combinations of q and a, these characteristics saturate when the modulation index increases above one. The reasons for such behavior have been discussed in section 5.2. Note that the fundamental component for combination 2 is lower than that for combination 1 and the fundamental component for combination 3 is lower than that for combination 2. This is because when operating with combination 1 the probability for the inverter to connect its output terminals to the first and fifth level of dc-bus voltage is the highest. When operating with combination 2 the probability is the second highest and when operating with combination 3 the probability is the lowest (see Figs. 5.27 (b) and 6.2). Note that the fundamental component is proportional to the probability for the inverter to connect its output terminals to the first and fifth level of dc-bus voltage.

Fig. 6.8 shows typical plots of third harmonic component versus modulation index.

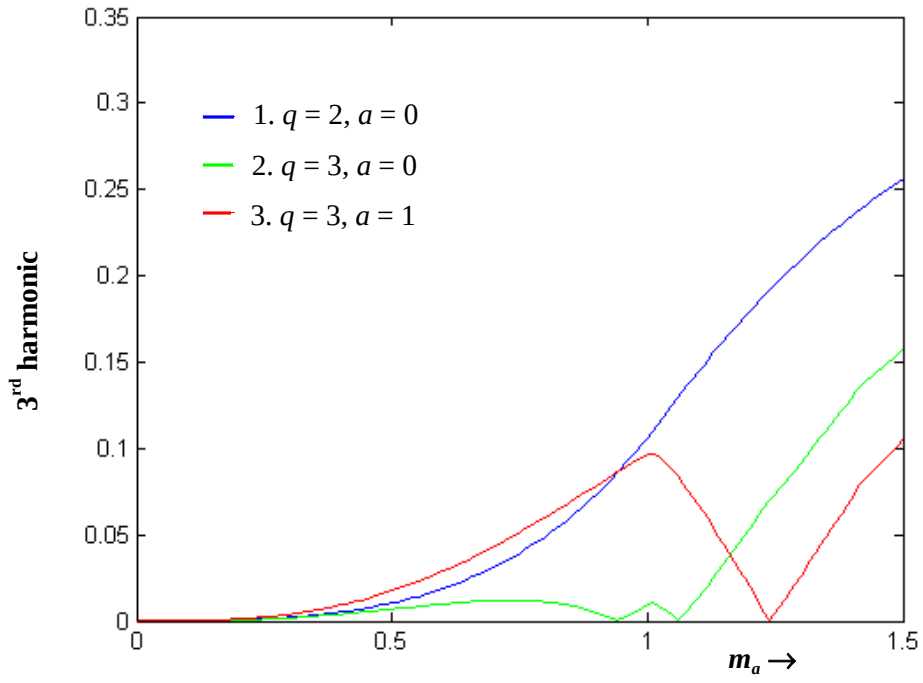

Fig. 6.8: Theoretical $2|c_3|$ versus modulation index with N = 6.

From Fig. 6.8, it can be seen that for N = 6, the WRPWM scheme operating with the various combinations that were considered have third harmonic boosting effect. It is also evident that in the linear modulation region the WRPWM scheme operating with combination 3 has the highest value of $|c_3|$. Further, the WRPWM scheme operating with the combination 2 has the lowest value of $|c_3|$ and is approximately zero at m_a = 0.94. For the range of m_a < 0.5, the WRPWM scheme with combinations 1 and 2 have similar third harmonic to fundamental ratio.

In the entire overmodulation region the WRPWM scheme with combination 1 has the highest value of $|c_3|$. It is also evident that the WRWPM scheme operating with combination 2 has the lowest value of $|c_3|$ at 1 < m_a < 1.12 and is approximately zero at m_a = 1.06. On the other hand, the WRPWM scheme operating with combination 3 has the lowest value of $|c_3|$ at 1.12 < m_a < 1.5.

In the linear region the WRPWM scheme operating with combination 2 offers the best performance because it has a lower value of $|c_3|$ than the WRPWM scheme operating with other combinations. The WRPWM scheme operating with combination 2 offers the best performance for modulation indices within the range 1 < m_a < 1.12. It is known that for most of the applications the modulation index rarely exceed over 1.2.
Fig. 6.9 shows typical plots of fifth harmonic component versus modulation index.

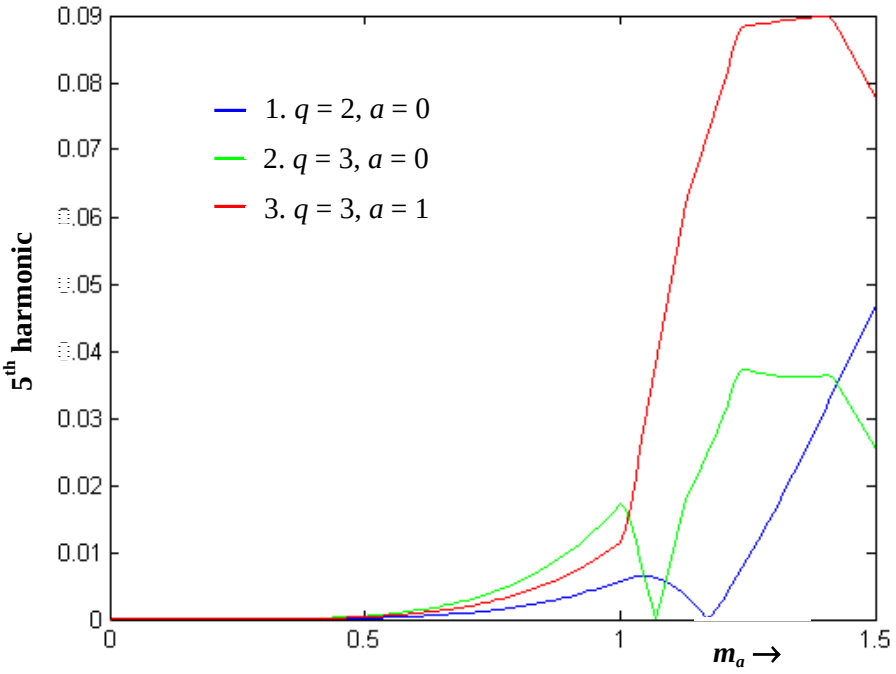

(c)

Fig. 6.9: Theoretical $2|c_5|$ versus modulation index with $N = 6$.

From Fig. 6.9 it is seen that the modified WRPWM scheme for a five-level inverter generates a fifth harmonic for all the combinations of q and a considered. In the linear modulation region, the WRPWM scheme operating with combination 1 has the lowest value of $|c_5|$ and the WRPWM scheme operating with combination 2 has the highest value of $|c_5|$.
In the overmodulation region, the fifth harmonic of the WRPWM scheme operating with combination 1 is insignificant within the range $1 < m_a < 1.25$. The fifth harmonic of the WRPWM scheme operating with combination 1 is approximately zero at $m_a = 1.17$. On the other hand, the fifth harmonic of the WRPWM scheme operating with combination 2 is approximately zero at $m_a = 1.07$.

The WRPWM scheme operating with combination 1 offers the best overall performance. This is due to the fact that it has a lower value of $|c_5|$ than the WRPWM scheme operating with other combinations of q and a.

Fig. 6.10 shows typical plot of seventh harmonic component versus modulation index.

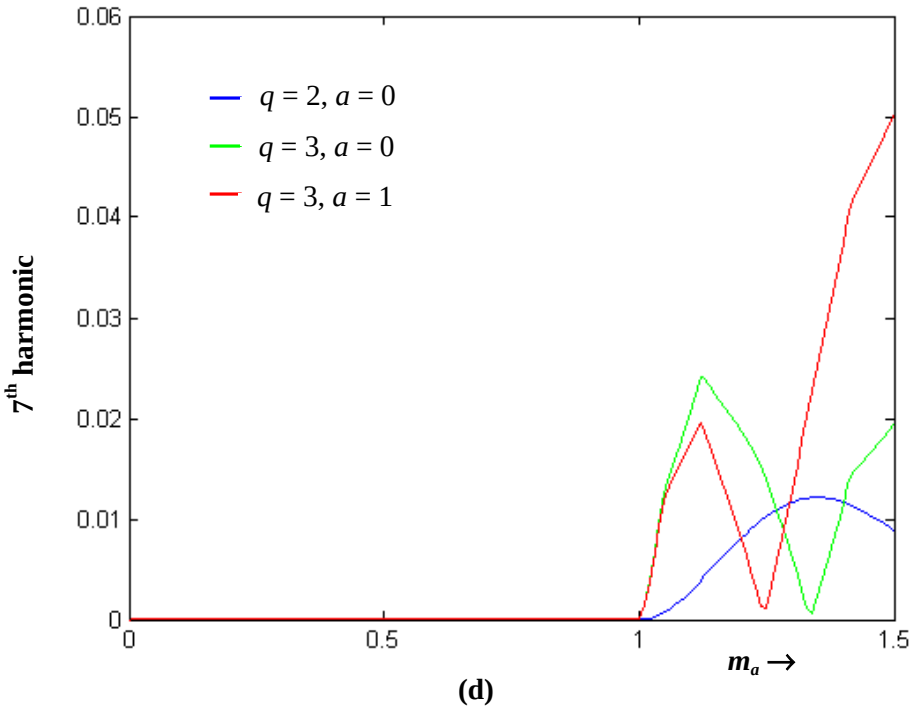

Fig. 6.10: Theoretical $2|c_7|$ versus modulation index with $N = 6$.

From Fig. 6.10 it can be seen that in the entire linear modulation region, the seventh harmonic of the WRPWM scheme operating with the combinations of q and a under consideration are insignificant and can be considered negligible.

In the overmodulation region, the WRPWM scheme operating with combination 1 has the lowest $|c_7| / |c_1|$ ratio within the range $1 < m_a < 1.2$ and $1 < m_a < 1.4$. The seventh harmonic reaches its minimum value at $m_a = 1.34$ with combination 2, and at $m_a = 1.25$ the $|c_7| / |c_1|$ ratio reaches approximately zero with combination 3.

In the linear region, the WRPWM scheme operating with all the combinations of q and a offer a good performance, as they give rise to an insignificant $|c_7|$. For the slightly overmodulated region $1 < m_a < 1.2$, the WRPWM scheme operating with combination 1 offers a better performance than the other combinations of q and a. It generates a lower $|c_7|$ than the WRPWM scheme operating with other combinations of q and a.

Figs. 6.11 (a) and (b) show the characteristic plots of the ninth harmonic $|c_9|$ and eleventh harmonic $|c_{11}|$ versus modulation index m_a, respectively.

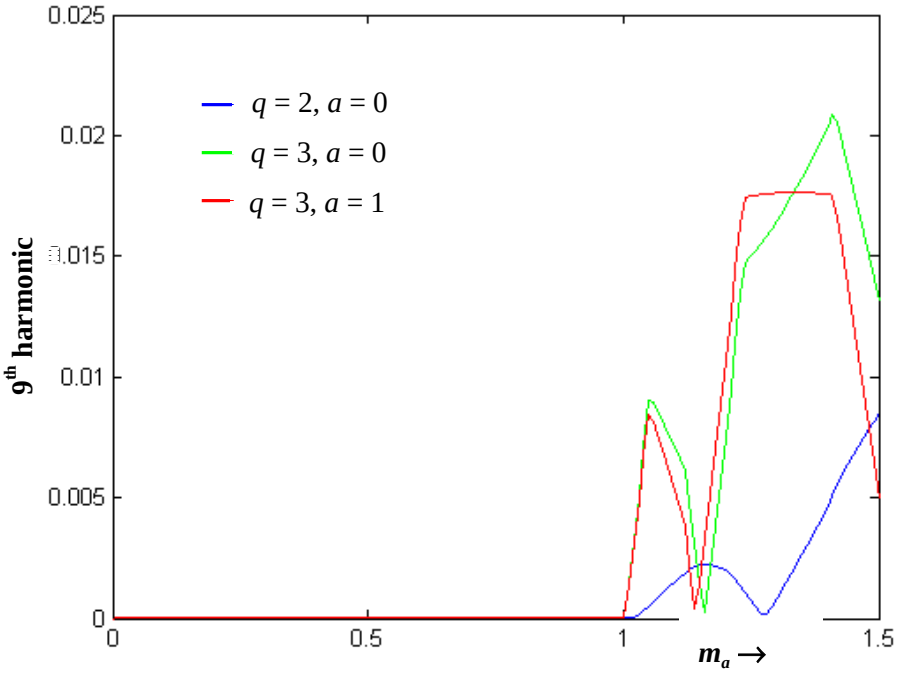

(a)

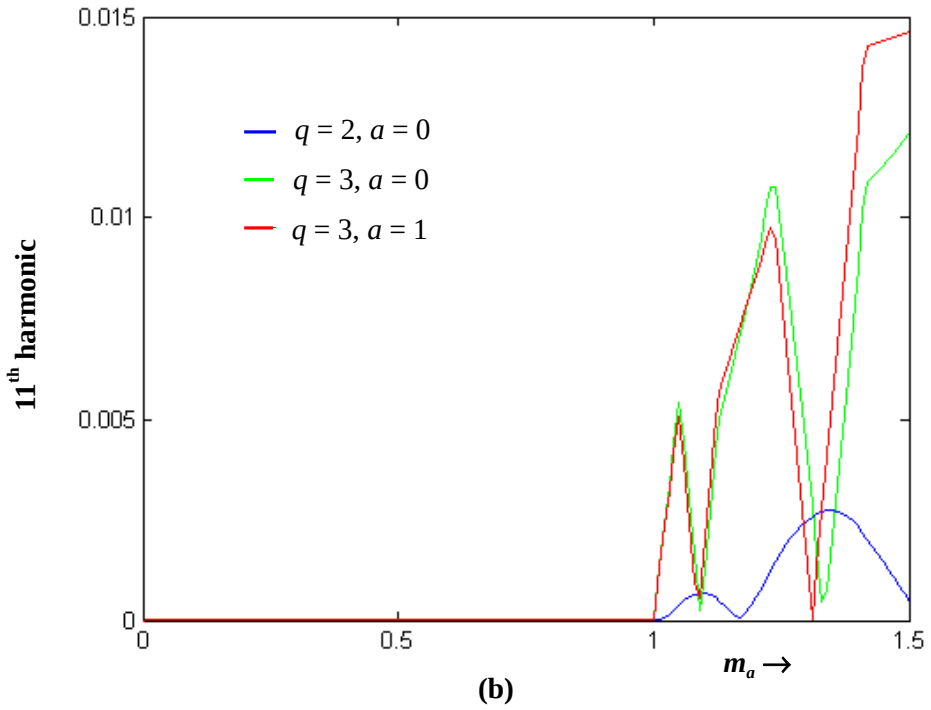

Fig. 6.11: Plots of harmonics vs. modulation index (a) 9th harmonic. (b) 11th harmonic.

From Fig. 6.11 (a) it can be seen that in the entire linear modulation region, the ninth harmonic of the WRPWM scheme operating with the combinations of q and a under consideration are insignificant and can be considered negligible.

In the overmodulation region, the ninth harmonic of the WRPWM scheme operating with combination 1 reaches its minimum value at m_a = 1.27. Furthermore, the ninth harmonic reaches its minimum at m_a = 1.16 with combination 2, and at m_a = 1.14 with combination 3.

In the linear region, the WRPWM scheme operating with all the combinations of q and a offer a good performance as they give rise to negligible $|c_9|$. For the slightly overmodulated region $1 < m_a < 1.2$, the WRPWM scheme operating with combination 1 offers a better performance than the other combinations of q and a.

From Fig. 6.11 (b) it can be seen that in the region of $0 < m_a < 1.3$, the ratio $|c_{11}| / |c_1|$ for the WRPWM schemes operating with the combinations under consideration are insignificant. In the overmodulation region, the eleventh harmonic reaches approximately zero at m_a = 1.17 with combination 1, the ratio $|c_{11}| / |c_1|$ becomes negligible at m_a = 1.09 and 1.34 with combination 2, and at m_a = 1.09 and 1.331 with combination 3.

In the linear region, the WRPWM schemes operating with the various combinations of q and a offer a good performance because they have negligible value of $|c_{11}|$. For the overmodulation region, the WRPWM scheme operating with combination 1 offers the best performance compared with the other combinations of q and a, because it has the lowest value of $|c_{11}|$ at m_a < 1.2.

6.3.2 Modified WRPWM Scheme Operating with N = 7

Fig. 6.12 shows typical plots of fundamental component $2|c_1|$ for the WRPWM scheme operating with N = 7 versus modulation index, m_a, for various combinations of q and a.

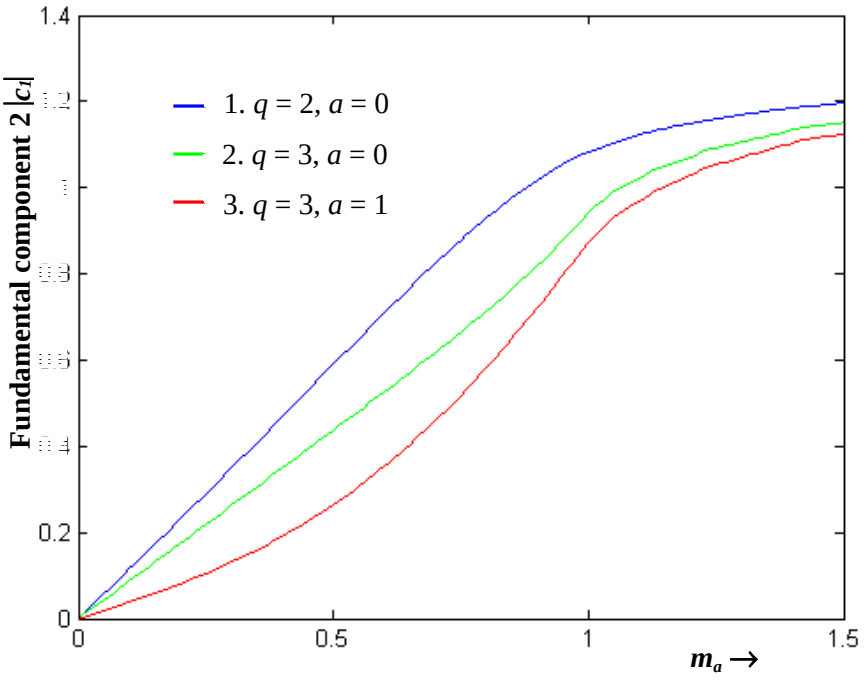

Fig. 6.12: Theoretical fundamental components versus modulation index with N = 7.

From Fig. 6.12, it is seen that unlike the standard WRPWM scheme with fixed q = 2, the modified WRPWM scheme operating with N = 7 does not give rise to linear fundamental-modulation index characteristics within the range $m_a < 1$ for all the combinations of q and a. In particular combinations 2 and 3 lead to slightly non-linear characteristics. For all the combinations of q and a, these characteristics saturate when the modulation index increases above one. Note that the fundamental component for combination 2 is lower than that for combination 1 and the fundamental component for combination 3 is lower than that for combination 2. This is because when operating with combination 1 the probability for the inverter to connect its output terminals to the first and fifth level of dc-bus voltage is highest, when operating with combination 2 the probability is the second highest and when operating with combination 3 the probability is the lowest (see Figs. 5.27 (c) and 6.3). Note that the fundamental component is proportional to the probability for the inverter to connect its output terminals to the first and fifth level of dc-bus voltage.

Fig. 6.13 shows typical plots of third harmonic component versus modulation index.

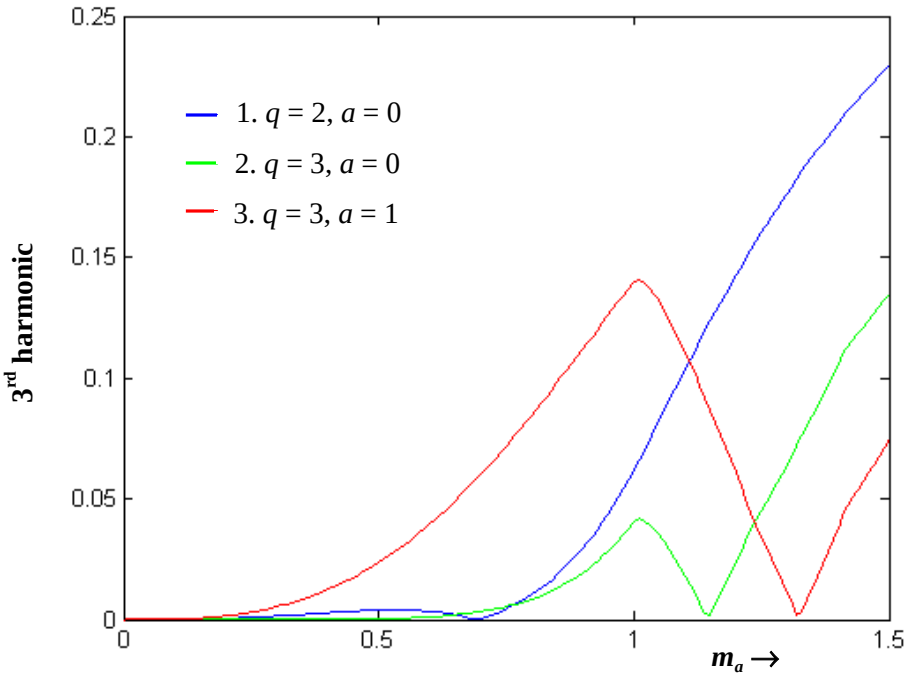

Fig. 6.13: Theoretical $2|c_3|$ versus modulation index with N = 7.

From Fig. 6.13, it can be seen that for N = 7, the WRPWM schemes for all the combinations that were considered have third harmonic boosting effect. In the linear modulation region the WRPWM scheme operating with combination 3 has the highest $|c_3|$. It is also evident that the WRPWM scheme operating with the combination 2 has the lowest value of $|c_3|$ at $0 < m_a < 0.63$ and $0.82 < m_a < 1$. The WRPWM scheme operating with the combination 1 has the lowest value of $|c_3|$ at $0.63 < m_a < 0.82$ and is approximately zero at $m_a = 0.69$.

In the overmodulation region the WRPWM scheme with combination 1 has the highest $|c_3| / |c_1|$ ratio at $1.13 < m_a < 1.5$. At the same time, the WRWPM scheme operating with combination 3 has the highest $|c_3| / |c_1|$ ratio at $1 < m_a < 1.13$ and is negligible at $m_a = 1.32$. Further, the WRPWM scheme operating with combination 2 has the lowest value of $|c_3|$ at $1 < m_a < 1.23$ and is negligible at $m_a = 1.15$.

The WRPWM scheme operating with combination 2 offers the best overall performance as it has the lowest value of $|c_3|$ at $0 < m_a < 0.63$ and $0.82 < m_a < 1.23$.

Fig. 6.14 shows typical plots of fifth harmonic component versus modulation index.

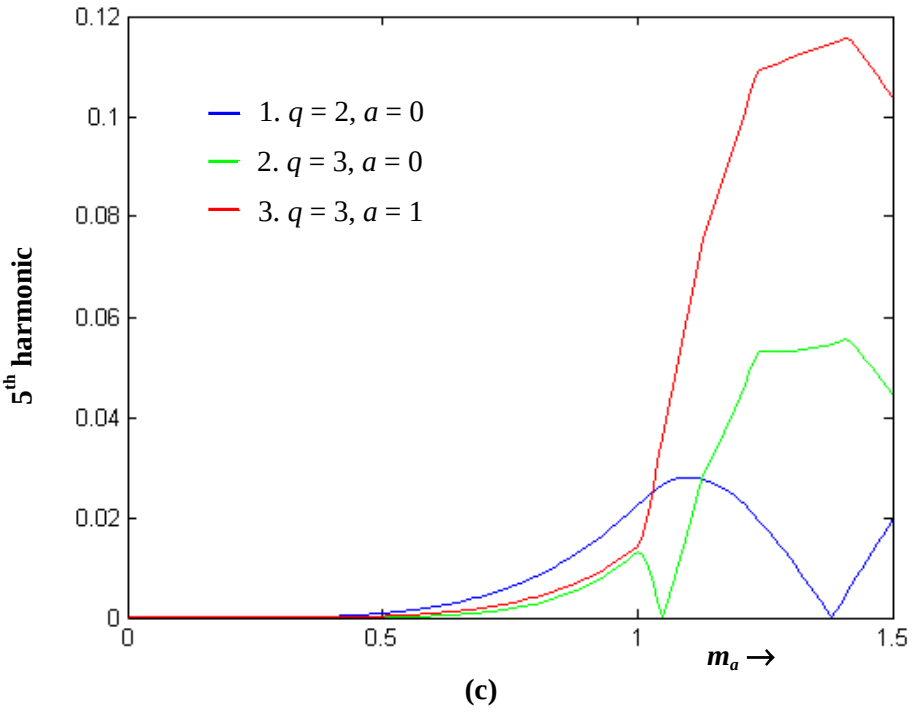

Fig. 6.14: Theoretical $2|c_5|$ versus modulation index with N = 7.

From Fig. 6.14 it is seen that the modified WRPWM scheme for a five-level inverter generates a fifth harmonic for all the combinations of q and a considered. In the linear modulation region, the WRPWM scheme operating with combination 1 has the highest $|c_5|$. The WRPWM scheme operating with combination 2 has the lowest value of $|c_5|$ and is insignificant at $0 < m_a < 0.94$ (i.e., almost the entire linear modulation region).

In the overmodulation region, the value of $|c_5|$ of the WRPWM scheme operating with combination 1 is the lowest at $1.12 < m_a < 1.5$ and is approximately zero at $m_a = 1.38$. The $|c_5| / |c_1|$ ratio of the WRPWM scheme operating with combination 2 is the lowest at $1 < m_a < 1.12$ and is approximately zero at $m_a = 1.05$.

The WRPWM scheme operating with combination 2 offers the best overall performance. It has the lowest $|c_5|$ compared with the WRPWM schemes operating with other combinations of q and a within the range $1 < m_a < 1.12$.

Fig. 6.15 shows typical plot of seventh harmonic component versus modulation index.

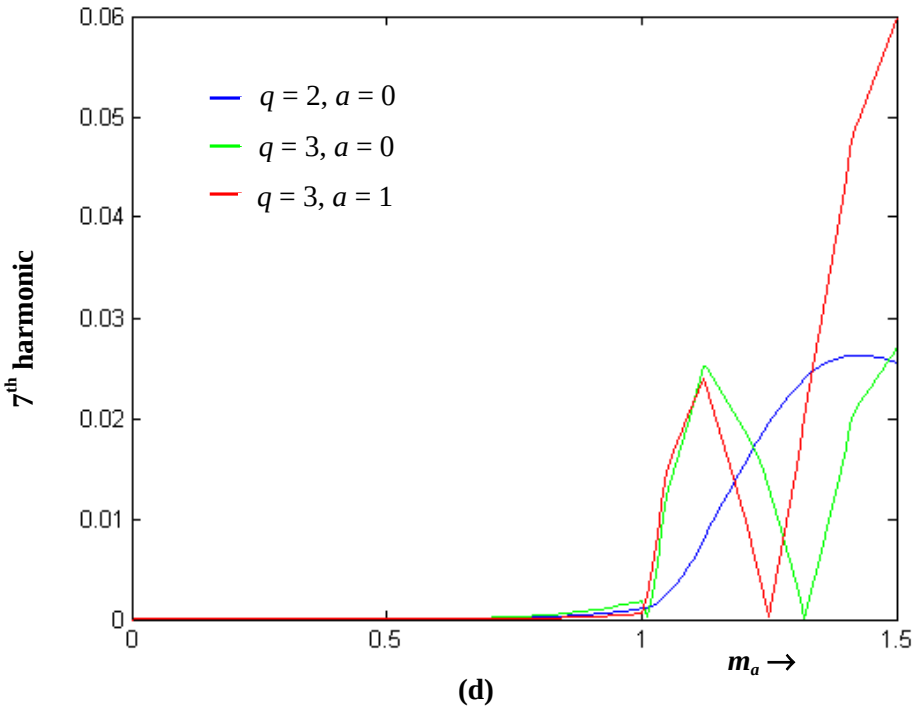

Fig. 6.15: Theoretica 2l$|c_7|$ versus modulation index with $N = 7$.

From Fig. 6.15 it can be seen that in the entire linear modulation region, the seventh harmonic of the WRPWM scheme operating with the combinations of q and a under consideration are insignificant and can be consider negligible.

In the overmodulation region, the value of $|c_7|$ for the WRPWM scheme operating with combination 1 is the lowest within the range $1.01 < m_a < 1.18$ and $1.48 < m_a < 1.5$. The value of $|c_7|$ for the WRPWM scheme operating with combination 2 is the lowest within the range $1.28 < m_a < 1.48$ and is approximately zero at $m_a = 1.32$. The value of $|c_7|$ of the WRPWM scheme operating with combination 3 is the lowest within the range $1.19 < m_a < 1.28$ and is approximately zero at $m_a = 1.25$.

In the linear region, the WRPWM schemes operating with the various combinations of q and a offer a good performance because they have insignificant value of $|c_7|$. For the slightly overmodulated region $1 < m_a < 1.18$, the WRPWM scheme operating with combination 1 offers the best performance. Compare with all the other combinations of q and a, it has the lowest $|c_7|$.

Figs. 6.16 (a) and (b) show the characteristic plots of the ninth harmonic $2|c_9|$ and eleventh harmonic $2|c_{11}|$ versus modulation index m_a, respectively.

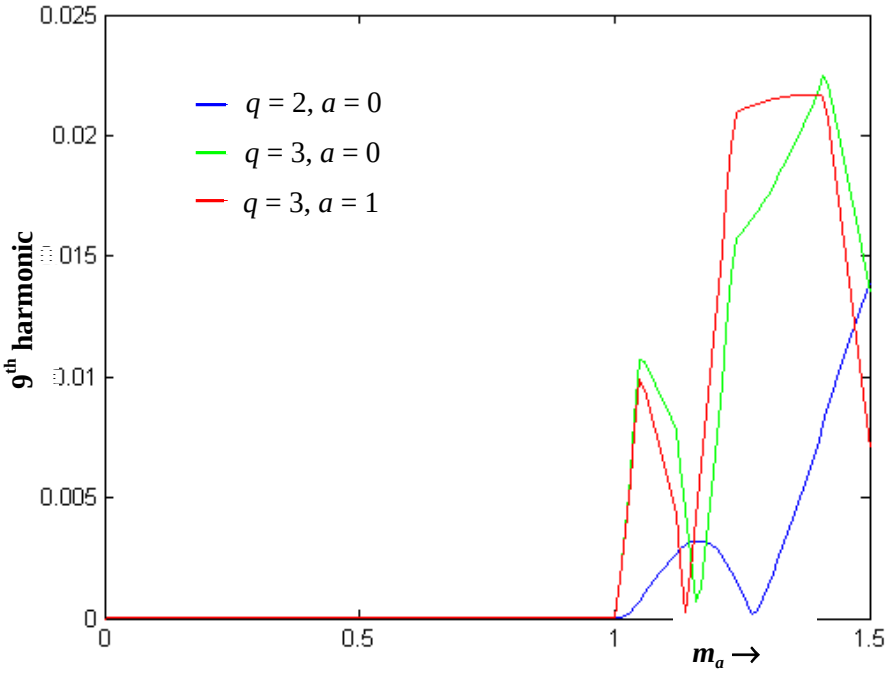

(a)

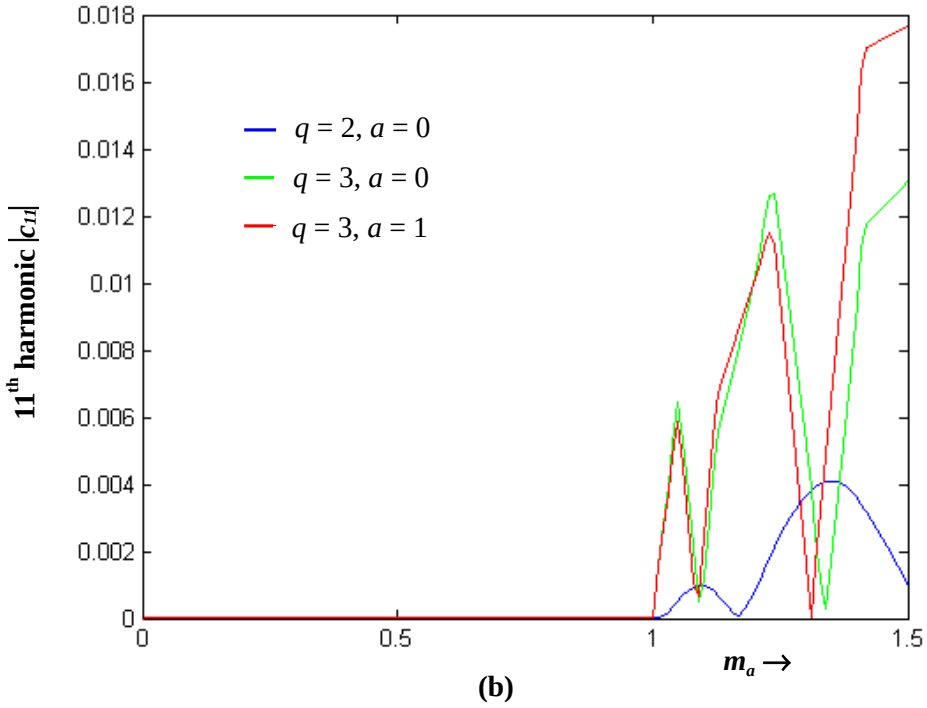

Fig. 6.16: Plots of harmonics vs. modulation index (a) 9^{th} harmonic. (b) 11^{th} harmonic.

From Fig. 6.16 (a) it can be seen that in the entire linear modulation region, the ninth harmonic of the WRPWM schemes operating with the combinations of q and a under consideration are insignificant and can be consider negligible.

The value of $|c_9|$ for the WRPWM scheme operating with combination 1 is the lowest within the range $1 < m_a < 1.12$ and $1.18 < m_a < 1.47$. It is approximately zero in the overmodulation region at $m_a = 1.27$. In the overmodulation region, the value of $|c_9|$ reaches its minimum value ($2|c_9| = 0.00068 \times V_d / 2$) at $m_a = 1.16$ with combination 2. For the WRPWM scheme operating with combination 3 the value $|c_9|$ reaches its minimum value ($2|c_9| = 0.00028 \times V_d / 2$) at $m_a = 1.14$.

In the linear region, the WRPWM schemes operating with the various combinations of q and a offer a good performance as they give rise to negligible value of $|c_9|$. For the slightly overmodulated region $1 < m_a < 1.2$, the WRPWM scheme operating with combination 1 offers the best performance compared with the other combinations of q and a.

From Fig. 6.16 (b) it can be seen that in the linear modulation region, the eleventh harmonic of the WRPWM schemes operating with the various combinations of q and a under consideration are insignificant. In the overmodulation region, the eleventh harmonic of the WRPWM

scheme operating with the combinations under consideration are fairly small (< 1.2 %) except for the WRPWM scheme operating with combination 3 at $1.4 < m_a < 1.5$.

In the linear region, the WRPWM schemes operating with the various combinations of q and a offer a good performance as they generate negligible $|c_{11}|$. For the overmodulation region, the WRPWM scheme operating with combination 1 offers the best performance. Compared with the other combinations of q and a, it has the lowest value of $|c_{11}|$ in the most of the overmodulation region.

6.3.3 Modified WRPWM Scheme Operating with $N = 8$

Fig. 6.17 shows typical plots of fundamental component $2|c_1|$ versus modulation index m_a with various combinations of q and a for the WRPWM scheme operating with $N = 8$.

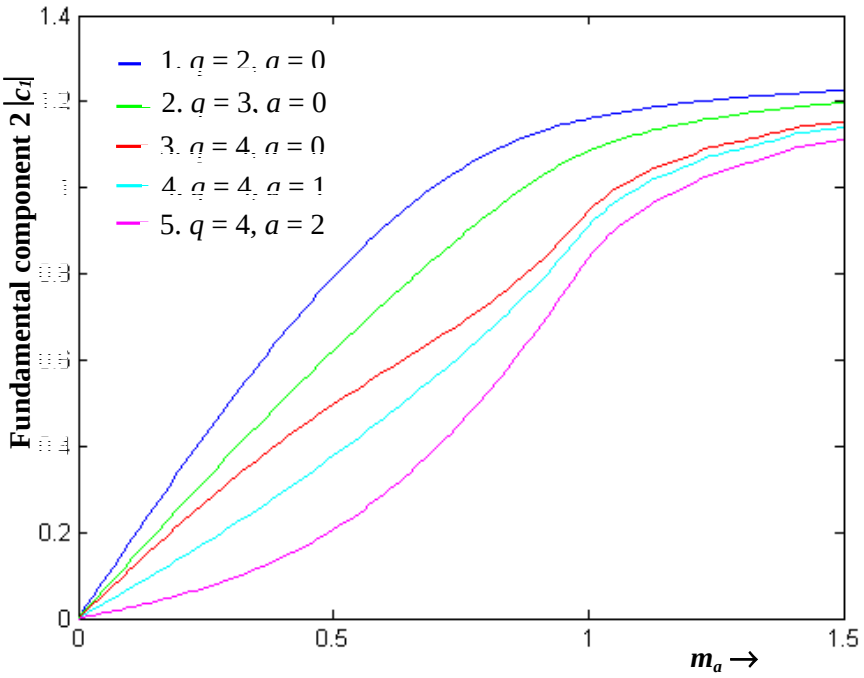

Fig. 6.17: Theoretical fundamental components versus modulation index with N = 8.

From Fig. 6.17, it is seen that unlike the standard WRPWM scheme with fixed q = 2, the modified WRPWM scheme operating with N = 8 does not give rise to linear fundamental-modulation index characteristics within the range $m_a < 1$ for all the combinations of q and a. In particular combinations 3 and 5 lead to slightly non-linear characteristics. For all the combinations of q and a, these characteristics saturate when the modulation index increases above one. It is evident that for all the schemes under consideration, the fundamental component for combination 1 is the highest amongst all those under consideration. The fundamental component for combination 5 on the other hand is the lowest. This is due to the fact that when operating with combination 1 the probability for the inverter to connect its output terminals to the first and fifth level of dc-bus voltage is the highest, when operating with combination 5 the probability is the highest. When operating with combination 3 the probability is the lowest (see Figs. 5.27 (d) and 6.5). Note that the fundamental component is proportional to the probability for the inverter to connect its output terminals to the first and fifth level of dc-bus voltage. The magnitude of the fundamental component in relation to the combinations under consideration can be sorted in descending order as combination 1, combination 2, combination 3, combination 4 and combination 5.

Fig. 6.18 shows typical plots of third harmonic component versus modulation index.

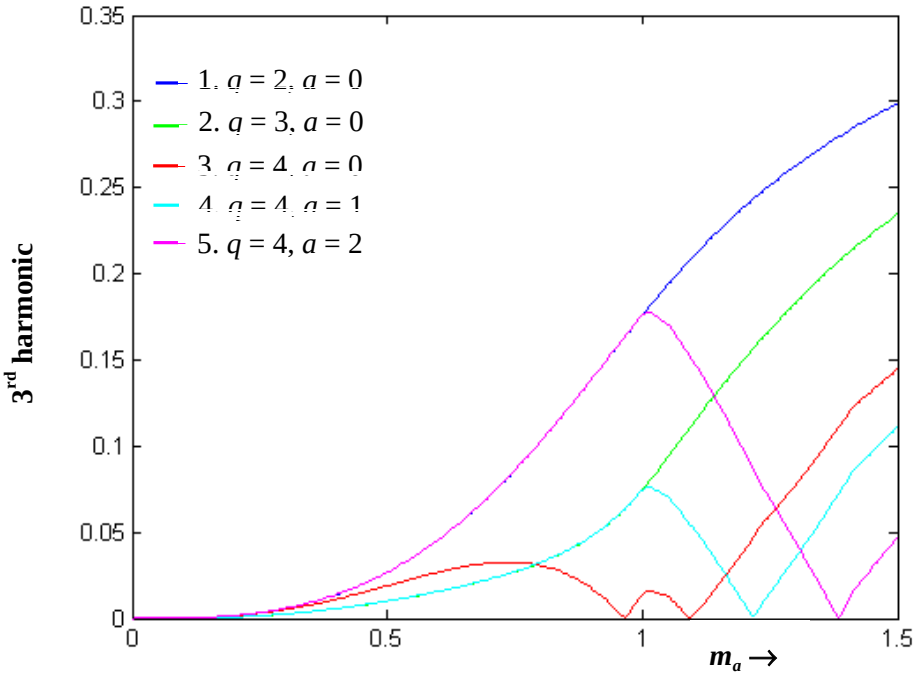

Fig. 6.18: Theoretical $2|c_3|$ versus modulation index with N = 8.

From Fig. 6.18, it can be seen that for N = 8, the WRPWM schemes operating with the combinations under consideration have third harmonic boosting effect. In the linear modulation region the WRPWM scheme operating with combination 5 has the highest value of $|c_3|$ and the WRPWM scheme operating with the combination 2 has the lowest $|c_3|$ within the range $0 < m_a < 0.83$. The WRPWM scheme operating with the combination 3 has the lowest $|c_3|$ within part of the linear modulation region (i.e., $0.83 < m_a < 1$) and is approximately zero at $m_a = 0.97$.

In the overmodulation region the WRPWM scheme operating with combination 3 has the lowest value of $|c_3|$ at $1 < m_a < 1.16$, and the WRPWM scheme operating with combination 4 has the lowest value of $|c_3|$ within the range $1.16 < m_a < 1.31$. It is also evident that the WRWPM scheme operating with combination 5 has the highest value of $|c_3|$ within the range $1 < m_a < 1.08$. The lowest value of $|c_3|$ is within the range $1.31 < m_a < 1.5$ falling to zero at $m_a = 1.39$.

The WRPWM scheme operating with combination 2 offers the best overall performance in the linear modulation region, and the WRPWM scheme operating with combination 3 offers the best overall performance in the overmodulation region.

Fig. 6.19 shows typical plots of fifth harmonic component versus modulation index.

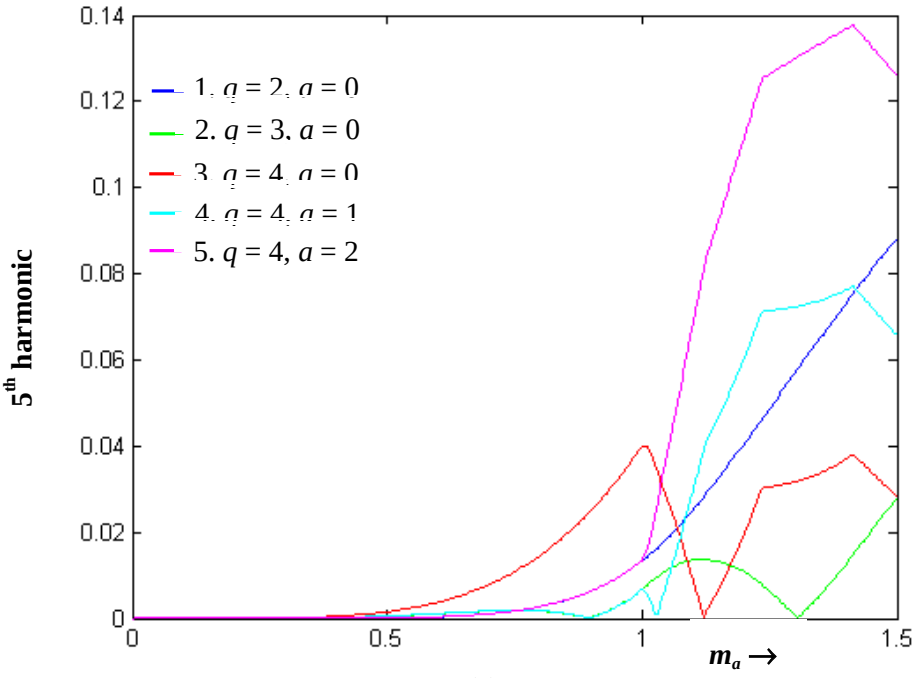

(c)

Fig. 6.19: Theoretical $2|c_5|$ versus modulation index with $N = 8$.

From Fig. 6.19 it is seen that the modified WRPWM scheme for a five-level inverter generates a fifth harmonic for all the combinations of q and a considered. In the linear modulation region, the WRPWM scheme operating with combination 2 has the highest $|c_5|$. On the other hand, the WRPWM schemes operating with combination 1, 2 and 4 give rise to insignificant $|c_5|$.

In the overmodulation region, the value of $|c_5|$ for the WRPWM scheme operating with combination 2 is insignificant at $1 < m_a < 1.4$ (almost the entire overmodulation region) and is approximately zero at $m_a = 1.31$.

The WRPWM scheme operating with combination 2 offers the best overall performance, as it has an insignificant $|c_5|$ within most of the modulation region considered.

Fig. 6.20 shows typical plots of seventh harmonic component versus modulation index.

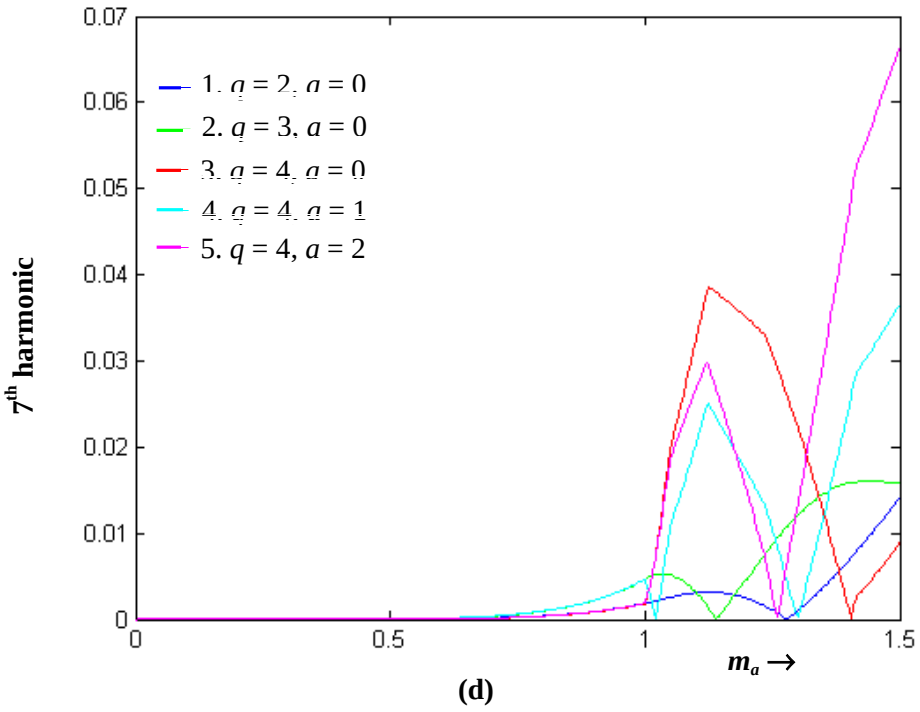

Fig. 6.20: Theoretical $2|c_7|$ versus modulation index with $N = 8$.

From Fig. 6.20 it can be seen that in the entire linear modulation region, the seventh harmonic components of the WRPWM scheme operating with the various combinations of q and a under consideration are insignificant and can be considered negligible.

In the overmodulation region, the value of $|c_7|$ of the WRPWM scheme operating with combination 1 is insignificant at $1 < m_a < 1.48$ and is approximately zero at $m_a = 1.28$. The value of $|c_7|$ of the WRPWM scheme operating with combination 2 is the lowest at $1 < m_a < 1.29$ and is approximately zero at $m_a = 1.14$.

In the linear region, the WRPWM schemes operating with the various combinations of q and a offer a good performance as they have insignificant value of $|c_7|$. For the overmodulation region, it is clear that the WRPWM scheme operating combination 1 offers a better performance than the other combinations of q and a.

Figs. 6.21 (a) and (b) show the characteristic plots of the ninth and eleventh components, respectively versus modulation index, m_a.

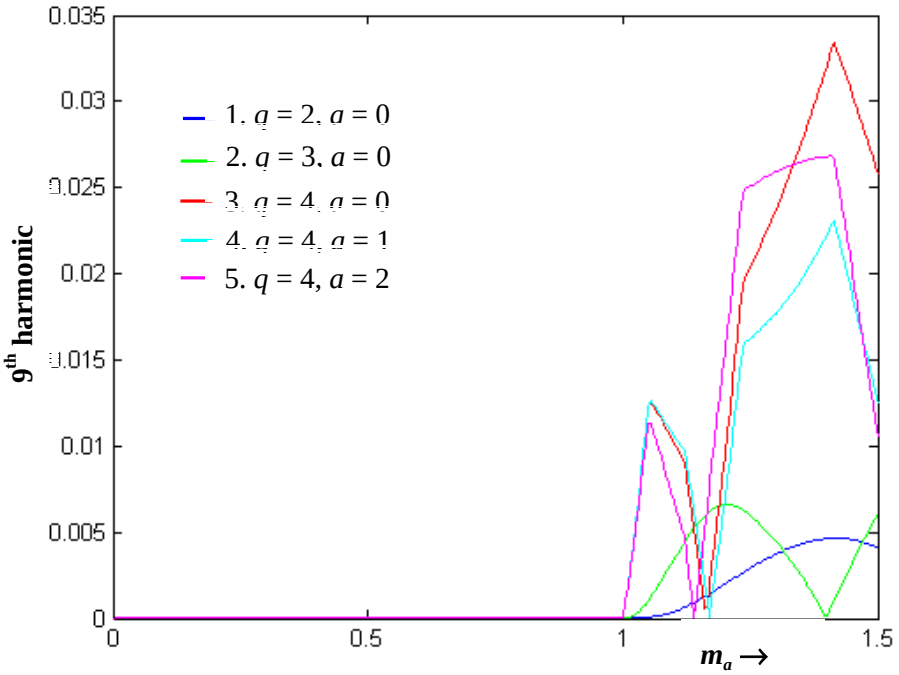

(a)

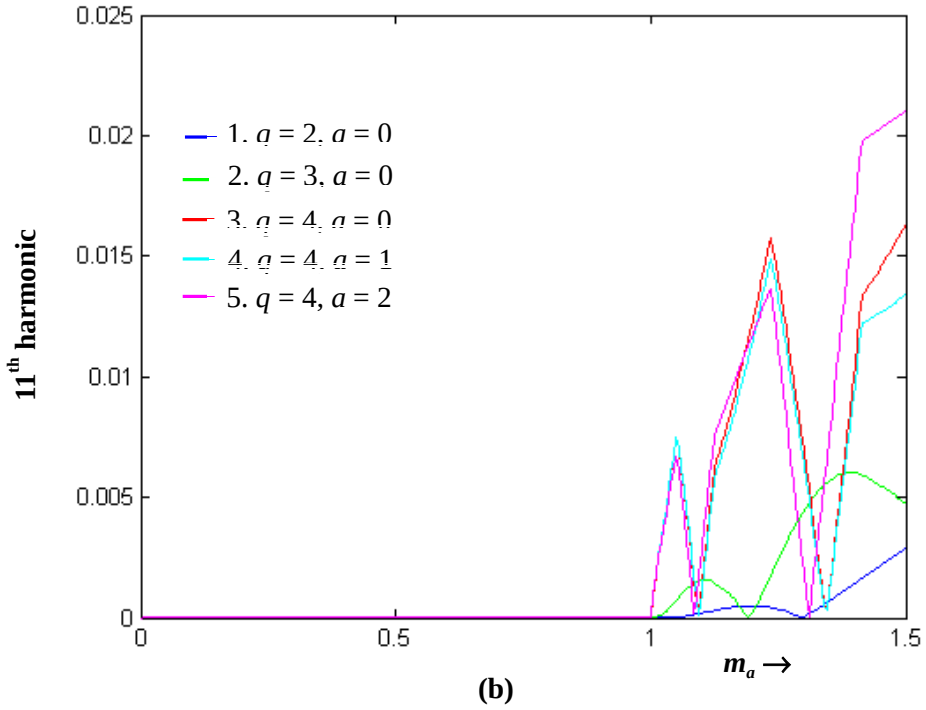

Fig. 6.21: Plots of harmonics vs. modulation index (a) 9th harmonic. (b) 11th harmonic.

From Fig. 6.21 (a) it can be seen that in the entire linear modulation region, the ninth harmonic components of the WRPWM scheme operating with the various combinations of q and a under consideration are insignificant and can be consider negligible.

The value of $|c_9|$ of the WRPWM scheme operating with combination 1 is insignificant over the entire overmodulation region and is the lowest at $1 < m_a < 1.14$, $1.18 < m_a < 1.32$ and $1.47 < m_a < 1.5$. The value of $|c_9|$ of the WRPWM scheme operating with combination 2 is insignificant over the entire overmodulation region. It is the lowest within the range $1.32 < m_a < 1.47$ and is approximately zero in the overmodulation region at $m_a = 1.4$.

In the linear region, the WRPWM schemes operating with the various combinations of q and a offer a good performance as they give rise to negligible $|c_9|$. For the overmodulation region, the WRPWM scheme operating with combination 1 offers the best performance compared with the other combinations of q and a.

From Fig. 6.21 (b) it can be seen that in the linear modulation region, the WRPWM scheme operating with combination 1 gives rise to an insignificant $|c_{11}|$ over the entire overmodulation region. It is the lowest within the range $1 < m_a < 1.18$ and $1.21 < m_a < 1.5$, and is approximately zero at $m_a = 1.3$. For the WPWM scheme operating with combination 2, $|c_{11}|$ is

insignificant over the entire overmodulation region. It is the lowest at $1.18 < m_a < 1.21$ and is approximately zero in the overmodulation region at $m_a = 1.19$.

In the linear region, the WRPWM scheme operating with the various combinations of q and a offer a good performance as they have negligible value of $|c_{11}|$. For the overmodulation region, the WRPWM scheme operating with combination 1 offers a better performance than the other combinations of q and a. It has the lowest value of $|c_{11}|$ over the most of the overmodulation region.

6.3.4 Modified WRPWM Scheme Operating with $N = 9$

Fig. 6.22 shows typical plots of fundamental component $2|c_1|$ versus modulation index, m_a, and various combinations of q and a for the WRPWM scheme operating with $N = 9$.

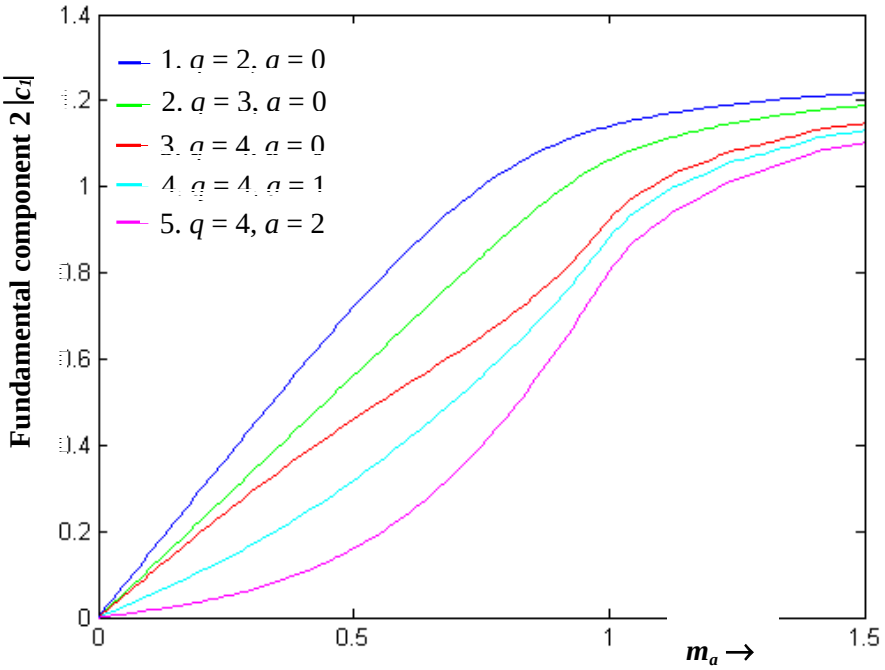

Fig. 6.22: Theoretical fundamental components versus modulation index with $N = 9$.

From Fig. 6.22, it is seen that unlike the standard WRPWM scheme with fixed q = 2, the modified WRPWM scheme operating with N = 9 does not give rise to linear fundamental-modulation index characteristics within the range $m_a < 1$ for all the combinations of q and a. In particular combinations 3 and 5 lead to slightly non-linear characteristics. For all the combinations of q and a, these characteristics saturate when the modulation index increases above one. It is also seen that the fundamental component for combination 1 is the highest amongst those for the WRPWM schemes operating with various combinations of q and a under consideration. The fundamental component for combination 5 is the lowest compared to those for the WRPWM schemes operating with other combinations of q and a. This is because when operating with combination 1 the probability for the inverter to connect its output terminals to the first and fifth level of dc-bus voltage is the highest. When operating with combination 5 the probability is the highest and when operating with combination 3 the probability is the lowest (see Figs. 5.27 (e) and 6.6). Note that the fundamental component is proportional to the probability for the inverter to connect its output terminals to the first and fifth level of dc-bus voltage. The magnitude of the fundamental component in relation to the combinations in consideration can be sorted in descending order as combination 1, combination 2, combination 3, combination 4 and combination 5.

Fig. 6.23 shows typical plots of third harmonic component versus modulation index.

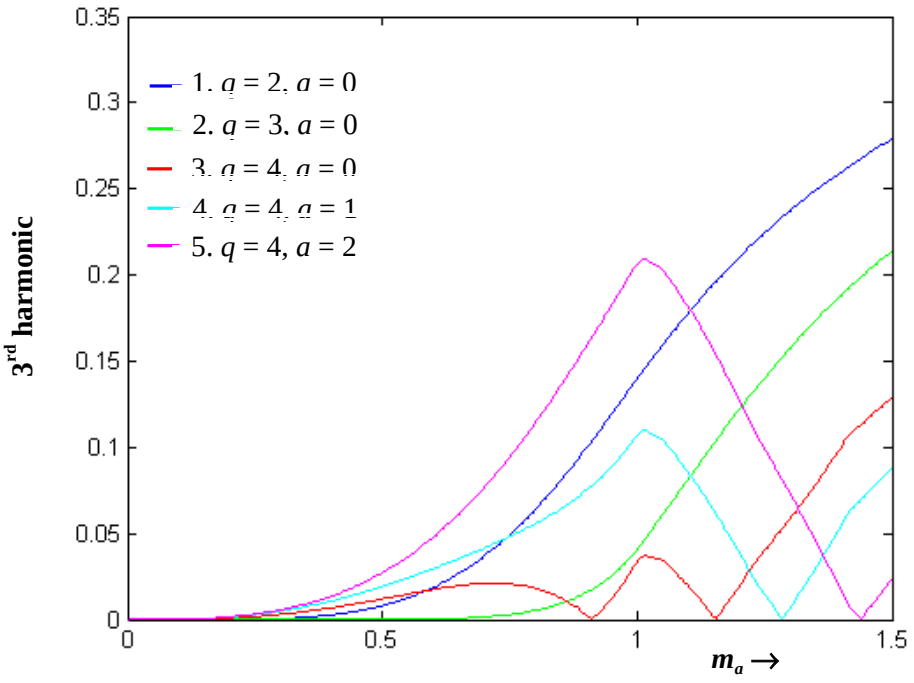

Fig. 6.23: Theoretical $2|c_3|$ versus modulation index with N = 9.

From Fig. 6.23, it can be seen that for N = 9, the WRPWM schemes for the various combinations q and a under consideration have third harmonic boosting effect. In the linear modulation region the WRPWM scheme operating with combination 5 has the highest value of $|c_3|$ and the WRPWM scheme operating with the combination 2 has the lowest $|c_3|$ within the range $0 < m_a < 0.87$. The WRPWM scheme operating with the combination 3 has the lowest $|c_3|$ for part of the linear modulation region at $0.87 < m_a < 1$ and is approximately zero at $m_a = 0.91$.

In the overmodulation region, the WRPWM scheme with combination 3 has the lowest $|c_3| / |c_1|$ ratio at $1 < m_a < 1.22$ and is approximately zero at $m_a = 1.16$. On the other hand, the WRPWM scheme operating with combination 4 has the lowest value of $|c_3|$ at $1.22 < m_a < 1.37$ and is approximately zero at $m_a = 1.29$. Additionally, the WRWPM scheme operating with combination 5 has the lowest value of $|c_3|$ at $1.37 < m_a < 1.5$ and is approximately zero at $m_a = 1.44$.

The WRPWM scheme operating with combination 2 offers the best overall performance in the linear modulation region, and the WRPWM scheme operating with combination 3 offers the best overall performance in the overmodulation region.
Fig. 6.24 shows typical plots of fifth harmonic component versus modulation index.

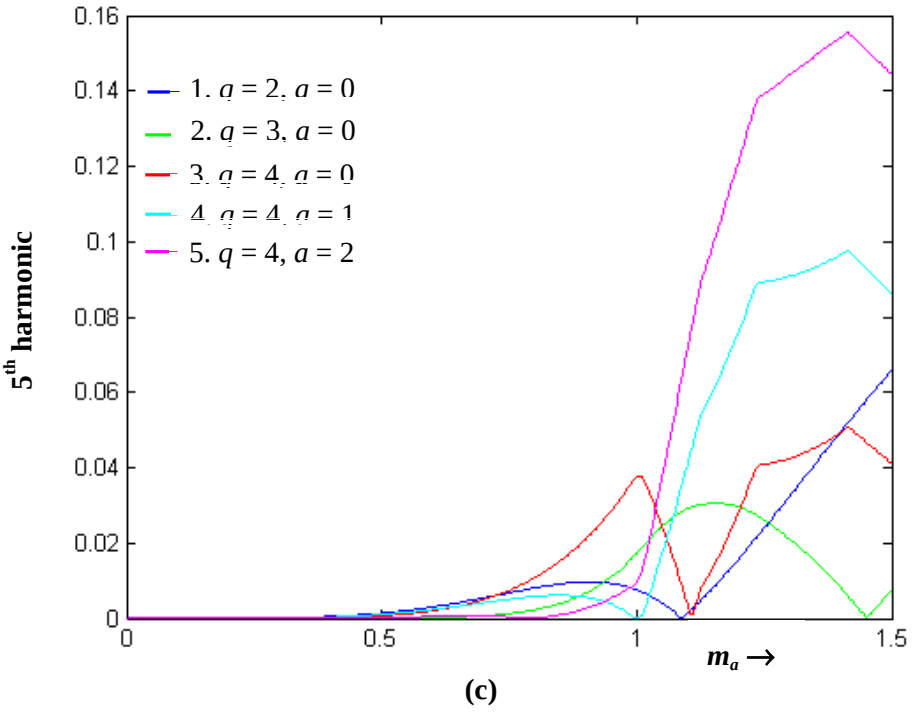

(c)

Fig. 6.24: Theoretical $2|c_5|$ versus modulation index with N = 9.

From Fig. 6.24 it is seen that the modified WRPWM scheme for five-level inverter generates a fifth harmonic for all the combinations of q and a considered. In the linear modulation region, the WRPWM scheme operating with combination 3 has the highest value of $|c_5|$ at $0.71 < m_a < 1$. The WRPWM scheme operating with combination 2 has insignificant value of $|c_5|$ at $0 < m_a < 0.94$. In the case of the WRPWM scheme operating with combination 5, $|c_5|$ is insignificant within the range $0 < m_a < 0.98$ and is approximately zero at $m_a = 0.8$.

In the overmodulation region, the WRPWM scheme operating with combination 1 has the lowest $|c_5|$ within the range $1.03 < m_a < 1.26$. It is also evident that the WRPWM scheme operating with combination 2 has the lowest value of $|c_5|$ at $1.27 < m_a < 1.5$ and is approximately zero at $m_a = 1.45$.

The WRPWM scheme operating with combination 1 offers the best overall performance in the overmodulation region, and the WRPWM scheme operating with combination 2 offers the best overall performance in the linear modulation region.

Fig. 6.25 shows typical plot of seventh harmonic component versus modulation index.

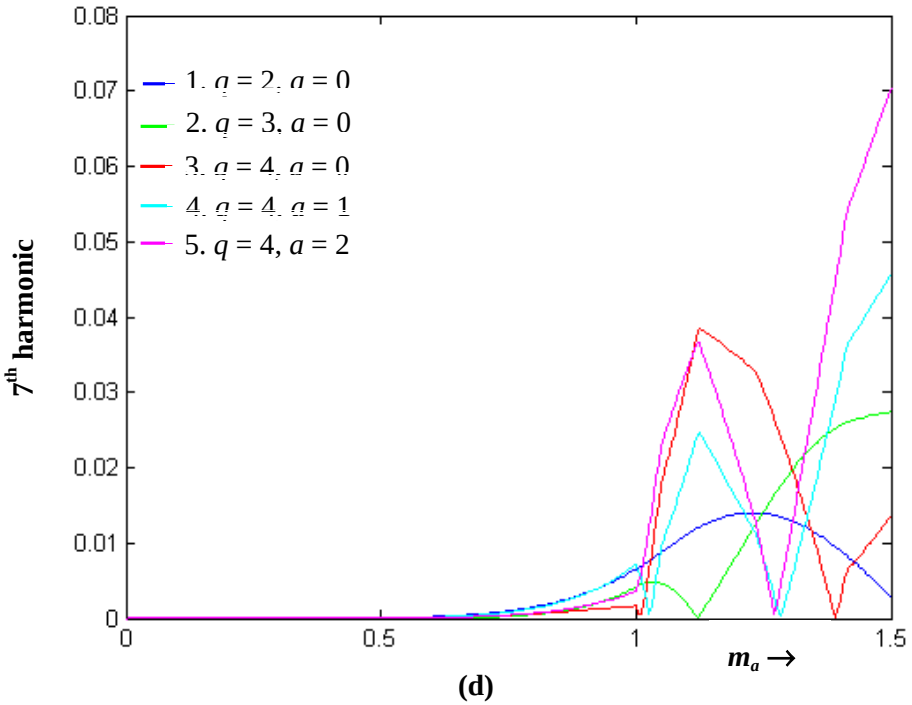

Fig. 6.25: Theoretical $2|c_7|$ versus modulation index with $N = 9$.

From Fig. 6.25 it can be seen that in the entire linear modulation region, the seventh harmonic of the WRPWM schemes operating with the various combinations of q and a under consideration are insignificant. The value of $|c_7|$ of the WRPWM scheme operating with combination 2 is the lowest within the range $0 < m_a < 0.87$ in the linear modulation region. The value of $|c_7|$ of the WRPWM scheme operating with combination 3 is the lowest within the range $0.87 < m_a < 1$ in the linear modulation region.

In the overmodulation region, the maximum value of $|c_7|$ of the WRPWM scheme operating with combination 1 is equal to $0.014 \times V_d / 2$ at $m_a = 1.23$. In the overmodulation region, the value of $|c_7|$ of the WRPWM scheme operating with combination 2 is the lowest at $1.04 < m_a < 1.23$ and is approximately zero at $m_a = 1.12$.

In the linear region, the WRPWM schemes operating with the various combinations of q and a under consideration offer a good performance because they have insignificant value of $|c_7|$. For the overmodulation region, it is clear that the WRPWM scheme operating combination 2 offers a better performance than the other combinations of q and a.

Figs. 6.26 (a) and (b) show the characteristic plots of the ninth harmonic $|c_9|$ and eleventh harmonic $|c_{11}|$ versus modulation index m_a, respectively.

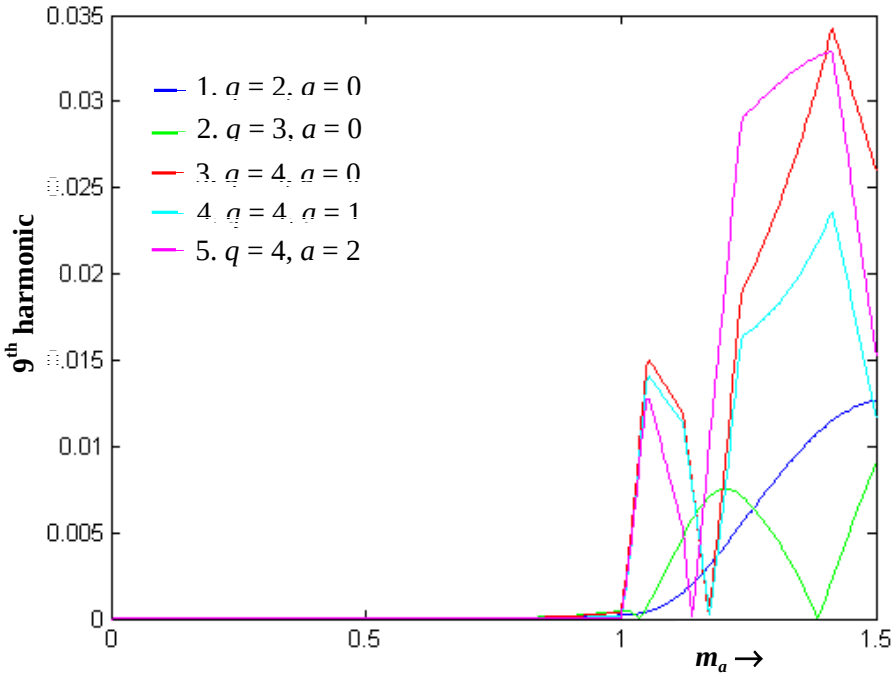

(a)

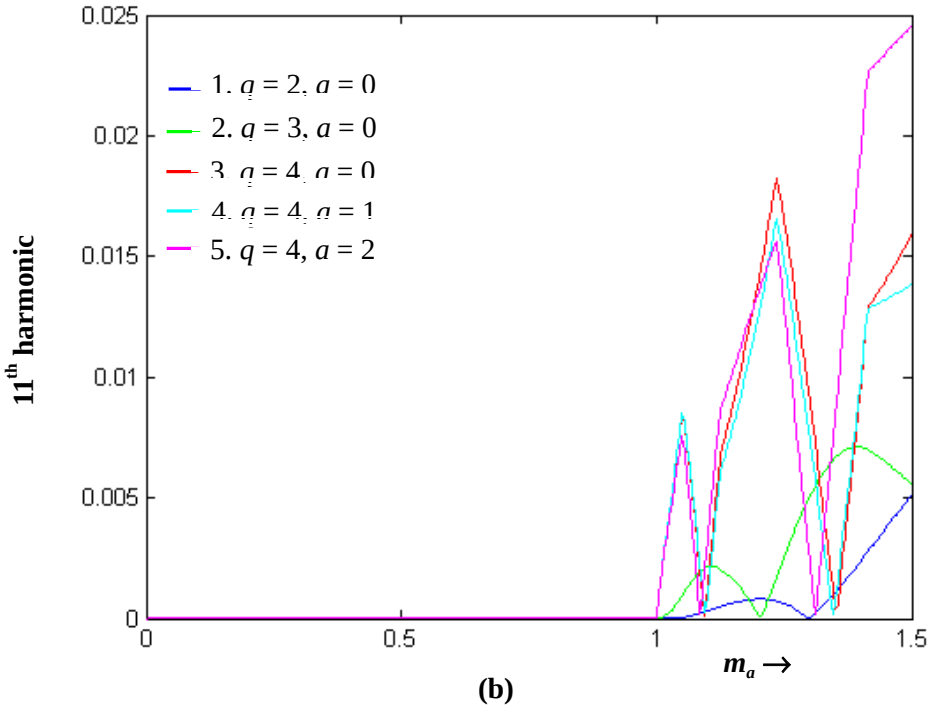

Fig. 6.26: Plots of harmonics vs. modulation index (a) 9th harmonic. (b) 11th harmonic.

From Fig. 6.26 (a) it can be seen that in the entire linear modulation region, the ninth harmonic component of the WRPWM schemes operating with the various combinations of q and a under consideration are insignificant and can be considered negligible.

In the overmodulation region, the WRPWM scheme operating with combination 1 gives rise to insignificant $|c_9|$ over the range $1 < m_a < 1.45$ (almost the entire overmodulation region) and is the lowest at $1.01 < m_a < 1.13$, $1.15 < m_a < 1.16$ and $1.19 < m_a < 1.26$. The WRPWM scheme operating with combination 2 generates insignificant $|c_9|$ within the range $1 < m_a < 1.5$.

In the linear region, the WRPWM schemes operating with the various combinations of q and a under consideration offer a good performance because they have negligible value of $|c_9|$. For the overmodulation region, the WRPWM scheme operating with combination 1 offers a better performance than the other combinations of q and a.

From Fig. 6.26 (b) it can be seen that in the linear modulation region, the WRPWM scheme operating with the combinations 1 generate an insignificant $|c_{11}|$ over the entire overmodulation region. It is the very low over most of the overmodulation region ($1 < m_a < 1.19$ and $2.22 < m_a < 1.5$), and approximately zero at $m_a = 1.3$. For the WRPWM scheme

operating with combination 2, $|c_{11}|$ is insignificant over the entire overmodulation region and is the lowest at $1.19 < m_a < 2.22$, and is approximately zero in the overmodulation region at $m_a = 1.2$.

In the linear region, the WRPWM schemes operating with the various combinations of q and a offer a good performance because they have negligible value of $|c_{11}|$. For the overmodulation region, the WRPWM scheme operating with combination 1 offers the best performance compared with the other combinations of q and a, because it has the lowest $|c_{11}|$ over most of the overmodulation region.

6.3.5 Section Conclusion

From Figs. 6.7 to 6.16, it is seen that for operation with $N = 6$ and 7, the WRPWM schemes operating with identical combination of q and a yield similar fundamental and harmonics versus modulation index characteristics. Moreover, from Figs. 6.17 to 6.26, it is seen that for operation with $N = 8$ and 9 the WRPWM schemes operating with identical combinations of q and a also yield similar fundamental and harmonics versus modulation index characteristics. Similar to the standard five-level WRWPM scheme, for each combination of q and a the fundamental component generated from the modified WRPWM scheme operating with an even number of comparisons, N, is higher than for operation with N odd. It is as a result of the ratio of probability for the inverter output terminals connecting to the first/fifth and third level of dc-bus voltage (i.e., P_1/P_3 and P_5/P_3) with an even number of comparisons, N, being higher than operating with N odd (see Figs. 6.2, 6.3, 6.5 and 6.6). This means that for an even number of comparisons, N, the inverter is more likely to connect its output terminal to first and fifth voltage level than it does when N being an odd number. Hence the total expected power of $k(t)$ for N even with the various combinations of q and a is higher than that for N odd with various combinations of q and a.

From Figs. 6.7-6.26 and the discussions in sections 6.3.1 to 6.3.4, three operations can be

considered as an optimal choice. Operation 1, the modified WRPWM scheme operating with N = 6, q = 2 and a = 0 (which is the standard five-level WRPWM scheme operating with N = 6), has the best overall fifth, seventh, ninth and eleventh harmonics content in the entire modulation region. Operation 2, the modified WRPWM scheme operating with N = 6, q = 3 and a = 0, has the best overall third harmonic content in the entire modulation region, and desirable seventh to eleventh harmonics content in the linear modulation region. Operation 3, the modified WRPWM scheme operating with N = 8, q = 3 and a = 0, generates lower third harmonic than operation 1 (the modified WRPWM scheme operating with N = 6, q = 2 and a = 0) in the entire modulation region. In the overmodulation region, operation 3 offers better fifth to eleventh harmonics content than operation 2. Moreover, operation 3 has insignificant seventh to eleventh harmonics content in the linear modulation. Thus, the modified WRPWM scheme operating with N = 6, q = 2 and a = 0 can be used in three phase applications. The modified WRPWM scheme operating with N = 6, q = 3 and a = 0 can be used in a single-phase application which only operates in linear modulation region. On the other hand, the modified WRPWM scheme operating with N = 8, q = 3 and a = 0 can be used in single-phase applications which operate within the range $0 < m_a < 1.2$ or high voltage applications where higher output voltage is required.

6.4 The Effect of Sampling Frequency on Noise Content

From section 5.4.1 it is known that the signal and discrete noise power $P_{1,noise}$ are virtually independent of f_{sp} and the continuous power $P_{2,noise}$ is inversely proportional to f_{sp}. Figs. 6.27, 6.28 and 6.29 show the normalized (with base value of $(V_d / 2)^2$) signal, discrete noise, and continuous noise power versus sampling frequency with m_a = 1. It is evident from Figs. 6.27 and 6.28 that changing the value of q and a does not affect this relationship.

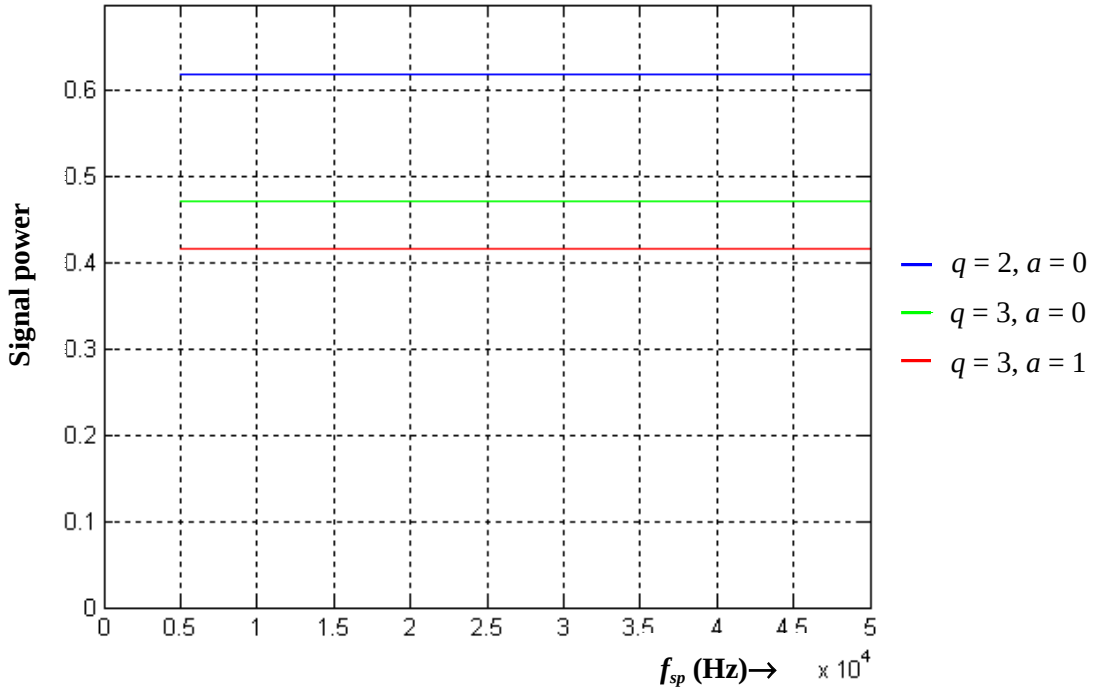

(a)

Fig. 6.27: Theoretical signal power versus f_{sp} (a) WRPWM with N = 6.

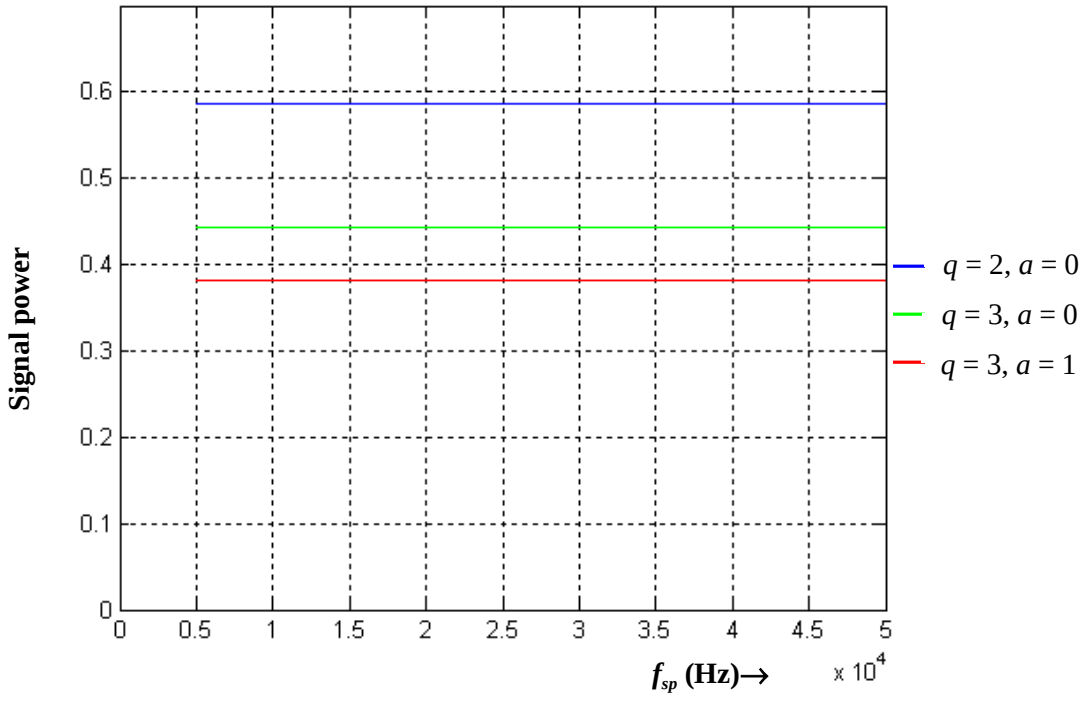

(b)

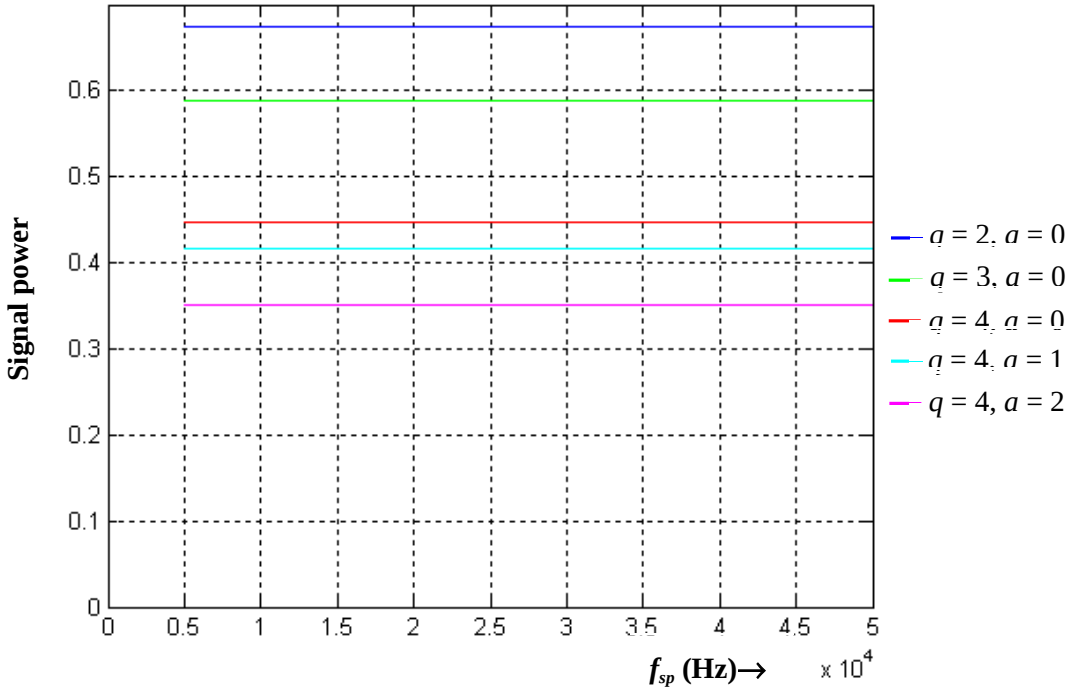

(c)

Fig. 6.27: (continued) (b) WRPWM with N = 7. (c) WRPWM with N = 8.

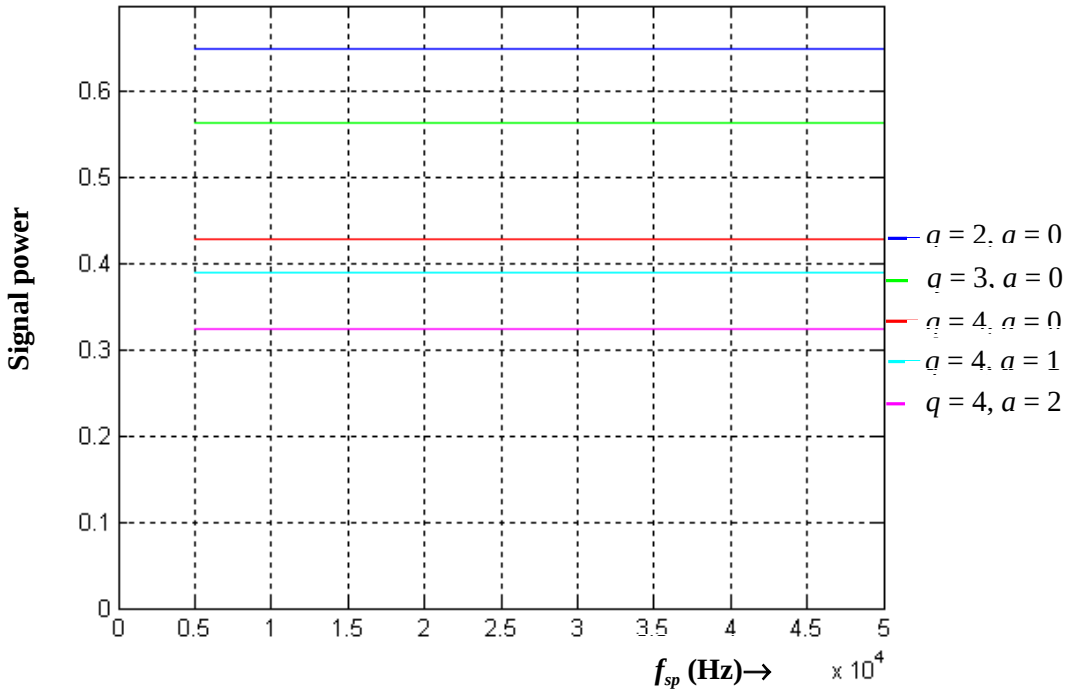

(d)

Fig. 6.27: (continued) (d) WRPWM with N = 9.

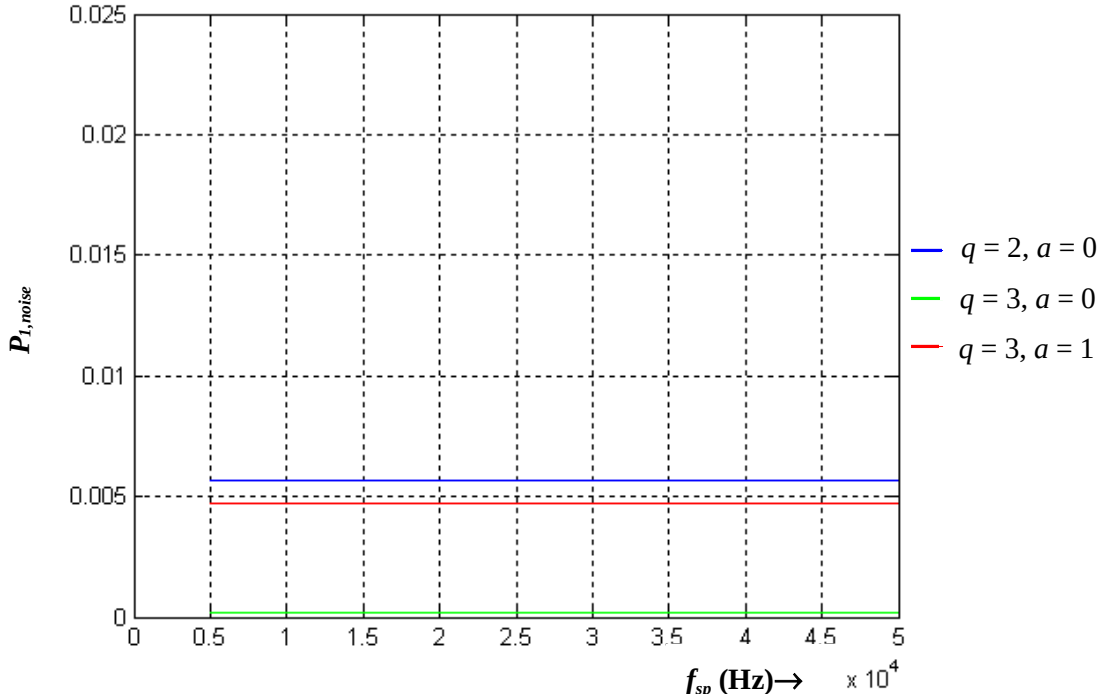

(a)

Fig. 6.28: Theoretical discrete noise ($P_{1,noise}$) power versus f_{sp} (a) WRPWM with N = 6.

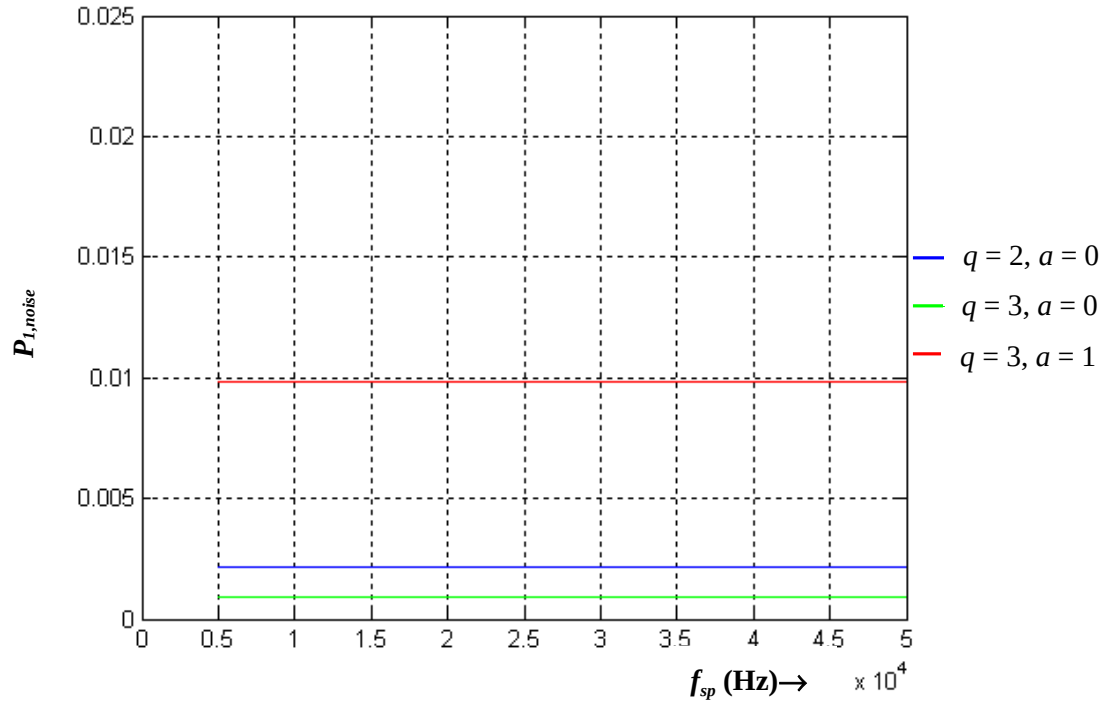

(b)

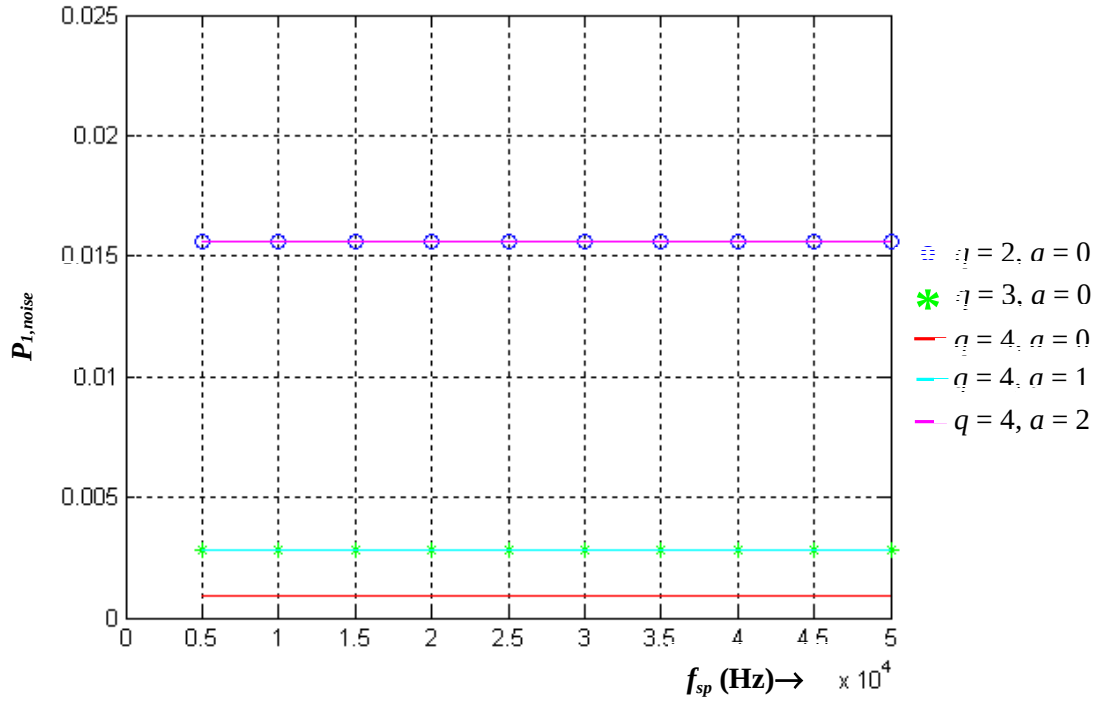

(c)

Fig. 6.28: (continued) (b) WRPWM with N = 7. (c) WRPWM with N = 8.

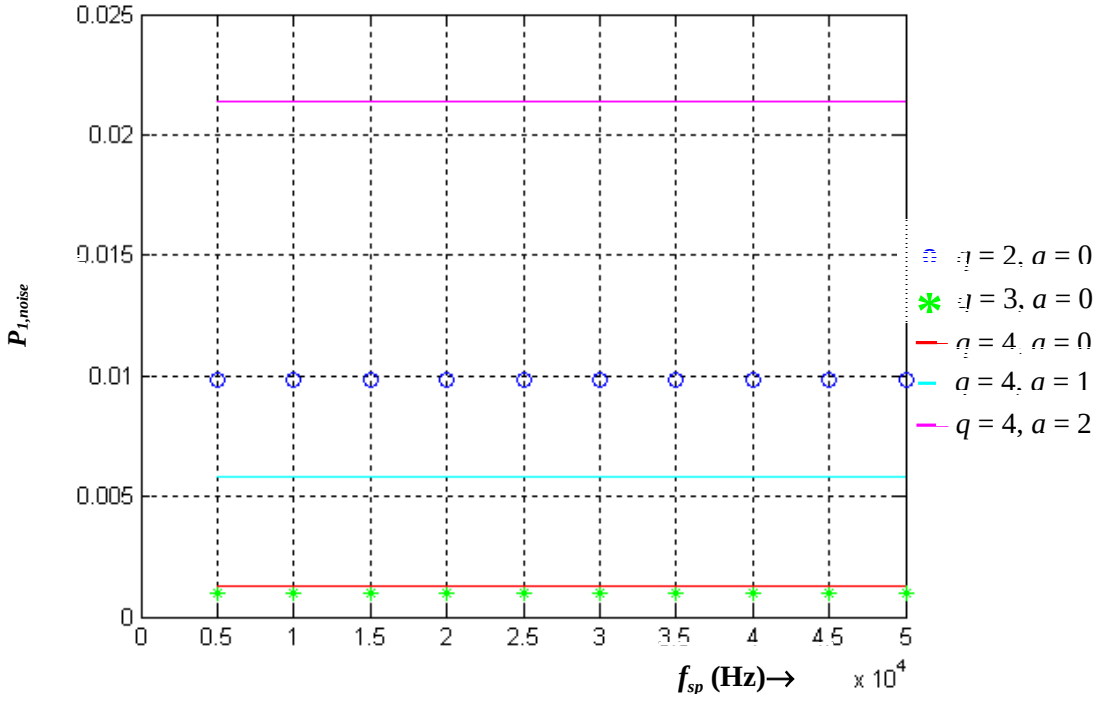

(d)

Fig. 6.28: (continued) (d) WRPWM with N = 9.

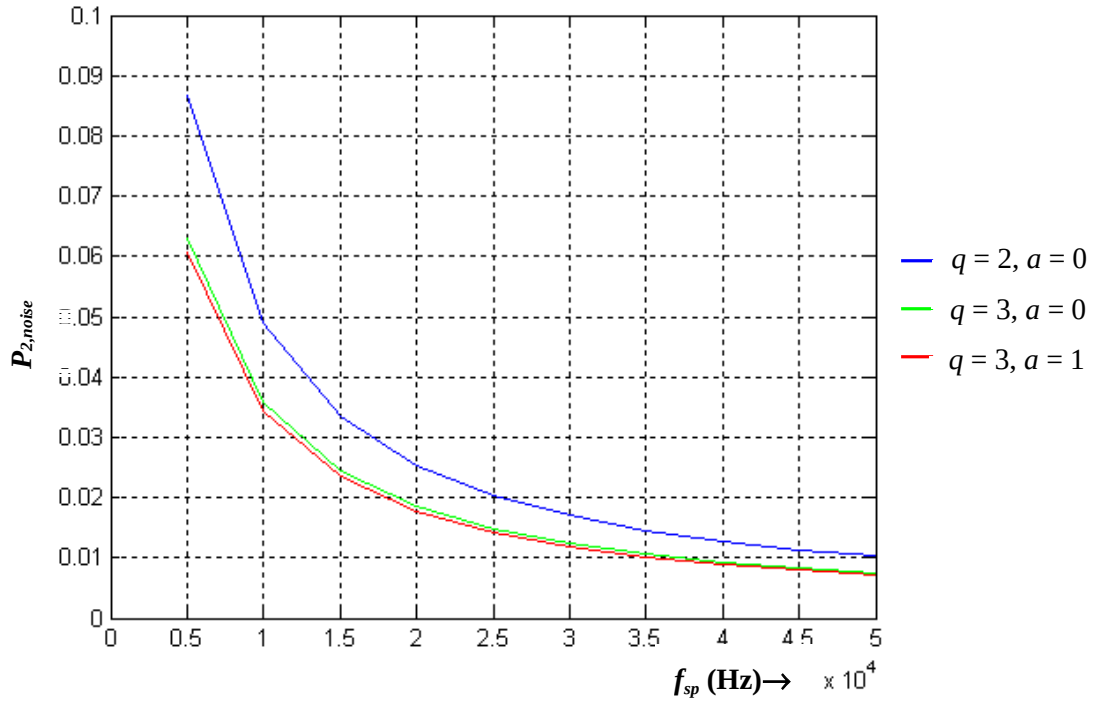

(a)

Fig. 6.29: Theoretical continuous noise ($P_{2,noise}$) power versus f_{sp} (a) WRPWM with N = 6.

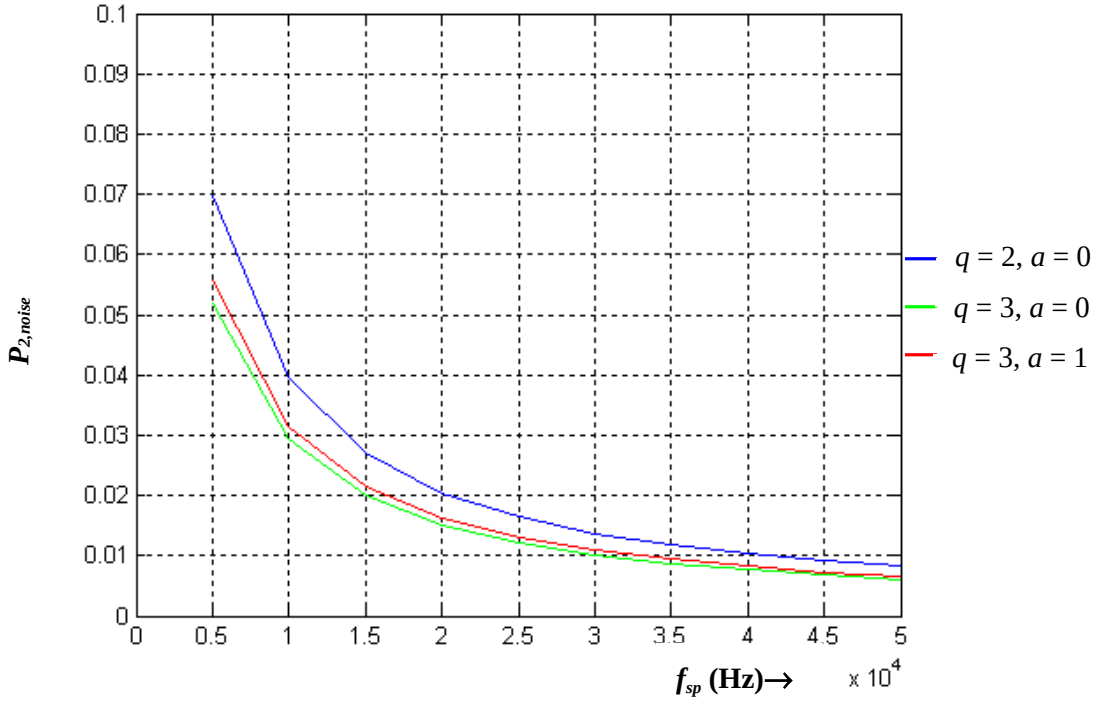

(b)

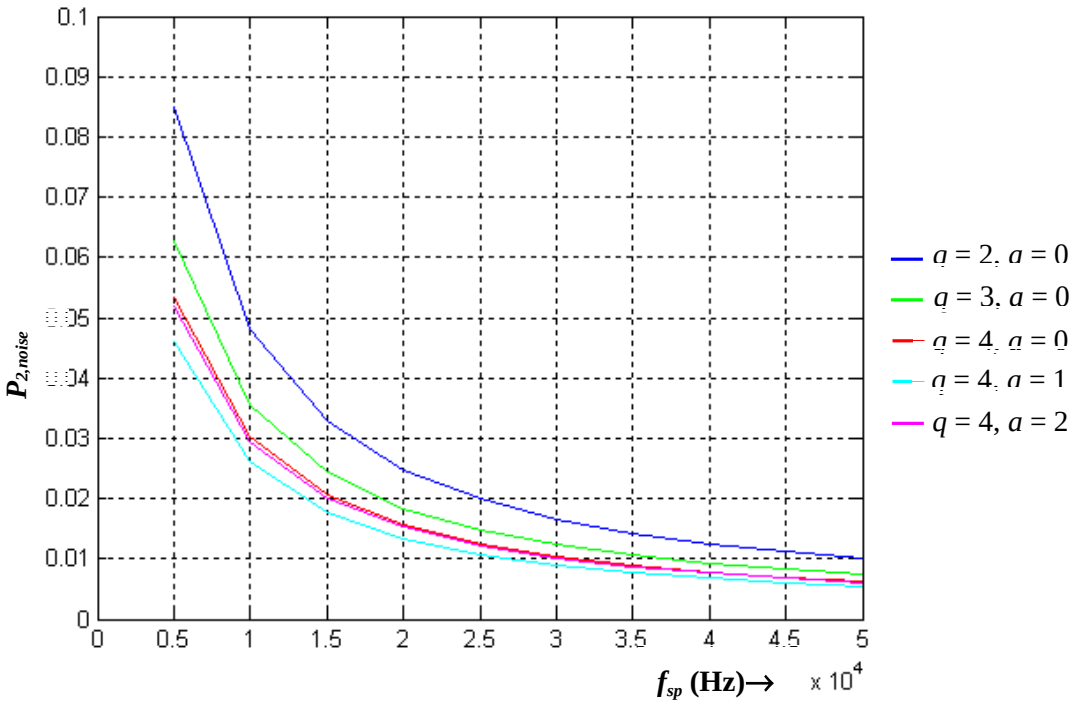

(c)

Fig. 6.29: (continued) (b) WRPWM with *N* = 7. (c) WRPWM with *N* = 8.

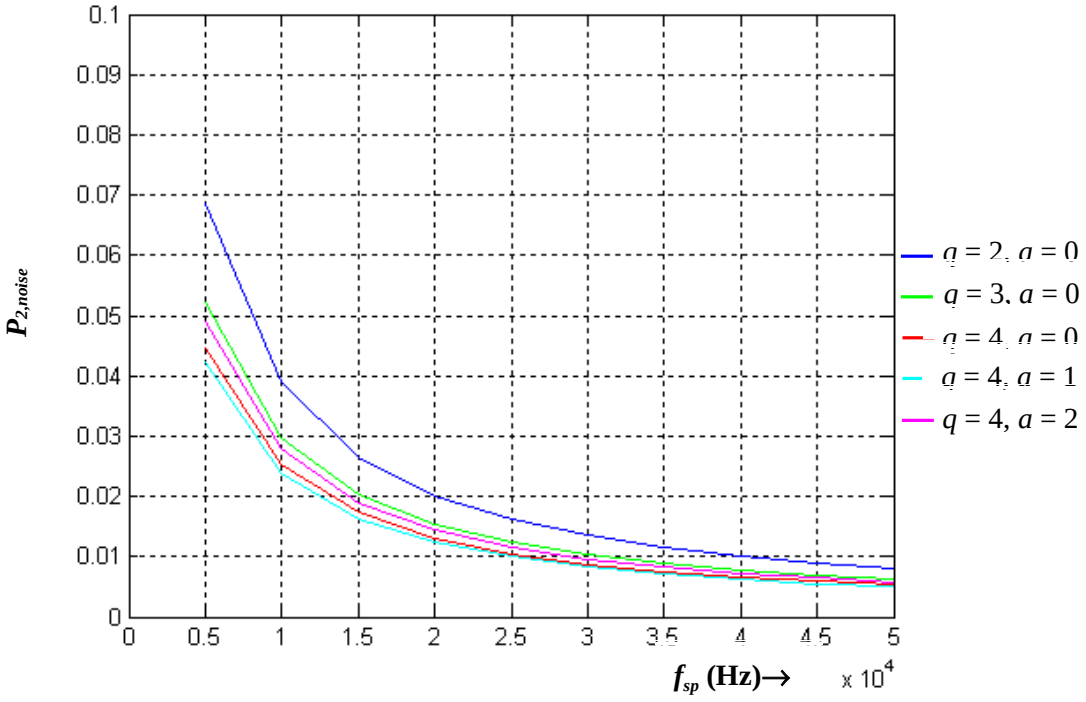

(d)

Fig. 6.29: (continued) (d) WRPWM with *N* = 9.

6.5 Effect of *q* and *a*

Unlike m_a and N, as q and a increase, it can be observed from Figs. 6.1 and 6.4 that $g(t)$ becomes more sinusoidal wave like function, up to a point, then it starts to become more impulse like function. This result in a decreasing value of the fundamental component $2|c_1|$ as q and a increase. However, the other harmonics behave in a mixed manner for different combinations of q and a (plots of the harmonics are shown in Figs. 6.7 to 6.26). Hence, the qualitative dependence of $P_{1,noise}$ on q and a is hard to predict. When q increases, the probabilities for the inverter to connect its output terminals to the second and fourth voltage level of dc-bus increases. Consequently, the chances of successive pulses joining together to form a wider second and fourth dc-bus voltage level pulse increases.

Similarly, when a increases, the probabilities for the inverter to connect its output terminals to the third dc-bus voltage level increases. As a result, the chances of successive pulses being joined together to form a wider third voltage level pulse increases. The merging of pulses results in various harmonic boosting and elimination effects. As q and a increases the average value of U_1 decreases and value of $|g(t)|^2$ decreases. This makes it hard to predict the value of U_1 - $|g(t)|^2$ and since d_{av} is proportional to U_1 - $|g(t)|^2$, hence, $P_{2,noise}$ is hard to predict.
From Figs. 6.27 (a) to (d), it can be seen that as the value of q and/or a increase the signal power decreases. The advantage of this degrading of fundamental component boosting effect is a decrease in continuous noise power, hence avoiding system resonances excitation.

6.6 The Effect of Modulation Index

In section 6.3.5, it was concluded that the WRPWM schemes operating with $N = 6$, $q = 2$ and $a = 0$ (operation1), $N = 6$, $q = 3$ and $a = 0$ (operation 2) and $N = 8$, $q = 3$ and $a = 0$ (operation 3) are the optimal choices for various applications. Thus, to illustrate the effect of modulation index, plots of normalized (with base value of $(V_d / 2)^2$) signal, discrete noise, and continuous noise power versus m_a with f_{sp} = 30 kHz are shown in Figs. 6.30 to 6.31, respectively. Fig. 6.33 shows the expected value $g(t)$ for operation 2 with various values of modulation index.

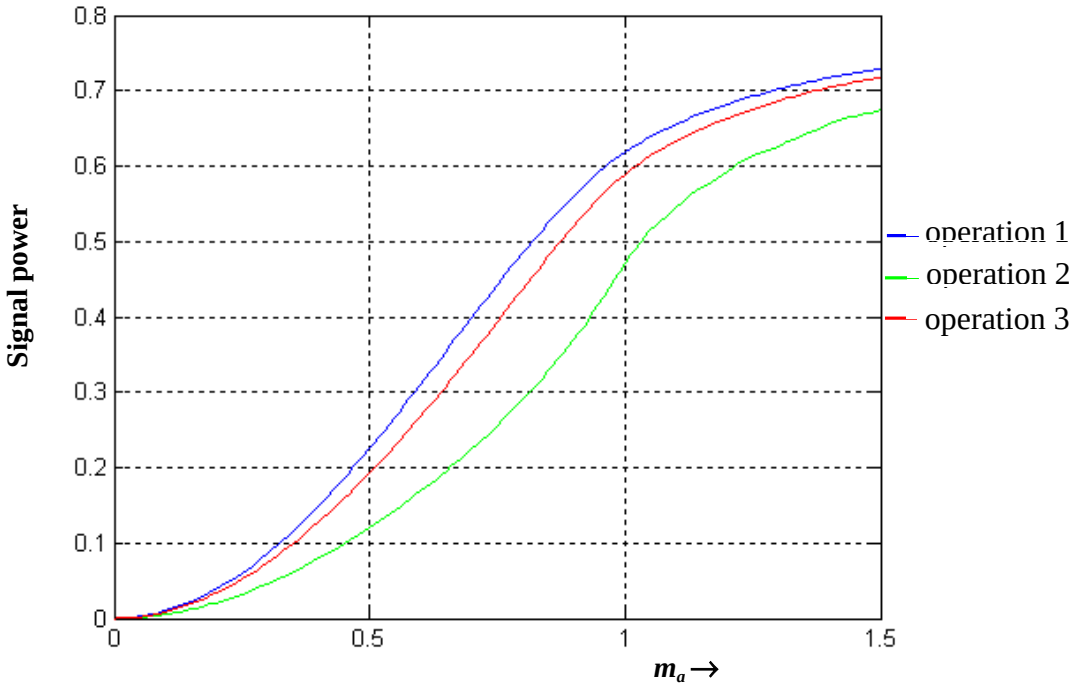

Fig. 6.30: Theoretical signal power versus m_a.

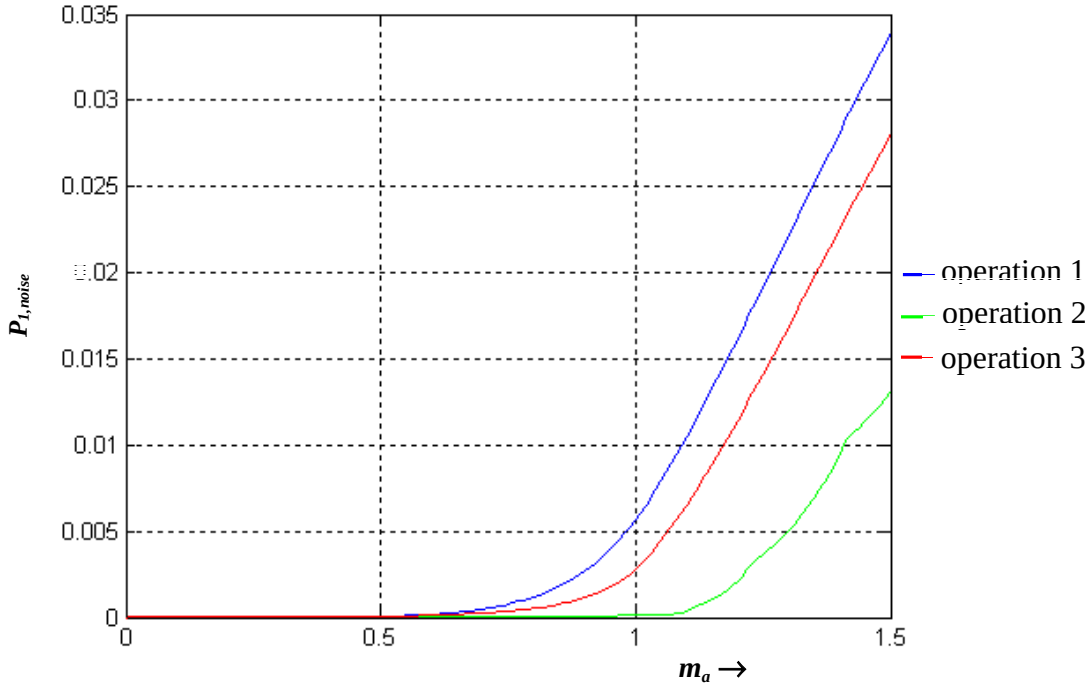

Fig. 6.31: Theoretical discrete noise power versus m_a.

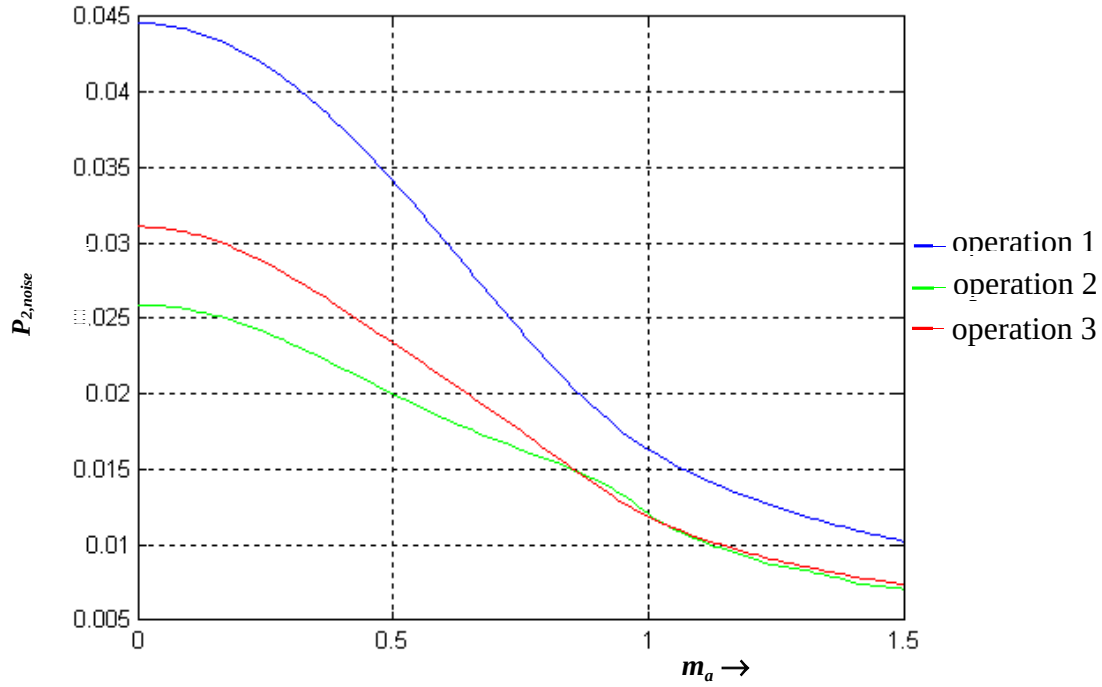

Fig. 6.32: Theoretical continuous noise power versus m_a.

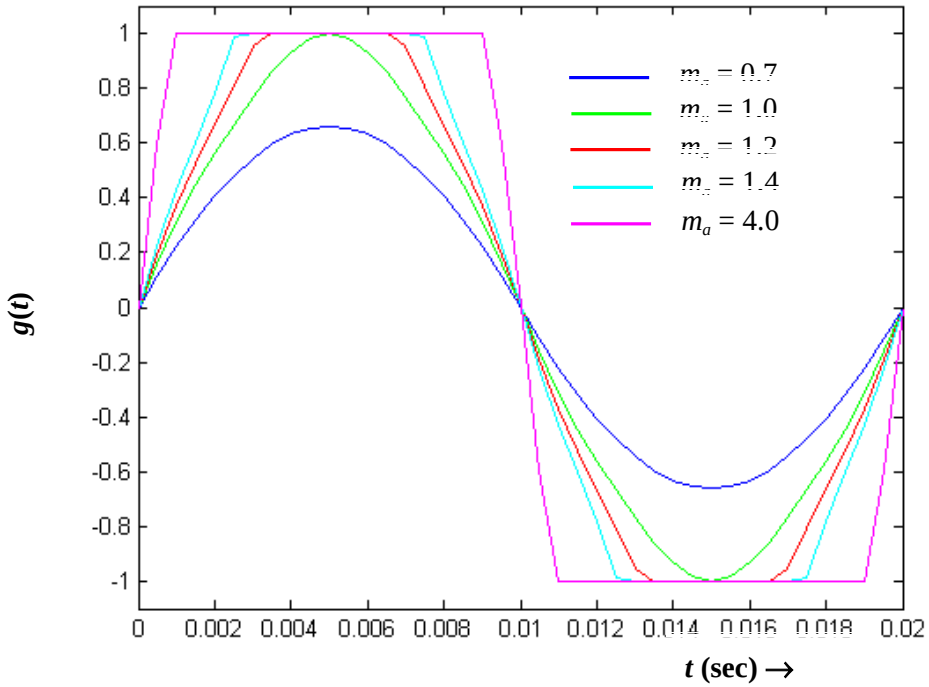

Fig. 6.33: Expected random PWM signal $g(t)$ of operation 2 with various modulation index.

From Fig. 6.33, it can be observed that similar to the standard WRPWM scheme discussed in

chapter 5, as modulation index m_a increases the expected value $g(t)$ becomes more and more square wave like function. Consequently, the signal power and the discrete noise power increases as m_a increases, as can be seen in Fig. 6.30 and 6.31. For large values of m_a, $g(t)$ approaches a square wave, hence, from (5.14), $P_{1,noise}$ will approach $0.19(2A)^2$. Moreover, from Fig. 6.32, it can be seen that as modulation index m_a increases the continuous noise power decreases. This is as it should since the total power of the WRPWM waveform is equal to the sum of signal power, discrete noise power and continuous noise power.

6.7 Comparison between the Standard Five-Level WRPWM and the Modified Five-Level WRPWM

In this section, a comparison is made between the standard five-level WRPWM and the modified five-level WRPWM.

As mentioned in section 6.2 the modified five-level WRPWM scheme operating with $q = 2$ and $a = 0$ is identical to the standard five-level WRPWM scheme. From sections 6.3 it is known that as the value of q and/or a increase the fundamental component decreases. Hence, the standard five-level WRPWM scheme yields a higher output fundamental component compared with the modified WRPWM scheme.

From section 6.3.5, it was found that regarding the harmonics content of the switching waveform, three operations can be considered as an optimal choice. They are operation 1, the modified WRPWM scheme operating with $N = 6$, $q = 2$ and $a = 0$ (which is the standard five-level WRPWM scheme operating with $N = 6$), operation 2, the modified WRPWM scheme operating with $N = 6$, $q = 3$ and $a = 0$ and operation 3, the modified WRPWM scheme operating with $N = 8$, $q = 3$ and $a = 0$.

From the plots of fundamental signal power versus sampling frequency in Fig. 6.27 it can be seen that the standard WRPWM scheme (q = 2, a = 0) has the highest signal power compared with the modified WRPWM schemes. However, from Figs. 6.3, 6.4, 6.7 and 6.8, it can be seen that the other harmonics behave in a mixed manner for different combinations of q and a. Therefore it is hard to predict the relationship between the discrete ($P_{1,noise}$), continuous ($P_{2,noise}$) noise power and the q-a combinations.

From Fig. 6.28 (a) it is seen that for N = 6 the standard WRPWM scheme has the highest $P_{1,noise}$, the modified WRPWM scheme operating with q = 3 and a = 1 has the second highest $P_{1,noise}$, and the modified WRPWM scheme operating with q = 3 and a = 0 has the lowest $P_{1,noise}$. From Fig. 6.29 (a) it is seen that for N = 6 the standard WRPWM scheme has the highest $P_{2,noise}$, the modified WRPWM scheme operating with q = 3 and a = 0 has the second highest $P_{2,noise}$, and $P_{2,noise}$ of the modified WRPWM scheme operates with q = 3 and a = 1 is slightly lower than $P_{2,noise}$ of the modified WRPWM scheme operating with q = 3 and a = 0. Thus, from noise power considerations, with N = 6, the modified WRPWM scheme operating with q = 3 and a = 0 is the optimal choice.

From Fig. 6.28 (b) it is seen that for N = 7, the modified WRPWM scheme operating with q = 3 and a = 1 has the highest $P_{1,noise}$, the standard WRPWM scheme has the second highest $P_{1,noise}$ and the modified WRPWM scheme operating with q = 3 and a = 0 has the least $P_{1,noise}$. From Fig. 6.29 (b) it is seen that for N = 7 the standard WRPWM has the highest $P_{2,noise}$, the modified WRPWM scheme operating with q = 3 and a = 1 has the second highest $P_{2,noise}$ and the modified WRPWM scheme operating with q = 3 and a = 0 has the least $P_{2,noise}$. Thus, from noise power considerations, with N = 7, the modified WRPWM scheme operating with q = 3 and a = 0 is the optimal choice.

From Fig. 6.28 (c) it is seen that for N = 8, the standard WRPWM scheme has the highest $P_{1,noise}$, the modified WRPWM scheme operating with of q = 4, a = 2 has the second highest $P_{1,noise}$, the modified WRPWM scheme operating with q = 3, a = 0 and q = 4, a = 1 has the third highest $P_{1,noise}$, and the modified WRPWM scheme operates with q = 4 and a = 0 has the lowest $P_{1,noise}$. From Fig. 6.29 (b) it is seen that for N = 8, the standard WRPWM has the highest $P_{2,noise}$, the modified WRPWM scheme operating with q = 3, a = 0, q = 4, a = 0, and q = 4, a = 2 have the second, third and fourth highest $P_{2,noise}$, respectively. The modified WRPWM scheme operating with q = 3, a = 1 has the least $P_{2,noise}$. Note that $P_{2,noise}$ of modified WRPWM scheme operating with q = 4, a = 0 is only slightly higher than $P_{2,noise}$ of the modified WRPWM scheme operating with q = 4, a = 2. Thus, from noise power considerations, with N = 8, the modified WRPWM scheme operating with q = 4 and a = 0 is

the optimal choice.

From Fig. 6.28 (d) it is seen that for N = 9, the modified WRPWM scheme operating with q = 4 and a = 2 has the highest $P_{1,noise}$. The standard WRPWM scheme has the second highest $P_{1,noise}$, and the modified WRPWM scheme operating with q = 4, a = 1, and q = 4, a = 0 have the third, fourth highest $P_{1,noise}$, respectively. The modified WRPWM operating with q = 3 and a = 0 has the lowest $P_{1,noise}$. Note that $P_{1,noise}$ of the modified WRPWM scheme operating with q = 4 and a = 0 is only slightly higher than $P_{1,noise}$ of the modified WRPWM scheme operating with q = 3 and a = 0. From Fig. 6.29 (d) it is seen that for N = 9 the standard WRPWM scheme has the highest $P_{2,noise}$, the modified WRPWM scheme operating with q = 3, a = 0, q = 4, a = 2, and q = 4, a = 0 have the second, third and fourth highest $P_{2,noise}$ respectively. The WRPWM scheme operating with q = 4 and a = 1 has the least $P_{2,noise}$. Thus, from noise power considerations, with N = 9, the modified WRPWM scheme operating with q = 4 and a = 0 is the optimal choice.

Note that with a fixed value of N the expected power of $k(t)$ varies with the combinations of q and a, thus, it is not necessary for the q-a combination with highest $P_{1,noise}$ to have the least $P_{2,noise}$.
In general, it seems that as far as noise power is concerned, for N = 6 and 7, the modified WRPWM scheme operating with q = 3 and a = 0 offers better performance than the standard WRPWM scheme, and for N = 8 and 9, the modified WRPWM scheme operating with q = 4 and a = 0 offers better performance than the standard WRPWM scheme.

From Figs. 6.7 to 6.26, 6.27 to 6.29, 6.31 and 6.32, with regard to the various performance parameters under consideration (i.e., the harmonics, discrete noise, continuous noise and switching loss), the modified five-level WRPWM scheme operating with N = 6, q = 3 and a = 0 seems to be the optimal choice.

6.8 Average Switching Frequency

Typical plots of the ratio of average switching frequency to sampling frequency (f_{sw}/f_{sp}) versus modulation index (m_a) are shown in Fig. 6.34. The maximum ratio and maximum switching frequency for sampling frequency of 30 kHz corresponding to the relative modulation index is shown in table 6.5. From table 6.5 it seems that with a fixed sampling frequency, as the value of q and/or a increases the maximum average switching frequency decreases.

TABLE 6.5

The maximum f_{sw} / f_{sp} ratio and switching frequency for sampling frequency of 30 kHz corresponding to the relative modulation index.

	N = 6			N = 7			N = 8			N = 9		
	MAX f_{sw}/f_{sp}	MAX f_{sw} kHz	m_a	MAX f_{sw}/f_{sp}	MAX f_{sw} kHz	m_a	MAX f_{sw}/f_{sp}	MAX f_{sw} kHz	m_a	MAX f_{sw}/f_{sp}	MAX f_{sw} kHz	m_a
q = 2 a = 0	0.3843	11.5	0	0.3358	10	0.4	0.3939	11.8	0	0.3488	10.5	0.3
q = 3 a = 0	0.3443	10.3	0	0.3026	9	0	0.3537	10.6	0	0.3236	9.7	0
q = 3 a = 1	0.2834	8.5	0.7	0.2598	7.8	0.8	N/A	N/A	N/A	N/A	N/A	N/A

q = 4 a = 0	N/A	N/A	N/A	N/A	N/A	N/A	0.3335	10	0	0.3154	9.5	0
q = 4 a = 1	N/A	N/A	N/A	N/A	N/A	N/A	0.2649	8	0.5	0.2477	7.4	0.8
q = 4 a =2	N/A	N/A	N/A	N/A	N/A	N/A	0.2395	7.1	0.8	0.2212	6.6	0.9

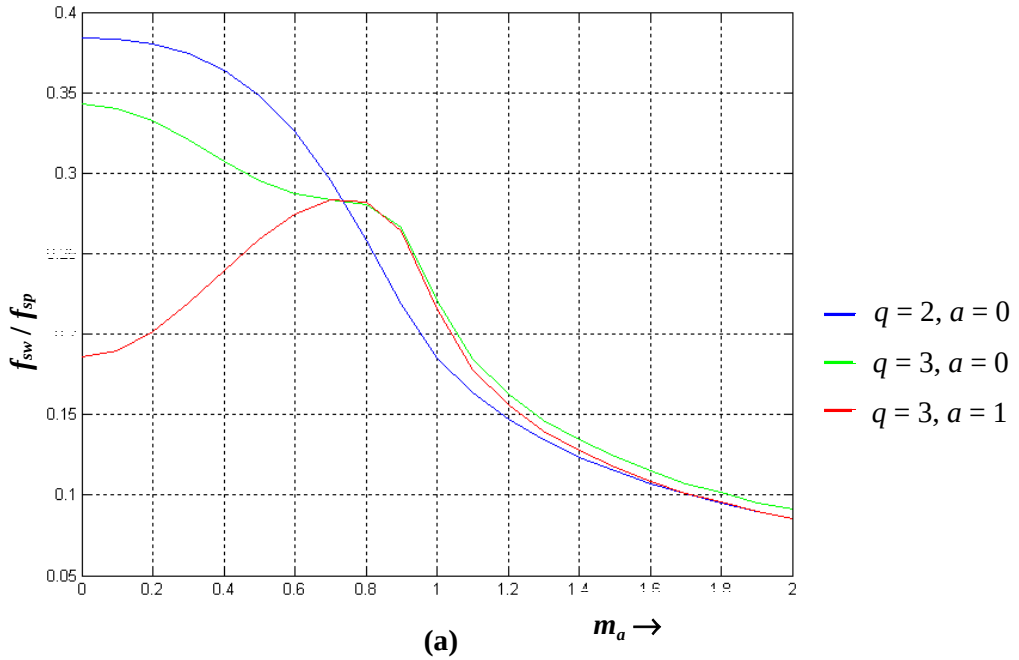

(a)

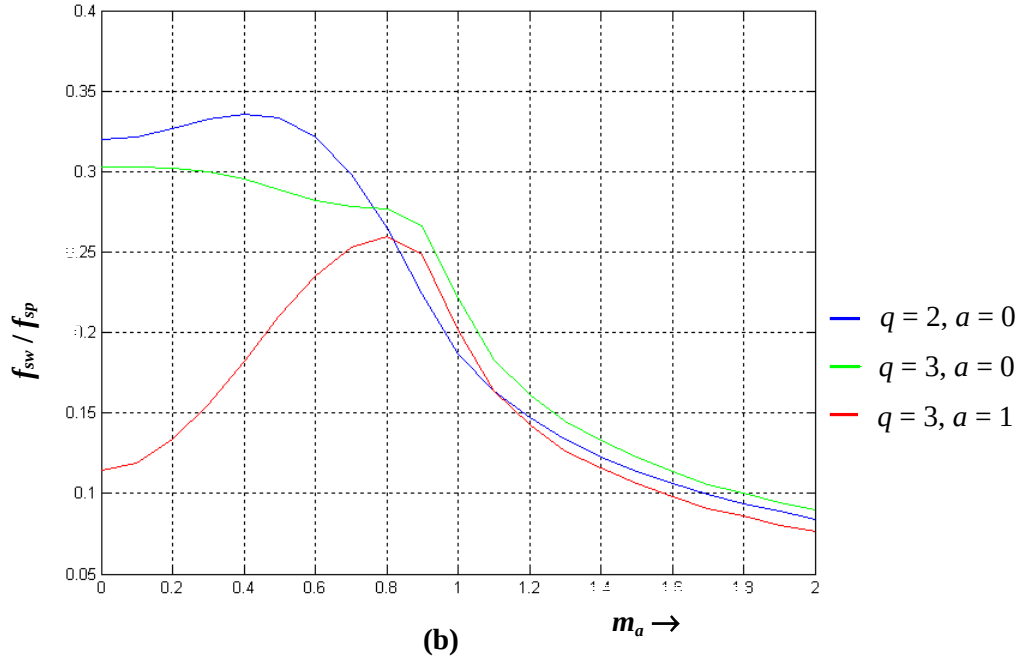

(b)

Fig. 6.34: Switching frequency versus modulation index for (a) N = 6 (b) N = 7.

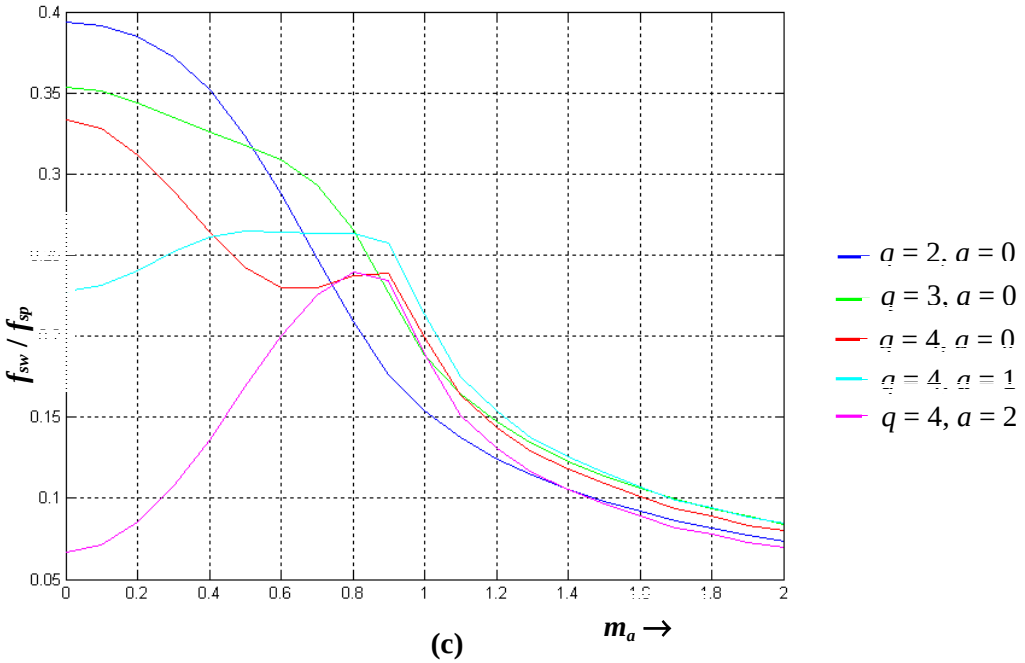

(c)

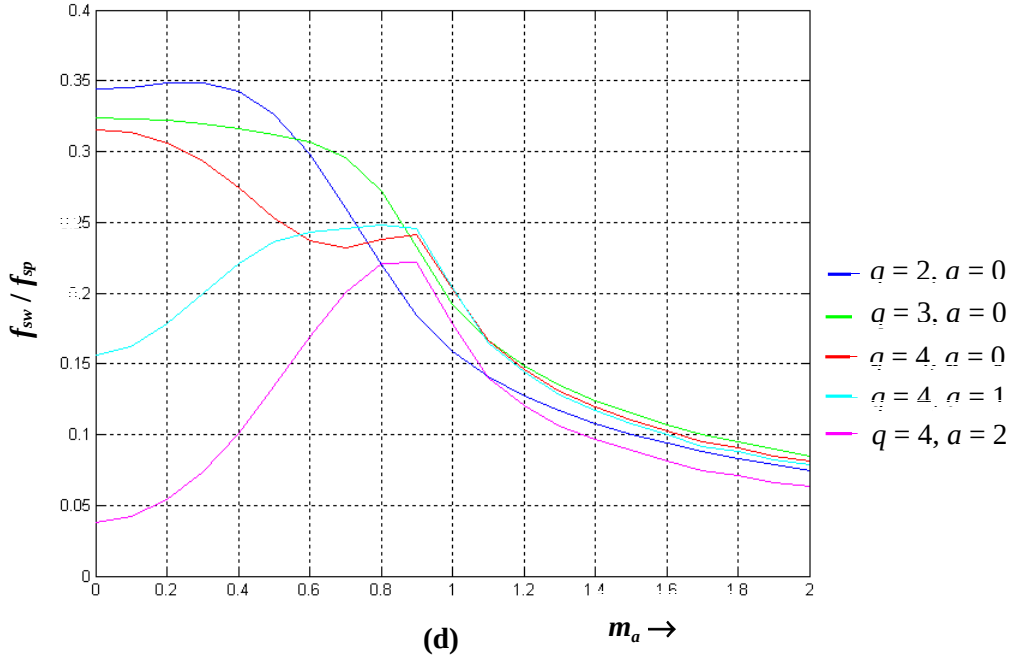

(d)

Fig. 6.34: (continued) (c) N = 8 (d) N = 9.

From Figs. 6.34 (a) to (d) it can be seen that over the interval $0 < m_a < 0.4$, as the value of q and/or a increase the switching frequency decreases and over the range $1 < m_a < 1.5$ all the plots have similar f_{sw}/f_{sp} versus m_a characteristic.

Similar to the standard WRPWM scheme, for the modified WRPWM scheme f_{sw}/f_{sp} is directly proportional to the sum of products of each possible combination of the five distribution functions (see equations (5.19) and (5.20)). The characteristic of f_{sw}/f_{sp} versus m_a behave in a mixed manner and therefore hard to predict, even over the range $0 < m_a < 0.2$ and $m_a > 1$, due to the parameters q and a, the level of dc-bus which has the dominant probability varies among the various schemes (see Figs. 5.27, 6.2, 6.3, 6.5 and 6.6).

CHAPTER SEVEN

PRACTICAL IMPLEMENTATION

In order to validate the results from the theoretical analysis, a 1 kW single-phase leg five-level diode clamped inverter was built. Both the standard five-level WRPWM and the modified WRPWM schemes were implemented in software and used to operate a five-level diode clamped inverter. The implemented single-phase leg five-level inverter is shown in Fig. 7.1. In this section, the design of the five-level diode clamped inverter and the implementation of both the standard and modified WRPWM is presented.

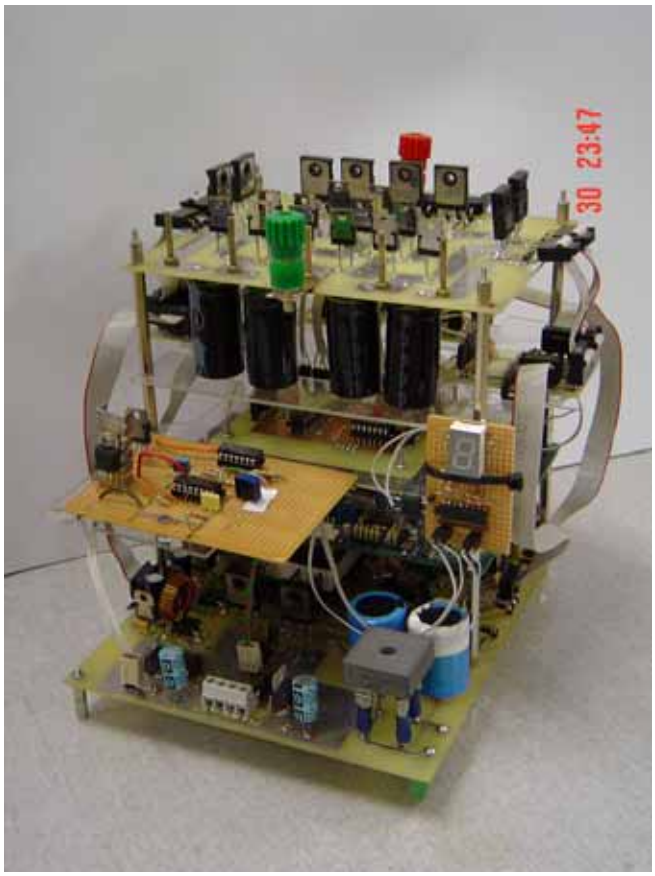

Fig. 7.1: The implemented single-phase leg five-level inverter.

7.1. Functional Design of Five-Level Inverter

Refer to Fig. 7.2 for a general functional block diagram. The random number generator and the reference sinusoidal wave look-up table implementation along with the switching decisions (WRPWM) are made within the Motorola DSP 56F807 evaluation module (FU 5). The DSP then sends the five level WRPWM signals through buffers in buffer chip1 (FU 3) to the driver circuitry (FU 2) to control the eight power MOSFETs in the five-level inverter (FU 1). When the driver circuitry detects that a fault has occurred in the power MOSFETs through the sensor tap, the driver circuitry will disable its-self and sends a fault signal through buffer chip 2 (FU 3) simultaneously to stop DSP generating WRPWM signals. To enable the driver circuitry a reset signal from DSP has to be sent through buffer chip 2 to the driver circuitry.

Due to the dc bus capacitors charge and discharge balancing problem four separate dc sources are used to provide the input dc voltage to the five-level inverter.

A push-pull converter (FU 4) was implemented to provide eight +15 V and eight -5 V dc source with isolated ground to the driver circuitry. The detail of the function unit 1 and flow diagram of DSP code for both the standard and modified WRPWM are provided in the following subsections and the design of function unit 2 and 4 is presented in appendix A and B, respectively.

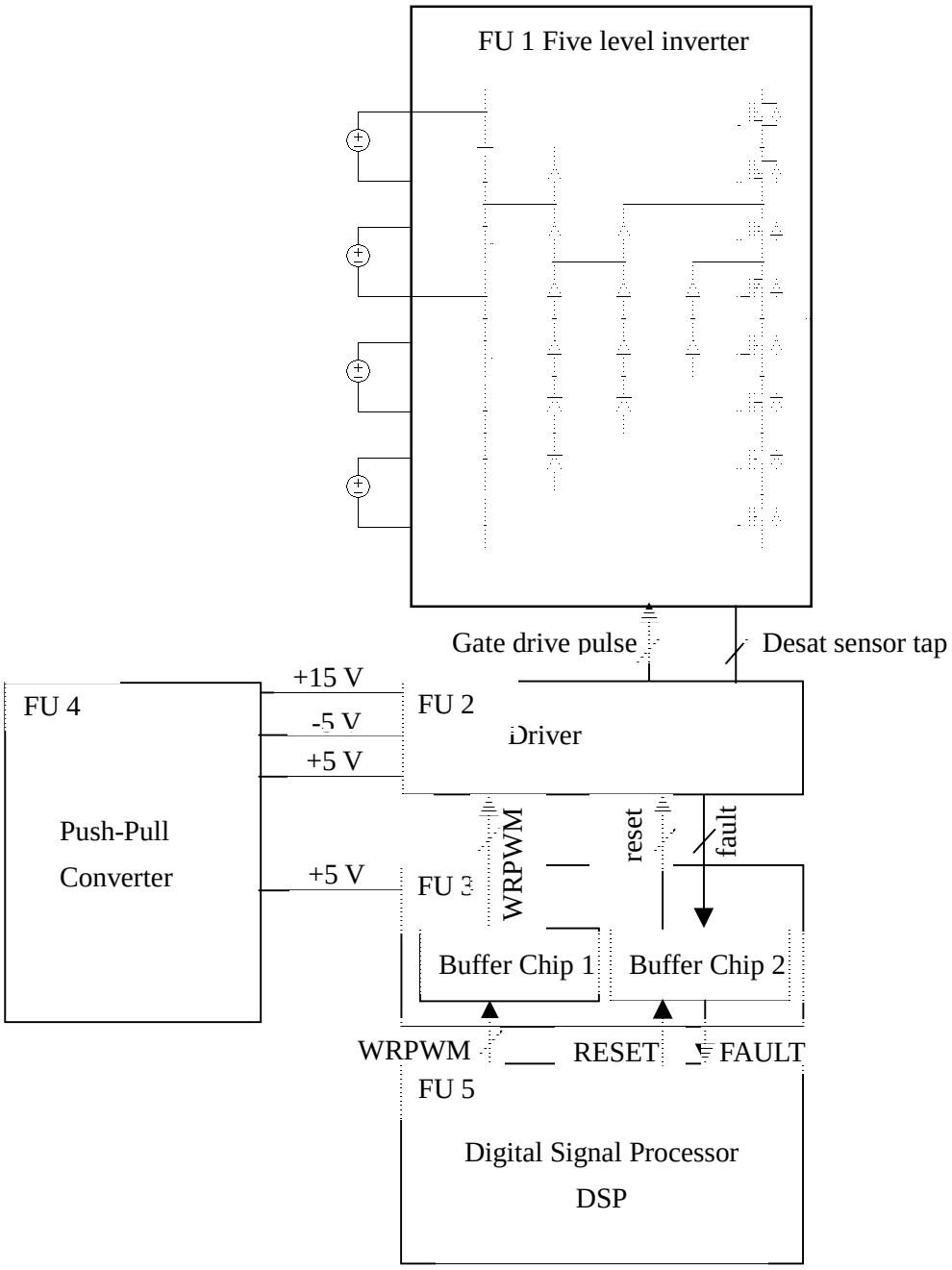

Fig. 7.2: Functional block diagram of five level inverter and control system.

7.2. The Five-Level Inverter Design

The diode clamped topology in Fig. 2.11 is used to implement the five-level inverter. In this topology, to built a five level inverter four dc link capacitor, eight power switching devices and twelve clamping diode is required.

The design of the five-level inverter is discussed below. The starting point parameters needed for the design are as follows.

- Maximum input voltage $V_{dc\ max}$ = 200 V.
- Maximum input current $I_{out\ max}$ = 5 A.
- Maximum switching frequency $f_{sw\ max}$ = 11.8 kHz.

7.2.1. dc link Capacitor Sizing

Four identical capacitors are used for the dc link each of them has to have same voltage capability:

$$V_{C\max} = 200/4 = 50\ \text{V}.$$

The maximum allowable voltage ripple is 10% of the dc source. Thus

$$\Delta V_{Cp-p} = 10\% \times 200\ \text{V} / 4 = 5\ \text{V}.$$

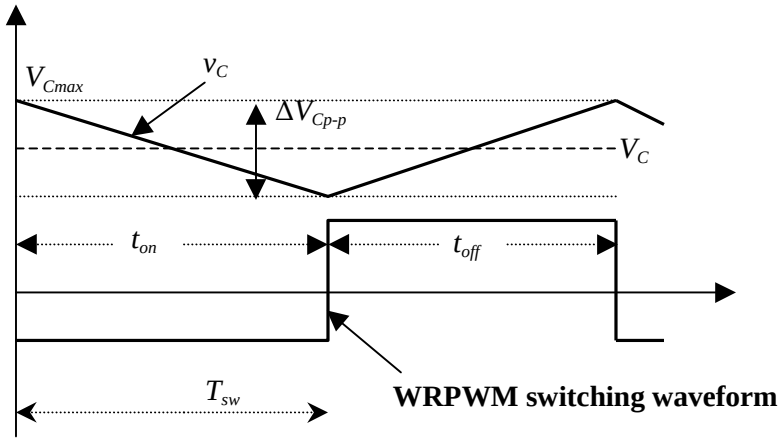

Fig. 7.3: Illustration of capacitor charging and discharging.

Fig. 7.3 shows the capacitor voltage waveform v_C corresponding to the PWM gate signal where V_{Cmax} is the maximum peak capacitor voltage, ΔV_{Cp-p} is the peak to peak capacitor voltage ripple and V_C is the capacitor dc component voltage. The capacitor voltage v_C is defined as

$$v_C = V_{Cmax} - (V_{Cmax} / RC) \times t \tag{7.1}$$

and the dc voltage component is defined as

$$V_C = V_{Cmax} - \Delta V_{Cp\text{-}p} / 2. \tag{7.2}$$

The worst case is when $t = 1 / f_{sw\ max}$ and from the theoretical analysis we know that at sampling frequency of 30 kHz the maximum ratio of f_{sw}/f_{sp} is 0.3939, this gives a switching frequency f_{sw} of 11.8 kHz. Now from (7.1) the minimum capacitance can be calculated as

$$\begin{aligned} T_{sw} &= 1/ f_{sw} \\ &= 84.7\ \mu\text{sec}, \end{aligned}$$

$$\Delta V_{Cp\text{-}p} = (V_{Cmax} / RC) \times t = 5\ \text{V}$$

and

$$V_{Cmax} / R = I_{in\ max} = 5\ \text{A}.$$

Thus, for the maximum allowable capacitor voltage ripple

$$C \geq 84.7\ \mu\text{F}.$$

From the above calculations four 3.3 mF capacitors are chosen to be used to realize the dc link capacitor. The expected maximum voltage ripple will then expected to be

$$\Delta V_{Cp\text{-}p} = (5\ \text{A} / 3.3\ \text{mF}) \times 84.7\ \mu\text{sec} = 128.3\ \text{mV}.$$

Capacitor Ripple Current:

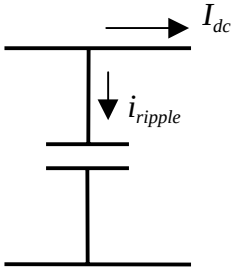

Fig. 7.4: Capacitor ripple and DC current.

Fig. 7.4 illustrates the current components of the dc link capacitor during the switching operation, where I_{dc} is the input current and i_{ripple} is the ripple current flow through the capacitor. From the relation $i = C\,dv/dt$, the ripple current flowing through the capacitor:

$$\begin{aligned} i_{ripple} &= C\,dv/dt \\ &= 3.3\,mF \times (128.3\,m\text{V}/84\,\mu\text{sec}) \\ &= 5\text{ A}. \end{aligned}$$

Therefore, for capacitance of 3.3 mF each of the capacitors should have at least 50 V and 5 A voltage and current capability.

7.2.2. MOSFET Selection

The MOSFET is chosen based on maximum stress voltage, maximum peak input current and maximum switching frequency.

From section 2.2.1.6.2, it is known that in the ideal condition the MOSFET should block nominal voltage of 50 V. The maximum stress voltage across drain source of switching power MOSFET should be the maximum blocking voltage plus the spike due to the stray inductance within the five-level inverter structure. Assume the spike is 100% of the maximum separated dc voltage. Thus

$$\begin{aligned} V_{stress} &= 50\text{ V} + 50\text{ V} \times 100\% \\ &= 100\text{ V}. \end{aligned}$$

Therefore, the drain to source breakdown voltage of the MOSFET should be greater than 100 V. The maximum continuous drain current is chosen to be greater than twice the maximum input current which is 10 A.

The sum of MOSFET turn on delay time $t_{d(\text{on})}$, rise-time t_r, turn-off-delay time $t_{d(\text{off})}$ and fall-time t_f should at least be less then half of the minimum switching interval (i.e., $1 / f_{sw\,max}$) minus the duty ratio (i.e., $1 / f_{sp}$). The maximum switching frequency is 12 kHz and the maximum sampling frequency is 30 kHz. Thus

$$t_{d(\text{on})} + t_r + t_{d(\text{off})} + t_f < (1 / 12\text{ kHz} - 1 / 30\text{ kHz}) / 2,$$
$$t_{d(\text{on})} + t_r + t_{d(\text{off})} + t_f < 25\ \mu\text{sec}.$$

According to the results of the calculations, IRFP264 HEXFET power MOSFET is selected to

be the power switching device. The important specifications are

Drain to source breakdown voltage	V_{DSS}	250 V
Continuous drain current	I_D	24 A
Maximum power dissipation	P_D	280 W
Static drain-to-source on-resistance	$R_{DS(on)}$	0.075 Ω
Maximum threshold voltage	$V_{GS(th)}$	4 V
Maximum junction temperature	T_j	150^o C
Total gate Charge	Q_g	210 nC
Turn-on delay time	$t_{d(on)}$	22 ns
Rise time	t_r	99 ns
Turn-off delay time	$t_{d(off)}$	110 ns
Fall time	t_f	92 ns

The current necessary to switch the IRFP264 on in 140 ns is given by

$$\begin{aligned} i &= dQ/dt \\ &= 210\ \text{nC}/140\ \text{nsec} \\ &= 1.5\ \text{A} \end{aligned}$$

and to switch off in 210 ns is

$$\begin{aligned} i &= dQ/dt \\ &= 210\ \text{nC}/210\ \text{nsec} \\ &= 1\ \text{A}. \end{aligned}$$

7.2.2.1 MOSFET Power Dissipation

The switching MOSFET has two major types of losses, which are conduction loss and switching loss.

7.2.2.1.1 Conduction Loss

Except at higher switching frequencies, nearly all of the power dissipated in a MOSFET in a switch mode power application occurs when the device is in the on state. The instantaneous power dissipation P_{on} in the on state of the MOSFET is given by

$$P_{on} = I_D^2 r_{DS(on)} = 5^2 \times 0.075 = 1.875\ \text{W}.$$

7.2.2.1.2 Switching Loss

In a switch mode power application MOSFET dissipate power during the turn-on and turn-off intervals. There are f_{sw} such turn-on and turn-off transients per second. Thus the average switching power loss P_{sw} in the MOSFET is given by

$$\begin{aligned} P_{sw} &= 1/2 \times V_{DS} I_D f_{sw} \left(t_{sw(on)} + t_{sw(off)} \right) \\ &= 1/2 \times 50\ \text{V} \times 5\ \text{A} \times 12\ \text{kHz} \times (140\ \text{nsec} + 210\ \text{nsec}) \\ &= 0.252\ \text{W} \end{aligned}$$

Therefore, the total power dissipation in the MOSFET is $P_{total} = P_{on} + P_{sw} = 2.127$ W

7.2.2.2 Heat Sink Requirement

Maximum junction temperature desired: $T_j = 100^o$ C
Maximum ambient temperature (assumption): $T_a = 25^o$ C
Junction to ambient thermal resistance required: $(T_j + T_a)/ P_{total} = 35.3\ ^oC/W$

7.2.3 Clamping Diode Selection

The clamping diode is chosen based on maximum stress voltage, maximum peak input current and should be ultra fast recovery diode.

From section 2.2.1.6.2, it is known that in the ideal condition the clamping diode should block maximum voltage of 150 V. The maximum stress voltage across the clamping diode should be the maximum block voltage plus the spike due to the stray inductance within the five-level inverter structure. Assume the spike is 100% of the maximum separated dc voltage. Thus

$$V_{stress} = 150\ \text{V} + 150\ \text{V} \times 100\% = 300\ \text{V}.$$

Therefore, the avalanche breakdown voltage of the clamping should be greater than 300 V. The maximum continuous forward conduction current is chosen to be greater than twice the maximum input current which is 10 A.

Based on the above requirements, HFA25TB60 HEXFRED ultrafast soft recovery diode is chosen to be the clamping diode. The important specifications are

Cathode-to-anode breakdown voltage	V_{BR}	600 V
Continuous forward current	I_F	25 A
Maximum power dissipation	P_D	125 W
Maximum forward voltage at I_F	V_F	1.5 V
Maximum reverse recovery time	t_{rr}	70 ns

7.2.3.1 Clamping Diode Power Dissipation

The HFA25TB60 ultrafast diode has t_{rr} of 70 ns thus nearly all the power dissipated in the diode occurs when it is in the on state. If the on state voltage drop is 1.5 V and the current through the diode is 5 A, then the on state power dissipation can be expressed as

$$P_{on} = 1.5 \times 5 = 7.5 \text{ W.}$$

7.2.3.2 Heat Sink Requirement

Maximum junction temperature desired: $T_j = 100^o$ C
Maximum ambient temperature (assumption): $T_a = 25^o$ C
Junction to ambient thermal resistance required: $(T_j + T_a)/ P_{total} = 10\ ^oC/W$

7.2.4 PCB Design

To reduce the stray inductance within the inverter the length of tracks are to be made as short as possible. The widths of the tracks are made wider to increase the current capability of the PCB. The layout of five-level inverter PCB is shown in appendix 2.

7.3 Switching Schemes Implementations on DSP

A digital controller using a Motorola digital signal processor (DSP) 56F807 evaluation module was used to control the five-level voltage source diode clamped WRPWM inverter. Figs. 7.4-7.6 illustrate the flowchart of the proposed five-level WRPWM algorithm.

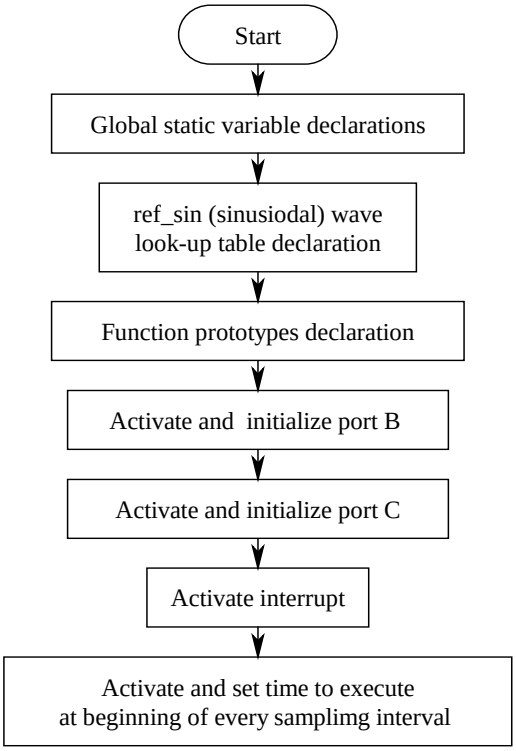

Fig. 7.5: Flowchart of the five-level algorithm.

From Fig. 7.5 the program start by first declaring all the global static variables, the reference sinusoidal wave look-up table and all the functions. Note that for sampling at 20 kHz, 600 samples are taken for one fundamental cycle. This is followed by activating and initializing all the pins in port B and C. After the fault condition interrupt is initiated, the timer for the WRPWM scheme which set to execute every $1/f_{sp}$ interval is then activating.

Fig. 7.6 shows the more detail algorithm of the fault interrupt. Note that the inverting buffer is used as the interface between the DSP and driver circuitry. Since the driver circuitry will send a high (i.e., a 1 in digital form) when fault occurred, thus the interrupt is set to execute when a 0 is received in pin C_1. When the interrupt execute it sent a 0 to disable the driver circuitry.

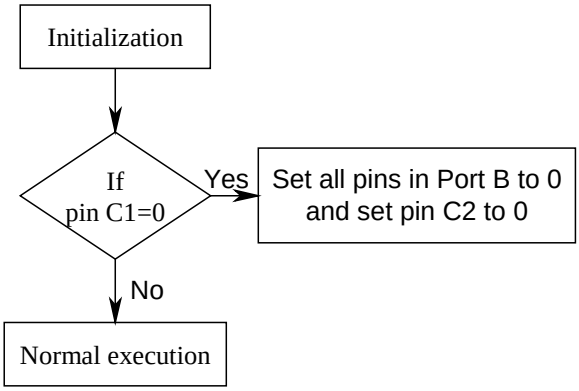

Fig 7.6: Flowchart of the fault interrupt algorithm.

Fig. 7.7 shows how the switching decision is made. The matrix row index (row) is set to be zero at the timer first activation. Then five random numbers are generated and compare with the reference sine wave form the look-up table. The counter (count) for counting how many random numbers is smaller than or equal to the reference sine wave is initialized to 0. The counter incremented by one for each random number that is smaller then or equal to the reference sine wave. The DSP will then decide which switching combination is performed base on the value of the counter. The matrix row index increased by one each timer cycle. The matrix row index is set to 0 when it reach a value of 599 (i.e., at end of each 50 Hz fundamental cycle).

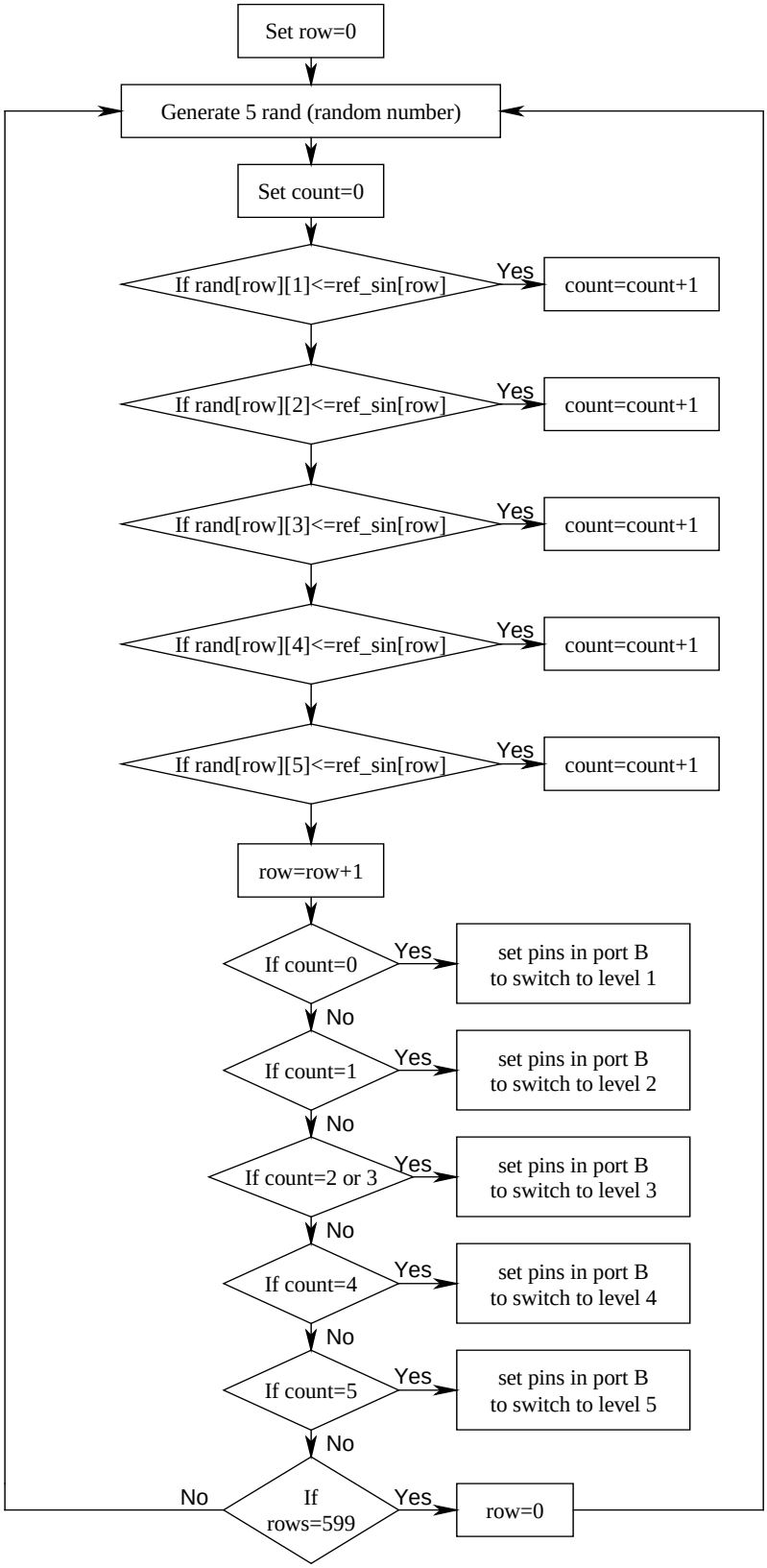

Fig. 7.7: Flowchart of the five-level switching algorithm within the timer.

CHAPTER EIGHT

EXPERIMENTAL RESULTS AND DISCUSSION

Chapter 8 presents and discusses the experimental results for both the standard and modified WRPWM switching schemes. This is for a five-level inverter operating with various numbers of comparisons, N, in one sampling interval and various combinations of q and a. Results will mainly comprise of the WRPWM output waveforms and signal power spectrum, harmonics versus modulation index, signal power versus sampling frequency, discrete noise power versus sampling frequency and continuous power versus sampling frequency plots.

The dc-bus is realized using four separated 40 V dc voltage sources to supply 160 V dc at the input of the five-level inverter. This gives -80 V, -40 V, 0 V, 40 V and 80 V as the first, second, third, fourth and fifth level of dc-bus voltage respectively.

Measurements were taken by measuring across points a and o of the new diode clamping five-level inverter in Fig. 2.11. Using an active probe with scale of 500 times, the oscilloscope was set at scale of 1000 times, therefore, the voltage measurements should be divided by two to get the actual value.

8.1 Standard Five-Level WRPWM

Typical output waveforms of a five-level inverter are used to illustrate the effects of the modulation index, m_a, on the switching decision for a standard five-level WRPWM scheme. Figs. 8.1 to 8.3 show the output waveform of the standard five-level WRPWM operating with $N = 5$ with modulation indices $m_a = 0.4$, 1.0 and 1.5 respectively. It is clear that as m_a increases, the chances or probability for the two outer levels of the dc-bus voltage (i.e. the first and the fifth level) being connected to the output terminal of the inverter within one fundamental cycle increases. At lower values of m_a, the probability of the third level of dc-bus voltage being connected to the output terminal of the inverter within one fundamental cycle increases. The observed output waveform is in agreement with the predicted performance in chapters 4 and 5.

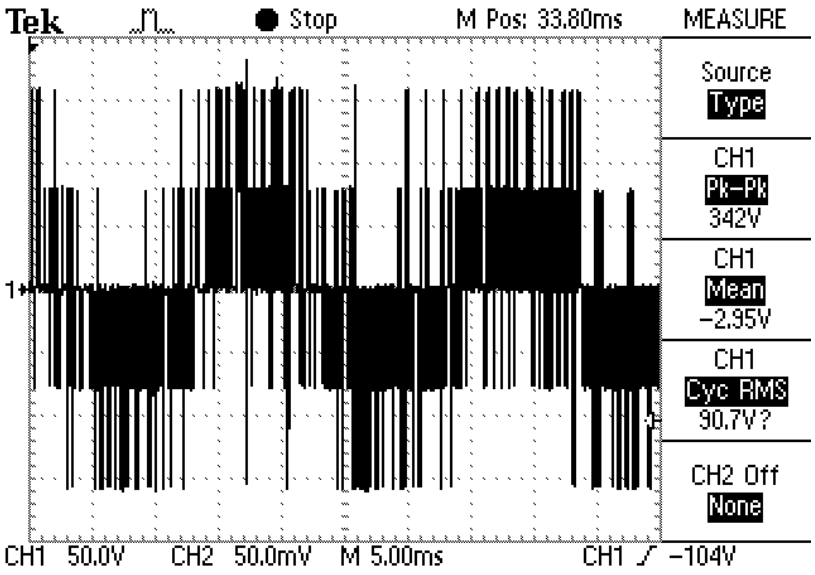

Fig. 8.1: Output waveform of standard five-level WRPWM operating with N = 5 at m_a = 0.4.

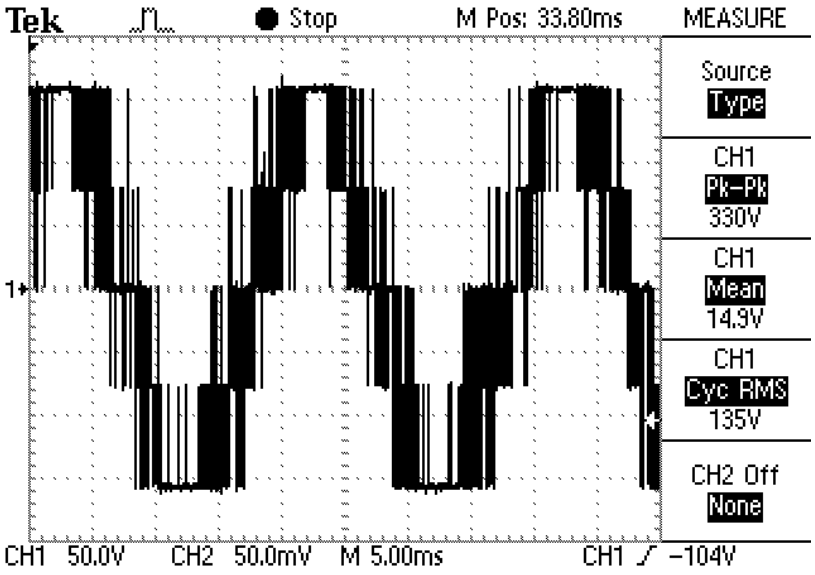

Fig. 8.2: Output waveform of standard five-level WRPWM operating with N = 5 at m_a = 1.0.

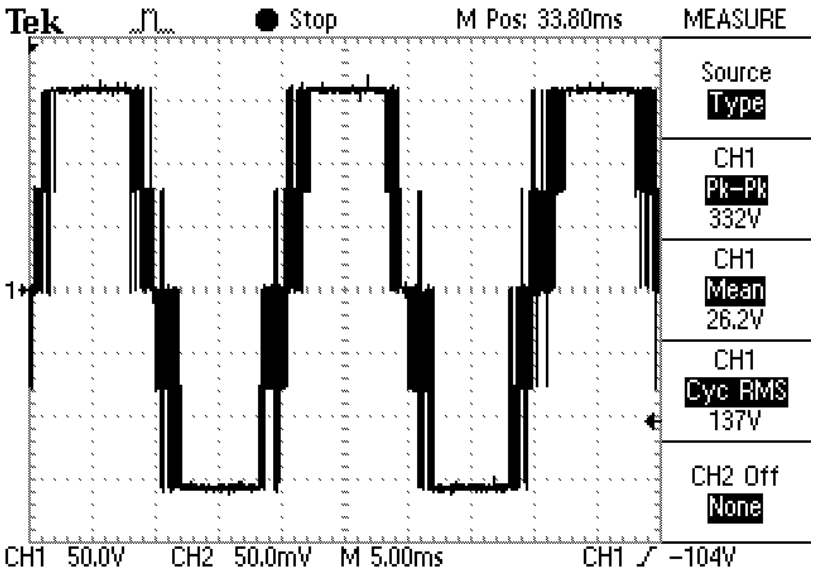

Fig. 8.3: Output waveform of standard five-level WRPWM operating with N = 5 at m_a = 1.5.

Figs. 8.4 to 8.6 show the voltage waveform and power spectrum of the five-level WRPWM scheme operating with N = 6 and modulation indices m_a = 0.4, 1.0 and 1.5. These are used to illustrate the effects of modulation index on the frequency spectrum of the standard five-level WRPWM output voltage waveform. It is clear that as m_a increases, the magnitude of fundamental component increases and the continuous noise power decreases.

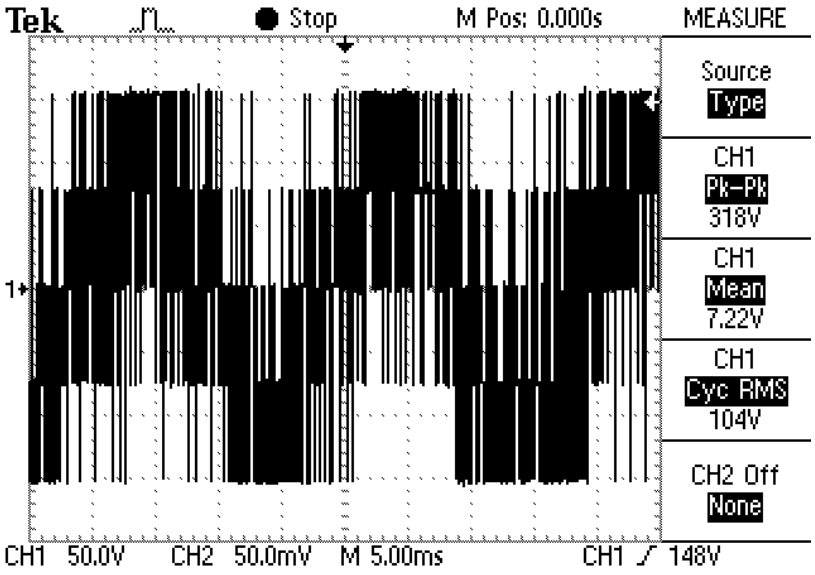

(a)

Fig. 8.4: Plots of standard five-level WRPWM operating with N = 6 at m_a = 0.4. (a) Output waveform.

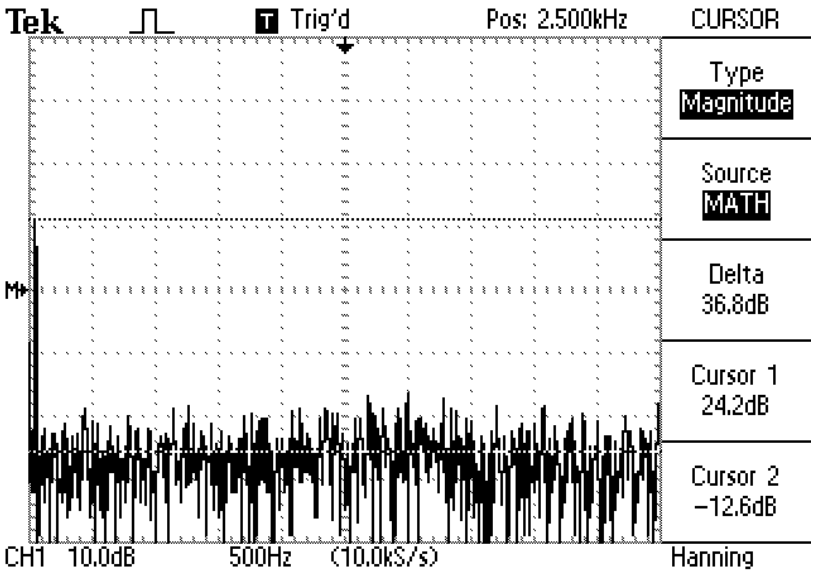

(b)

Fig. 8.4: (Continued) (b) Power spectrum.

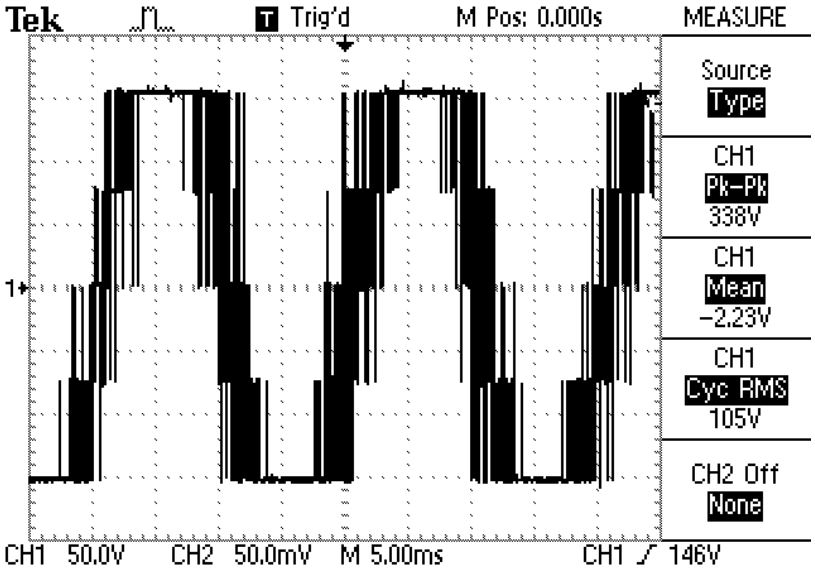

(a)

Fig. 8.5: Plots of standard five-level WRPWM operating with N = 6 at m_a = 1.0. (a) Output waveform.

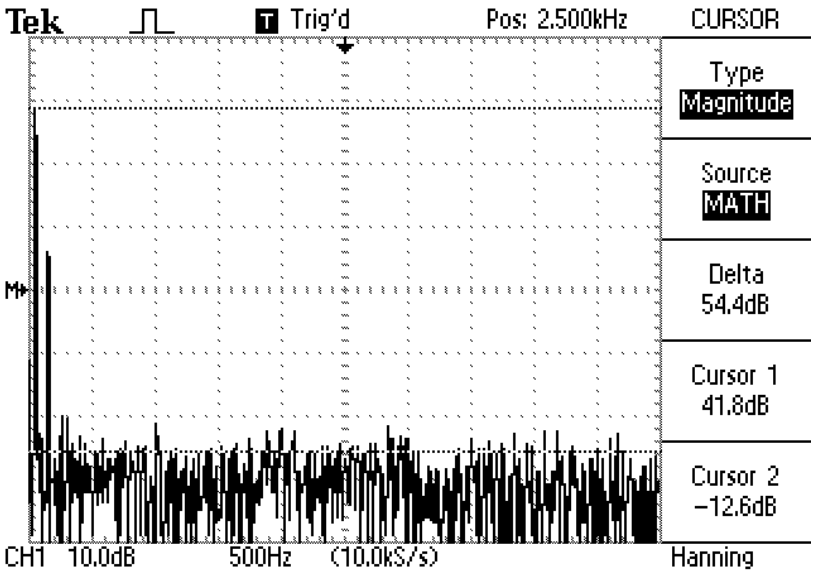

(b)

Fig. 8.5: (Continued) (b) Power spectrum..

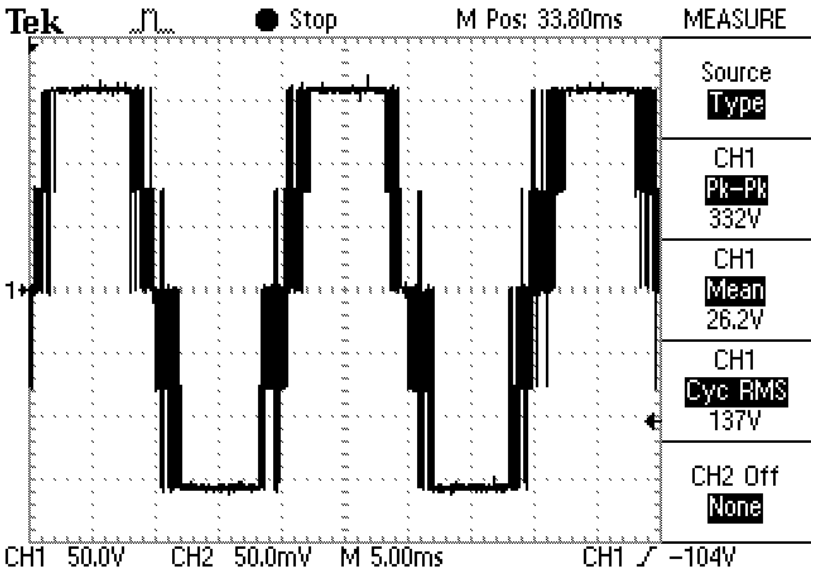

(a)

Fig. 8.6: Plots of standard five-level WRPWM operating with N = 6 at m_a = 1.5. (a) Output waveform.

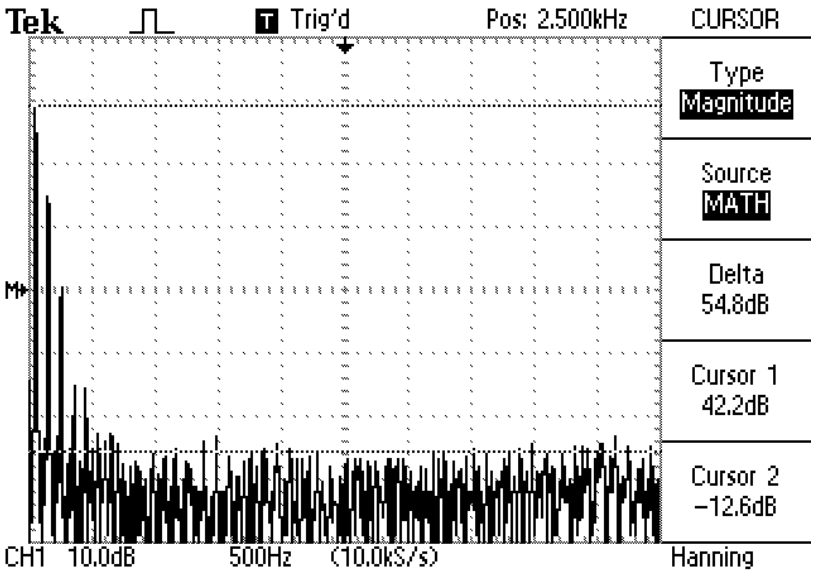

(b)

Fig. 8.6: (Continued) (b) Power spectrum.

The effect of sampling frequency on the output voltage waveform and the power spectrum of the standard five-level WRPWM schemes are illustrated. Examples of the output voltage waveform and power spectrum of the five-level WRPWM scheme operating with N = 9, and modulation index, m_a = 1.0 at sampling frequencies of f_{sp} = 10 kHz and 16 kHz are shown in Figs. 8.7 and 8.8, respectively. From Figs. 8.7 and 8.8, it can be seen that the continuous noise is in agreement with the derived function of $Td_{av}\text{sinc}^2(fT)$ in section 4.2.3. Moreover, as the sampling frequency increases the continuous noise power decreases, this can be observed from Figs. 8.4 to 8.6 as well.

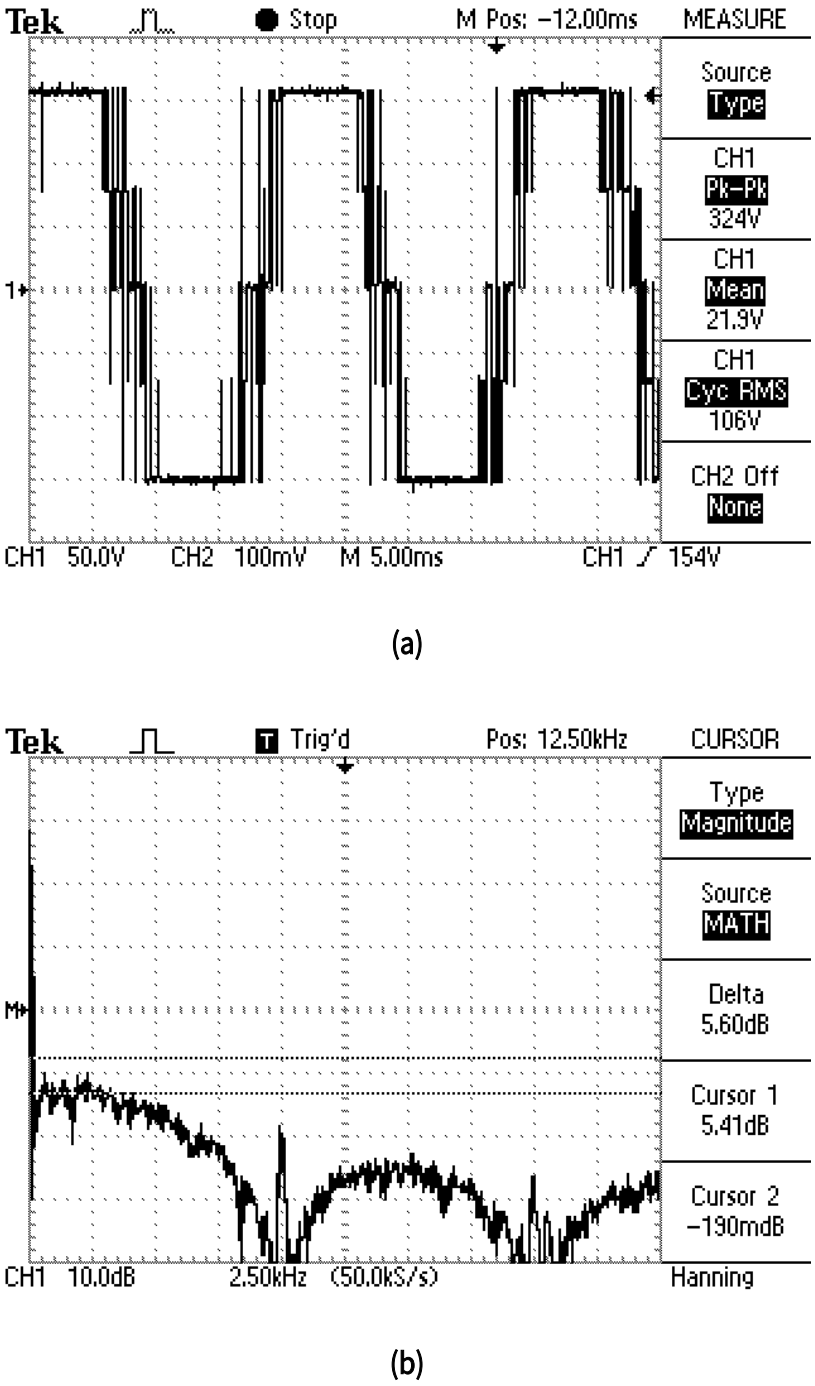

Fig. 8.7: Plots of standard five-level WRPWM operating N = 9 at m_a = 1.0 and f_{sp} = 10 kHz. (a) Output waveform. (b) Power spectrum.

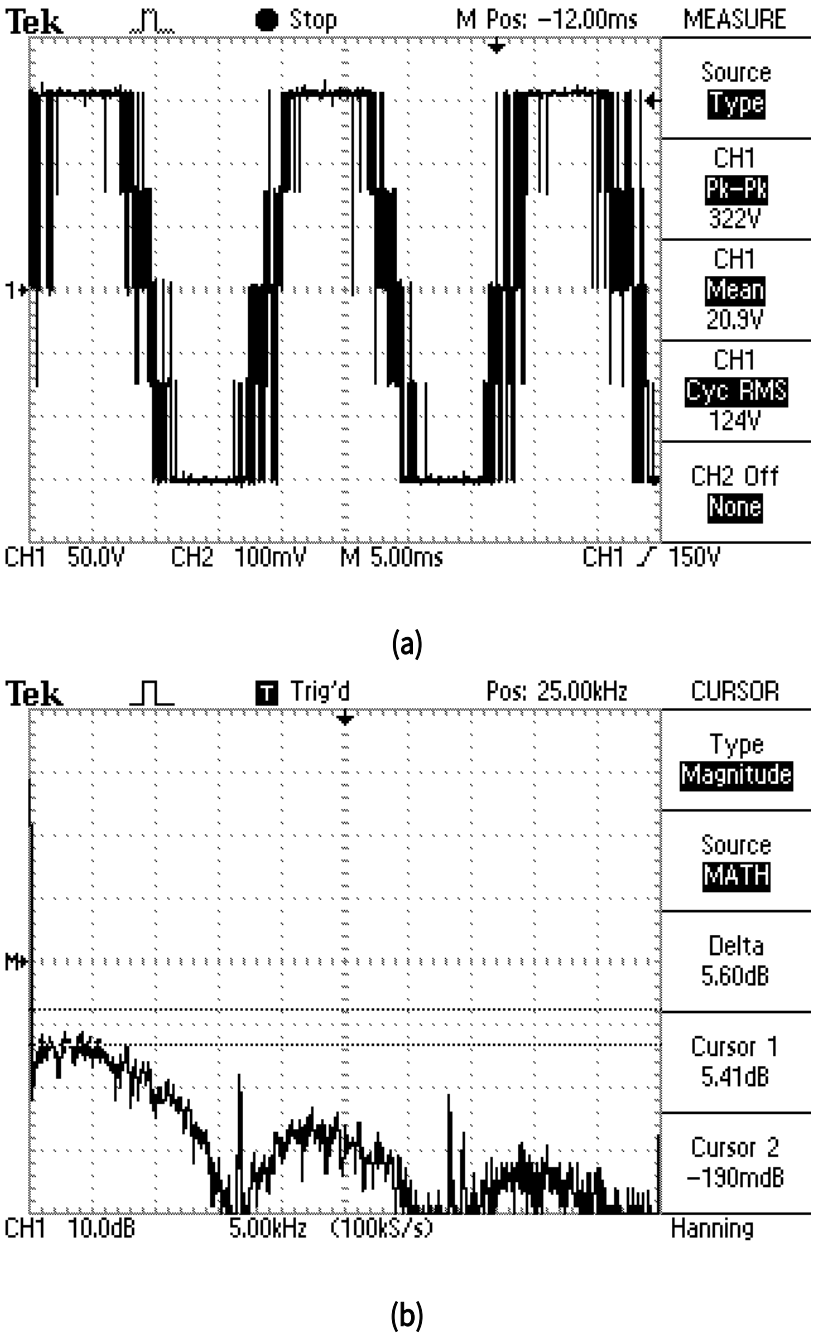

Fig. 8.8: Plots of standard five-level WRPWM operating N = 9 at m_a = 1.0 and f_{sp} = 16 kHz. (a) Output waveform. (b) Power spectrum.

8.1.1 Fundamental and Harmonic Components Measurements for Standard Five-Level WRPWM Scheme

In this section, plots of measured fundamental and harmonic components versus modulation

index are presented.

The measurements were taken by using the averaging function provided by the Tektronix TDS 220 oscilloscope in acquire mode. This gives the mean value of the fundamental and harmonics components generated most frequently and the range is shown with two points. Note that due to the magnitude of certain order of harmonics being lower than the magnitude of the continuous noise, it is difficult to measure them and, therefore, they will not be presented. However, the measurements included are adequate to validate the theoretical predictions.

8.1.1.1 Standard Five-Level WRPWM Operating with $N = 5$

The plot of measured fundamental component versus modulation index is shown in Fig. 8.9. The plots of third, fifth, seventh and ninth harmonic components versus modulation index are shown in Figs. 8.10, 8.11, 8.12 and 8.13, respectively. Note that the predicted values are plotted using a dotted line and the measured values are represented by star symbols. From Figs. 8.9 to 8.13, it can be seen that the measurements are in good agreement with predictions.

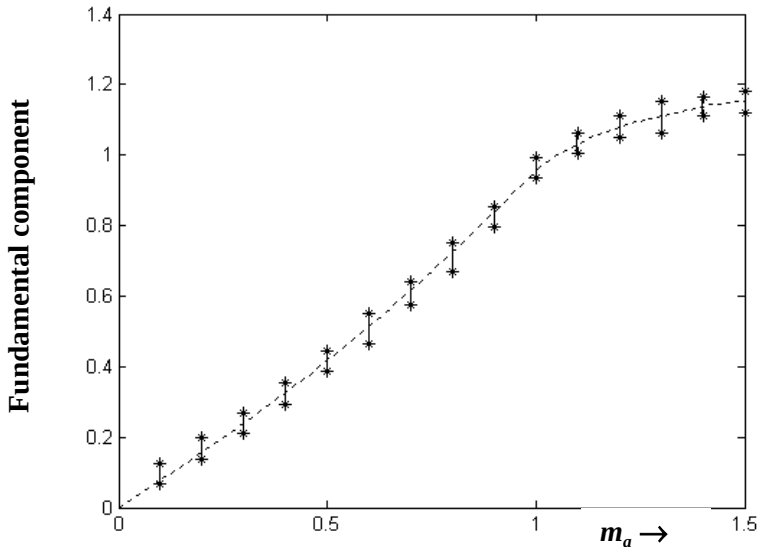

Fig. 8.9: Theoretical and measured fundamental component versus modulation index for standard five-level WRPWM scheme operating with $N = 5$.

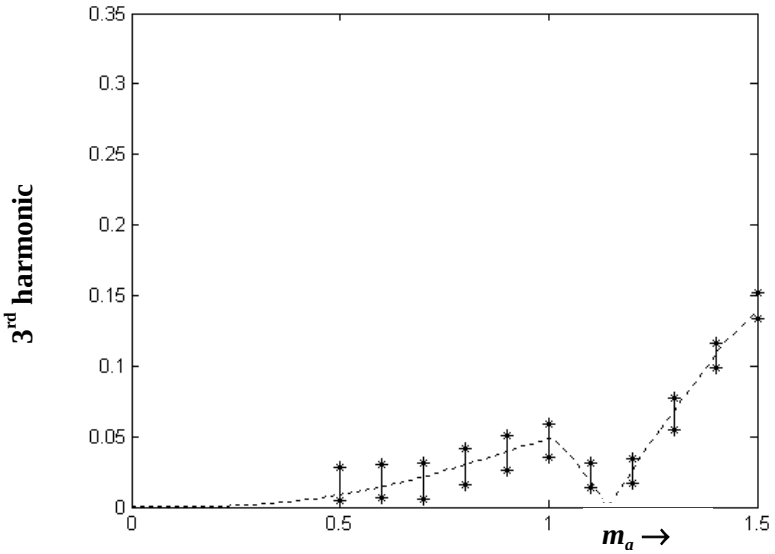

Fig. 8.10: Theoretical measured third harmonic component versus modulation index for standard five-level WRPWM scheme operating with N = 5.

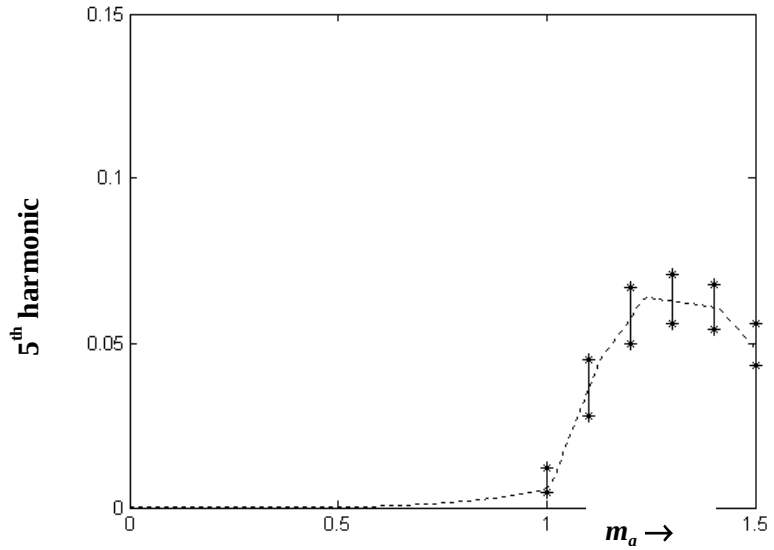

Fig. 8.11: Theoretical and measured fifth harmonic component versus modulation index for standard five-level WRPWM scheme operating with N = 5.

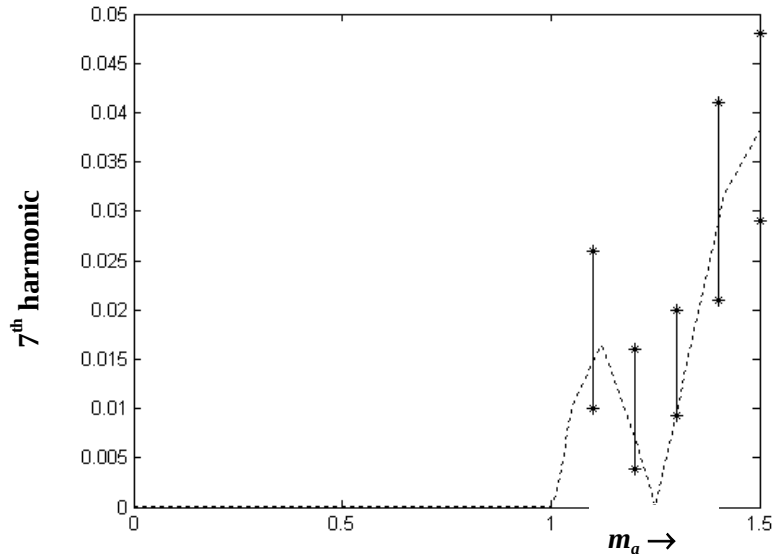

Fig. 8.12: Theoretical and measured seventh harmonic component versus modulation index for standard five-level WRPWM scheme operating with N = 5.

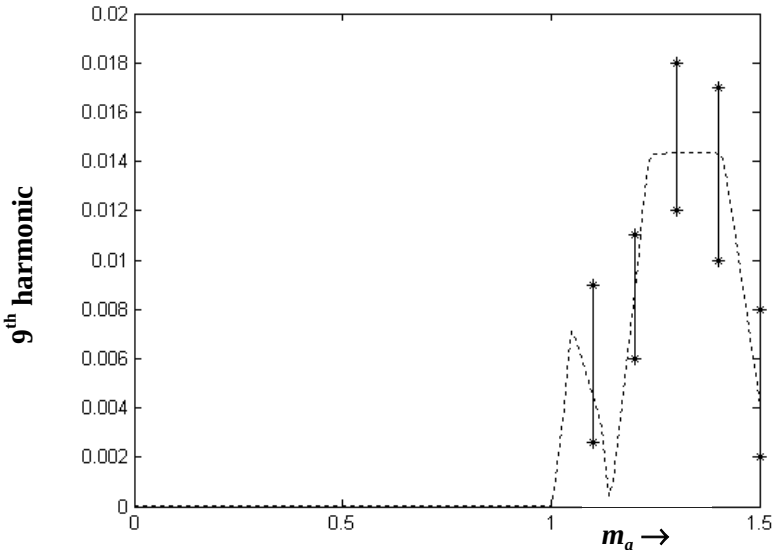

Fig. 8.13: Theoretical and measured ninth harmonic component versus modulation index for standard five-level WRPWM scheme operating with N = 5.

8.1.1.2 Standard Five-Level WRPWM Operating with N = 6

The plot of measured fundamental component versus modulation index is shown in Fig. 8.14. The plots of third, fifth and seventh harmonic components versus modulation index are shown in Figs. 8.15, 8.16 and 8.17, respectively. Note that the predicted values are plotted using a dotted line and the measured values are represented by star symbols. From Figs. 8.14 to 8.17, it can be seen that the measurements are in good agreement with predictions.

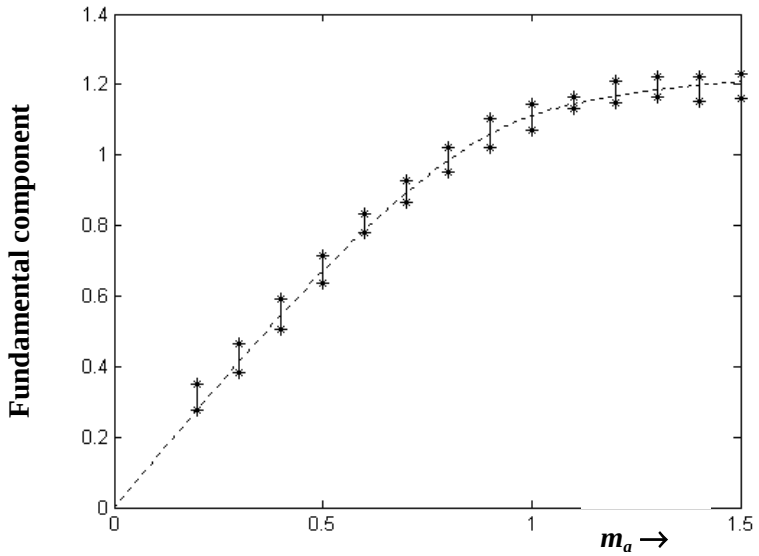

Fig. 8.14: Theoretical and measured fundamental component versus modulation index for standard five-level WRPWM scheme operating with N = 6.

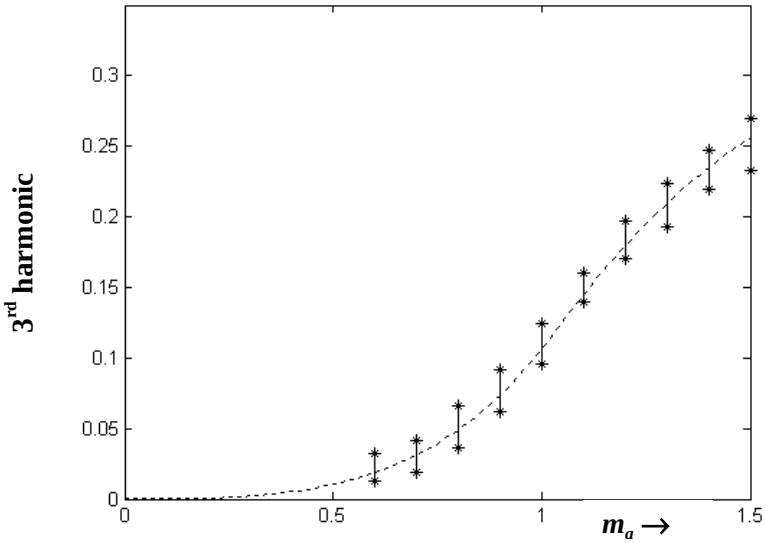

Fig. 8.15: Theoretical and measured third harmonic component versus modulation index for standard five-level WRPWM scheme operating with N = 6.

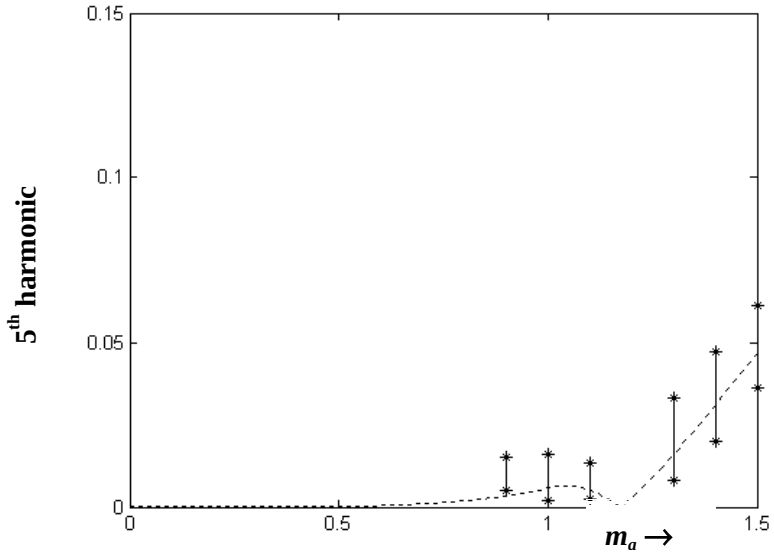

Fig. 8.16: Theoretical and measured fifth harmonic component versus modulation index for standard five-level WRPWM scheme operating with N = 6.

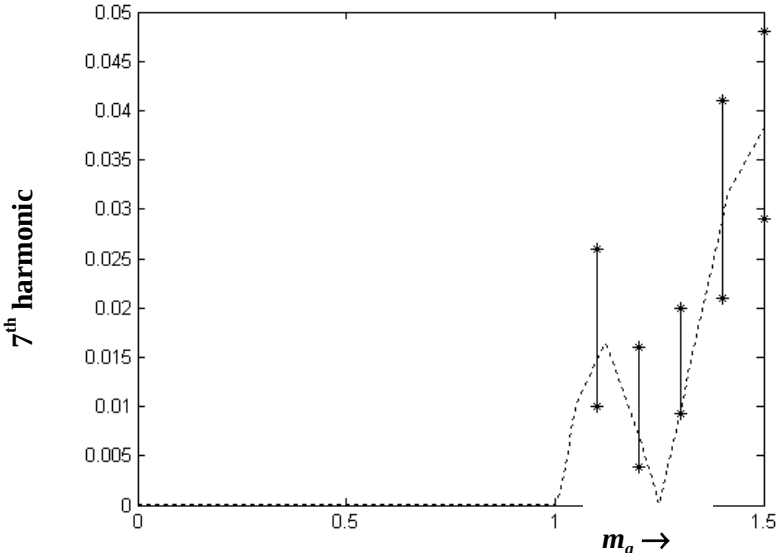

Fig. 8.17: Theoretical and measured seventh harmonic component versus modulation index for standard five-level WRPWM scheme operating with N = 6.

8.1.1.3 Standard Five-Level WRPWM Operating with N = 7

The plot of measured fundamental component versus modulation index is shown in Fig. 8.18. The plots of third, fifth and seventh harmonic components versus modulation index are shown in Figs. 8.19, 8.20 and 8.21, respectively. Note that the predicted values are plotted using a dotted line and the measured values are represented by star symbols. From Figs. 8.18 to 8.21, it can be seen that the measurements are in good agreement with predictions.

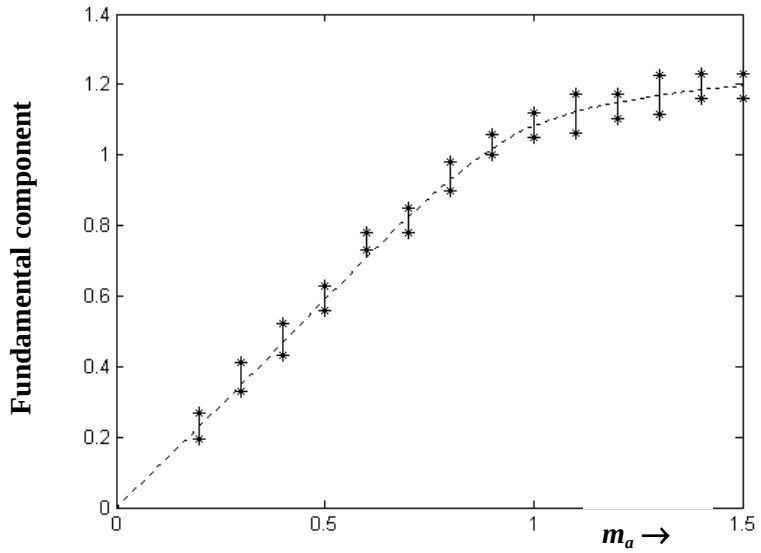

Fig. 8.18: Theoretical and measured fundamental component versus modulation index for standard five-level WRPWM scheme operating with N = 7.

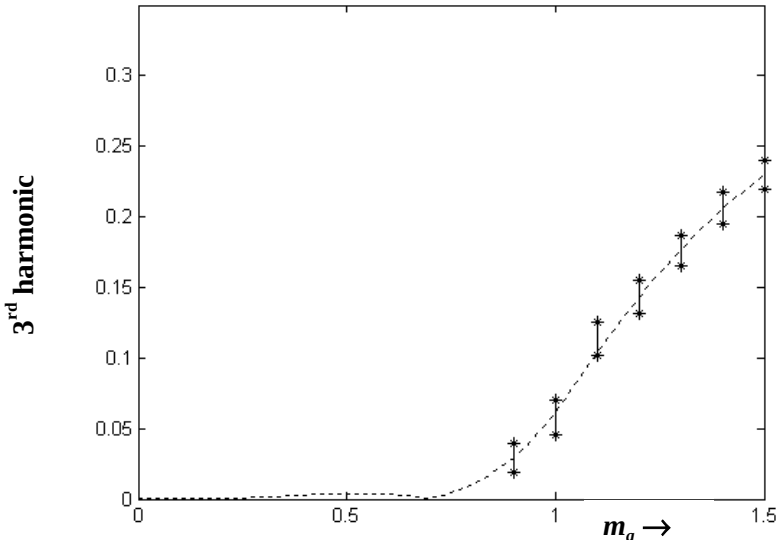

Fig. 8.19: Theoretical and measured third harmonic component versus modulation index for standard five-level WRPWM scheme operating with N = 7.

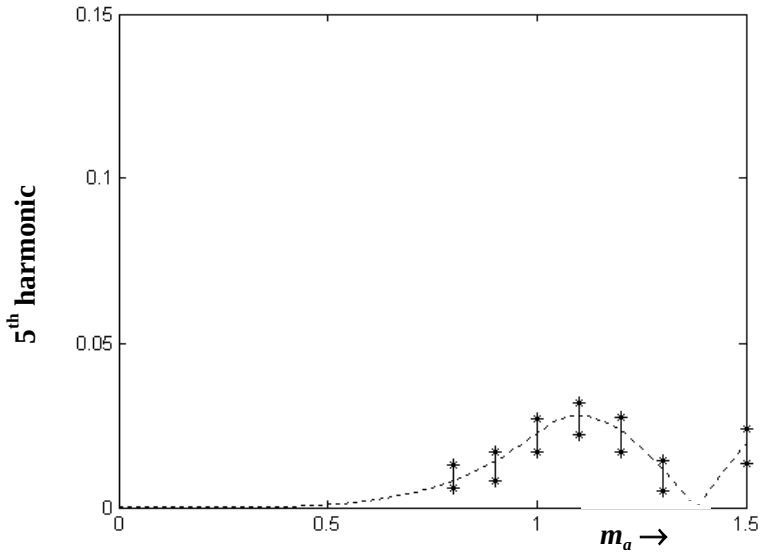

Fig. 8.20: Theoretical and measured fifth harmonic component versus modulation index for standard five-level WRPWM scheme operating with N = 7.

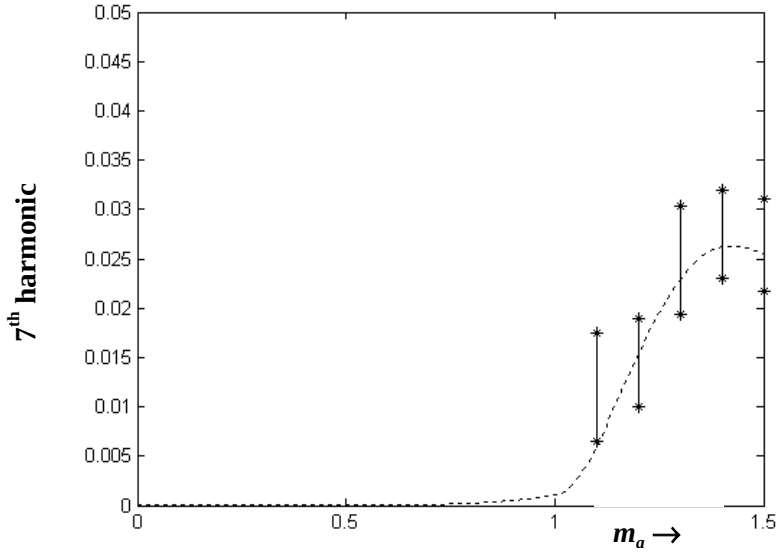

Fig. 8.21: Theoretical and measured seventh harmonic component versus modulation index for standard five-level WRPWM scheme operating with N = 7.

8.1.1.4 Standard Five-Level WRPWM Operating with N = 8

The plot of measured fundamental component versus modulation index is shown in Fig. 8.22. The plots of third, fifth and seventh harmonic components versus modulation index are shown in Figs. 8.23, 8.24 and 8.25, respectively. Note that the predicted values are plotted using a dotted line and the measured values are represented by star symbols. From Figs. 8.22 to 8.25, it can be seen that the measurements are in good agreement with predictions.

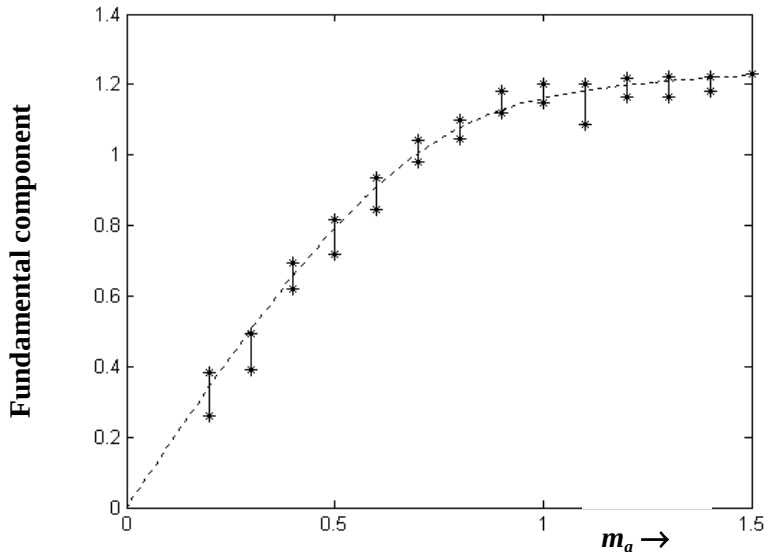

Fig. 8.22: Theoretical and measured fundamental component versus modulation index for standard five-level WRPWM scheme operating with N = 8.

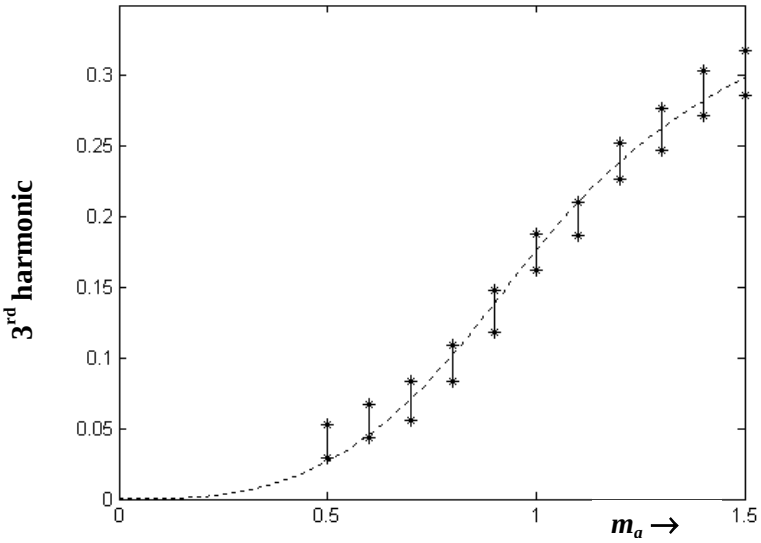

Fig. 8.23: Theoretical and measured third harmonic component versus modulation index for standard five-level WRPWM scheme operating with N = 8.

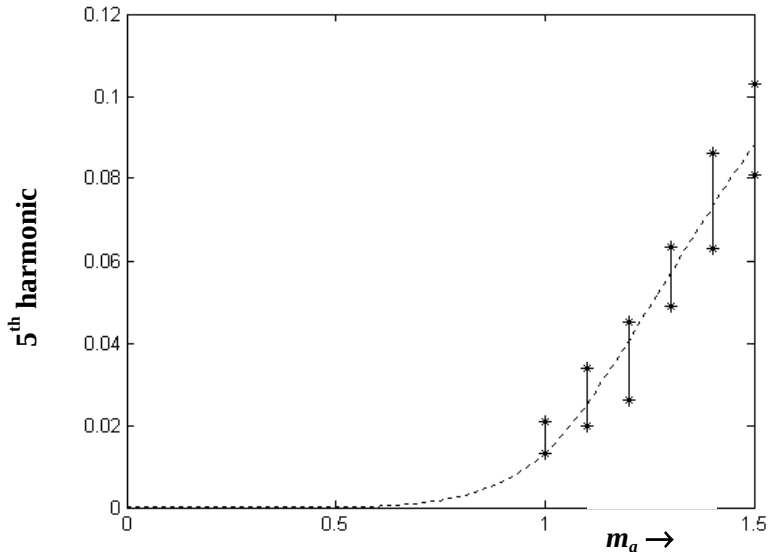

Fig. 8.24: Theoretical and measured fifth harmonic component versus modulation index for standard five-level WRPWM scheme operating with N = 8.

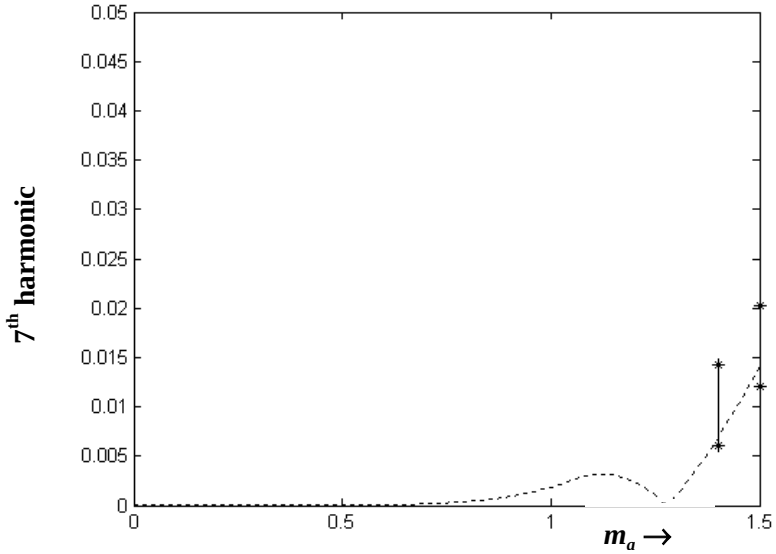

Fig. 8.25: Theoretical and measured seventh harmonic component versus modulation index for standard five-level WRPWM scheme operating with N = 8.

8.1.1.5 Standard Five-Level WRPWM Operating with N = 9

The plot of measured fundamental component versus modulation index is shown in Fig. 8.26. The plots of third, fifth and seventh harmonic components versus modulation index are shown in Figs. 8.27, 8.28 and 8.29, respectively. Note that the predicted values are plotted using a dotted line and the measured values are represented by star symbols. From Figs. 8.26 to 8.29, it can be seen that the measurements are in good agreement with predictions.

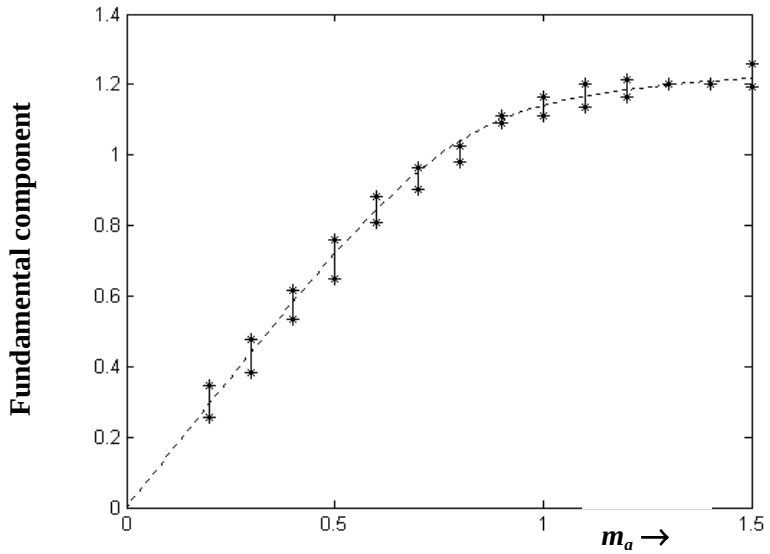

Fig. 8.26: Theoretical and measured fundamental component versus modulation index for standard five-level WRPWM scheme operating with N = 9.

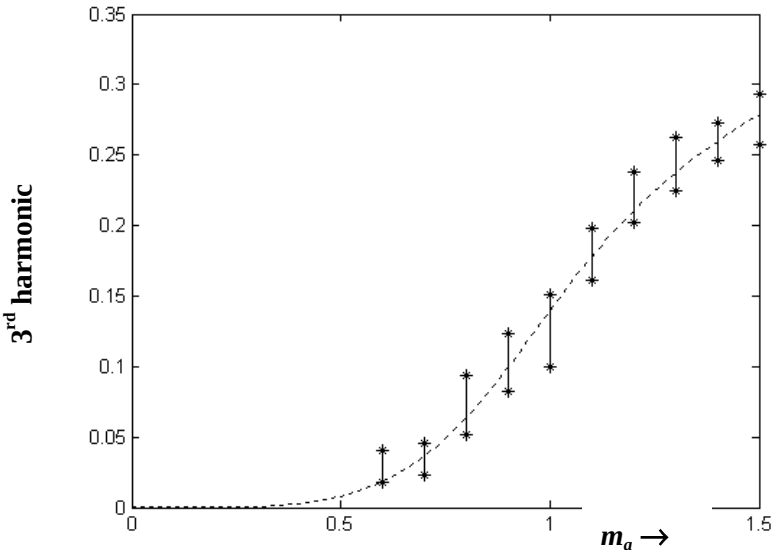

Fig. 8.27: Theoretical and measured third harmonic component versus modulation index for standard five-level WRPWM scheme operating with N = 9.

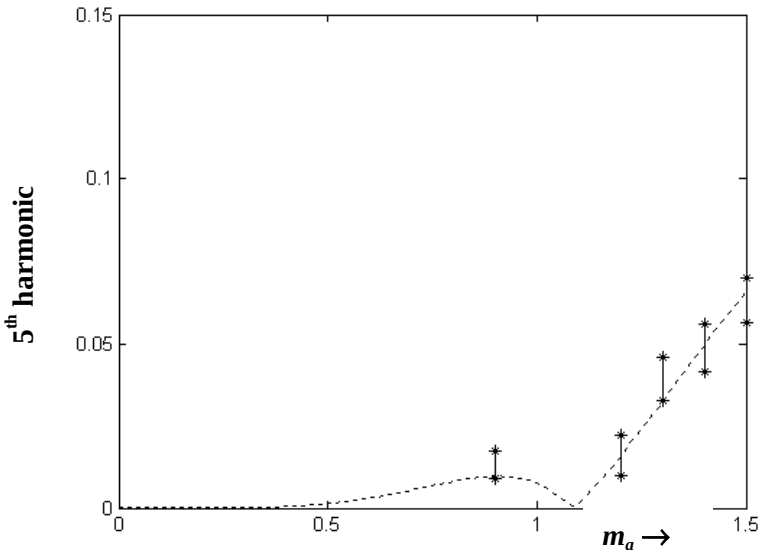

Fig. 8.28: Theoretical and measured fifth harmonic component versus modulation index for standard five-level WRPWM scheme operating with N = 9.

8.1.2 Signal, Discrete and Continuous Noise Power

In this section, plots of measured signal, discrete noise and continuous noise power versus sampling frequency are presented.

8.1.2.1 Signal Power

The signal power was calculated by first squaring and then averaging the value of the two points from the fundamental component measurements (i.e. $(V_{1\max}{}^2 + V_{1\min}{}^2)/2$, where V_1 is the amplitude of the fundamental component of voltage spectrum).

Figs. 8.29 and 8.30 show the plots of signal power versus sampling frequency characteristic for the standard five-level WRPWM scheme operating with N = 5 and 6, respectively. Measurements were taken at the sampling frequencies of f_{sp} = 10 kHz, 20 kHz and 25 kHz.

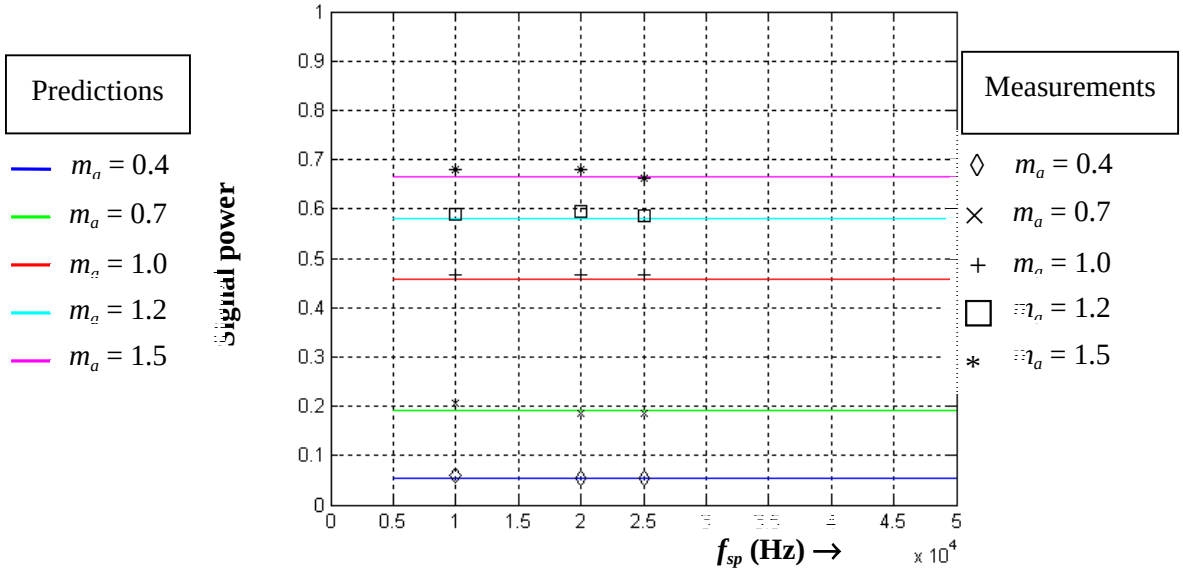

Fig. 8.29: Theoretical and measured signal power versus sampling frequency for standard five-level WRPWM scheme operating with N = 5.

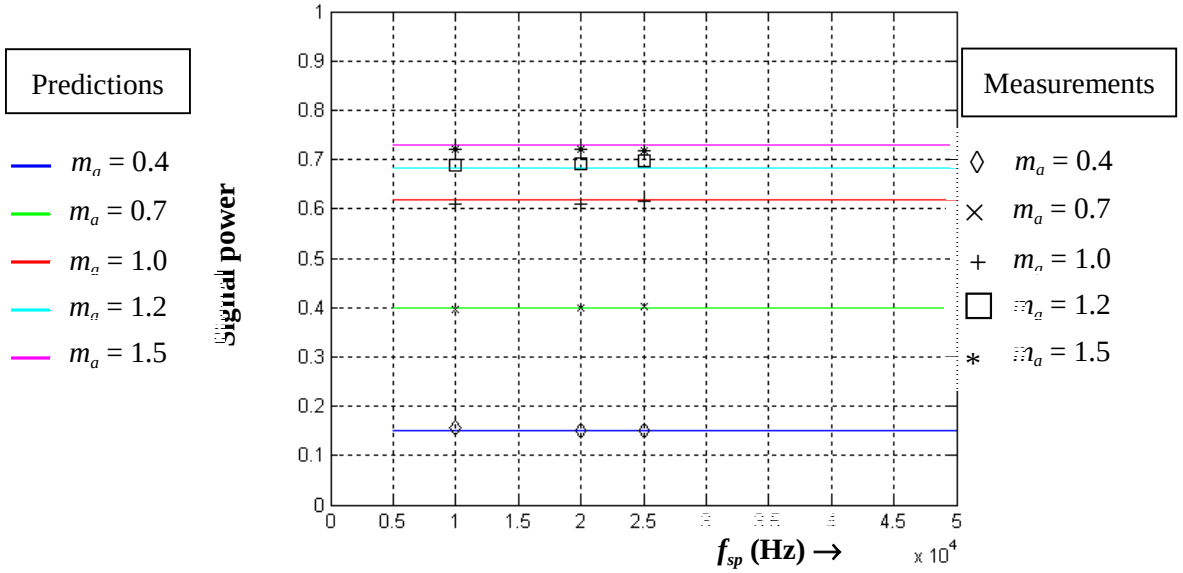

Fig. 8.30: Theoretical and measured signal power versus sampling frequency for standard five-level WRPWM scheme operating with N = 6.

Figs. 8.31 and 8.32 show the plots of signal power versus sampling frequency characteristic for the standard five-level WRPWM scheme N = 7 and 8. Measurements were taken at the sampling frequencies of f_{sp} = 10 kHz and 20 kHz.

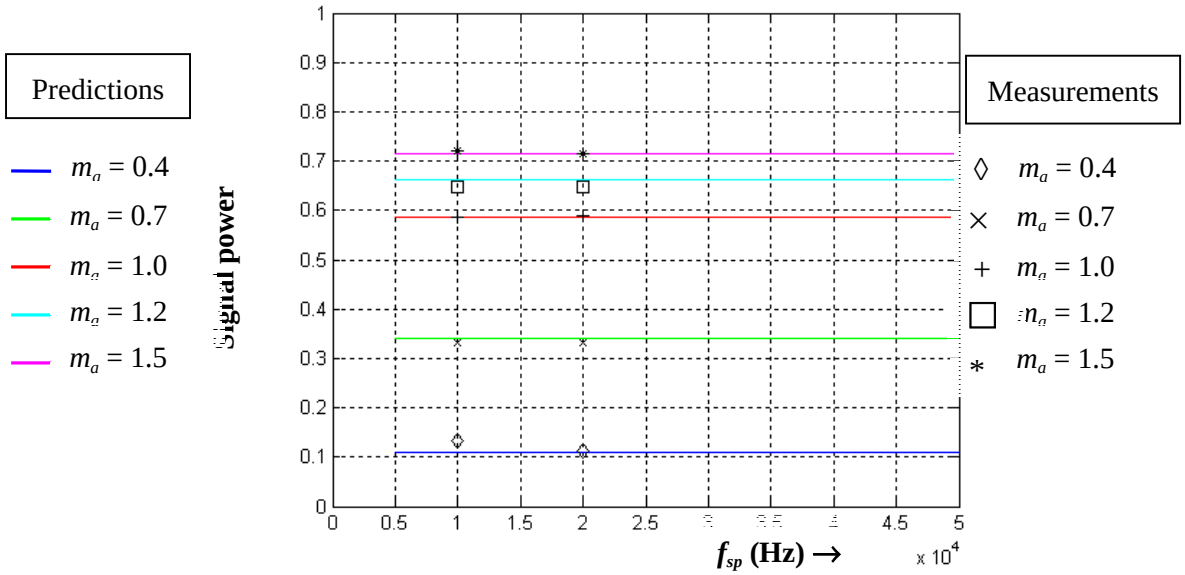

Fig. 8.31: Theoretical and measured signal power versus sampling frequency for standard five-level WRPWM scheme operating with N = 7.

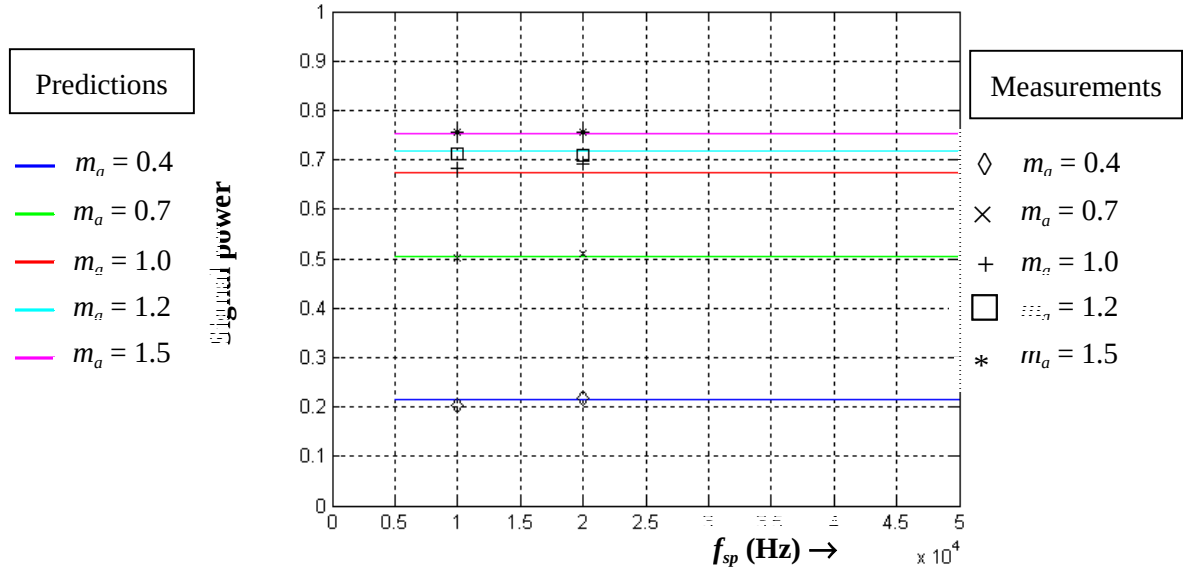

Fig. 8.32: Theoretical and measured signal power versus sampling frequency for standard five-level WRPWM scheme operating with N = 8.

Fig. 8.33 show the plots of signal power versus sampling frequency characteristic for the standard five-level WRPWM scheme N = 9. Measurements were taken at the sampling frequencies of f_{sp} = 10 kHz and 16 kHz.

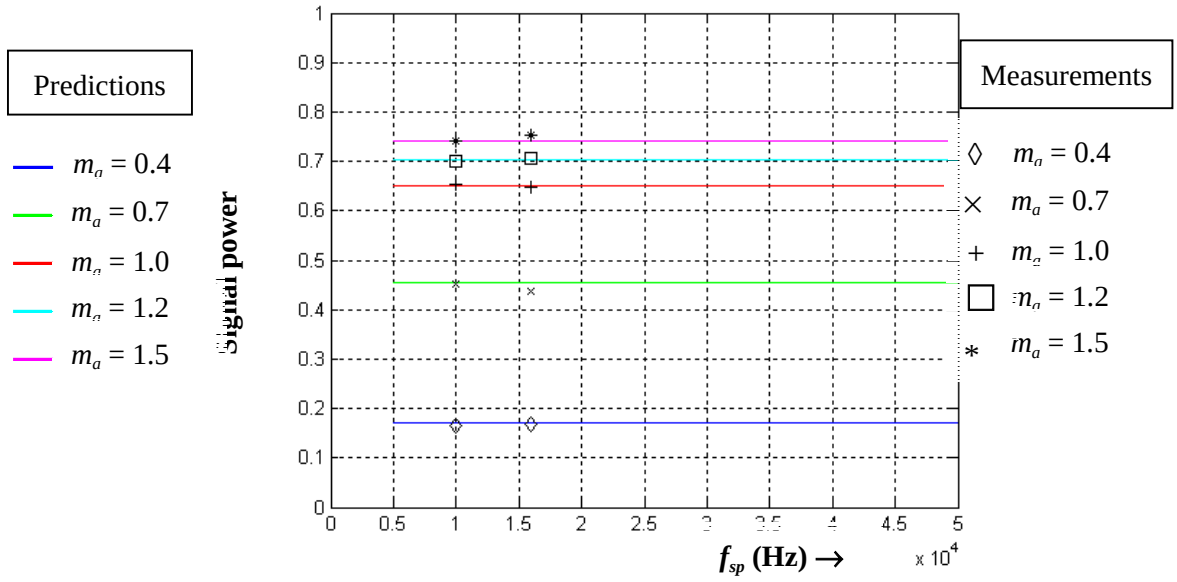

Fig. 8.33: Theoretical and measured signal power versus sampling frequency for standard five-level WRPWM scheme operating with N = 9.

8.1.2.2 Discrete Noise Power

The discrete noise power was also calculated by first squaring and then averaging the value of the two points from the harmonic components measurements (i.e. $(V_{h\max}{}^2 + V_{h\min}{}^2)/2$, where V_h is the amplitude of the harmonic component of voltage spectrum and h = 3, 4, 5 …).

Figs. 8.34 and 8.35 show the plots of discrete noise power versus sampling frequency characteristic for the standard five-level WRPWM scheme operating with N = 5 and 6, respectively. Measurements were taken at the sampling frequencies of f_{sp} = 10 kHz, 20 kHz and 25 kHz.

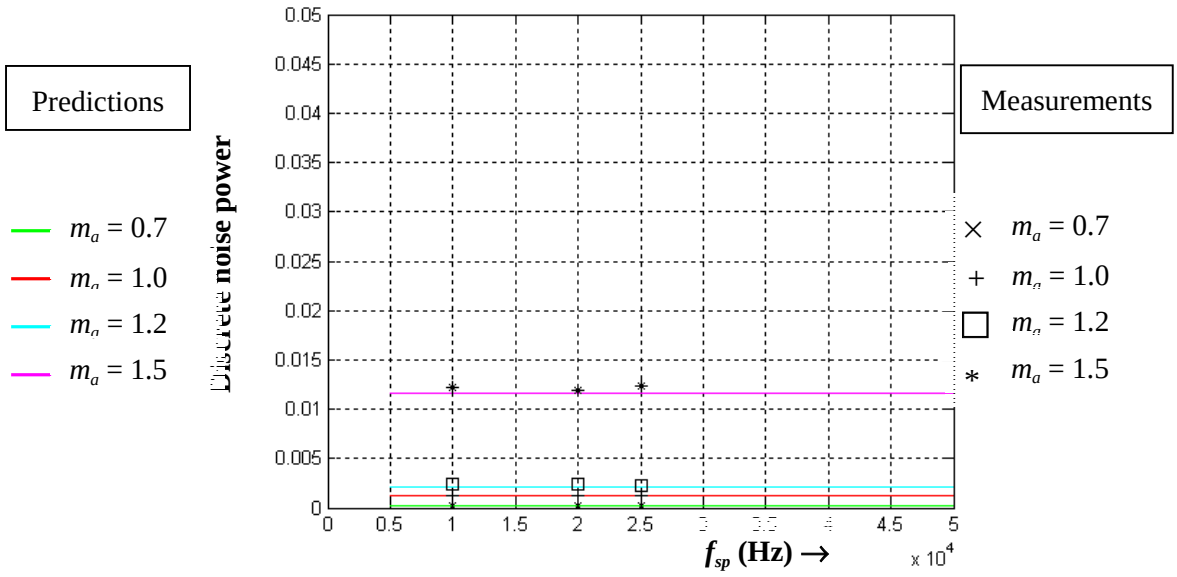

Fig. 8.34: Theoretical and measured discrete noise power versus sampling frequency for standard five-level WRPWM scheme operating with N = 6.

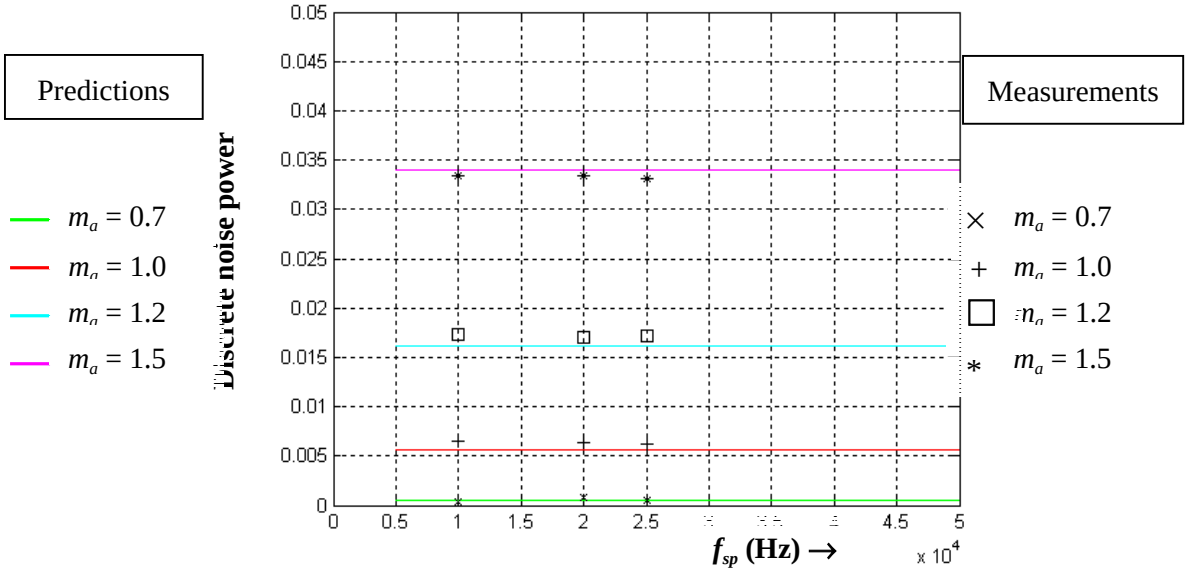

Fig. 8.35: Theoretical and measured discrete noise power versus sampling frequency for standard five-level WRPWM scheme operating with N = 6.

Figs. 8.36 and 8.37 show the plots of discrete noise power versus sampling frequency characteristic for the standard five-level WRPWM scheme N = 7 and 8. Measurements were taken at the sampling frequencies of f_{sp} = 10 kHz and 20 kHz.

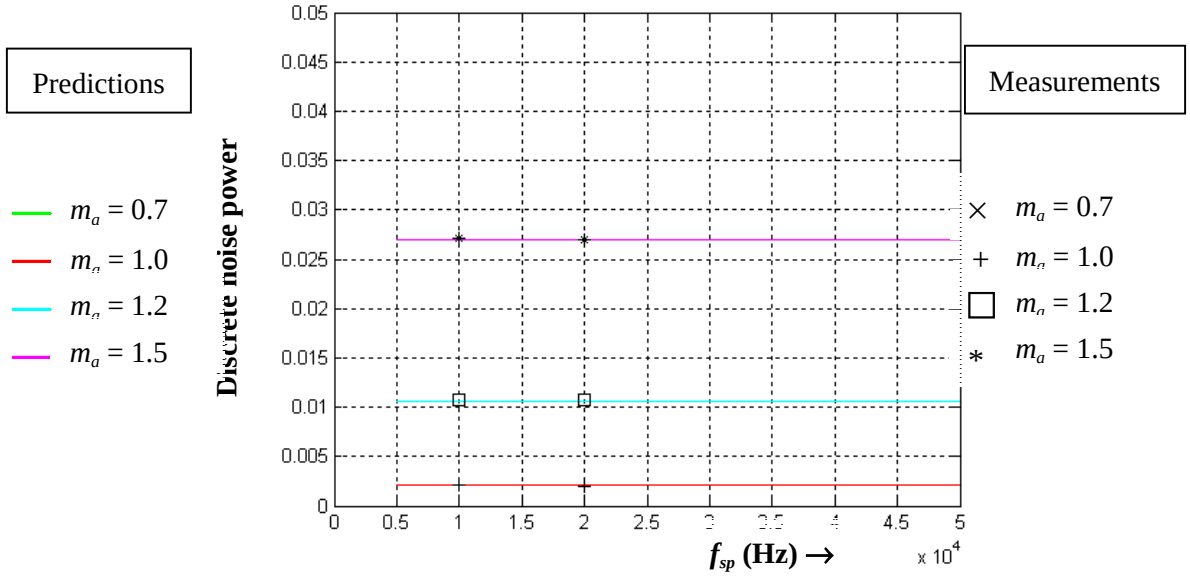

Fig. 8.36: Theoretical and measured discrete noise power versus sampling frequency for standard five-level WRPWM scheme operating with N = 7.

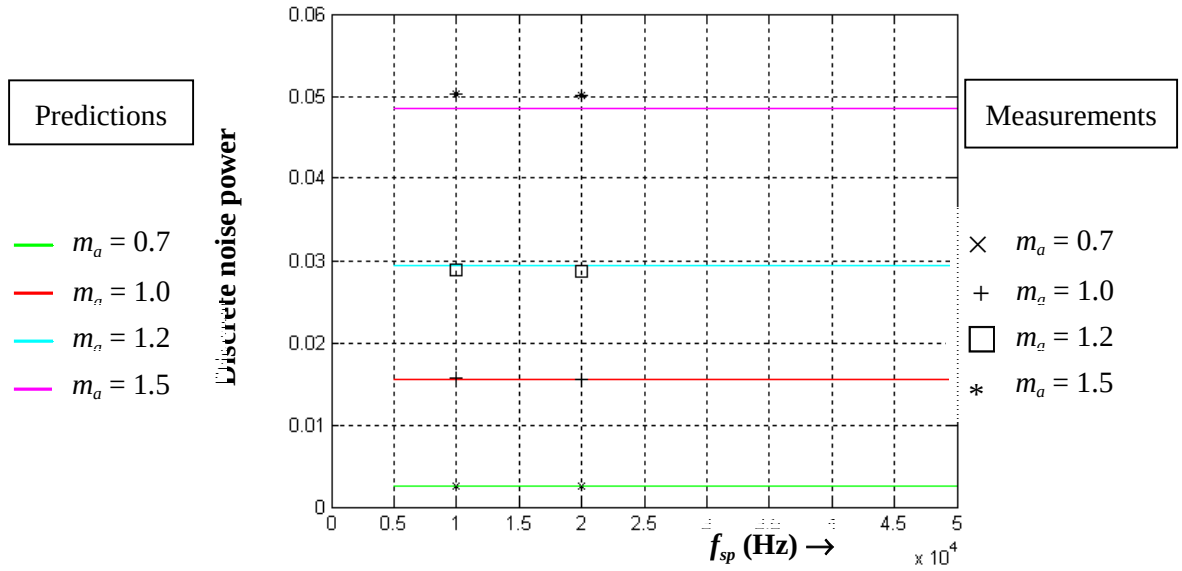

Fig. 8.37: Theoretical and measured discrete noise power versus sampling frequency for standard five-level WRPWM scheme operating with N = 8.

Fig. 8.38 show the plots of discrete noise power versus sampling frequency characteristic for the standard five-level WRPWM scheme N = 9. Measurements were taken at the sampling frequencies of f_{sp} = 10 kHz and 16 kHz.

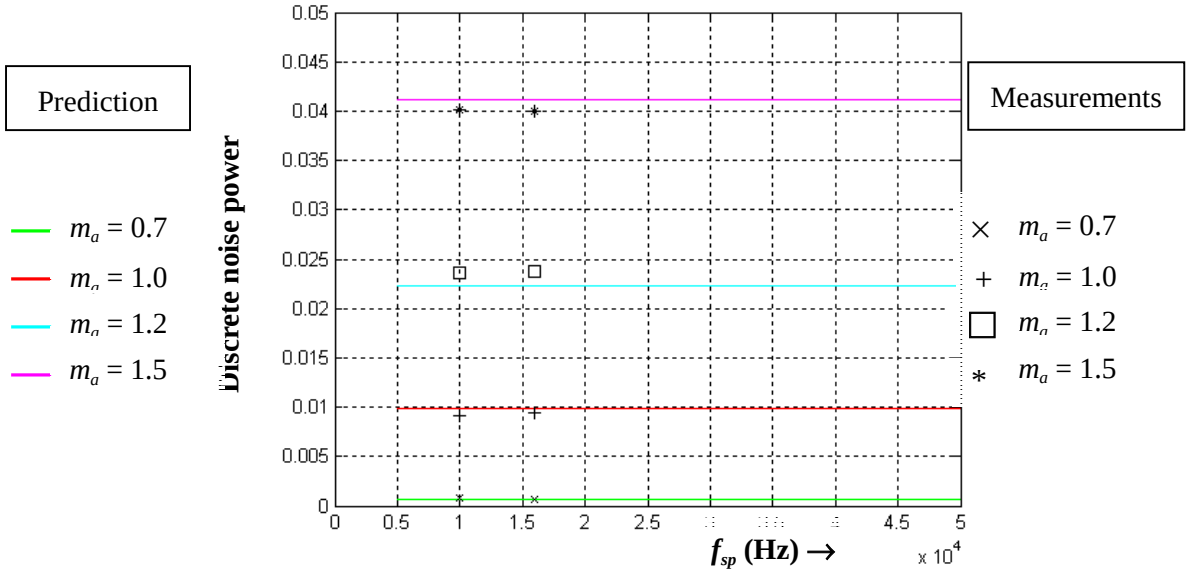

Fig. 8.38: Theoretical and measured discrete noise power versus sampling frequency for standard five-level WRPWM scheme operating with N = 9.

8.1.2.3 Continuous Noise Power

The measurements of continuous noise power were taken by averaging the value of power spectrum of the WRPWM waveform using the function provided in Tektronix TDS 220 oscilloscope in acquire mode. The data was then transferred to a PC using WaveStar. Microsoft Excel was then used to sum up after the fundamental and harmonics components were subtracted. The sum was averaged by dividing with number of data within 2000 Hz, and then integrated by multiplying with 2000.

Figs. 8.39 and 8.40 show the plots of continuous noise power versus sampling frequency characteristic for the standard five-level WRPWM scheme operating with N = 5 and 6, respectively. Measurements were taken at the sampling frequencies of f_{sp} = 10 kHz, 20 kHz and 25 kHz.

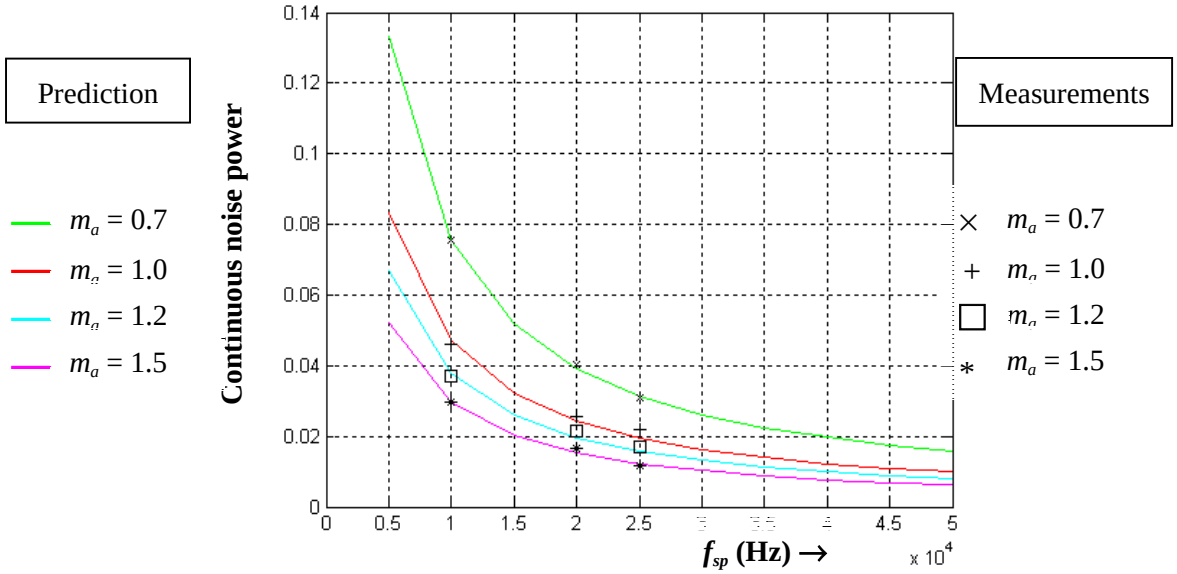

Fig. 8.39: Theoretical and measured continuous noise power versus sampling frequency for standard five-level WRPWM scheme operating with N = 5.

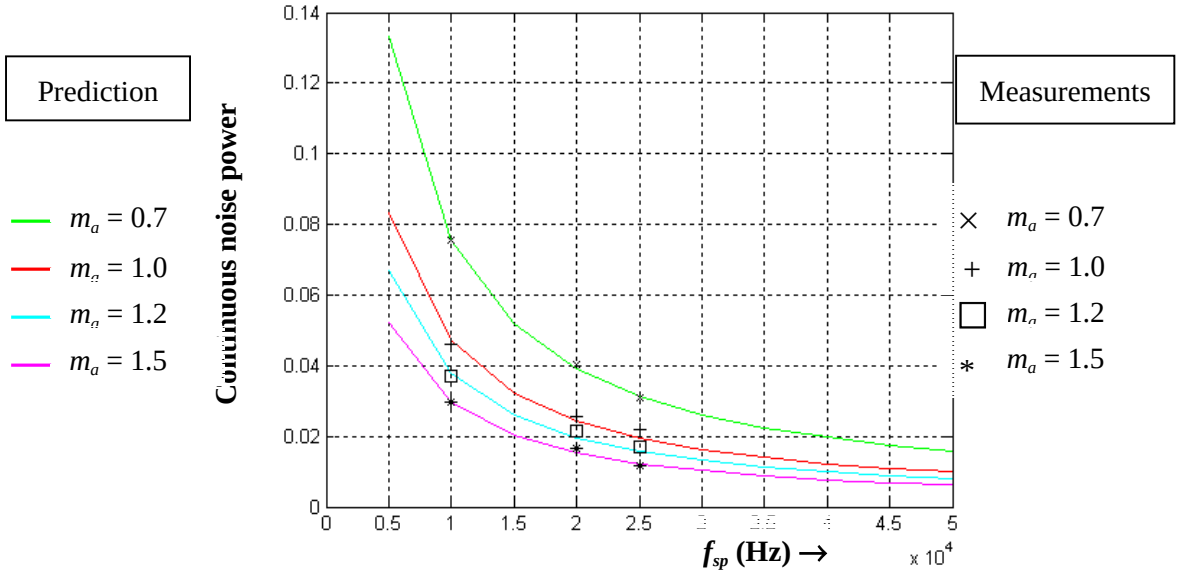

Fig. 8.40: Theoretical and measured continuous noise power versus sampling frequency for standard five-level WRPWM scheme operating with N = 6.

Figs. 8.41 and 8.42 show the plots of continuous noise power versus sampling frequency characteristic for the standard five-level WRPWM scheme N = 7 and 8. Measurements were taken at the sampling frequencies of f_{sp} at 10 kHz and 20 kHz.

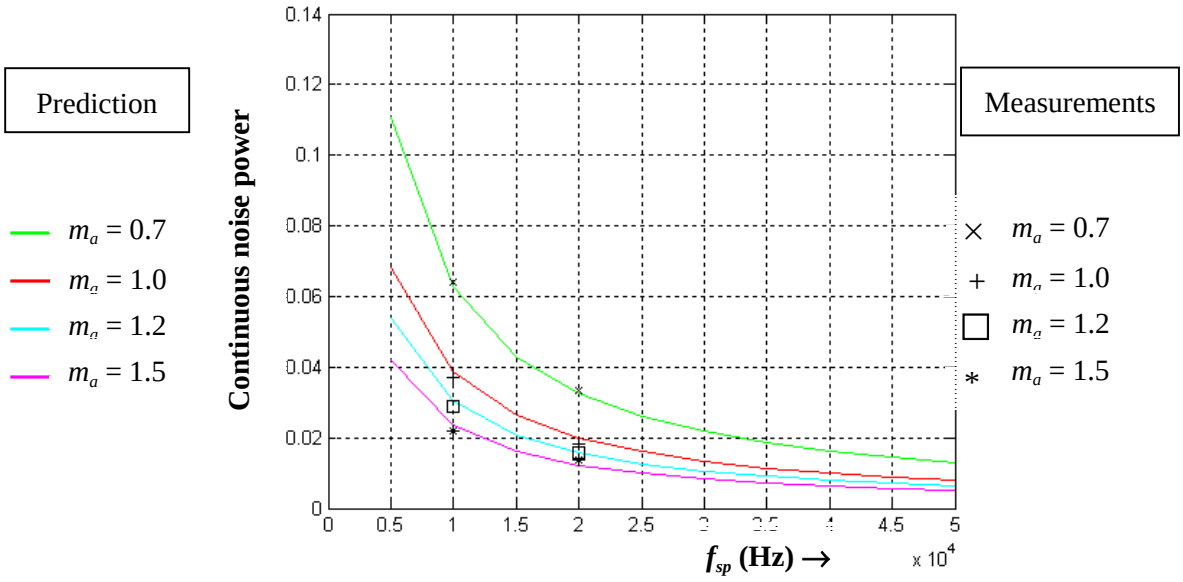

Fig. 8.41: Theoretical and measured continuous noise power versus sampling frequency for standard five-level WRPWM scheme operating with N = 7.

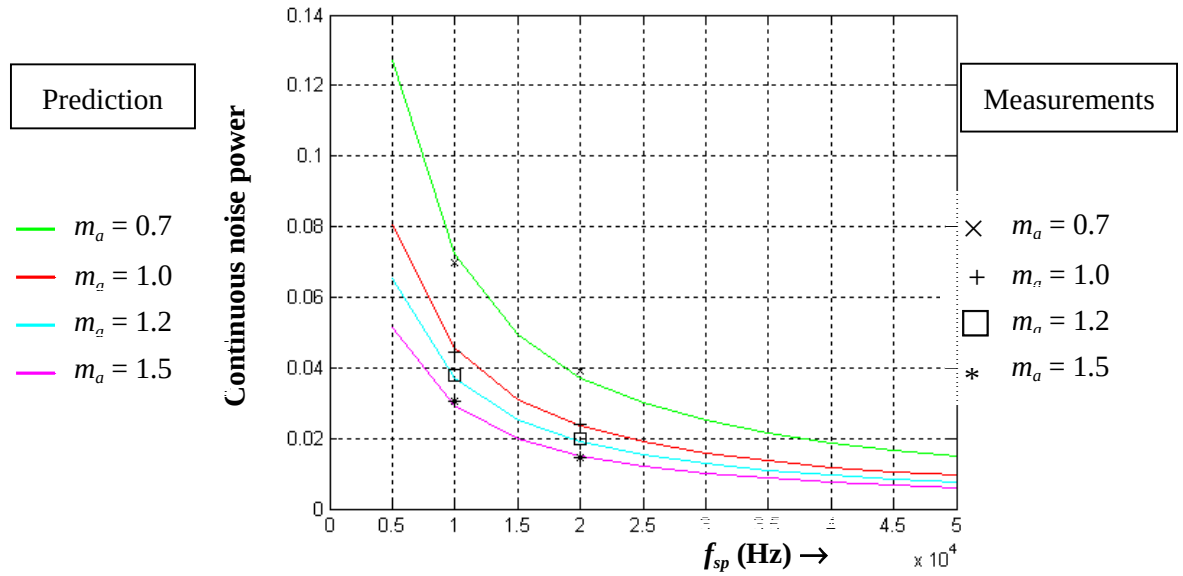

Fig. 8.42: Theoretical and measured continuous noise power versus sampling frequency for standard five-level WRPWM scheme operating with N = 8.

Fig. 8.43 show the plots of continuous noise power versus sampling frequency characteristic for the standard five-level WRPWM scheme N = 9. Measurements were taken at the sampling frequencies of f_{sp} = 10 kHz and 16 kHz.

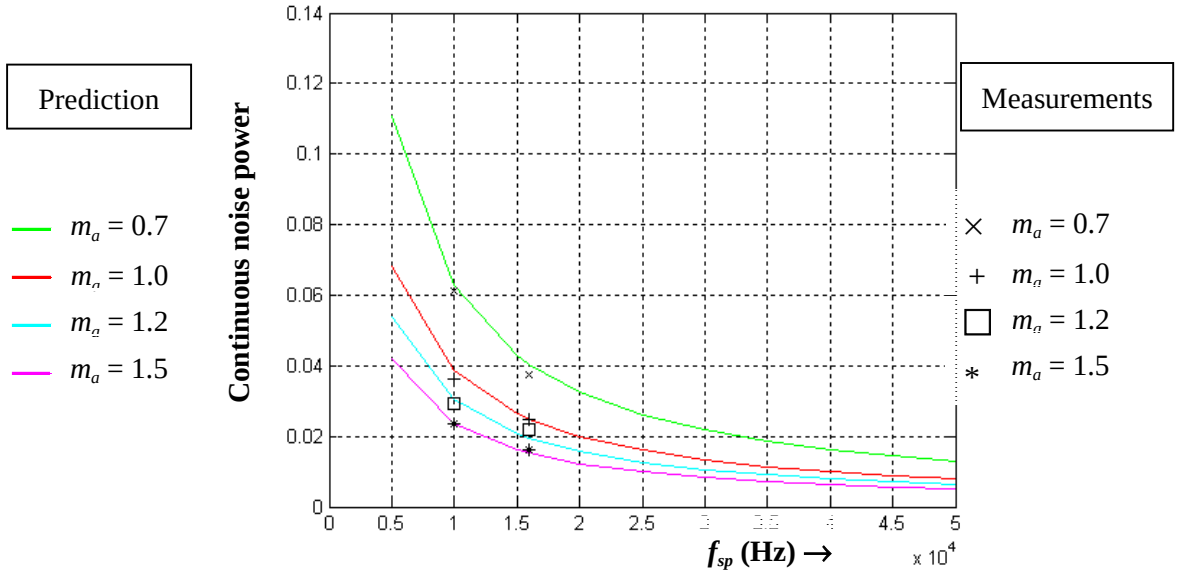

Fig. 8.43: Theoretical and measured continuous noise power versus sampling frequency for standard five-level WRPWM scheme operating with N = 9.

8.2 Modified Five-Level WRPWM

Figs. 8.44 to 8.45 show the output voltage waveform of the five-level WRPWM scheme operating with N = 8, q = 3 and a = 0; N = 8, q = 4 and a = 2 and modulation indices m_a = 0.4, 1.0 and 1.5 respectively. These are used to illustrate the effects of combinations q and a and modulation index on switching decisions of modified five-level WRPWM output voltage waveform. It is clear that as the values of q and a increase, the probability of the outer levels of the dc-bus voltage (i.e. the first and the fifth levels) being connected to the output terminals of the inverter in any one fundamental cycle decreases. On the other hand, the probability of the third level of the dc-bus voltage being connected to the output terminal of the inverter within one fundamental cycle increases.

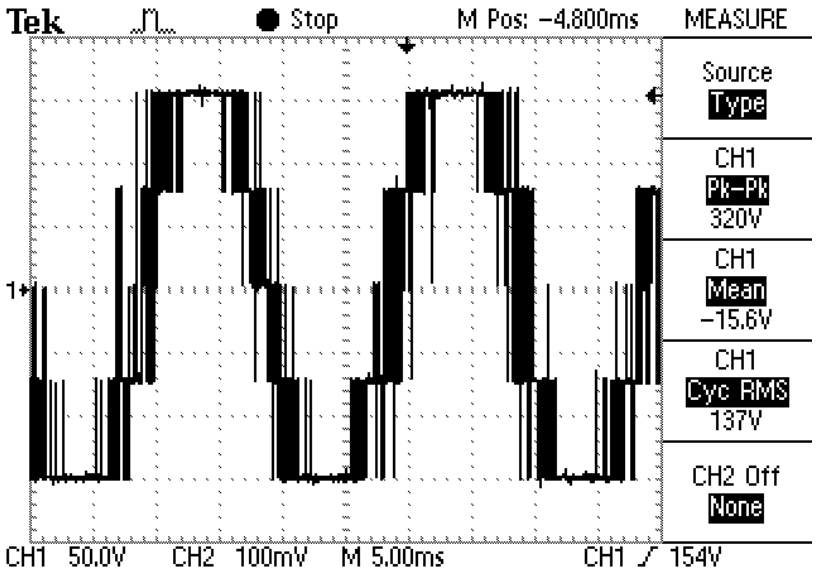

Fig. 8.44: Output waveform of modified five-level WRPWM operating with N = 8, q = 3 and a = 0 at m_a = 1.0.

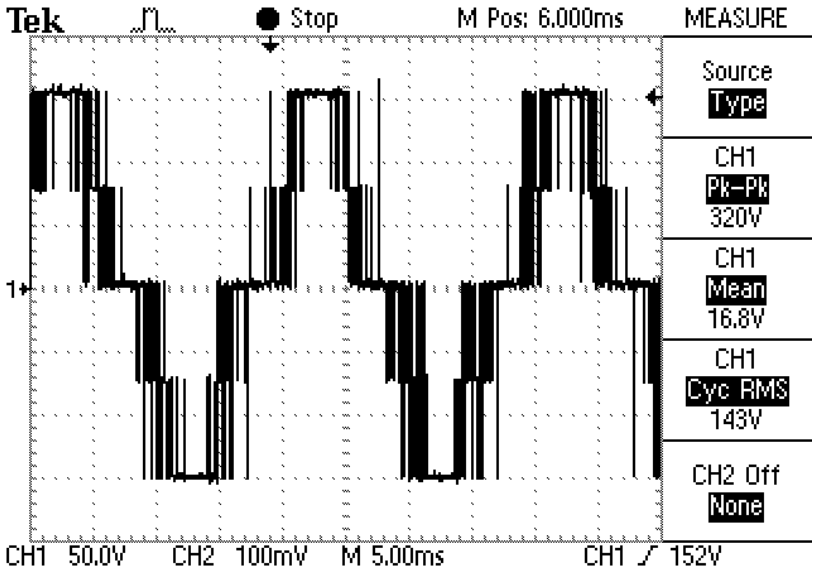

Fig. 8.45: Output waveform of modified five-level WRPWM operating with N = 8, q = 4 and a = 2 at m_a = 1.0.

Figs. 8.46 to 8.47 show the power spectrum of the five-level WRPWM scheme operating with N = 8 for combinations of q = 3 a = 0 and q = 4 a = *2* and modulation index m_a = 1.0 respectively. These are used to illustrate the effects of sampling frequency, combinations of q and a and modulation index on the power spectrum of the modified five-level WRPWM. It is clear that as the values of q and a increase, the magnitude of fundamental component decreases.

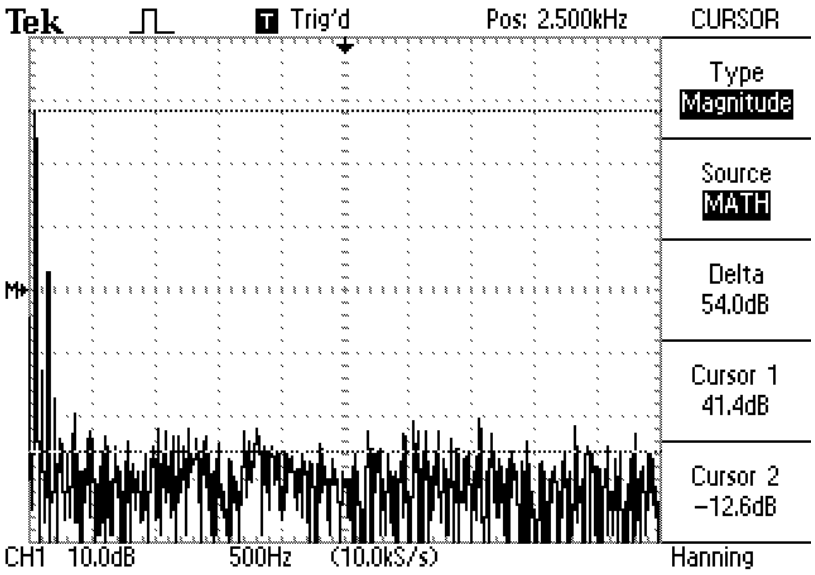

Fig. 8.46: Power spectrum of modified five-level WRPWM output waveform operating with N = 8, q = 3 and a = 0 at m_a = 1.0.

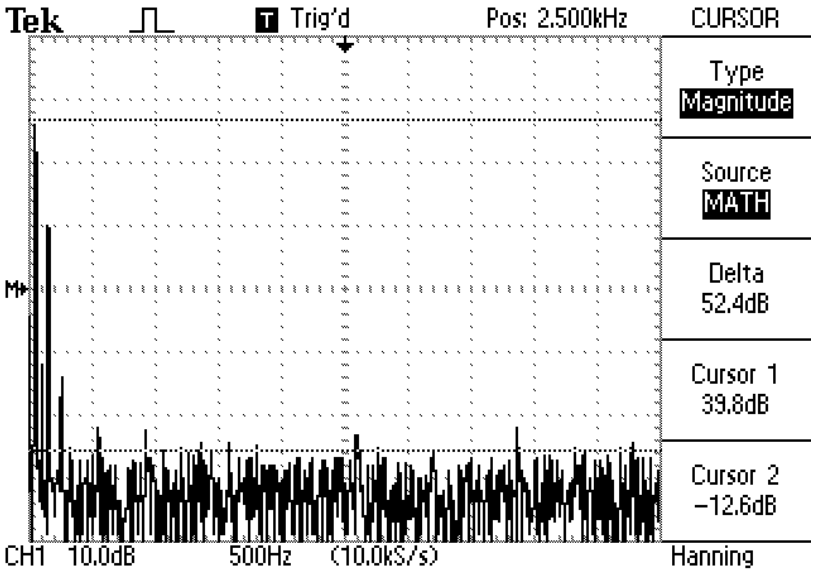

Fig. 8.47: Power spectrum of modified five-level WRPWM output waveform operating with N = 8, q = 4 and a = 2 at m_a = 1.0.

8.2.1 Fundamental and Harmonic Components Measurements for Modified Five-Level WRPWM Scheme

In this section, plots of measured fundamental and harmonic components versus modulation index are presented.

The measurements were taken by approximating the range of amplitude of the fundamental and harmonic components generated most frequently and the range is shown with two points. Due to the magnitude of certain order of harmonics being lower than the magnitude of the continuous noise. However, the measurements included are adequate to validate the theoretical predictions.

8.2.1.1 Modified Five-level WRPWM Operating with $N = 6$ and Combination $q = 3$ $a = 0$

The plot of measured fundamental component versus modulation index is shown in Fig. 8.48. The plots of third, fifth and seventh harmonic components versus modulation index are shown in Figs. 8.49, 8.50 and 8.51, respectively. From Figs. 8.48 to 8.51, it can be seen that the measurements are in good agreement with predictions.

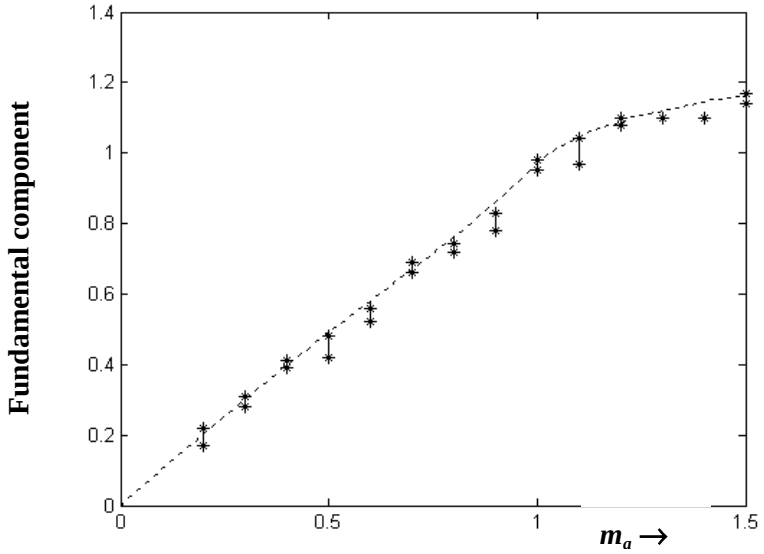

Fig. 8.48: Theoretical and measured fundamental component versus modulation index for modified five-level WRPWM scheme operating with $N = 6$, $q = 3$ and $a = 0$.

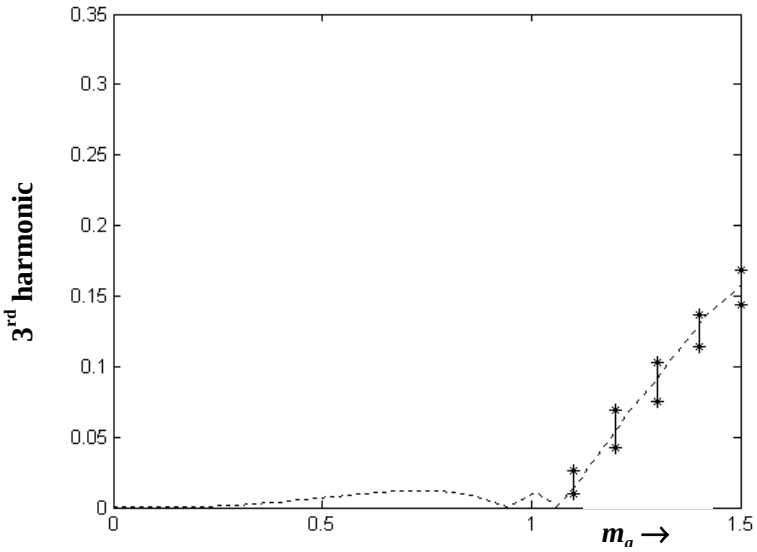

Fig. 8.49: Theoretical and measured third harmonic component versus modulation index for modified five-level WRPWM scheme operating with N = 6, q = 3 and a = 0.

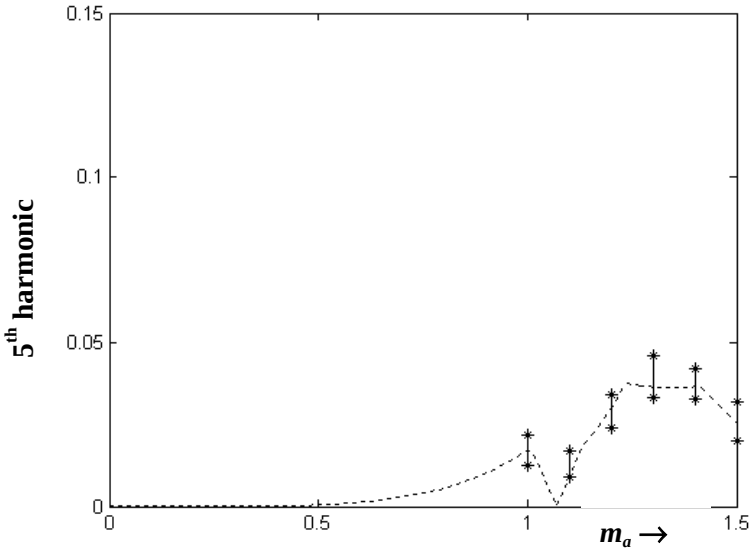

Fig. 8.50: Theoretical and measured fifth harmonic component versus modulation index for modified five-level WRPWM scheme operating with N = 6, q = 3 and a = 0.

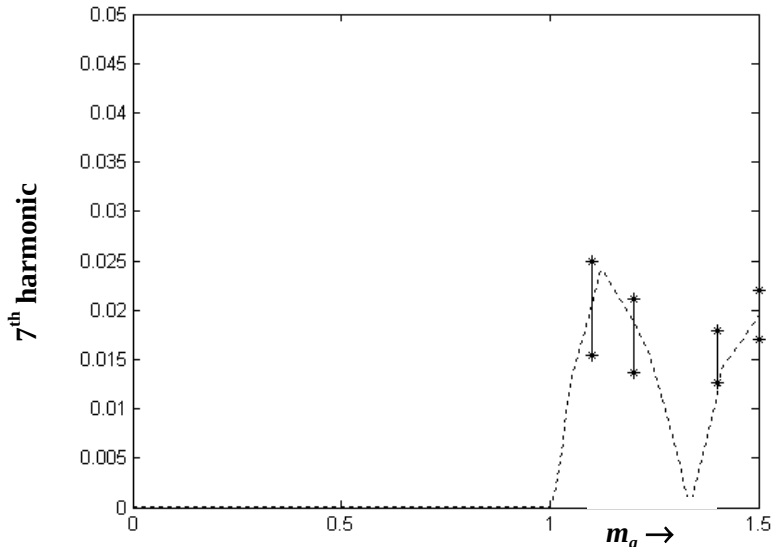

Fig. 8.51: Theoretical and measured seventh harmonic component versus modulation index for modified five-level WRPWM scheme operating with N = 6, q = 3 and a = 0.

8.2.1.2 Modified Five-Level WRPWM Operating with N = 6 and Combination q = 3 a = 1

The plot of measured fundamental component versus modulation index is shown in Fig. 8.52. The plots of third, fifth and seventh harmonic components versus modulation index are shown in Figs. 8.53, 8.54 and 8.55, respectively. From Figs. 8.52 to 8.55, it can be seen that the measurements are in good agreement with predictions.

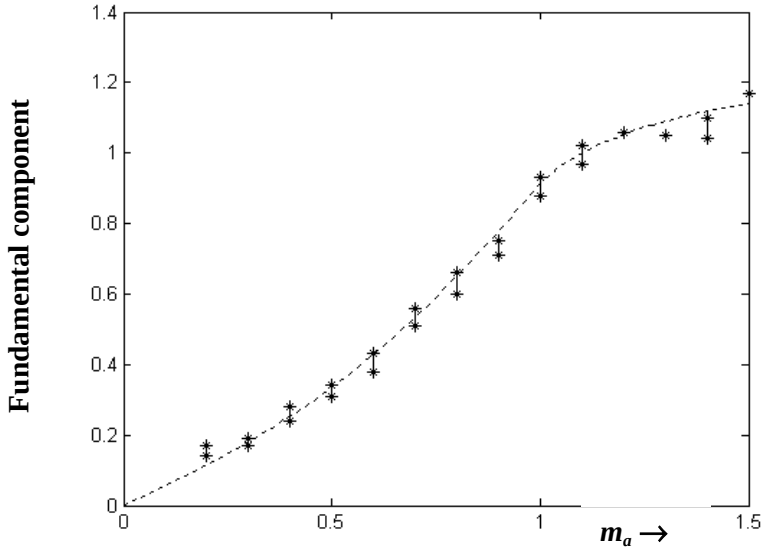

Fig. 8.52: Theoretical and measured fundamental component versus modulation index for modified five-level WRPWM scheme operating with N = 6, q = 3 and a = 1.

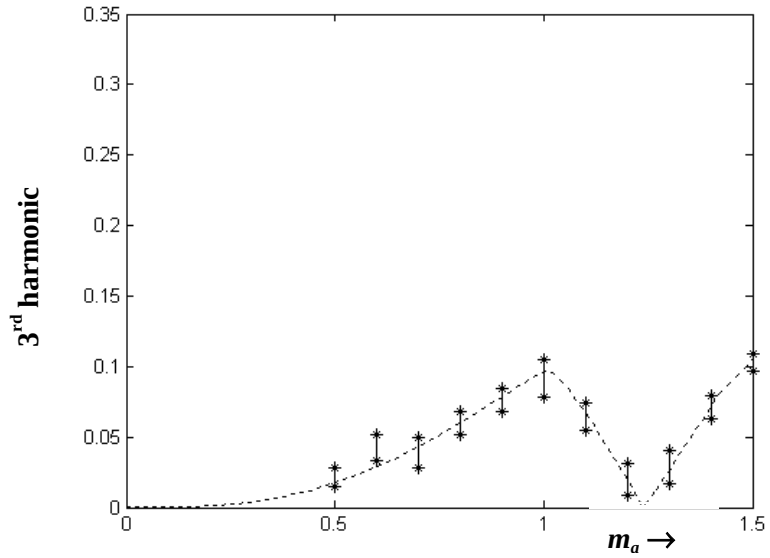

Fig. 8.53: Theoretical and measured third harmonic component versus modulation index for modified five-level WRPWM scheme operating with N = 6, q = 3 and a = 1.

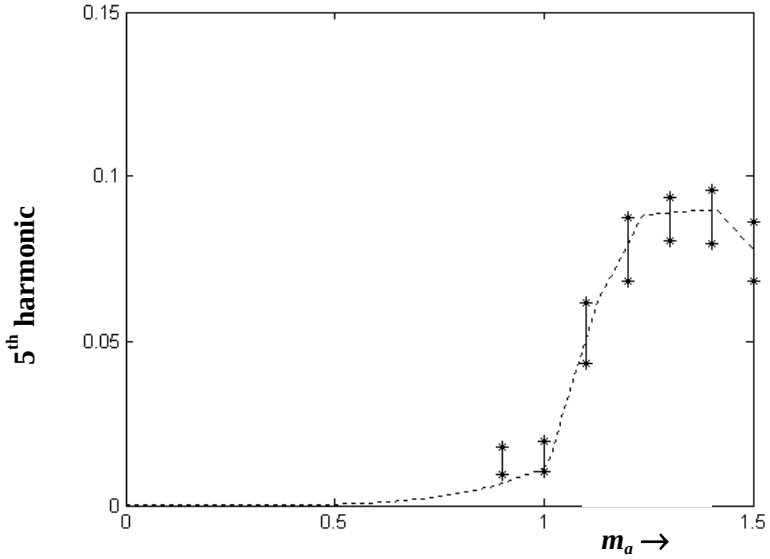

Fig. 8.54: Theoretical and measured fifth harmonic component versus modulation index for modified five-level WRPWM scheme operating with N = 6, q = 3 and a = 1.

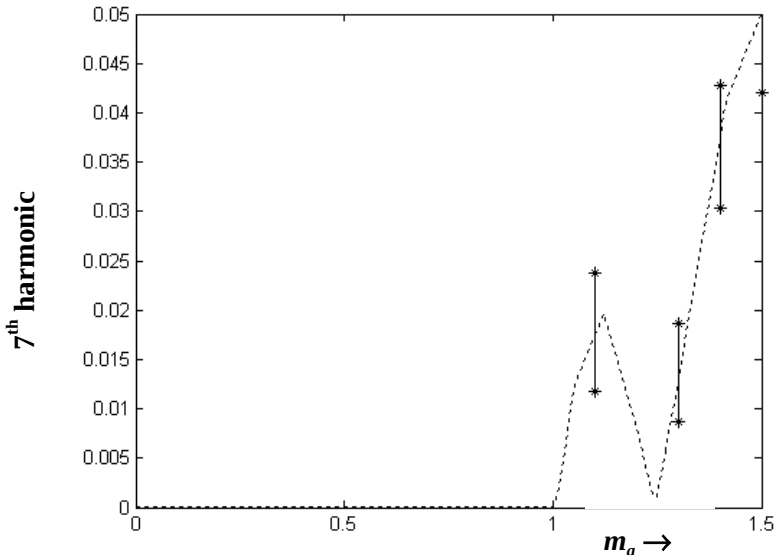

Fig. 8.55: Theoretical and measured seventh harmonic component versus modulation index for modified five-level WRPWM scheme operating with N = 6, q = 3 and a = 1.

8.2.1.3 Modified Five-Level WRPWM Operating with N = 7 and Combination q = 3 a = 0

The plot of measured fundamental component versus modulation index is shown in Fig. 8.56. The plots of third, fifth and seventh harmonic components versus modulation index are shown in Figs. 8.57, 8.58 and 8.59, respectively. From Figs. 8.56 to 8.59, it can be seen that the measurements are in good agreement with predictions.

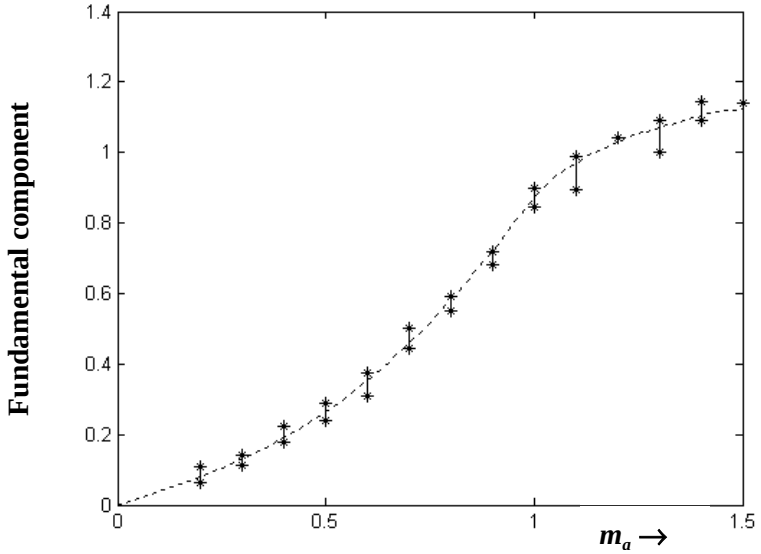

Fig. 8.56: Theoretical and measured fundamental component versus modulation index for modified five-level WRPWM scheme operating with N = 7, q = 3 and a = 0.

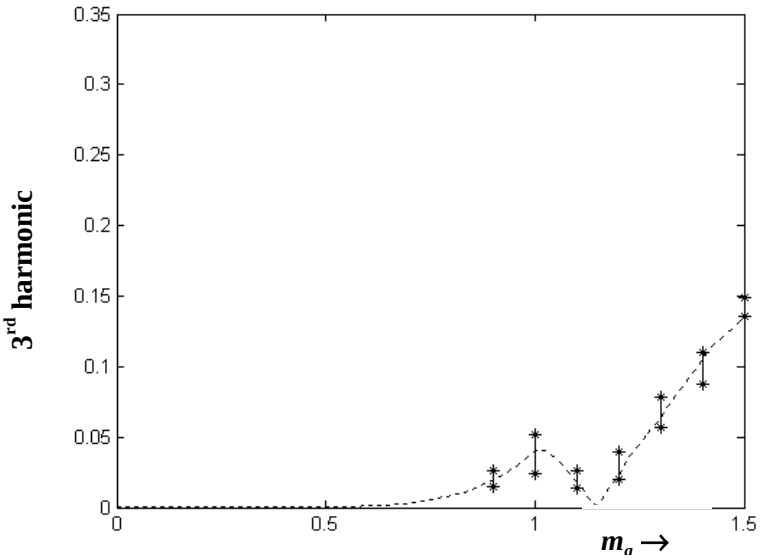

Fig. 8.57: Theoretical and measured third harmonic component versus modulation index for modified five-level WRPWM scheme operating with N = 7, q = 3 and a = 0.

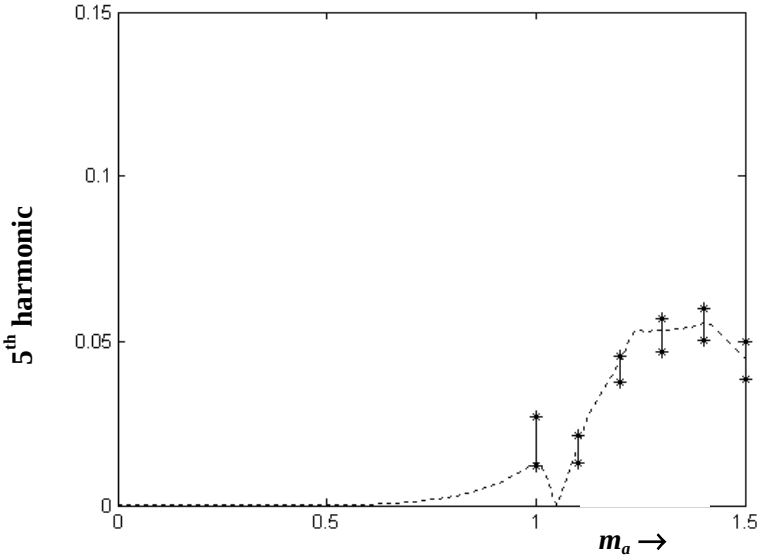

Fig. 8.58: Theoretical and measured fifth harmonic component versus modulation index for modified five-level WRPWM scheme operating with N = 7, q = 3 and a = 0.

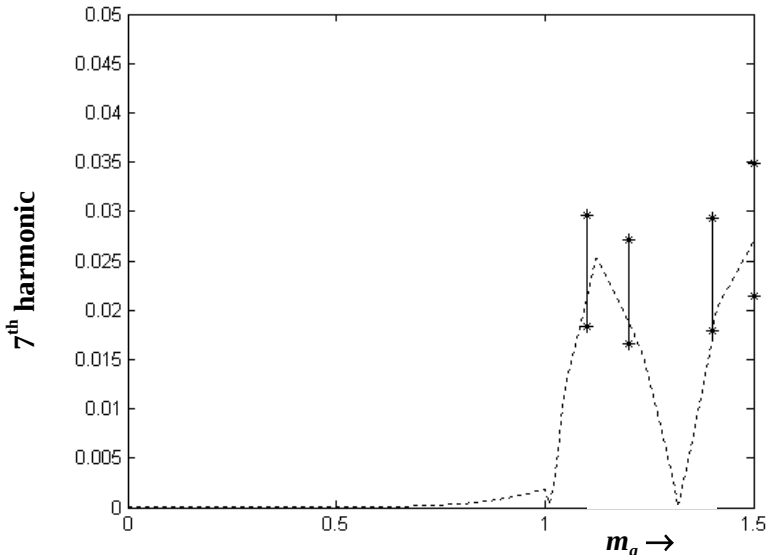

Fig. 8.59: Theoretical and measured seventh harmonic component versus modulation index for modified five-level WRPWM scheme operating with N = 7, q = 3 and a = 0.

8.2.1.4 Modified Five-Level WRPWM Operating with N = 7 and Combination q = 3 a = 1

The plot of measured fundamental component versus modulation index is shown in Fig. 8.60. The plots of third, fifth and seventh harmonic components versus modulation index are shown in Figs. 8.61, 8.62 and 8.63, respectively. From Figs. 8.60 to 8.63, it can be seen that the measurements are in good agreement with predictions.

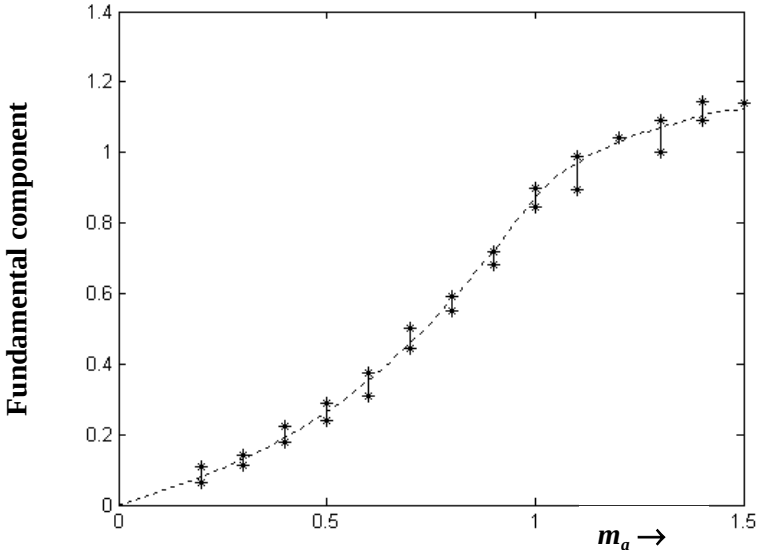

Fig. 8.60: Theoretical and measured fundamental component versus modulation index for modified five-level WRPWM scheme operating with N = 7, q = 3 and a = 1.

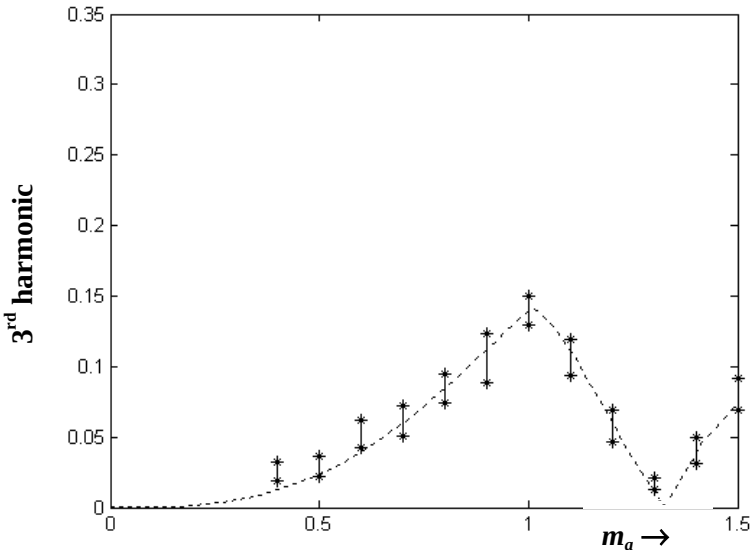

Fig. 8.61: Theoretical and measured third harmonic component versus modulation index for modified five-level WRPWM scheme operating with N = 7, q = 3 and a = 1.

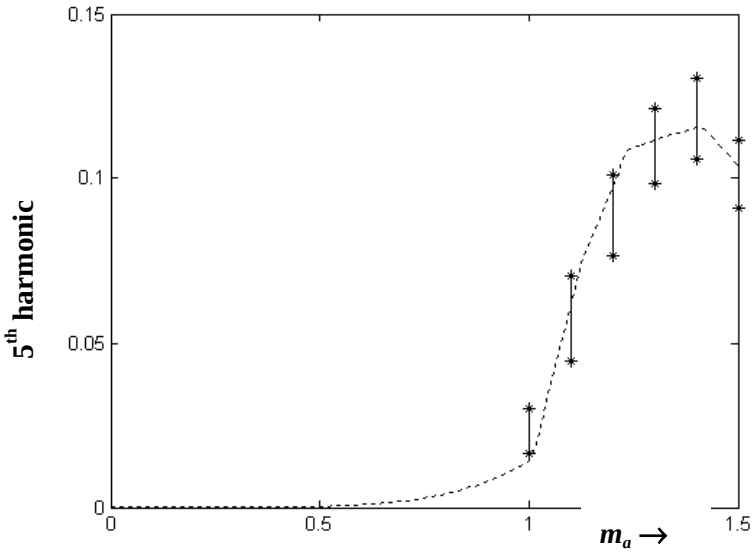

Fig. 8.62: Theoretical and measured fifth harmonic component versus modulation index for modified five-level WRPWM scheme operating with N = 7, q = 3 and a = 1.

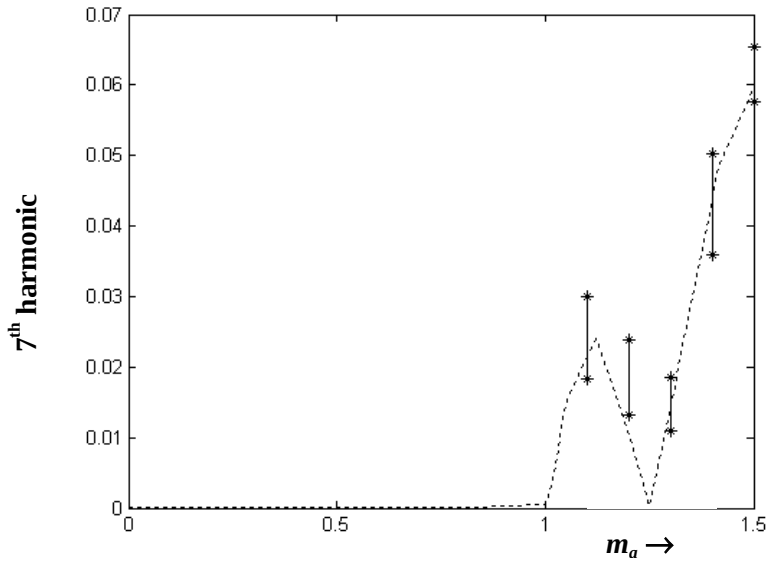

Fig. 8.63: Theoretical and measured seventh harmonic component versus modulation index for modified five-level WRPWM scheme operating with N = 7, q = 3 and a = 1.

8.2.1.5 Modified Five-Level WRPWM Operating with N = 8 and Combination q = 3 a = 0

The plot of measured fundamental component versus modulation index is shown in Fig. 8.64. The plots of third and fifth harmonic components versus modulation index are shown in Figs. 8.65 and 8.66, respectively. From Figs. 8.64 to 8.66, it can be seen that the measurements are in good agreement with predictions.

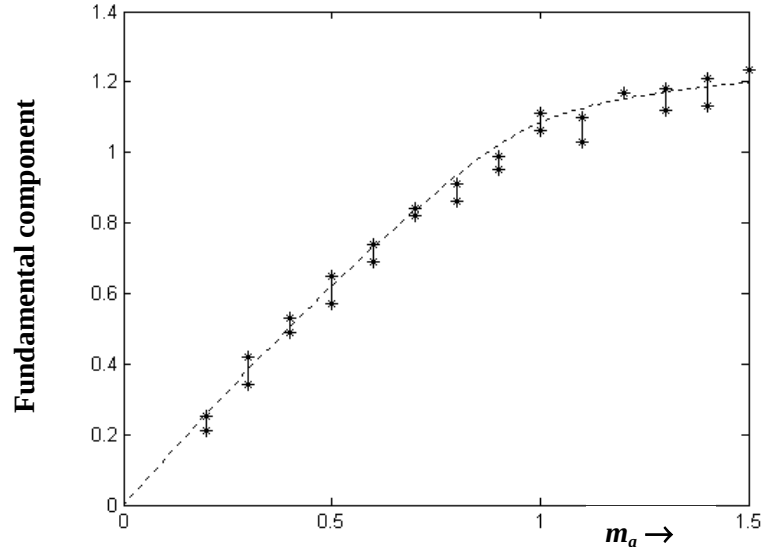

Fig. 8.64: Theoretical and measured fundamental component versus modulation index for modified five-level WRPWM scheme operating with N = 8, q = 3 and a = 0.

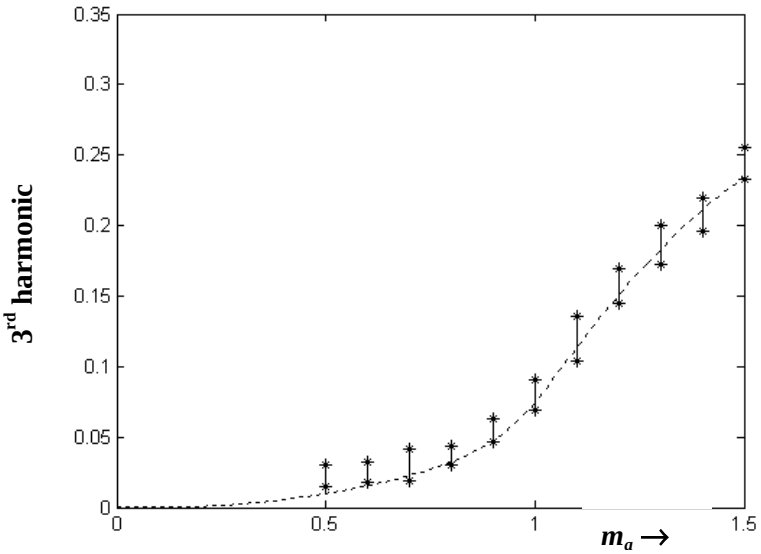

Fig. 8.65: Theoretical and measured third component versus modulation index for modified five-level WRPWM scheme operating with N = 8, q = 3 and a = 0.

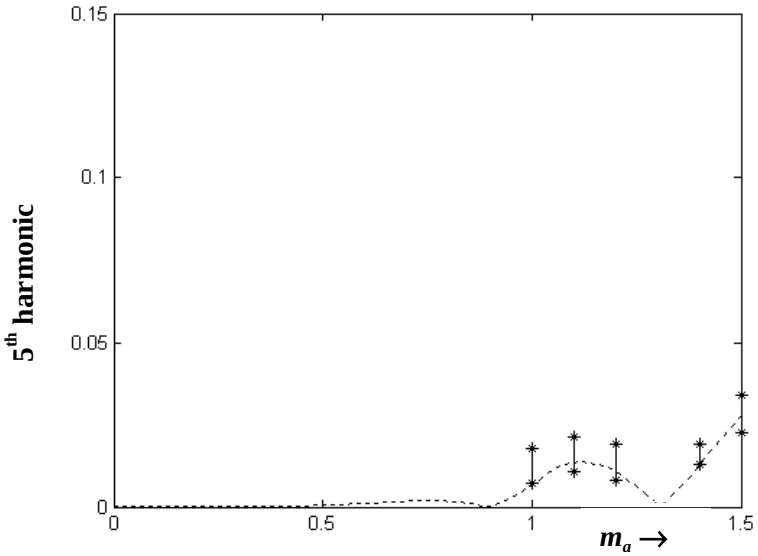

Fig. 8.66: Theoretical and measured fifth component versus modulation index for modified five-level WRPWM scheme operating with N = 8, q = 3 and a = 0.

8.2.1.6 Modified Five-Level WRPWM Operating with N = 8 and Combination q = 4 a = 0

The plot of measured fundamental component versus modulation index is shown in Fig. 8.67. The plots of third, fifth, seventh and ninth harmonic components versus modulation index are shown in Figs. 8.68, 8.69, 8.70 and 8.71, respectively. From Figs. 8.67 to 8.71, it can be seen that the measurements are in good agreement with predictions.

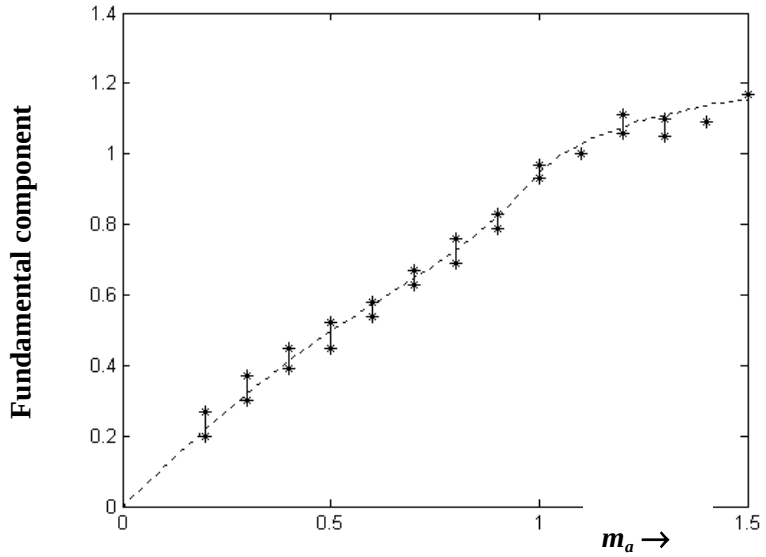

Fig. 8.67: Theoretical and measured fundamental component versus modulation index for modified five-level WRPWM scheme operating with N = 8, q = 4 and a = 0.

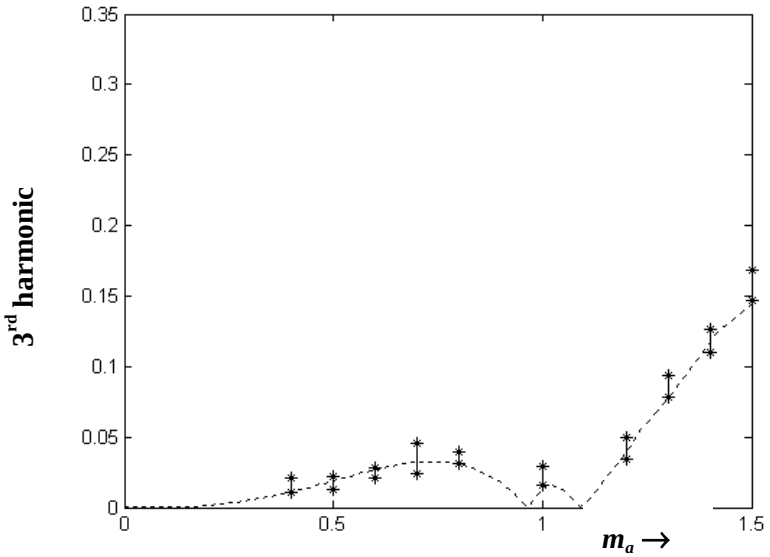

Fig. 8.68: Theoretical and measured third harmonic component versus modulation index for modified five-level WRPWM scheme operating with N = 8, q = 4 and a = 0.

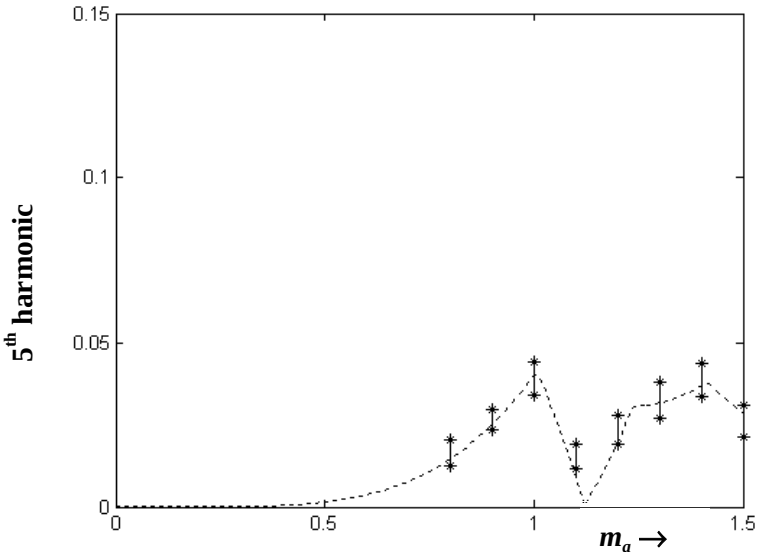

Fig. 8.69: Theoretical and measured fifth harmonic component versus modulation index for modified five-level WRPWM scheme operating with N = 8, q = 4 and a = 0.

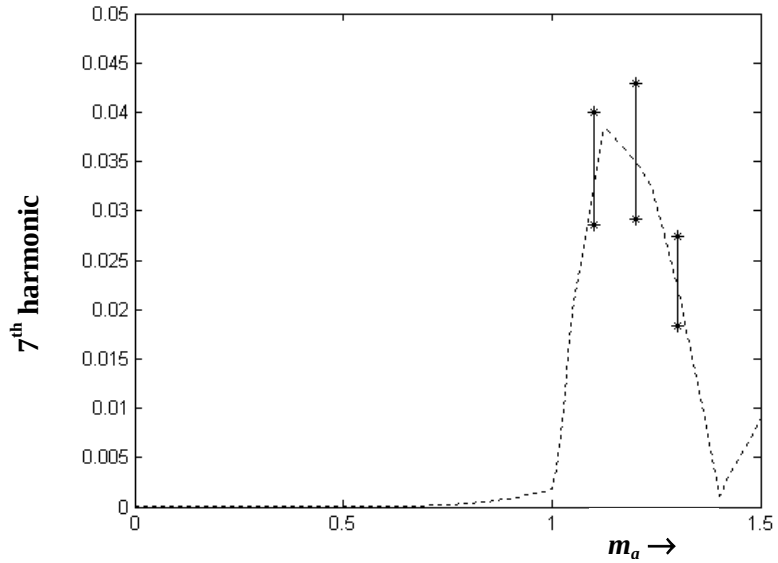

Fig. 8.70: Theoretical and measured seventh harmonic component versus modulation index for modified five-level WRPWM scheme operating with N = 8, q = 4 and a = 0.

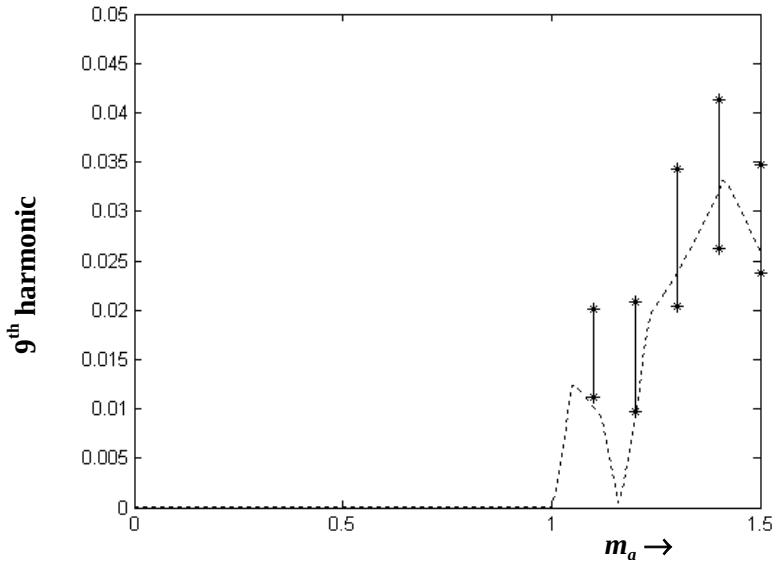

Fig. 8.71: Theoretical and measured ninth harmonic component versus modulation index for modified five-level WRPWM scheme operating with N = 8, q = 4 and a = 0.

8.2.1.7 Modified Five-Level WRPWM Operating with N = 8 and Combination q = 4 a = 1

The plot of measured fundamental component versus modulation index is shown in Fig. 8.72. The plots of third, fifth, seventh and ninth harmonic components versus modulation index are shown in Figs. 8.73, 8.69, 8.70 and 8.71, respectively. From Figs. 8.67 to 8.71, it can be seen that the measurements are in good agreement with predictions.

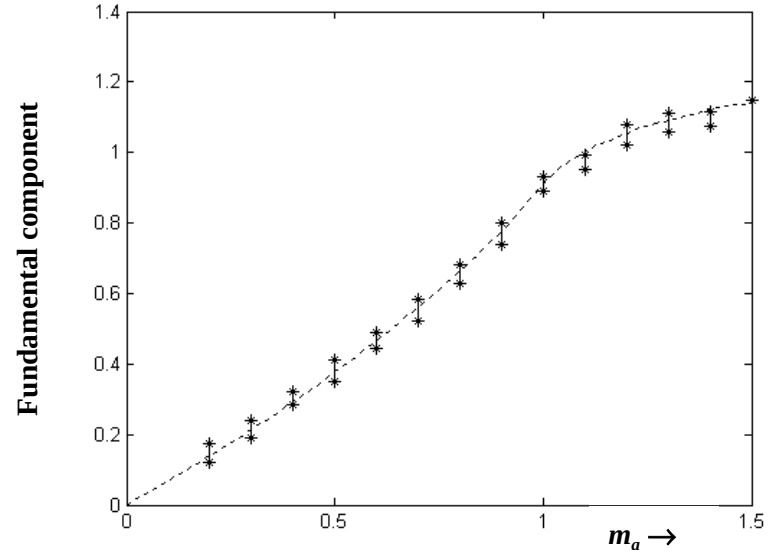

Fig. 8.72: Theoretical and measured fundamental component versus modulation index for modified five-level WRPWM scheme operating with N = 8, q = 4 and a = 1.

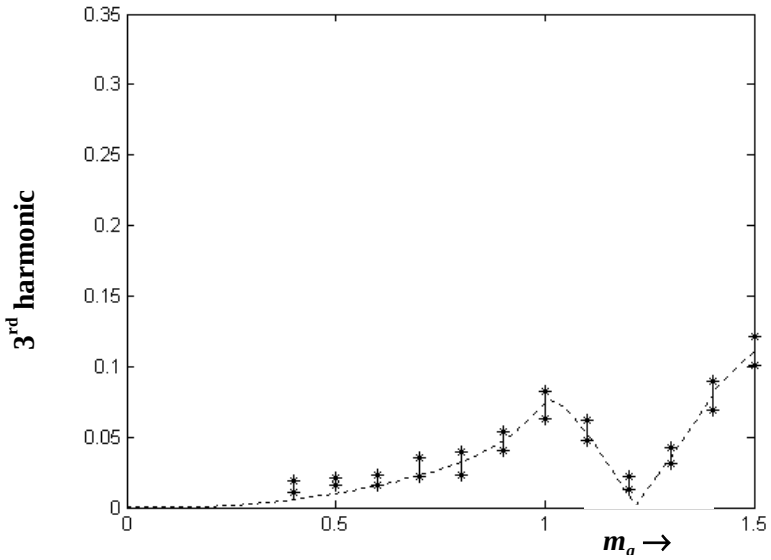

Fig. 8.73: Theoretical and measured third harmonic component versus modulation index for modified five-level WRPWM scheme operating with N = 8, q = 4 and a = 1.

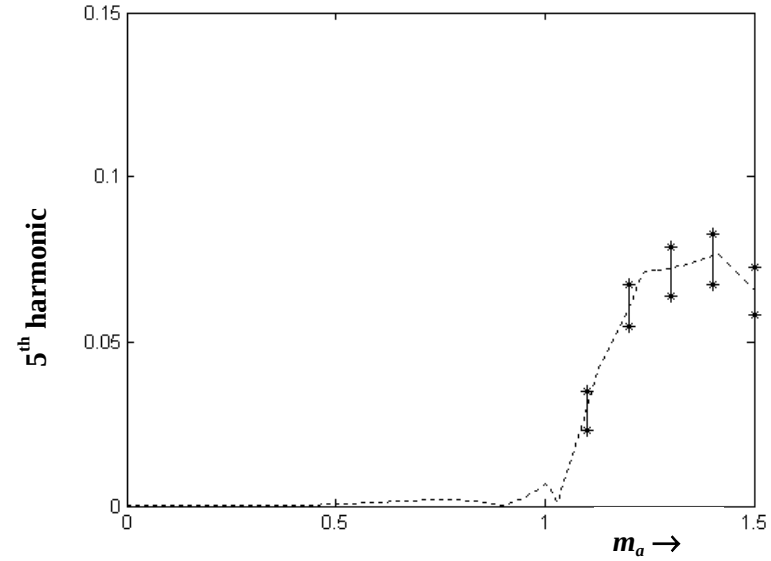

Fig. 8.74: Theoretical and measured fifth harmonic component versus modulation index for modified five-level WRPWM scheme operating with N = 8, q = 4 and a = 1.

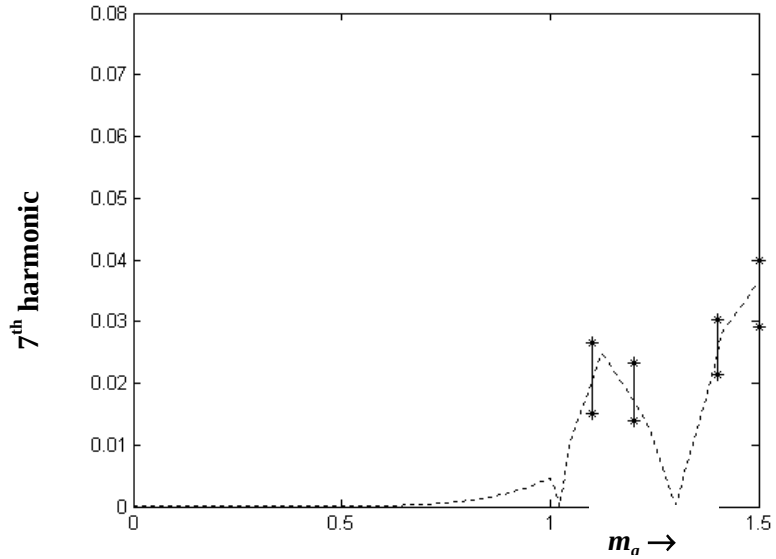

Fig. 8.75: Theoretical and measured seventh harmonic component versus modulation index for modified five-level WRPWM scheme operating with N = 8, q = 4 and a = 1.

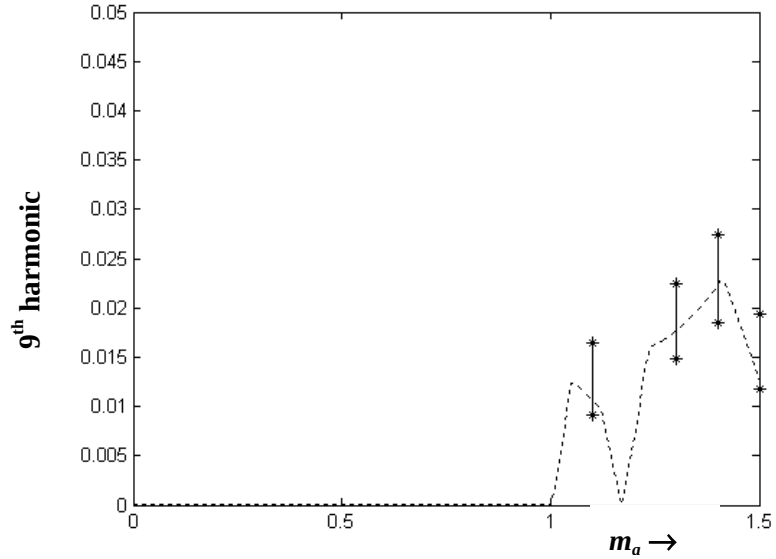

Fig. 8.76: Theoretical and measured ninth harmonic component versus modulation index for modified five-level WRPWM scheme operating with N = 8, q = 4 and a = 1.

8.2.1.8 Modified Five-level WRPWM Operating with N = 8 and Combination q = 4 a = 2

The plot of measured fundamental component versus modulation index is shown in Fig. 8.77. The plots of third, fifth, seventh, ninth and eleventh harmonic components versus modulation index are shown in Figs. 8.78, 8.79, 8.80, 8.81 and 8.82, respectively. From Figs. 8.77 to 8.82, it can be seen that the measurements are in good agreement with predictions.

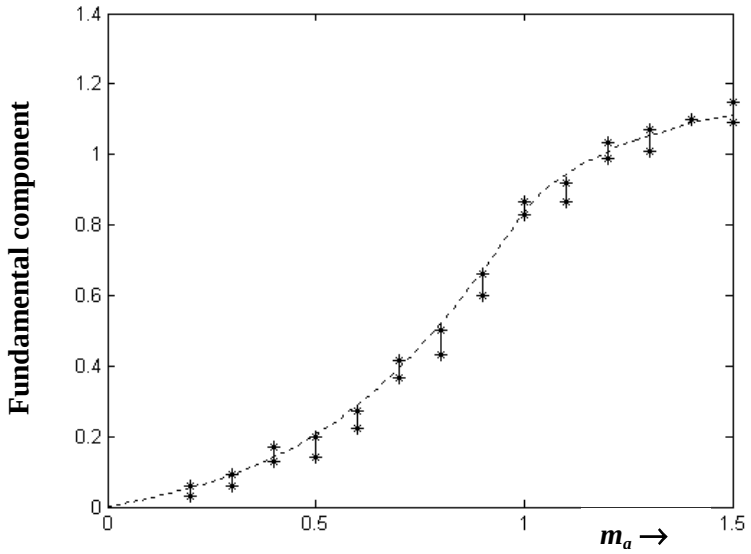

Fig. 8.77: Theoretical and measured fundamental component versus modulation index for modified five-level WRPWM scheme operating with N = 8, q = 4 and a = 2.

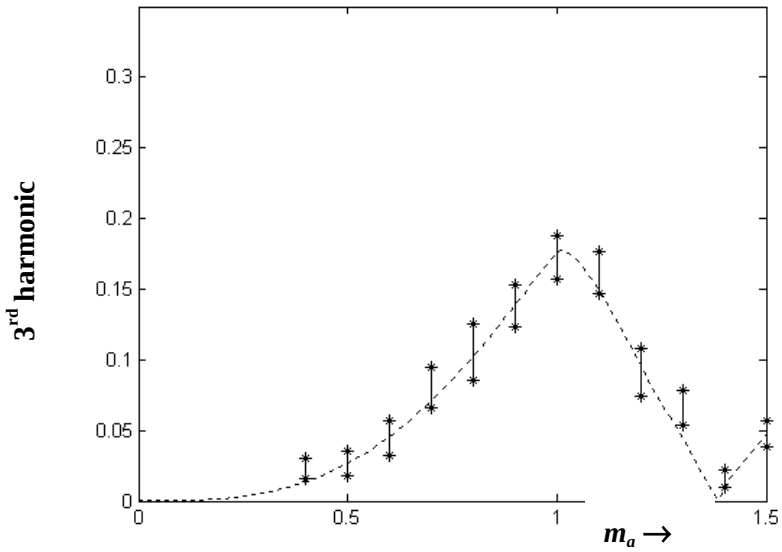

Fig. 8.78: Theoretical and measured third harmonic component versus modulation index for modified five-level WRPWM scheme operating with N = 8, q = 4 and a = 2.

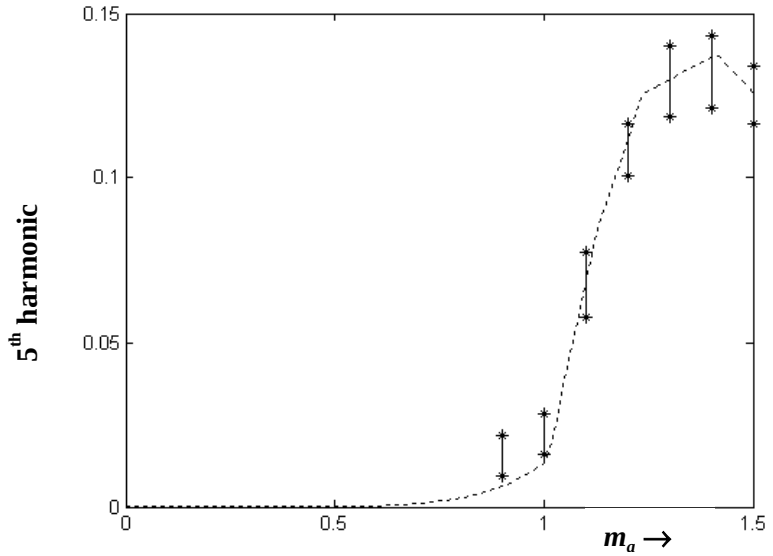

Fig. 8.79: Theoretical and measured fifth harmonic component versus modulation index for modified five-level WRPWM scheme operating with N = 8, q = 4 and a = 2.

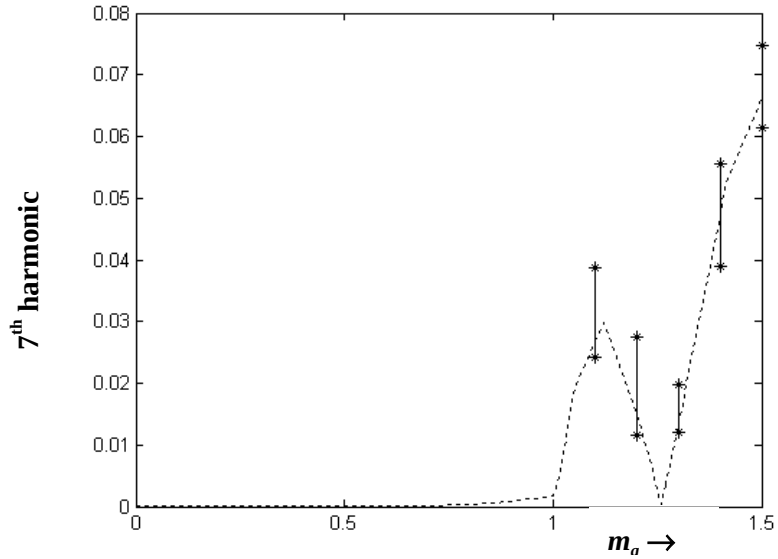

Fig. 8.80: Theoretical and measured seventh harmonic component versus modulation index for modified five-level WRPWM scheme operating with N = 8, q = 4 and a = 2.

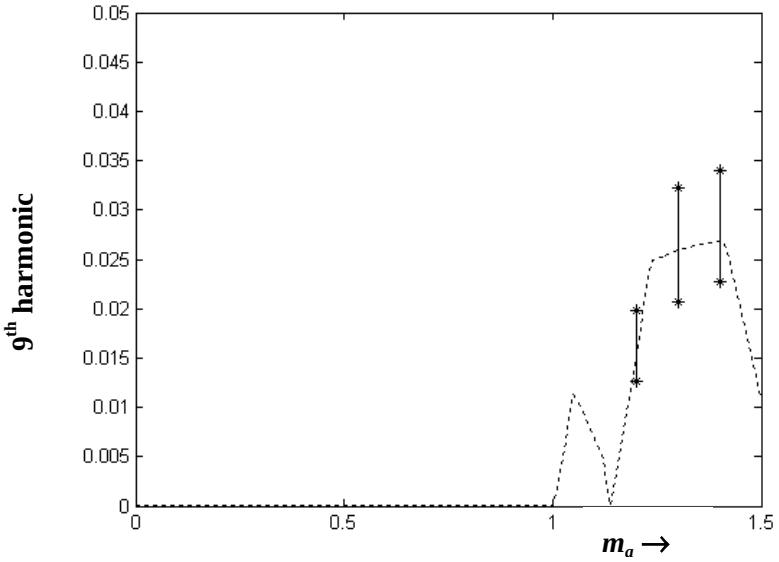

Fig. 8.81: Theoretical and measured ninth harmonic component versus modulation index for modified five-level WRPWM scheme operating with N = 8, q = 4 and a = 2.

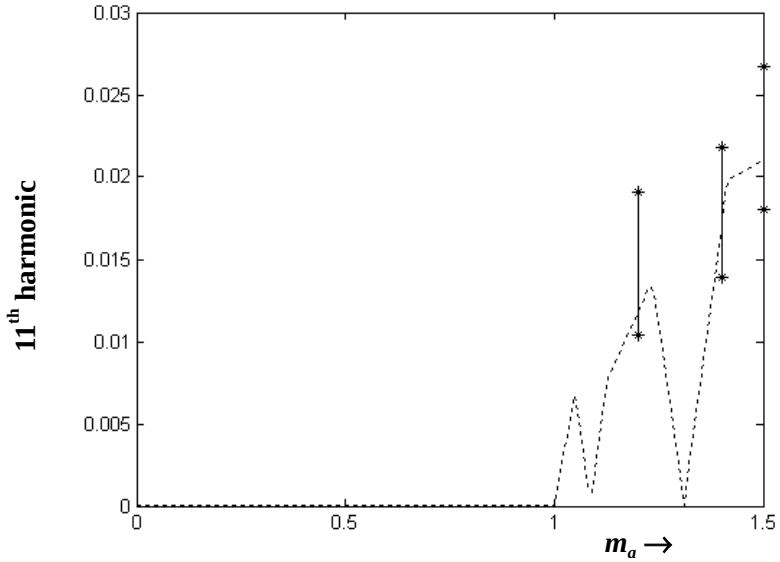

Fig. 8.82: Theoretical and measured eleventh harmonic component versus modulation index for modified five-level WRPWM scheme operating with N = 8, q = 4 and a = 2.

8.2.1.9 Modified Five-Level WRPWM Operating with N = 9 and Combination q = 3 a = 0

The plot of measured fundamental component versus modulation index is shown in Fig. 8.83. The plots of third, fifth and seventh harmonic components versus modulation index are shown in Figs. 8.84, 8.85 and 8.86, respectively. From Figs. 8.83 to 8.86, it can be seen that the measurements are in good agreement with predictions.

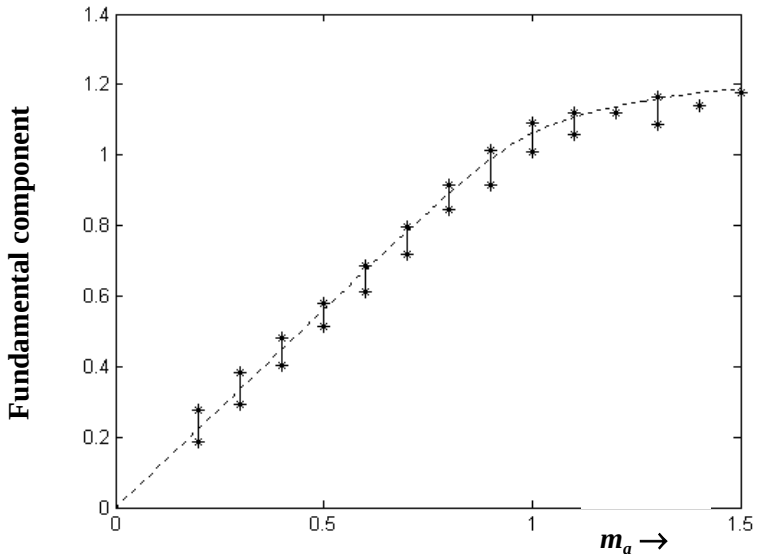

Fig. 8.83: Theoretical and measured fundamental component versus modulation index for modified five-level WRPWM scheme operating with N = 9, q = 3 and a = 0.

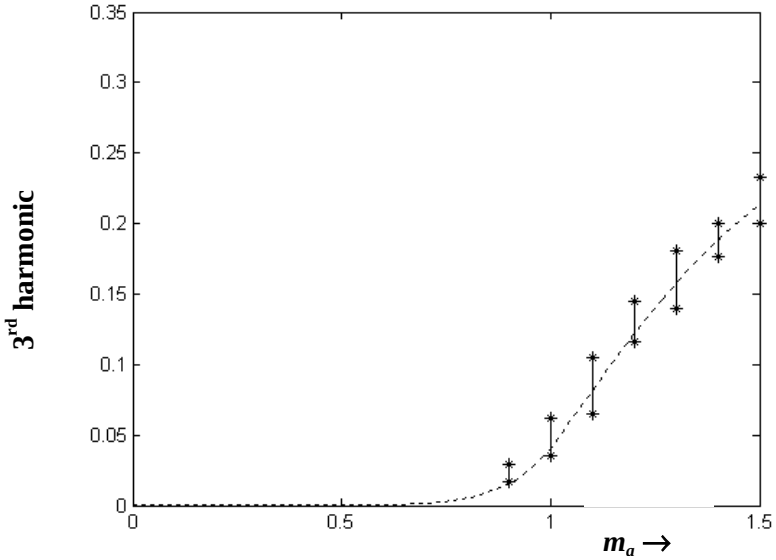

Fig. 8.84: Theoretical and measured third harmonic component versus modulation index for modified five-level WRPWM scheme operating with N = 9, q = 3 and a = 0.

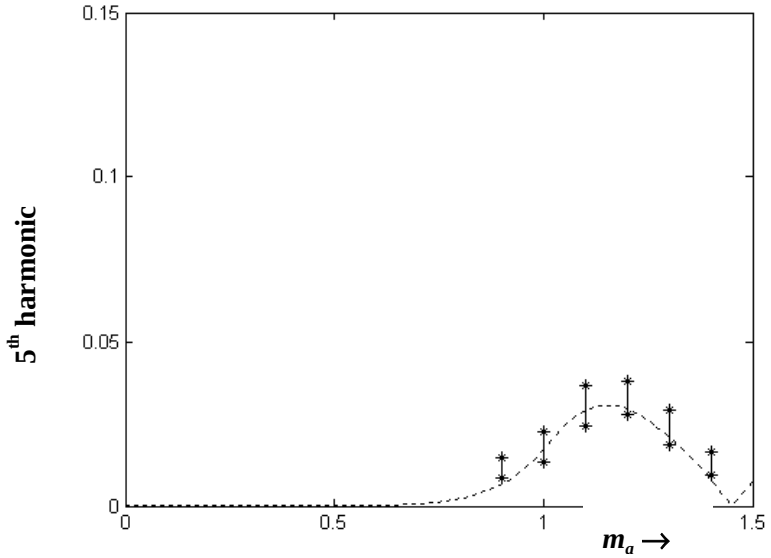

Fig. 8.85: Theoretical and measured fifth harmonic component versus modulation index for modified five-level WRPWM scheme operating with N = 9, q = 3 and a = 0.

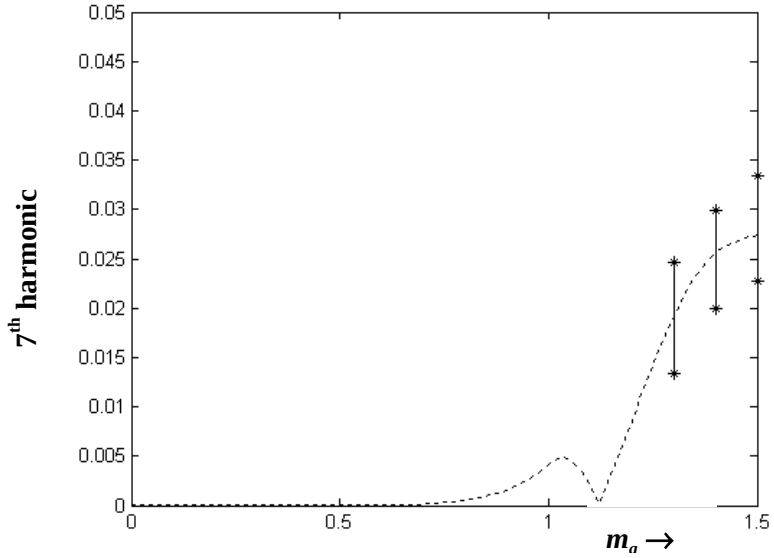

Fig. 8.86: Theoretical and measured seventh harmonic component versus modulation index for modified five-level WRPWM scheme operating with N = 9, q = 3 and a = 0.

8.2.1.10 Modified Five-Level WRPWM Operating with N = 9 and Combination q = 4 a = 0

The plot of measured fundamental component versus modulation index is shown in Fig. 8.87. The plots of third, fifth, seventh and ninth harmonic components versus modulation index are shown in Figs. 8.88, 8.89, 8.90 and 8.91, respectively. From Figs. 8.87 to 8.91, it can be seen that the measurements are in good agreement with predictions.

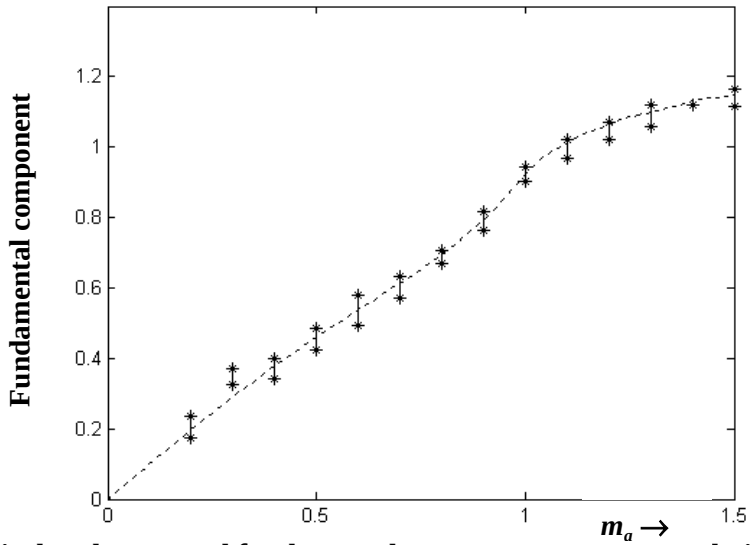

Fig. 8.87: Theoretical and measured fundamental component versus modulation index for modified five-level WRPWM scheme operating with N = 9, q = 4 and a = 0.

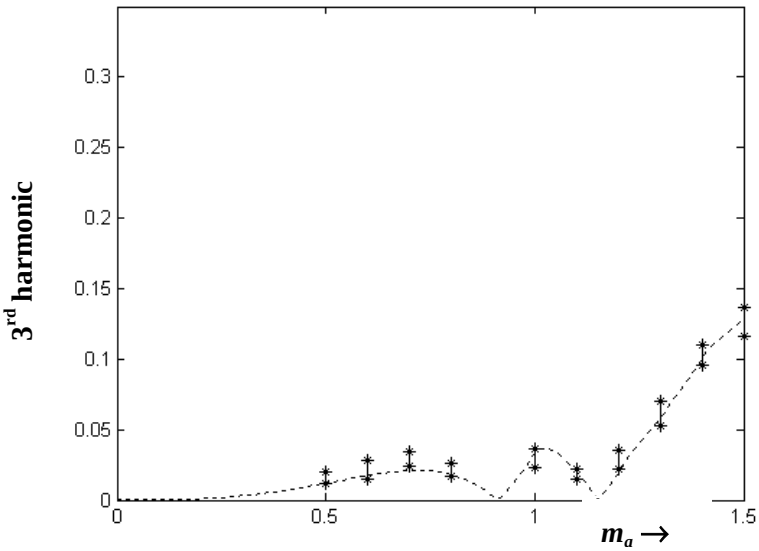

Fig. 8.88: Theoretical and measured third harmonic component versus modulation index for modified five-level WRPWM scheme operating with N = 9, q = 4 and a = 0.

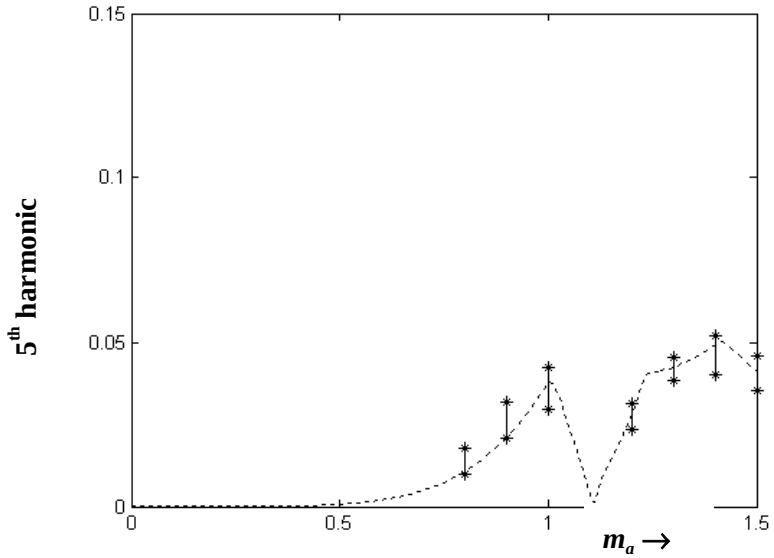

Fig. 8.89: Theoretical and measured fifth harmonic component versus modulation index for modified five-level WRPWM scheme operating with N = 9, q = 4 and a = 0.

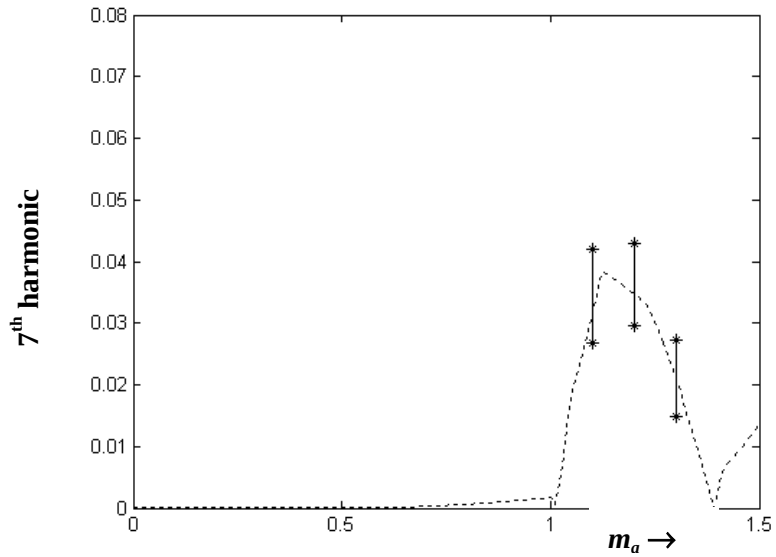

Fig. 8.90: Theoretical and measured seventh harmonic component versus modulation index for modified five-level WRPWM scheme operating with N = 9, q = 4 and a = 0.

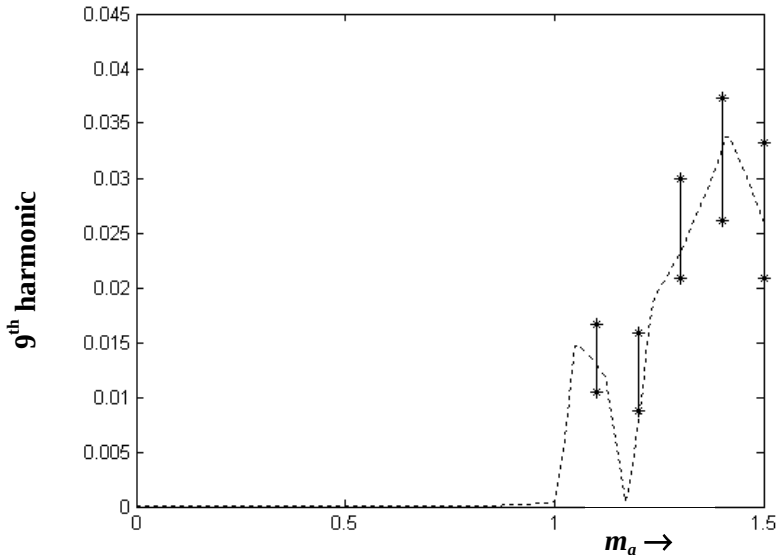

Fig. 8.91: Theoretical and measured ninth harmonic component versus modulation index for modified five-level WRPWM scheme operating with N = 9, q = 4 and a = 0.

8.2.1.11 Modified Five-Level WRPWM Operating with N = 9 and Combination q = 4 a = 1

The plot of measured fundamental component versus modulation index is shown in Fig. 8.92. The plots of third, fifth and seventh harmonic components versus modulation index are shown in Figs. 8.93, 8.94 and 8.95, respectively. From Figs. 8.92 to 8.95, it can be seen that the measurements are in good agreement with predictions.

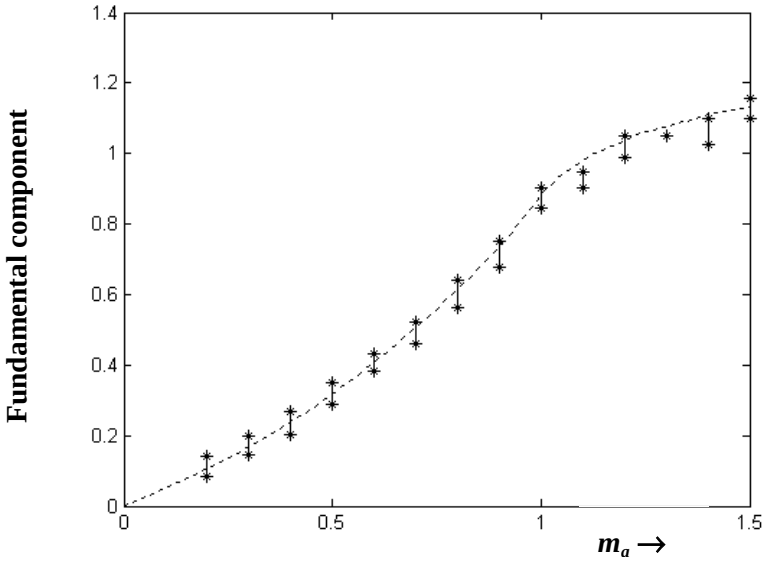

Fig. 8.92: Theoretical and measured fundamental component versus modulation index for modified five-level WRPWM scheme operating with N = 9, q = 4 and a = 1.

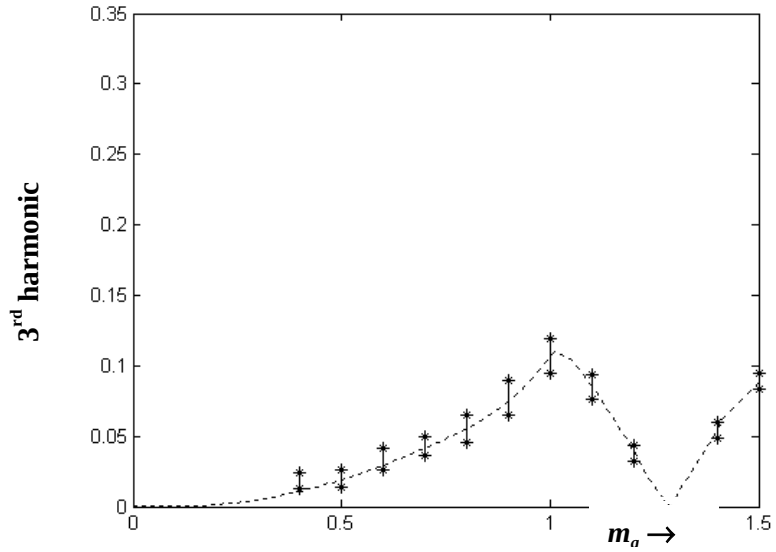

Fig. 8.93: Theoretical and measured third harmonic component versus modulation index for modified five-level WRPWM scheme operating with N = 9, q = 4 and a = 1.

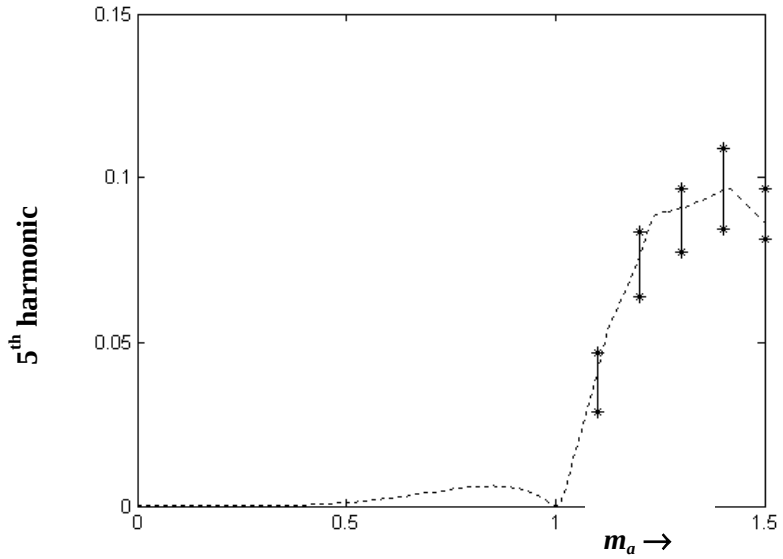

Fig. 8.94: Theoretical and measured fifth harmonic component versus modulation index for modified five-level WRPWM scheme operating with N = 9, q = 4 and a = 1.

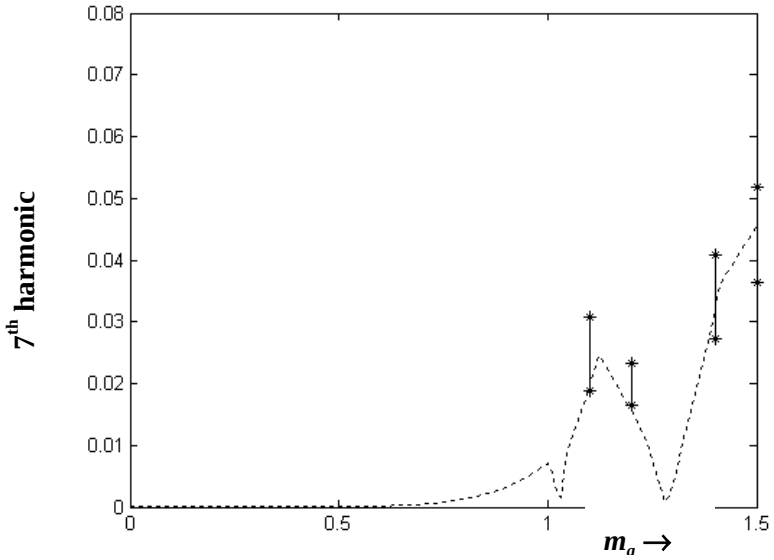

Fig. 8.95: Theoretical and measured seventh harmonic component versus modulation index for modified five-level WRPWM scheme operating with N = 9, q = 4 and a = 1.

8.2.1.12 Modified Five-Level WRPWM Operating with N = 9 and Combination q = 4 a = 2

The plot of measured fundamental component versus modulation index is shown in Fig. 8.96. The plots of third, fifth and seventh harmonic components versus modulation index are shown in Figs. 8.97, 8.98 and 8.99, respectively. From Figs. 8.96 to 8.99, it can be seen that the measurements are in good agreement with predictions.

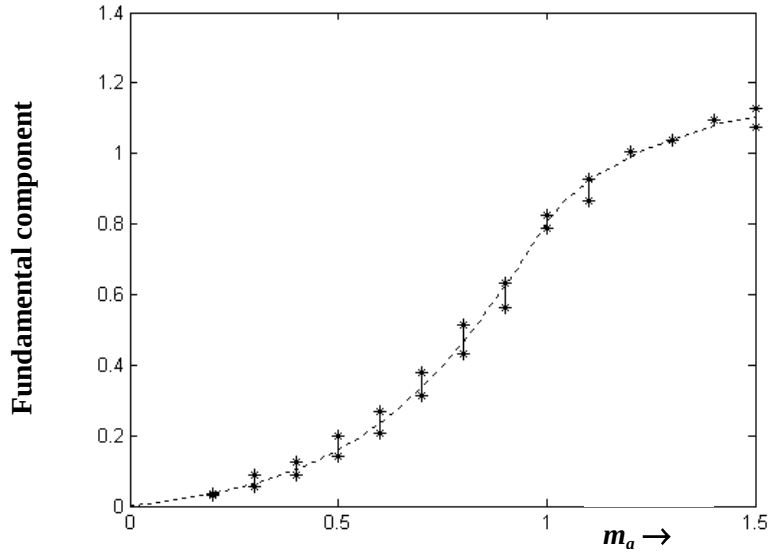

Fig. 8.96: Theoretical and measured fundamental component versus modulation index for modified five-level WRPWM scheme operating with N = 9, q = 4 and a = 2.

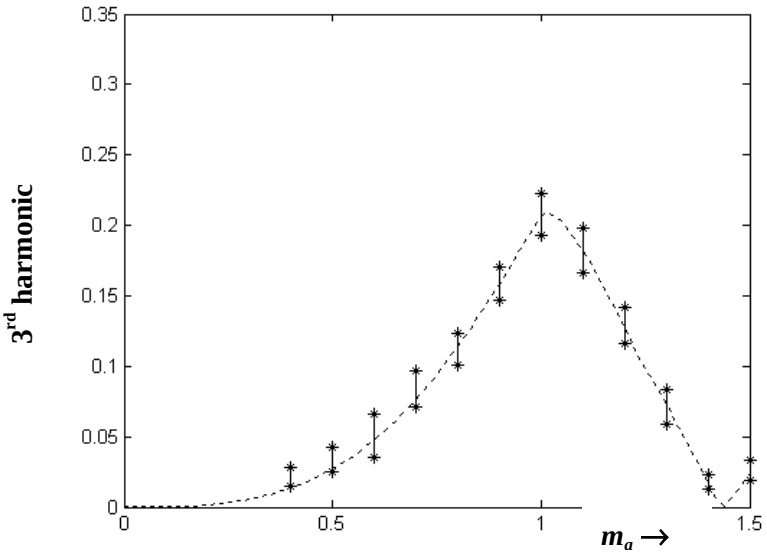

Fig. 8.97: Theoretical and measured third harmonic component versus modulation index for modified five-level WRPWM scheme operating with N = 9, q = 4 and a = 2.

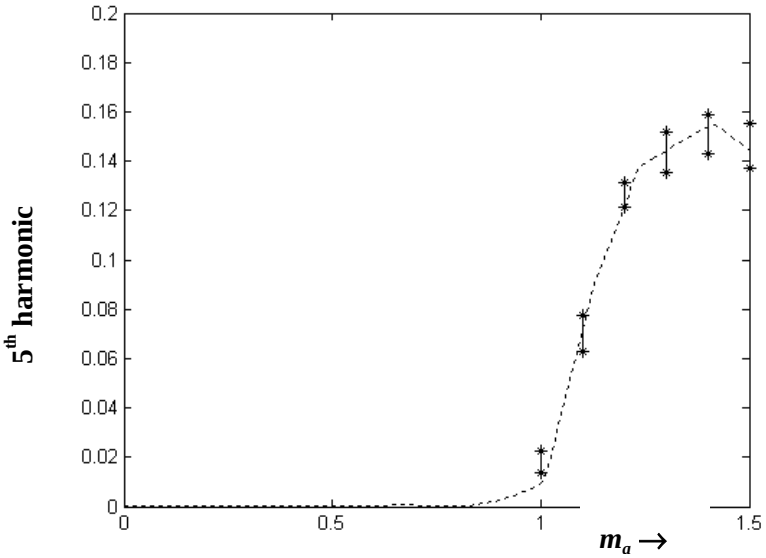

Fig. 8.98: Theoretical and measured fifth harmonic component versus modulation index for modified five-level WRPWM scheme operating with N = 9, q = 4 and a = 2.

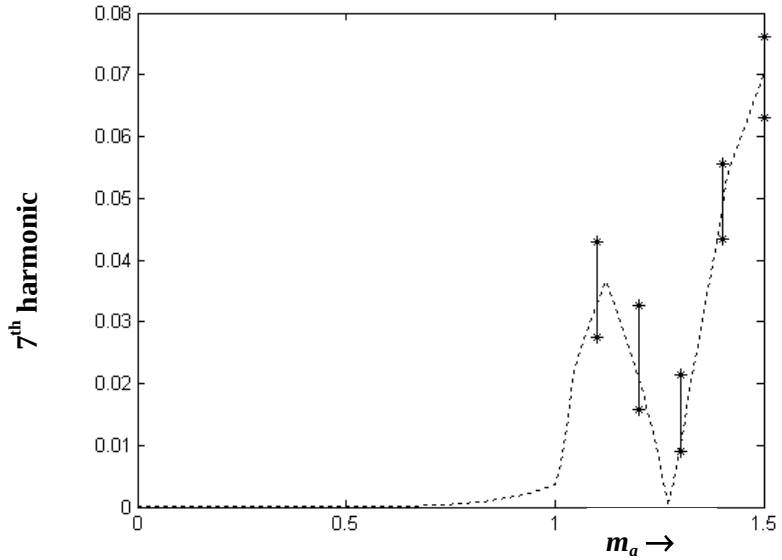

Fig. 8.99: Theoretical and measured seventh harmonic component versus modulation index for modified five-level WRPWM scheme operating with N = 9, q = 4 and a = 2.

8.2.2 Signal, Discrete and Continuous Noise Power

In this section, plots of measured signal, discrete noise and continuous noise power versus sampling frequency are presented.

8.2.2.1 Signal Power

The signal power is calculated by first squaring and then averaging the value of the two points from the fundamental component measurements (i.e. $(V_{1\max}{}^2 + V_{1\min}{}^2)/2$, where V_1 is the amplitude of the fundamental component of voltage spectrum).

Fig. 8.100 shows the plots of signal power versus sampling frequency characteristic for the modified five-level WRPWM scheme operating with N = 6 and for various combinations of q and a. Measurements were taken at the sampling frequencies of f_{sp} = 10 kHz, 20 kHz and 25 kHz.

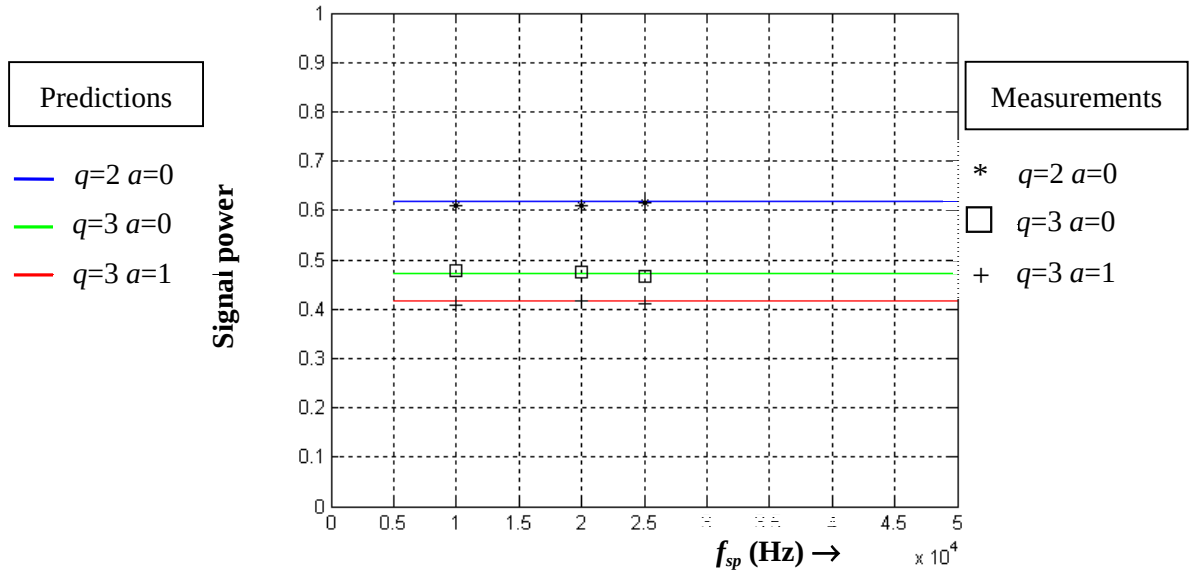

Fig. 8.100: Measured signal power versus sampling frequency for modified five-level WRPWM scheme operating with N = 6 and various combinations of values q and a.

Figs. 8.101 and 8.102 show the plots of signal power versus sampling frequency characteristic for the modified five-level WRPWM scheme operating with N = 7 and 8 and for various combinations of q and a. Measurements were taken at the sampling frequencies of f_{sp} = 10 kHz and 20 kHz.

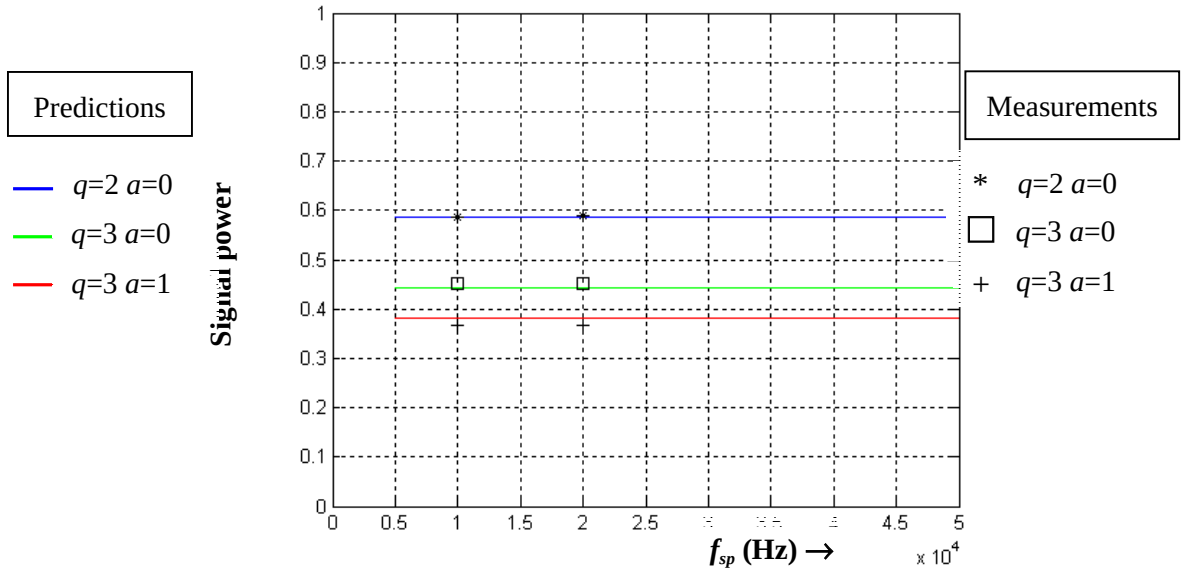

Fig. 8.101: Measured signal power versus sampling frequency for modified five-level WRPWM scheme operating with N = 7 and various combinations of values q and a.

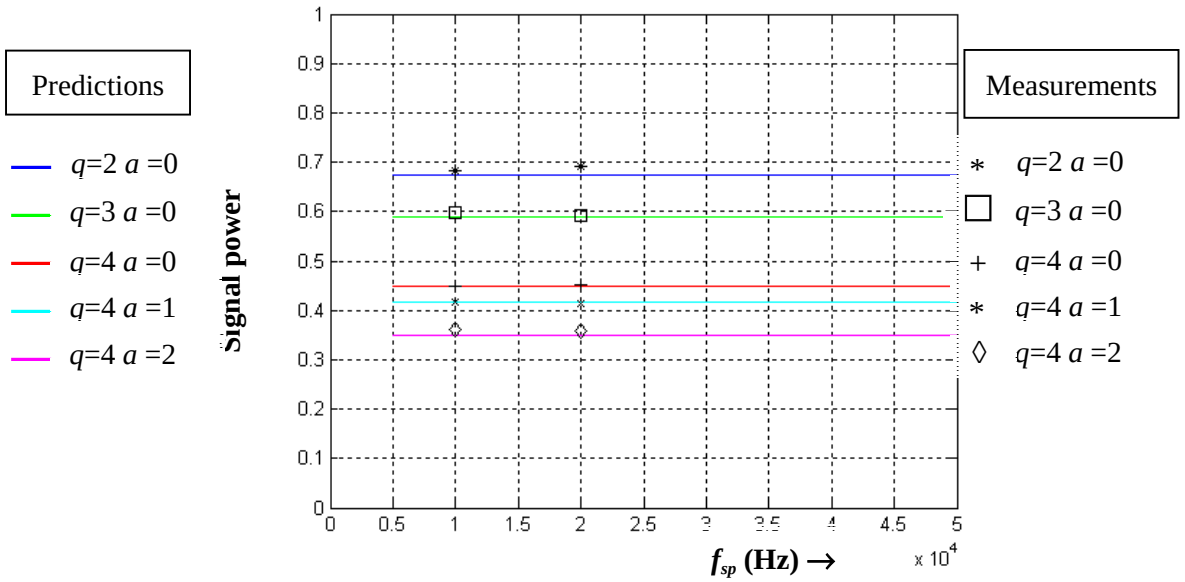

Fig. 8.102: Measured signal power versus sampling frequency for modified five-level WRPWM scheme operating with N = 8 and various combinations of values q and a.

Fig. 8.103 shows the plots of signal power versus sampling frequency characteristic for the modified five-level WRPWM scheme operating with N = 9 and for various combinations of q and a. Measurements were taken at the sampling frequencies of f_{sp} = 10 kHz and 16 kHz.

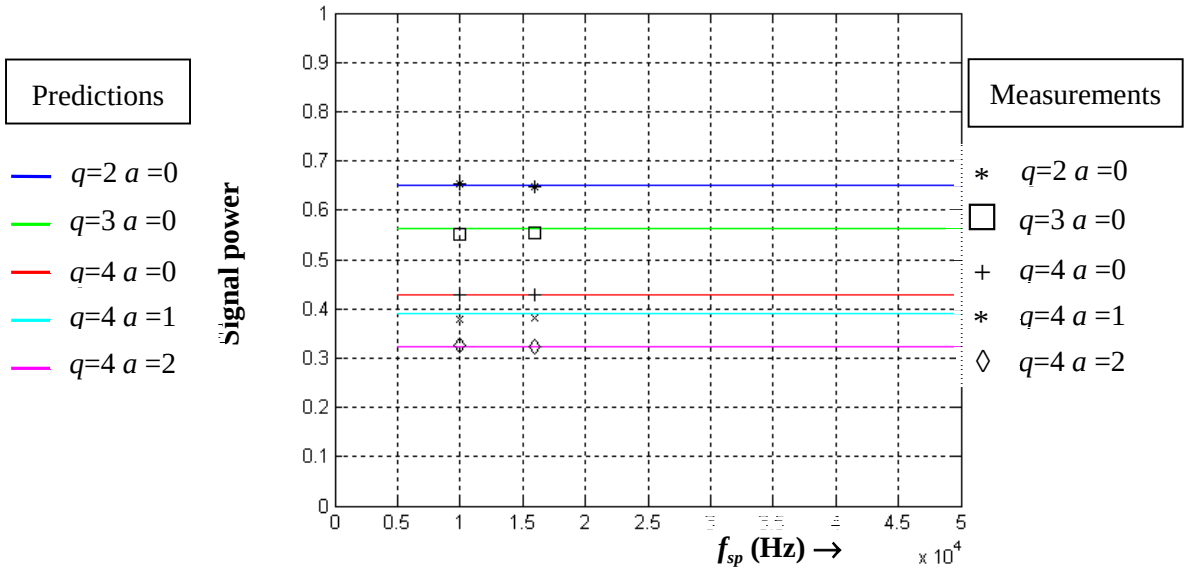

Fig. 8.103: Measured signal power versus sampling frequency for modified five-level WRPWM scheme operating with N =9 and various combinations of values q and a.

8.2.2.2 Discrete Noise Power

The discrete noise power is calculated by first squaring and then averaging the value of the two points from the harmonic components measurements (i.e. $(V_{h\max}{}^2 + V_{h\min}{}^2)/2$, where V_h is the amplitude of the harmonic component of voltage spectrum and h = 3, 4, 5 …).

Fig. 8.104 shows the plots of discrete noise power versus sampling frequency characteristic for the modified five-level WRPWM scheme operating with N = 6 and various combinations of q and a. Measurements are taken at sampling frequency f_{sp} at 10 kHz, 20 kHz and 25 kHz.

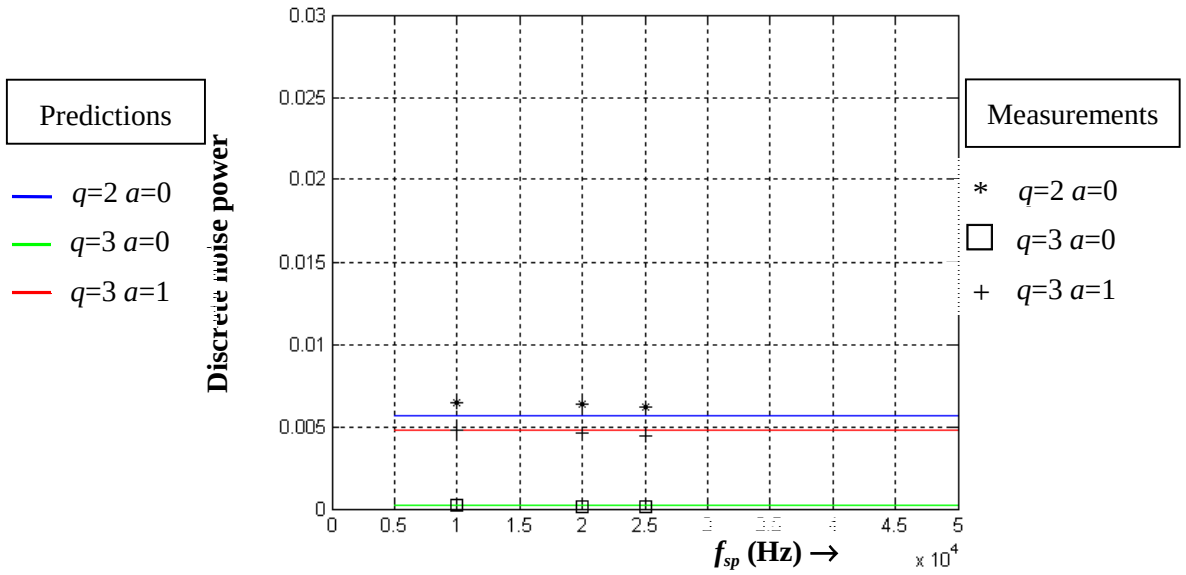

Fig. 8.104: Measured signal power versus sampling frequency for modified five-level WRPWM scheme operating with N =6 and various combinations of values q and a.

Figs. 8.105 and 8.106 show the plots of discrete noise power versus sampling frequency characteristics for the modified WRPWM scheme operating with N = 7 and 8 and for various combinations of q and a. Measurements were taken at the sampling frequencies of f_{sp} = 10 kHz and 20 kHz. In the prediction of the modified WRPWM scheme operating with N = 8, the discrete noise power for operation with q = 2, a = 0 (standard five-level WRPWM scheme) and q = 4 a = 2 are identical but the measured noise power for operation with q = 2, a = 0 are slightly higher.

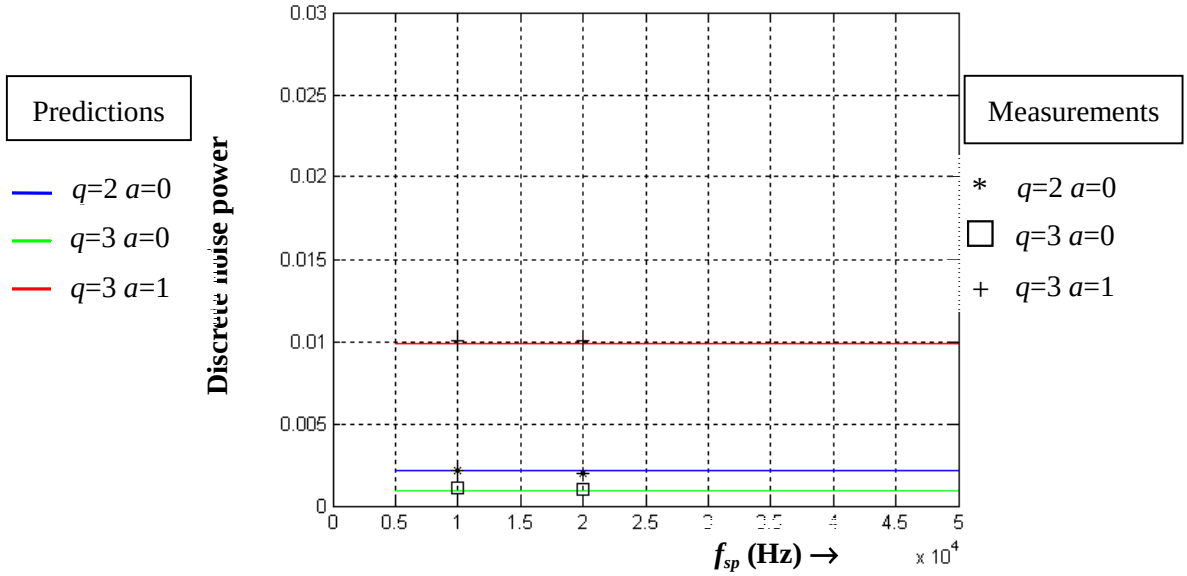

Fig. 8.105: Measured signal power versus sampling frequency for modified five-level WRPWM scheme operating with *N* =7 and various combinations of values *q* and *a*.

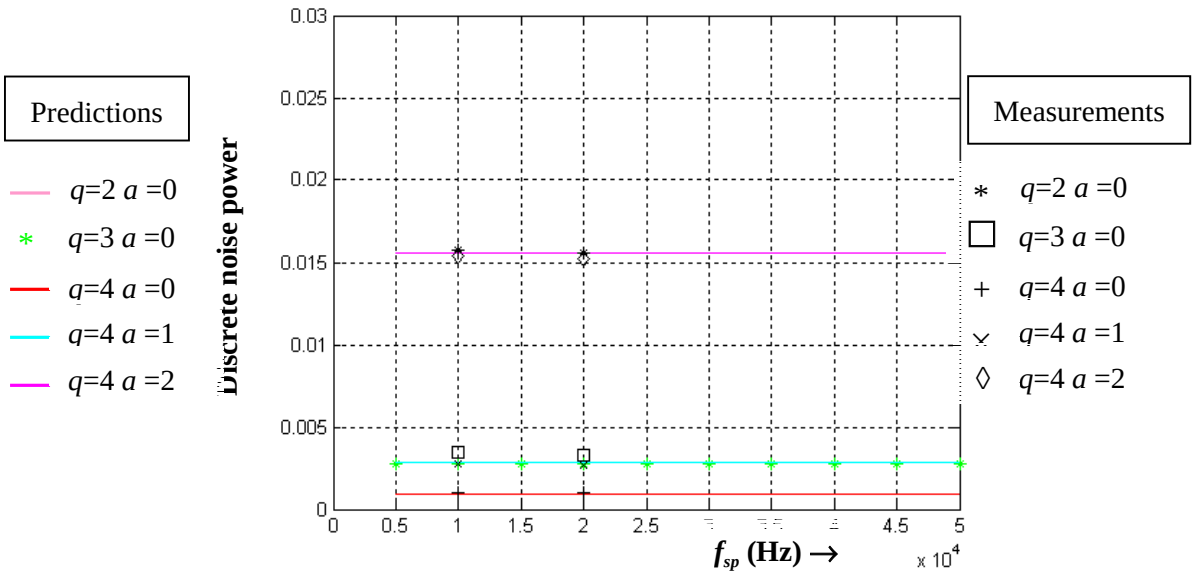

Fig. 8.106: Measured signal power versus sampling frequency for modified five-level WRPWM scheme operating with *N* =8 and various combinations of values *q* and *a*.

Fig. 8.107 shows the plots of discrete power versus sampling frequency characteristic for the modified five-level WRPWM scheme operating with N = 9 and various combinations of q and a. Measurements were taken at the sampling frequencies of f_{sp} = 10 kHz and 16 kHz.

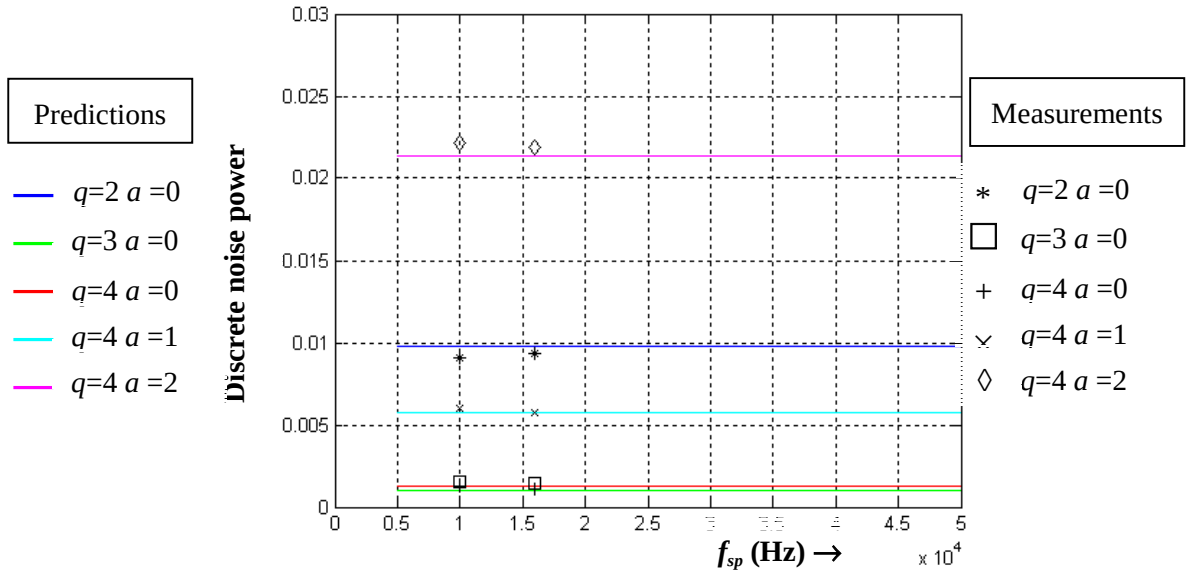

Fig. 8.107: Measured signal power versus sampling frequency for modified five-level WRPWM scheme operating with *N* =9 and various combinations of values *q* and *a*.

8.2.2.3 Continuous Noise Power

The measurements of continuous noise power were taken by averaging the value of power spectrum of the WRPWM waveform using the function provided in Tektronix TDS 220 oscilloscope in acquire mode. The data was then transferred to a PC using WaveStar. Microsoft Excel was then used to sum up after the fundamental and harmonics components were subtracted. The sum was averaged by dividing with number of data within 2000 Hz, and then integrated by multiplying with 2000.

Fig. 8.108 shows the plots of continuous noise power versus sampling frequency characteristic for the modified five-level WRPWM scheme operating with N = 6. Measurements were taken at the sampling frequencies of f_{sp} = 10 kHz, 20 kHz and 25 kHz. It can be seen that the continuous power of the modified WRPWM scheme operating with q = 3 and a = 0 is slightly higher than that for the modified WRPWM scheme operating with q = 3 and a =1.

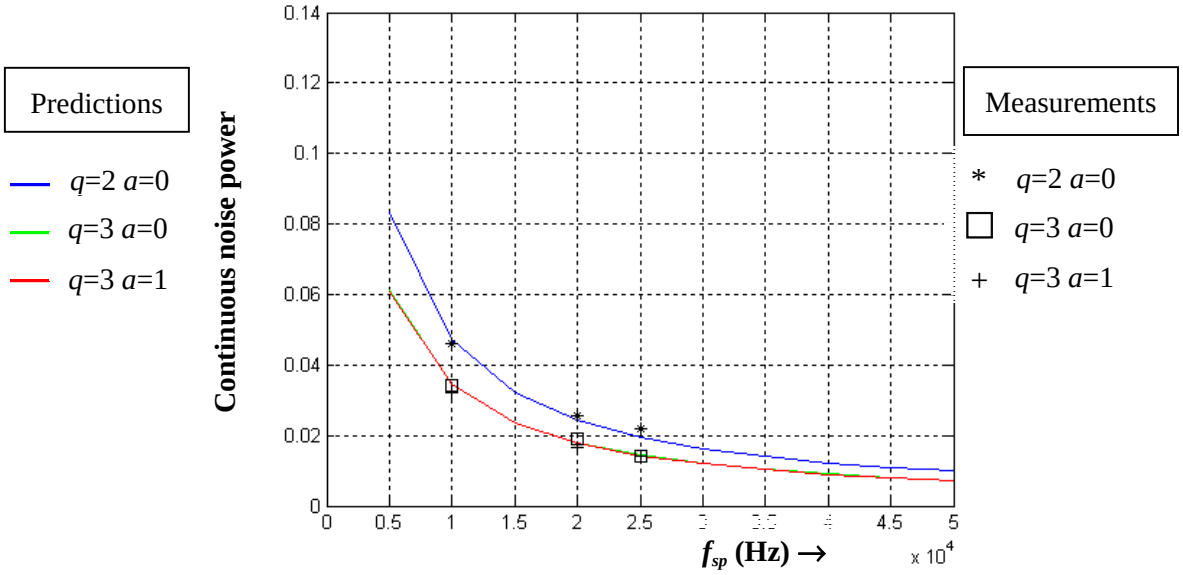

Fig. 8.108: Measured continuous noise power versus sampling frequency for modified five-level WRPWM scheme operating with N = 6 and various combinations of q and a.

Fig. 8.109 shows the plots of continuous noise power versus sampling frequency characteristic for the modified five-level WRPWM scheme operating with N = 7. Measurements were taken at the sampling frequencies of f_{sp} at 10 kHz and 20 kHz.

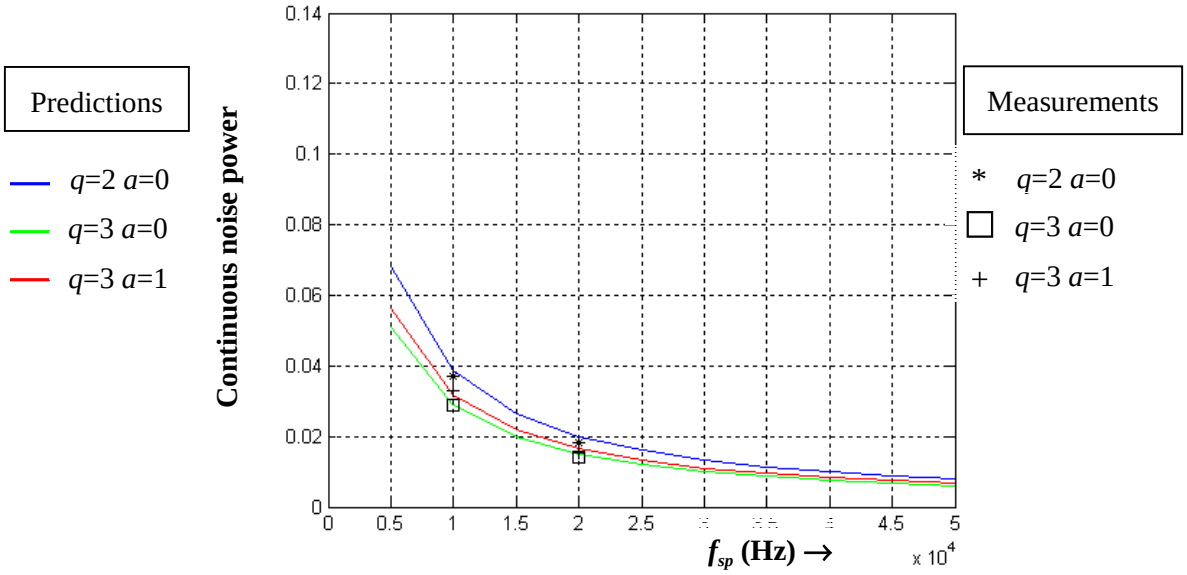

Fig. 8.109: Measured continuous noise power versus sampling frequency for modified five-level WRPWM scheme operating with N = 7 and various combinations of q and a.

Fig. 8.110 shows the plots of continuous noise power versus sampling frequency characteristic for the modified five-level WRPWM scheme operating with N = 8. Measurements were taken at the sampling frequencies of f_{sp} = 10 kHz and 20 kHz. It can be seen that with N = 8, the continuous noise of modified WRPWM scheme operating with q = 4 and a = 2 is slightly higher than that for the modified WRPWM scheme operating with q = 4 and a = 0. The modified WRPWM operating with N = 8, q = 4 and a =1 has the lowest continuous noise.

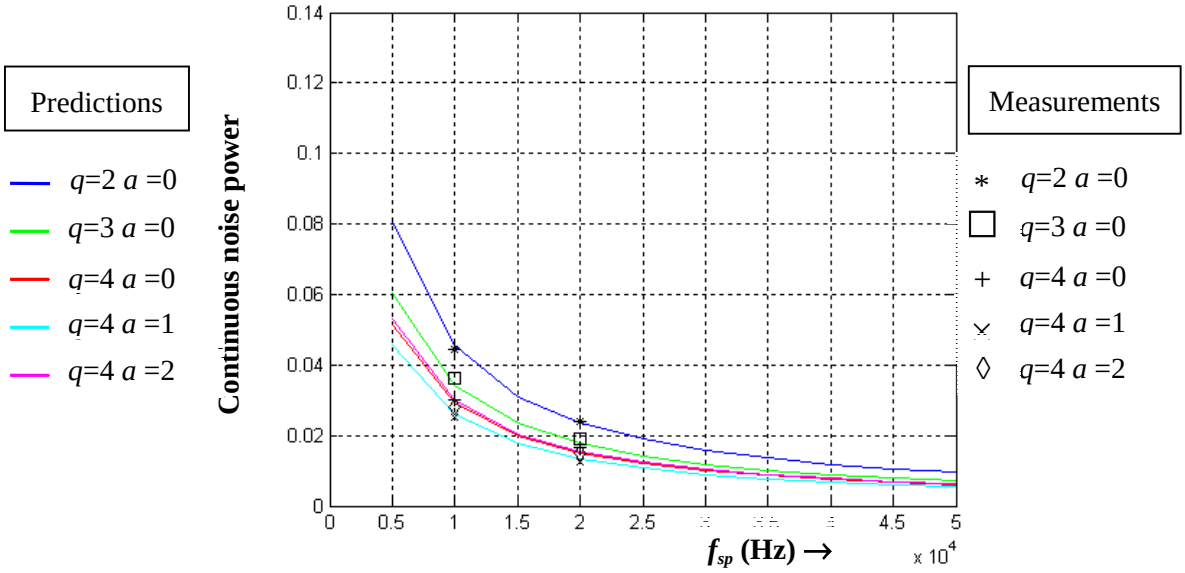

Fig. 8.110: Measured continuous noise power versus sampling frequency for modified five-level WRPWM scheme operating with N = 8 and various combinations of q and a.

Fig. 8.111 shows the plots of continuous noise power versus sampling frequency characteristic for the modified five-level WRPWM scheme operating with N = 9. Measurements were taken at the sampling frequencies of f_{sp} = 10 kHz and 16 kHz. It can be observed that with N = 9, the continuous noise of modified WRPWM scheme operating with q = 3 and a = 0 is slightly higher than that for the modified WRPWM scheme operating with q = 4 and a = 2. It is also evident that the continuous noise of modified WRPWM scheme operating with q = 4 and a = 0 is slightly higher than the modified WRPWM scheme operating with q = 4 and a = 1. Additionally, the modified WRPWM operating with N = 8, q = 4 and a =1 has the lowest continuous noise.

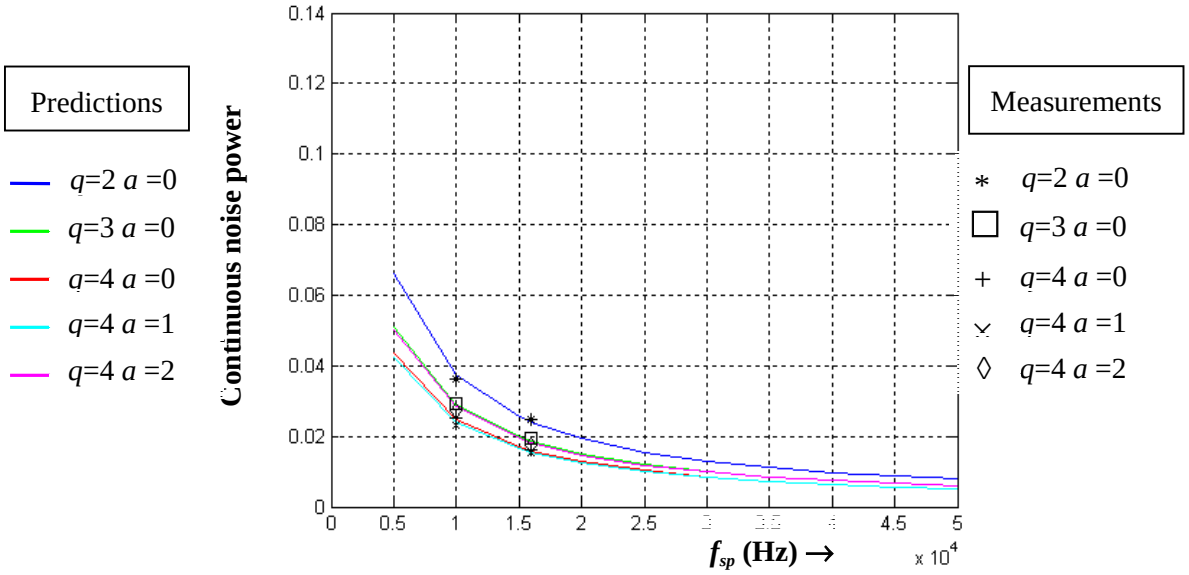

Fig. 8.111: Measured continuous noise power versus sampling frequency for modified five-level WRPWM scheme operating with *N* = 9 and various combinations of *q* and *a*.

In section 6, the five-level WRPWM schemes operating with $N = 6$, $q = 2$, $a = 0$ (i.e. operation 1); $N = 6$, $q = 3$, $a = 0$ (i.e. operation 2); $N = 8$, $q = 3$ and $a = 0$ (i.e. operation 3) were found to be the optimal choices depending on the application. The output voltage waveform and power spectrum of the five-level WRPWM with operation 1 with modulation index $m_a = 1.0$ are shown in Figs. 8.5 (a) and (b) respectively. Figs. 8.112 (a) and (b) show the output voltage waveform and power spectrum of the five-level WRPWM with operation 2 with modulation index $m_a = 1.0$ respectively. On the other hand, Figs. 8.113 (a) and (b) respectively show the output voltage waveform and power spectrum of the five-level WRPWM scheme employing operation 3 and modulation index, $m_a = 1.0$.

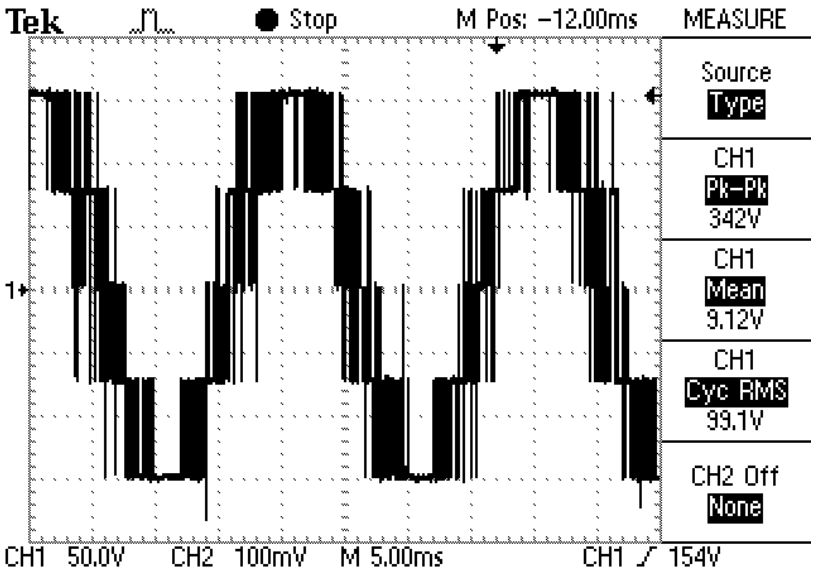

(a)

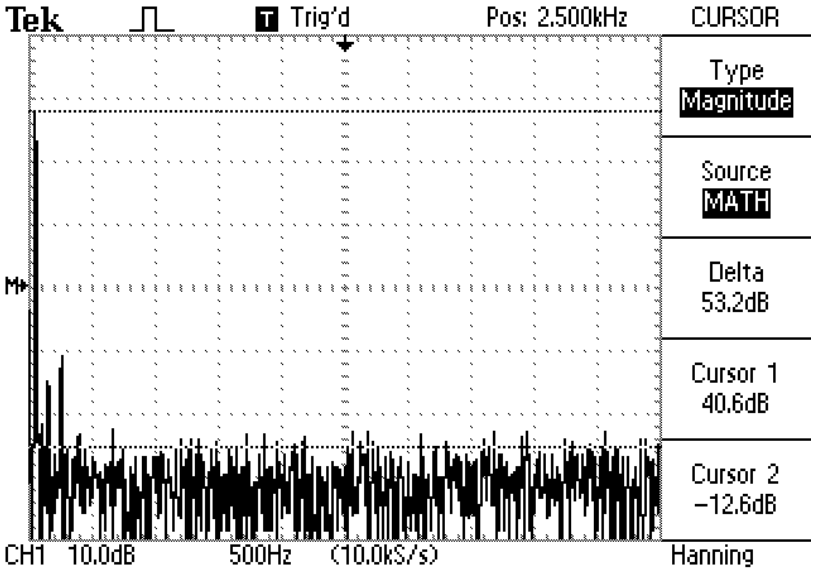

(b)

Fig. 8.112: Plots of standard five-level WRPWM with operation 1 at m_a = 1.0. (a) Output waveform. (b) Power spectrum.

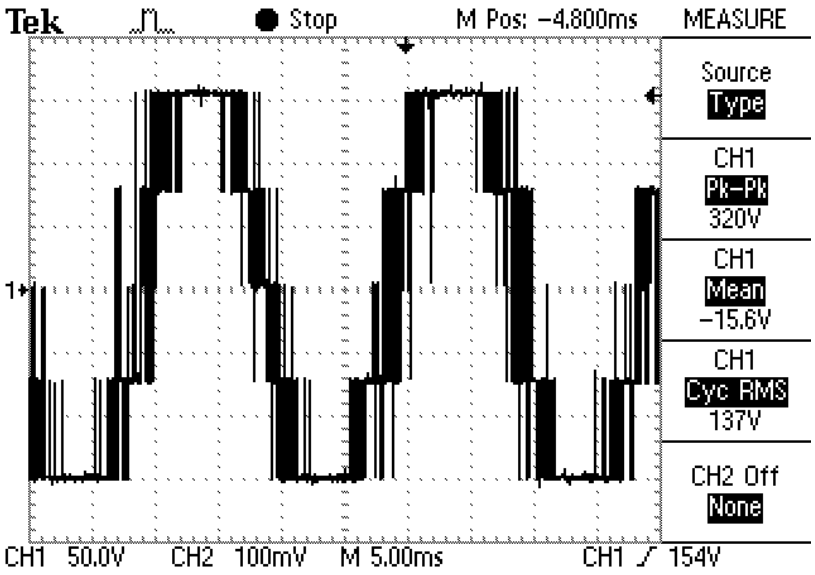

(a)

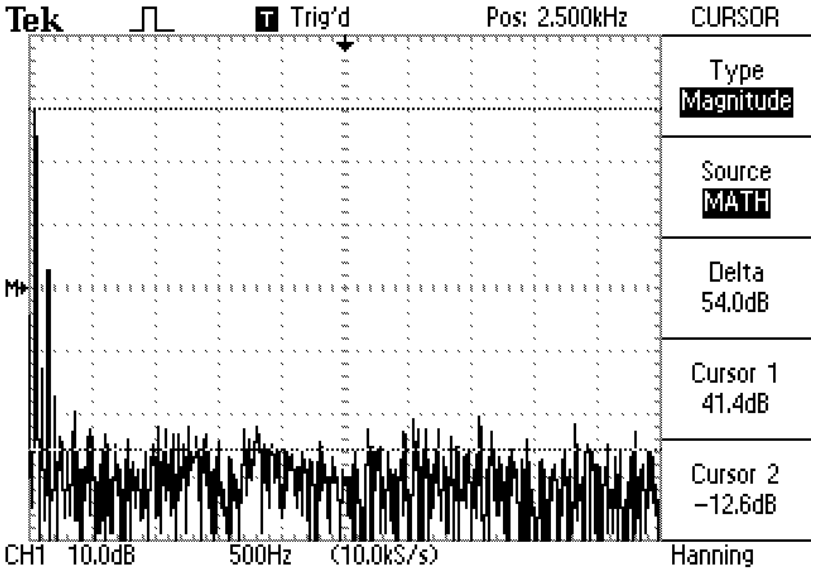

(b)

Fig. 8.113: Plots of standard five-level WRPWM with operation 3 at m_a = 1.0. (a) Output waveform. (b) Power spectrum.

CHAPTER NINE

CONCLUSION

Multilevel random PWM (RPWM) schemes have drawn increasing attention in the past few years. Multilevel topologies provide high voltage and high power capabilities and random PWM schemes offer reduction in discrete harmonics. Most researches have focused on the three-level random PWM schemes while this report focused on WRPWM schemes for five-level converters. In the available literature, no other report that attempted to apply WRPWM schemes to five-level converters was found.

In this report a standard five-level WRPWM and a modified WRPWM scheme have been proposed. A statistical approach for analysis of the standard and modified five-level WRPWM was presented. This statistical theory was used to predict the spectral performance, noise power content and average switching frequency of the standard and modified five-level WRPWM schemes. The effects of various parameters on the noise power were investigated. A scaled laboratory prototype diode clamping five-level inverter was built for verification of the standard and the proposed modified WRPWM schemes. For the half bridge five-level prototype, four 40 V dc power sources were employed as the dc supplies for the dc link. The measurements and the theoretical results were all in good agreement. The two WRPWM schemes offer significant improvements on the spectrum content compared with the conventional PWM schemes as was evident in Figs. 8.4-8.8, 8.46 and 8.47.

Utilizing the redundancy of the switching decisions of the five-level inverter, an extra parameter was introduced into the standard WRPWM to realize the modified WRPWM. From the proposed modified five-level inverter, it was found that as the level of inverter increases, the redundancy for the inverter to make its switching decisions increases as well. As a result, the inverter becomes more flexible in manipulating the harmonics content of the output waveform. Depending on its applications, the modified WRPWM scheme can be configured to generate an output voltage waveform with or without third harmonic boosting effect by changing the values of parameters q and a. Moreover, the values of parameters q and a can be changed to optimize the spectrum content, depending on the operating modulation index.

Both standard and modified five-level WRPWM schemes were found to have switching

frequencies that were lower than 40 % of the sampling frequency. Therefore, not only did the topology of the inverter reduce the switching stress of the power switching devices, the switching scheme also provides additional improvements as well. Moreover, It was proved mathematically that similar to the three-level WRPWM scheme all the even discrete harmonic components are absent from the spectrum if the ratio of sampling frequency to fundamental frequency is an even integer. For a sufficiently large value of the ratio, the quantitative picture remains the same, i.e., even harmonic are very small.

The analytical and experimental results have shown that both the standard and the modified five-level WRPWM schemes were effective in causing the harmonics to be spread over the frequency spectrum. Therefore, no harmonic component has significant magnitude. Both the standard and the modified WRPWM schemes have fairly linear fundamental-modulation index characteristic within the range m_a<1. These characteristics saturate when the modulation index increases over one which is similar to the conventional sinusoidal PWM techniques. It was found that for a given value of N the standard five-level WRPWM scheme yields a higher output fundamental component than the modified WRPWM scheme.

Both standard and modified schemes have their optimum harmonic contents depending on the operating region of modulation index and value of N. From the theoretical analysis and measurement results, it was found that both the standard WRPWM scheme operating with N = 6 (operation 1) and modified WRPWM scheme operating with N = 8, q = 3 and a = 0 (operation 3) offer the best overall performance if the third harmonic boosting effect is desired (e.g. three-phase inverter). For some applications where it is not desirable to have third harmonic boosting effect (e.g. single-phase inverter), it was found that the modified WRPWM scheme operating with N = 6, q = 3 and a = 0 (operation 2) offers the best overall performance.

The signal and noise power of both standard and modified five-level WRPWM schemes have been characterized and experimentally verified. For both standard and modified five-level WRPWM schemes, if the ratio (f_{sp} / f_r) ≥ 100, the signal power and the discrete noise power are independent of sampling frequency. It was found that continuous noise power is sampling frequency dependent and decreases as the sampling frequency increases. The effect of the modulation index, m_a and number of comparisons N were also investigated. The signal and discrete noise power increases as m_a increased whereas continuous noise decreases as m_a increased. It was also found that as N increases (in odd increment or in even increment) the continuous power deceases and as N increases (in odd increment or in even increment) both signal and discrete noise power increases. Moreover, the signal power and discrete noise

power for N even are higher than that for N odd (e.g., the signal power and discrete noise power for $N = 6$ are higher than $N = 7$). In contrast, the continuous noise power for N even is lower than that for N odd (e.g., the continuous noise power for $N = 6$ is lower than $N = 7$).

From the noise power analysis, it was found that the continuous noise power of modified WRPWM scheme was lower than that for the standard WRPWM scheme. At fixed modulation index, by setting the optimum values of q and a the discrete noise power for modified WRPWM scheme was lower than that for the standard WRPWM scheme. In general, over the modulation region of $0<m_a<1.2$, the standard five-level WRPWM offers high signal power. On the other hand, the modified five-level WRPWM scheme has low continuous noise power which reduces the chance for system excitation at high power applications.

It was observed that similar to the conventional multilevel PWM (e.g., SH-PWM), as the modulation index m_a approaches infinity the output voltage waveform of the inverter becomes square wave. Moreover, similar to two-level and three-level WRPWM, when the modulation index m_a or the number of comparisons N approaches infinity, the output waveform of the standard and modified five-level WRPWM tends to be square wave like. Therefore, when the standard or modified WRPWM scheme is applied, the five-level inverter performance degenerates to that of a two level inverter at fairly large value of m_a and/or N.

A comparison was made between the theoretically predicted performance of the standard five-level WRPWM scheme and that of a three-level WRPWM scheme. It was found that the three-level WRPWM scheme operating with $N = 3$ has a slightly better harmonic content than the five-level WRPWM scheme. However it should be noted that the five-level WRPWM scheme would most likely be used in systems which requires higher dc-bus voltages than those for the three-level WRPWM schemes. This makes the improvements achieved by employing the five-level WRPWM schemes that much more significant. It was also found that the five-level WRPWM scheme has lower continuous noise power making it less likely to excite systems resonances than the three-level WRPWM scheme.

The comparison between the theoretically predicted spectral performance of the standard five-level WRPWM scheme and that of the conventional carrier based five-level PWM scheme further confirmed that the five-level WRPWM scheme does indeed improve the spectral content. The five-level WRPWM scheme not only significantly improves the harmonic content, but also provides approximately the same fundamental component as the five-level SH-PWM.

The attractive features of five-level inverter employing five-level WRPWM scheme with operations 1, 2 and 3 include: 1) low undesirable low-order harmonics; 2) low continuous noise; 3) low switching frequency; 4) switching device stresses are reduced; 5) no voltage sharing problems exists for series connected devices. Furthermore, both standard and modified five-level WRPWM schemes reduce the EMI, switching loss, system resonance excitation and acoustic noise, and provide high input voltage capability. These features are suitable for large VA rated applications.

REFERENCES

[1] H. L. Liu, G. H. Cho, and S. S. Park, "Optimal PWM Design for High Power Three-Level Inverter Through Comparative Studies" *IEEE Trans. Power Electron.*, vol. 10, no. 1, pp. 38-47, Jan., 1995.

[2] C. Newton, and M. Sumner, "Novel technique for maintaining balanced internal DC link voltages in diode clamped five-level inverters" *Proc. IEE, Electr. Power Appl.*, vol. 146, no. 3, pp. 341-349, May, 1999.

[3] S. Y. R. Hui, S. Sathiakumar, and K. K. Sung, "Novel Random PWM Schemes with Weighted Switching Decision" *IEEE Trans. Power Electron.*, vol. 12, no. 6, pp. 945-952, Nov., 1997.

[4] Y. Shrivastava, and S. Y. R. Hui, "Analysis of Random PWM Switching Methods for Three-Level Power Inverters" *IEEE Trans. Power Electron.*, vol. 14, no. 6, pp. 1156-1163, Nov., 1999.

[5] Y. Shrivastava, S. Y. R. Hui, and S. Sathiakumar, "Noise Analysis of DC-AC Random PWM Schemes" *IEEE Trans. Power Electron.*, vol.14, no. 4, pp. 761-770, July, 1999.

[6] X. Yuan, and I. Barbi, "Fundamental of a New Diode Clamping Multilevel Inverter" *IEEE Trans. Power Electron.*, vol. 15, no. 4, pp. 711-718, July, 2000.

[7] J. S. Lai, and F. Z. Peng "Multilevel Converters—A New Breed of Power Converters" *IEEE Trans. Ind. Applicat.*, vol. 32, no. 3, pp. 509-517, May/June, 1996,

[8] X. Yuan, and I. Barbi, "Zero-Voltage Switching for Three-Level Capacitor Clamping Inverter" *IEEE Trans. Power Electron.*, vol. 14, no. 4, pp. 771-781, July, 1999.

[9] S. Y. R. Hui, I. Oppermann, and S. Sathiakumar, "Microprocessor-Based Random PWM Schemes for DC-AC Power Conversion" *IEEE Trans. Power Electron.*, vol. 12, no. 2, pp. 253-260, March, 1997.

[10] Y. Shirvastava, S. Sathiakumar, and S. Y. R. Hui, “Improved Spectral Performance of Random PWM Scheme with Weighted Switching Decision” *IEEE Trans. Power Electron.*, vol. 13, no. 6, pp. 1038-1045, Nov., 1998.

[11] N. Mohan, T. M. Undeland, and W. P. Robbins, “POWER ELECTRONICS”. John Wiley and Sons INC, 1995, pp. 200-245.

[12] A. M. Trzynadlowski, “Introduction to Modern Power Electronics”. John Wiley and Sons INC, 1998, pp. 200-243.

[13] P. C. Sen, “Principle of Electric Machine and Power Electronics”. John Wiley and Sons, 1996, pp. 79-272.

[14] L. M. Tolbert, F. Z. Peng, D. J. Adams, and J. W. Mckeever, “Multilevel Inverters for Large Automotive Electric Drives”, *All Electric Combat Vehicle Second International Conf.*, vol. 2, 8-12 June 1997, Dearborn Michigan, pp. 209-214.

[15] R. A. Gabel, and R. A. Roberts, “SIGNALS AND LINEAR SYSTEMS”. John Wiley and Sons INC, 1987, pp. 239-274.

[16] J. G. Proakis, and M. Salehi, “COMUNICATION SYSTEMS ENGINEARING”. Prentice Hall International INC, 1994, pp. 26-93, 143-188.

[17] S. R. Bowes, M. I. Mech and B. M. Bird, “Novel approach to the analysis and synthesis of modulation processes in power inverters”, *Proc. IEE. Electr. Power Appl.*, vol. 122, no. 5, pp. 507-513, May, 1975.

[18] S. R. Bowes, and M. I. Mech, “New sinusoidal pulsewidth-modulatioed inverter”, *Proc. IEE. Electr. Power Appl.*, vol. 122, no. 11, pp. 1279-1285, Nov., 1975.

[19] D. G. Holmes, “A General Analytical Method for Determining the Theoretical Harmonic Components of Carrier Based PWM Strategies”, *Conf. Rec. 1998 IEEE Ind. Applicat. Conf.*, 1998, pp. 1207-1214.

[20] D. G. Holmes, and B. P. McGrath, “Opportunities for Harmonic Cancellation with Carrier-Based PWM for Two-level and Multilevel Cascaded Inverters”, *Conf. Rec. 1999 IEEE-IAS Ann. Mtg.*, 1999, pp.781-788.

[21] J. K. Steinke, "Switching Frequency Optimal PWM Control of a Three-level Inverter", *IEEE Trans. Power Electron*, vol. 7, no. 3, pp. 487-496, July, 1992.

[22] J. Song, S. Cho, L. Choy and J. Choi, "New PWM Method for single-phase Three-level Rectifier", *Proc. IEEE Ind. Electron. 1997 ISIE'97 int.*, vol. 2, 1997, pp.283-287.

[23] A. Nabae, I. Takahashi, H. Akagi "A New Neutral-Point-Clamped PWM Inverter", *IEEE Trans. Power Electron*, vol. 17, no. 5, pp. 518-522, Sept/Oct., 1981.

[24] P.M. Bhagwat, and V. R. Stefanovic, "Generalized Structure of a Multilevel PWM Inverter", *IEEE Trans. Ind. Applicat.*, vol. 19, no. 6, pp. 1057-1069, Nov/Dec., 1983.

[25] M. Manjrekar, G. Venkataramanan, "Advanced Topologies and Modulation Strategies", *Conf. Rec. PESC*'96, 1996, pp. 1013-1018.

[26] C. Hochgraf, R. Lasseter, D. Divan, T. A. Lipo. "Comparison of Multilevel Inverter For Static Var Compensation", *Conf. Rec. 1994 IEEE-IAS Ann. Mtg.*, 1994, pp.921-928.

[27] L. M. Tolbert, F. Z. Peng, T. G. Habetler, "Multilevel PWM Methods at Low Modulation Indices", *IEEE Trans. Power Electron*, vol. 15, no. 4, pp. 719-725, July, 2000.

[28] J. Rodriguez, J. S. Lai, and F. Z. Peng, "Multilevel Inverters: A Survey of Topologies, Controls, and Applications", *IEEE Trans. Ind. Electron*, vol. 49, no. 4, pp. 724-738, Aug., 2002.

[29] G. Carrara, S. Gardella, M. Marchesoni, R. Salutari, and G. Sciutto, "A New Multilevel PWM Method: A Theoretical Analysis", *IEEE Trans. Power Electron.*, vol. 7, no. 3, pp. 497-505, July, 1992.

[30] B. P. McGrath, and D. G. Holmes, "An Analytical Technique for the Determination of Spectral Components of Multilevel Carrier-Based PWM Methods", *IEEE Trans. Power Electron.*, vol. 49, no. 4, pp. 847-857, Aug., 2002.

[31] L. M. Tolbert, and T. G. Habetler, "Novel Multilevel Inverter Carrier-Based PWM Method", *IEEE Trans. Ind. Applicat.*, vol. 35, no. 5, pp. 1098-1107, Sept/Oct., 1999.

[32] J. R. Espinoza, G. Joos, and H. Jin "MODELLING AND IMPLEMENTATION OF SPACE VECTOR PWM TECHNIQUES IN ACTIVE FILTER APPLICATIONS" *Conf. Rec. 1996 IEEE Power Electron. Conf.*, 1996, pp. 142-146.

[33] R. L. Kirlin, S. Kowk, S. Legowski, and A. M. Trzynadlowski, " Power Spectra of a PWM Inverter with Randomized Pulse Position", *IEEE Trans. Power Electron.*, vol. 9, no. 5, pp. 463-472, Aug., 1994.

[34] B. Huo, A. M. Trynadlowski, I. Panahi, and Z. Yu, "Novel Random Pulse Width Modulator with Constant Sampling Frequency Based on the TMS320F240 DSP Controller", *Proc. IECON'99*, 1999, pp. 342-347.

[35] A. M. Trzynadlowski, Z. W. Wang, J. M. Nagashima, C. stancu, and M. H. Zelechowski, "Comparative Investigation of PWM Techniques for a New Drive for Electric Vehicles", *IEEE Trans. Ind. Electron.*, vol. 39, no. 5, pp. 1396-1403, Aug., 2003.

[36] A. M. Stankovic, G. C. Verghese, and D. J. Perreault, "Analysis and Synthesis of Randomized Modulation Schemes for Power Converters" *IEEE Trans. Power Electron.*, vol. 10, no. 6, pp. 680-693, Aug., 1995.

[37] M. M. Bech, J. K. Pederson, F. Blaabjerg, and A. M. Trzynadloski, "A Methodology for true Comparison of Analytical and Measured Frequency Domain Spectra in Random PWM Converters", *IEEE Trans. Power Electron.*, vol. 14, no. 3, pp. 578-586, May, 1999.

[38] A. M. Trzynadlowski, F. Blaabjerg, J. K. Pederson, R. L. Kirlin, and S. Legowski, "Random Pulse Width Modulation Techniques for Converter-Fed Drive System-A Review", *IEEE Trans. Ind. Electron.*, vol. 35, no. 5, pp. 1166-1175, Sept/Oct., 1994.

[39] R. L. Kirlin, S. F. Legowski, and A. M. Trzynaldlowski, "An optimal Approach to Random Pulse Width modulation in Power Inverters", *Conf. Rec. PESC'*95, 1995, pp. 313-318.

[40] T. G. Habetler, and D. M. Divan, "Acoustic Noise Reduction in Sinusoidal PWM Drives Using a Randomly Modulated Carrier", *IEEE Trans. Power Electron.*, vol. 6, no. 3, pp. 356-363, July, 1991.

[41] C. M. Liaw, Y. M. lin, C. H. Wu, and K. I. Hwu, "Analysis, Design, and Implementation of a Random Frequency PWM Inverter", *IEEE Trans. Power Electron.*, vol. 15, no. 5, pp. 843-854, May, 2001.

[42] G. A. Covic, and J. T. Boys, "Noise quieting with random PWM AC drives", *IEE Proc. Electric. Power Appl.*, vol. 145, no. 1, pp. 1-10, Jan., 1998.

[43] A. M. Trzynadlowski, R. L. Kirlin, and S. F. Legowski, "Space Vector PWM Technique with Minimum Switching Losses and a Variable Pulse Rate", *IEEE Trans. Ind. Electron.*, vol. 44, no. 2, pp. 173-181, April, 1997.

[44] V. Blasko "Analysis of a Hybrid PWM Based on Modified Space-Vector Triangle-Comparison Methods", *IEEE Trans. Ind. Appl.*, vol. 33, no. 3, pp. 756-764, May/June, 1997.

[45] M. M. Bech, F. Blaabjerg, and J. K. Pederson, "Random Modulation Techniques with Fixed Switching Frequency for Three-Phase Power Converters", *IEEE Trans. Power Electron.*, vol. 15, no. 4, pp. 753-761, July, 2000.

[46] J. L. Shyu, T. J. Liang, and J. F. Chen, "Digitally-controlled PWM inverter modulated by multi-random technique with fixed switching frequency", *IEE Proc. Electric. Power Appl.*, vol. 148, no. 1, pp. 62-68, Jan., 2001.

[47] C. K. Lee, S. Y. R. Hui, H. S. Chung, and Y. Shrivastava, "A Randomized Voltage Vector Switching Scheme for Three-Level Power Inverters", *IEEE Trans. Power Electron.*, vol. 17, no. 1, pp. 94-100, July, 2002.

[48] S. Legowski, and A. M. Trzynadlowski, “HYPERSONIC MOSFET-BASED POWER INVERTER WITH RANDOM PULSE WIDTH MODULATION”, *Conf. Rec. 1989 IEEE-IAS Ann. Mtg.*, 1989, pp.901-903.

[49] S. Legowski, and A. M. Trzynadlowski, “POWER-MOSFET, HYPERSONIC INVERTER WITH HIGH-QUALITY OUTPUT CURRENT”, *Proc. APEC’90*, 1990, pp. 3-7.

[50] S. Legowski, and A. M. Trzynadlowski, “ADVANCED RANDOM PULSE WIDTH MODULATION TECHNIQUE FOR VOLTAGE-CONTROLLED INVERTER DRIVE SYSTEM”, *Proc. APEC’91*, 1991, pp. 100-106.

[51] B. P. McGrath, and D. G. Holmes, “Multicarrier PWM Strategies for Multilevel Inverters”, *IEEE Trans. Ind. Appl.*, vol. 49, no. 4, pp. 858-867, May/June, 2002.

[52] L. Garcia, “Probability and Random Processes for Electrical Engineering”, Addison Wesley, INC, 1994, pp. 60-98.

APPENDIX A. PUSH-PULL CONVERTER DESIGN

In this section, the design of the push-pull converter with eight +15 V and eight -5 V isolated dc voltage output is presented.

A.1 Operation of Push-pull converter

Fig. A.1 shows the circuit arrangement for a push-pull dc-dc converter. Push-pull topology is derivatives of two forward converters operating out of phase 180 degrees to produce a square wave ac at the input of the center tapped high frequency transformer. The output of the transformer is rectified to produce a dc output. A center tapped secondary is used, which results in only one diode voltage drop on the secondary side. This configuration allows operating in the first and the third quadrant of the hysteresis loop, with better a utilization of the magnetic core of the transformer. The maximum voltage stress of the power switches is twice the input voltage as same as the forward topology.

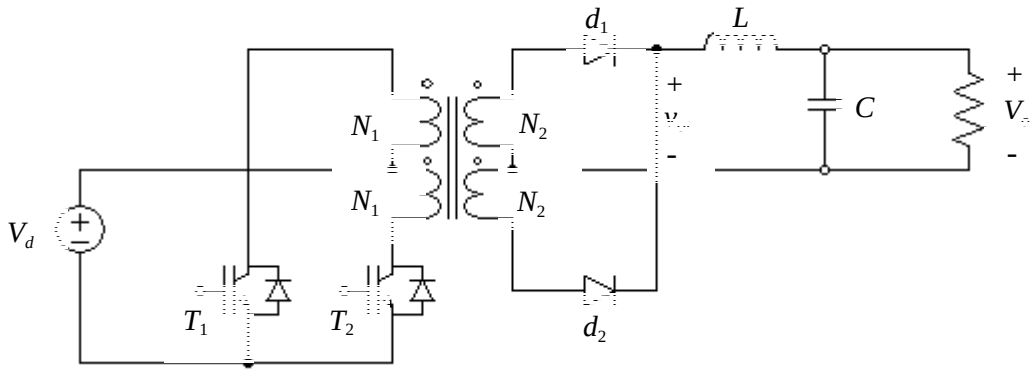

Fig. A.1: Push-pull converter

In the push-pull converter, where the converter output is rectified to produce a dc output, the dc output voltage V_o is controlled by using the PWM scheme shown in Fig. A.2, which controls the interval Δ during which all the switches are off simultaneously. In Fig. A.1, when T_1 is on, d_1 conducts and d_2 gets reverse biased. This results in the voltage v_{oi} across the cathode of the output diodes d_1 and d_2 and the center tap of the secondary winding of the transformer equal to $(N_2 / N_1)V_d$ (assuming there are no losses in the MOSFET's and output diodes).

A.2 Push-pull converter Design

Design inputs

Input voltage: V_d = 280 V
Output voltage 1:V_{o1} = 15 V
Maximum output voltage ripple 1: V_{rp1} = 0.15 V
Output current 1: I_{o1} = 2 A
Output voltage 2: V_{o2} = 5 V
Maximum output voltage ripple 2: V_{rp2} = 0.05 V
Output current 2: I_{o2} = 0.7 A
On resistance of power MOSFET: R_{Ton} = 0.27 Ω
Diode forward drop voltage: Vd_{fw} = 1.2 V
Switching frequency: f_{sw} = 100 kHz
Transformer efficiency: η = 0.9

From Fig. A.2 each switch switches at half the switching frequency thus the switching frequency for each of the power MOSFET f_T is 50 kHz.

Total output power P_o for the push-pull converter is

$$P_o = 8(V_{o1} + Vd_{fw})\, I_{o1} + 8(V_{o2} + Vd_{fw})\, I_{o2} = 293.9 \text{ W},$$

choose P_o to be 300 W.

Voltage drop across power MOSFET V_{Ton} during the on time is

$$V_{Ton} = \frac{P_o}{\eta \times V_d} \times R_{Ton} \qquad \text{(A.1)}$$
$$V_{Ton} \approx 0.32 \text{ V}$$

A.2.1 Selection of the Duty cycle and the Transformer Turn Ratio

The maximum duty ratio D of switches T_1 and T_2 can attain is 0.5. Thus, choose the duty ratio D to be 0.35.

The on time of each switching interval for each MOSFET is therefore

$$T_{Ton} = \frac{1}{f_T} \times D = 7\ \mu\text{sec} \tag{A.2}$$

The transformer turn ratio N_{sp} for the 15 V and 5 V supply are

$$N_{sp1} = \frac{N_2}{N_1} = \frac{V_{o1}/2D + Vd_{fw}}{V_d - V_{Ton}} = 0.08 \qquad \text{for 15 V supply} \tag{A.3}$$

$$N_{sp2} = \frac{N_2}{N_1} = \frac{V_{o2}/2D + Vd_{fw}}{V_d - V_{Ton}} = 0.03 \qquad \text{for 5 V supply} \tag{A.4}$$

A.2.2 Maximum voltage stress across Drain to Source of the Switching MOSFET

The maximum voltage stress across Drain to Source $V_{T\max}$ of the Switching MOSFET (assume the voltage spike is 30% of the input dc voltage) is

$$V_{T\max} = 2(1.30 \times V_d) = 728\ \text{V} \tag{A.5}$$

A.2.3 Maximum voltage stress across Drain to Source of the Switching MOSFET

The maximum voltage stress $V_{diode\max}$ across the output diode d_1 and d_2 is

$$V_{diode\max} = V_d \times N_{sp1} = 22.4\ \text{V} \tag{A.6}$$

A.2.4 Selection of output Inductor and Capacitor

The output inductor should not permit to go discontinuous, this occurred when the output dc current has dropped to half the span of the inductor current dI_L. The span of the inductor current dI_L can be defined as

$$\begin{aligned} dI_L &= V_L \times \frac{T_{Ton}}{L} \\ &= (V_{oi} - V_o) \times \frac{T_{Ton}}{L} \end{aligned} \tag{A.7}$$

where the output voltage V_o of the converter is defined as

$$V_o = 2 \times \frac{T_{Ton}}{1/f_{sw}} \times v_{io} \tag{A.8}$$

and the voltage across the cathode of the output diode and the center tap of the secondary winding v_{oi} can be defined as

$$v_{oi} = \frac{V_o}{2 \times T_{Ton}} \times \frac{1}{f_T} \tag{A.9}$$

Thus, v_{oi} for the 15 V and 5 V supplies are

v_{oi1} = 21.43 V for 15 V supply
v_{oi2} = 7.14 V for 5 V supply

The minimum inductance to operating at continuous mode for 15 V and 5 V supplies are

$$L_{1\min} = \frac{(V_{oi1} - V_{o1})T_{Ton}}{2 \times I_{o1}} = 11.25\,\mu\text{H} \quad \text{for 15 V supply} \tag{A.10}$$

$$L_{2\min} = \frac{(V_{oi2} - V_{o2})T_{Ton}}{2 \times I_{o2}} = 10.7\,\mu\text{H} \quad \text{for 5 V supply} \tag{A.11}$$

The inductance of the output inductors are chosen to be much greater than the minimum inductance in (A.10) and (A.11). Thus

$$L_1 = 47\ \mu\text{H}$$
$$L_2 = 47\ \mu\text{H}$$

The span of the inductor current dI_L for the 15 V and 5 V supplies can be calculated using (A.7) as

$$dI_{L1} = 0.96\ \text{A} \qquad \text{for 15 V supply}$$
$$dI_{L2} = 0.32\ \text{A} \qquad \text{for 15 V supply}$$

The output capacitors are chosen to satisfy the standard capacitance definition, which is

$$I_C = C\frac{dV_C}{dt} \tag{A.12}$$

where t is the MOSFET on time T_{Ton} , and V_C is chosen to be 25% of the maximum output ripple voltage. Thus, from (A.12), the minimum capacitance of the output capacitors for 15 V and 5 V supplies are

$$C_{1\min} = dI_{L1} \times \frac{T_{Ton}}{V_{rp1} \times 0.25} = 179.2\ \mu\text{F}$$
$$C_{2\min} = dI_{L2} \times \frac{T_{Ton}}{V_{rp2} \times 0.25} = 179.2\ \mu\text{F}$$

Thus, the capacitance of the output capacitors for both 15 V and 5 V supplies are chosen to be 220 μF.

A.2.5 Transformer Primary and Secondary Current

Fig. A.3 shows the typical plot of current waveform in the push-pull transformer windings. For primary current, it is assumed that the top of the current waveform in Fig. A.3 is flat and is equal to I_{pft}. The equivalent flat topped primary current is defined as

$$I_{pft} = \frac{P_o}{(V_d - V_{Ton}) \times \eta \times 2 \times D} = 1.7 \text{ A} \tag{A.13}$$

The primary rms current I_{prms} can be expressed [] as

$$I_{prms} = I_{pft} \times \sqrt{D} = 1 \text{ A} \tag{A.14}$$

As for the secondary rms current, it is assumed that the center ramp top is equal to the dc output current. Thus, the secondary rms current I_{srms} of 15 V and 5 V supplies can be expressed as

$$I_{s1rms} = I_{o1} \times \sqrt{D} = 1.183 \text{ A} \qquad \text{for 15 V supply} \tag{A.15}$$

$$I_{s2rms} = I_{o2} \times \sqrt{D} = 0.414 \text{ A} \qquad \text{for 5 V supply} \tag{A.16}$$

A.2.6 High Frequency Transformer Design

The number of turns for primary winding is expressed as

$$N_p = \frac{(V_d - V_{Ton}) \times D}{f_T \times \Delta B \times Ac} = 87.4 \text{ turns} \tag{A.17}$$

where the change in flux density ΔB is chosen to be 0.2 T and the core area Ac is 112×10^{-6} m^2. Note that the numbers of turns should be rounded to higher or lower integer value, thus, the number of turns chosen for primary winding N_p is 88 turns.

The number turns for secondary winding is expressed as

$$N_s = \left(\frac{V_o \times 1/f_T}{2 \times T_{Ton}} + Vd_{fw} \right) \times \frac{N_p}{V_d - V_{Ton}} \tag{A.18}$$

From (A.18), the numbers of turns of secondary winding for 15 V and 5 V supplies are

N_{s1} = 8 turns for 15 V supply
N_{s2} = 3 turns for 5 V supply

A.2.6.1 Selection of Primary and Secondary wire size

Primary side:

The current density J is chosen to be 3.9 A/mm^2 and from section A.2.5, the primary rms current is found to be 1 A. The cross sectional area W_{pcu} and the diameter d_{pcu} of the wire can be calculated as follows

$$W_{pcu} = \frac{I_{prms}}{J} = 0.256\,\text{mm}^2 \tag{A.19}$$

$$d_{pcu} = 2\times\sqrt{\frac{W_{pcu}}{\pi}} = 0.571\,\text{mm} \tag{A.20}$$

Secondary side:

The current density J is chosen to be 3.9 A/mm^2 and from section A.2.5, the primary rms current is found to be 1.183 A and 0.414 A for 15 V and 5 V supplies, respectively. The cross sectional area W_{pcu} and the diameter d_{pcu} of the wire can be calculated as follows

$$W_{s1cu} = \frac{I_{s1rms}}{J} = 0.303\,\text{mm}^2 \quad \text{for 15 V supply} \tag{A.21}$$

$$W_{s2cu} = \frac{I_{s2rms}}{J} = 0.106\,\text{mm}^2 \quad \text{for 5 V supply} \tag{A.22}$$

$$d_{s1cu} = 2\times\sqrt{\frac{W_{s1cu}}{\pi}} = 0.621\,\text{mm} \quad \text{for 15 V supply} \tag{A.23}$$

$$d_{s2cu} = 2\times\sqrt{\frac{W_{s2cu}}{\pi}} = 0.38\,\text{mm} \quad \text{for 15 V supply} \tag{A.24}$$

A.2.7 Push-Pull converter PCB layout

The PCB layout of the push-pull converter which contents eight isolated +15 V and -5 V dc voltage output are presented in Fig. A.3.

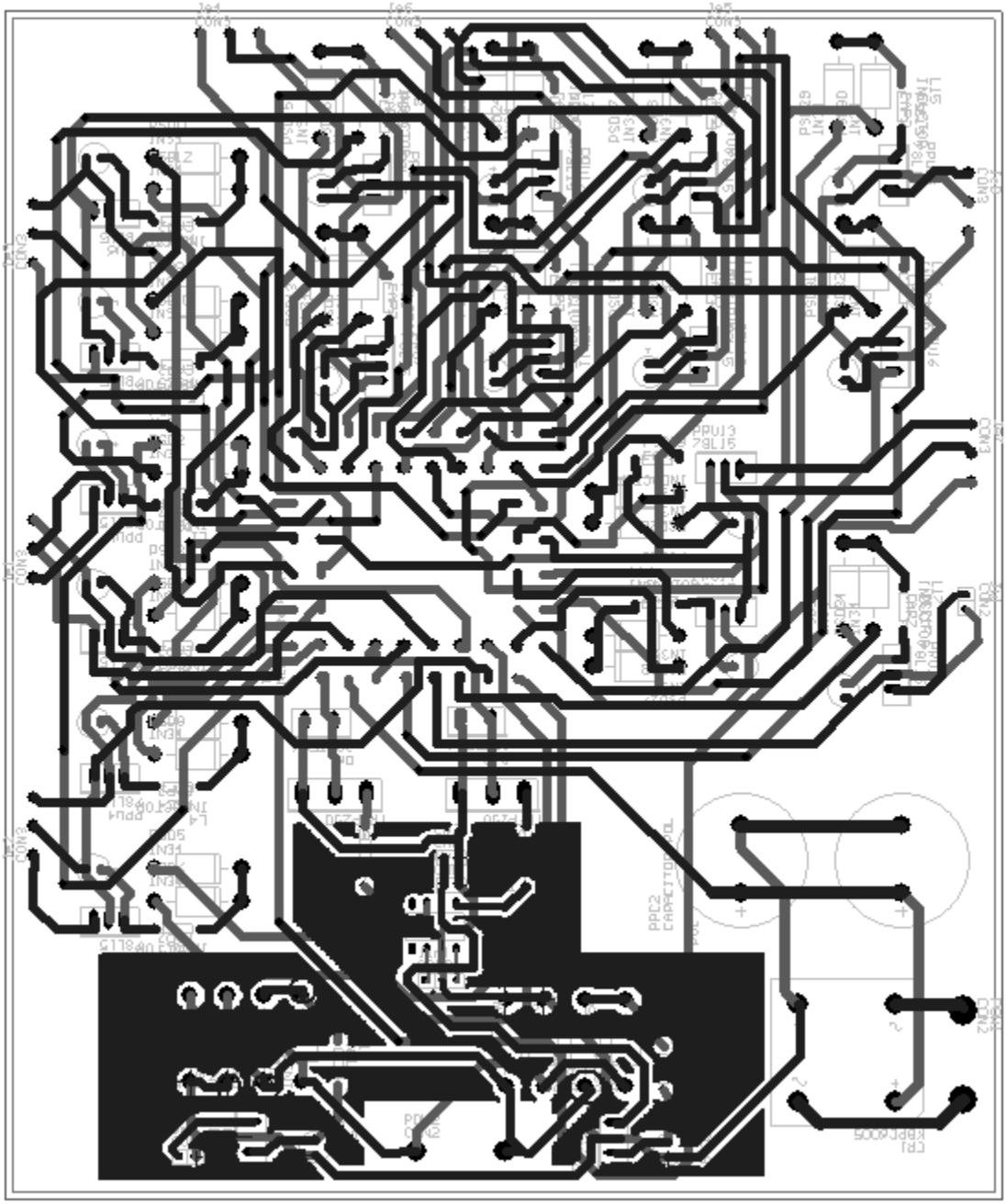

Fig. A.3: PCB layout of the push-pull inverter.

APPENDIX B. GATE DRIVE CIRCUITRY

In this section, the design of the gate drive circuitry which is able to output switching signal from +15 V to -5 V is presented.

B.1. Gate Drive Design

The HCPL-316J 2 A gate drive optocoupler from Agilent is used to implement the gate drive circuitry. The HCPL-316J offers an on-chip integrated V_{DS} desaturation detection and fault status feedback. Fig. B.1 shows the schematic of the gate drive circuitry.

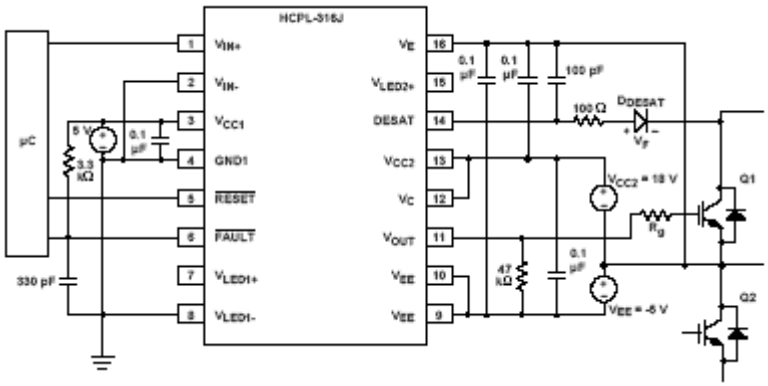

Fig. B.1: Schematic of the gate drive circuitry.

The maximum gate to source voltage of the power MOSFET is 20 V, thus 15 V dc voltage is choose to switch on the MOSFETs. To improve the discharging response of the MOSFETs additional -5 V is used.

The power stage of an inverter is susceptible to several types of failures, most of which are potentially destructive to the power MOSFETs. These failure modes can be grouped into four basic categories: Input supply sort circuits due to user misconnect or bad wiring, control signal failures due to noise or computational errors, overload conditions induced by the load, and component failures in the gate drive circuitry. Under any of these fault conditions, the current through the MOSFETs can increase rapidly, causing excessive power dissipation and heating. The MOSFETs become damaged when the current load approaches the saturation current of the device, and the drain to source voltage V_{DS} raises above the saturation voltage level. The drastically increased power dissipation very quickly overheats the power device and destroys it.

HCPL-316J monitors the saturation (drain) voltage of the MOSFET and to trigger a local fault shutdown sequence if the drain voltage exceeds a predetermined threshold by the DESAT diode. The value of V_{DS} which triggers DESAT to signal a fault condition, is 7 V – V_F, where V_F is the forward on voltage of the diode. The General Semiconductor UF4007 ultra fast diode is used in this application.

With a fixed value of switch on voltage, the value of the gate resistor R_G determines the maximum amount of gate-charging/discharging current

To find the peak charging I_{OL} assume that the gate is initially charged. Therefore R_G can be determined by applying the following relationship:

$$R_G = \frac{[V_{CC2} - 1 - (V_{OL} + V_{EE})]}{I_{OL}}$$
$$= \frac{15\,\text{V} - 1\,\text{V} - (1.5\,\text{V} - 5\,\text{V})}{2\,\text{A}}$$
$$= 8.75\,\Omega$$

B.2 Gate Drive Circuitry PCB layout

The PCB layout of the gate drive circuitry is presented in Fig. B.2. The PCP contents two sets of the gate drive circuitry.

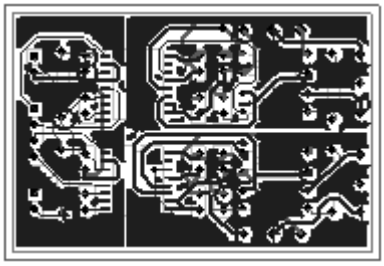

Fig. B.2: PCB layout of the gate drive circuitry.